T H E

E L E C T R O M A G N E T I C

F L O W M E T E R

by

W. D. JACKSON
B.Sc.
(Glasgow)

A Thesis Presented to the University of Glasgow
for the Degree of Doctor of Philosophy

May 1960

ProQuest Number: 10646803

ProQuest 10646803

PREFACE

The development of a flowmeter based on motional electro-
magnetic induction in a fluid was first recorded almost thirty
years ago and had been preceded by applications of the effect
to measurement of the speed of ships and to a study of tides
and waves. The authors of the latter acknowledged that their
work was based on experiments conducted in 1832 by Faraday
from Waterloo Bridge, London in an unsuccessful attempt to
detect the motion of the river Thames through the magnetic
field of the Earth.

Since the date of the first report, the electromagnetic
flowmeter has become established as an instrument for the
measurement of blood flow and, more recently, of liquid metal
flow in atomic reactors. Many of these applications have been
described in the now comparatively extensive literature on the
subject and a considerable amount of repetition of techniques
and results is to be found. In contrast to this, however, no
truly general study of the device has previously been given
and the few efforts which have been made in this direction
have been limited in their scope. One of the objects of this
report is to provide for this interesting device the general
evaluation which has hitherto been lacking.

At the outset of the study reported here, use of the
electromagnetic flowmeter for blood flow measurement was well
developed and its application to liquid metals was actively
in hand, particularly in the laboratories of the United States
Atomic Energy Commission. The first intention was that it
should be concerned with an application of the method to steam
plant flow metering, but the nature and extent of prior and
then current work indicated that it would be more profitable
to work along the lines of a general treatment of the device.
Two main points arose in the course of this, as related below,
and the innovations and improvements in electromagnetic flow-
meter practice and theory stemming from them are recorded in
detail in the text.

Much of the early flowmeter development was undertaken by
Kolin and the availability of this device in 1945 as a
practical measuring instrument was due largely to his efforts.
One of his initial contributions was the replacement of the
permanent magnet or d.c. excited magnetic field by sinusoidal
time variation of the flux density, thus minimising electrode
polarisation effects in the measurement of the flow of
electrolytes. As an alternative to this arrangement, a flow-
meter operating on a pulsed magnetic field with rectangular

flux waveform was proposed and developed during the course of this study.

Interest in blood flow measurement led to the initial development of this flowmeter being concentrated on a range of fluid electrical conductivities which, in the presence of the required magnetic field, are neither low enough to produce noticeable dielectric polarisation nor high enough to yield significant energy interaction effects due to fluid motion. While the latter had been investigated in 1936 by Hartmann and Lazarus and also utilised in the development of electromagnetic pumps, they had not been taken into account in other flowmeter studies. Recognition that the electromagnetic flowmeter could be regarded as a magnetohydrodynamic device and application of the ideas and methods of that relatively new subject to the study of it constituted the second major point.

The work on which this report is based was undertaken from September 1948 to July 1951 in the Electrical Engineering Department of the Royal College of Science and Technology, Glasgow, and completed during the following year in the Electrical Engineering Department of the Manchester College of Science and Technology. Chapter 1 follows closely the notes prepared (but otherwise unpublished) for an informal paper presented to the North-Western Graduates and Students Section of the Institution of Electrical Engineers in December, 1952. While the text is broadly restricted to cover the work completed during the period mentioned, use is made of subsequent work, including that by other investigators, where it leads to a better interpretation of the results obtained. The list of references to the measurement of fluid flow by electromagnetic methods and to related matters in magnetohydrodynamics has been brought up to date as of June, 1959.

It is a pleasure to conclude with acknowledgements to those who have helped this work towards its completion. Professor F. M. Bruce served as supervisor of the research, made numerous valuable suggestions and provided much patient guidance. Dr. E. S. Fairley first indicated the possibilities of the electromagnetic flowmeter as a research topic and participated in many useful discussions of the work. Professors J. Hollingworth and E. Bradshaw kindly consented to use of the facilities of the Electrical Engineering Department of the Manchester College of Science and Technology. Construction of the experimental apparatus was largely due to the skillful work of Mr. J. Brown, Mr. L. Davis and Mr. G. Nelson.

April, 1960   W. D. JACKSON

Table of Contents

Table of Contents (contd.)

Table of Contents (contd.)

Table of Contents (contd.)

List of Figures

List of Figures (contd.)

List of Figures (contd.)

List of Tables

Units and List of Symbols

Notes:

1. All equations are written for the rationalised system of M.K.S. units:

2. Where it is necessary to distinguish between moving and stationary reference frames, quantities in the latter are denoted by primes:

3. Under- and over-scored symbols denote vector quantities and time means respectively.

4. Volume measure in gallons is by the Imperial Standard unit.

Symbols are defined by the following list:

A magnetic vector potential

A_g effective airgap area

a half internal dimension, rectangular channel

B magnetic flux density

B_o uniform applied magnetic flux density

b half internal dimension, rectangular channel; or induced magnetic flux density

$b_e = B/\mu\sqrt{v\rho\sigma}$ "magnetic velocity" variable

b_n Fourier coefficient

C capacitance (in space, per unit length)

C, C_i etc.   integration constants

C_b barrier capacitance

C_{ci} flowmeter internal capacitance

C_{in} amplifier input capacitance

C_s flowmeter shunt capacitance

D electric flux density

E electric field intensity

F electromagnetic force on unit charge

F_p electromagnetic polarising force

Units and List of Symbols (contd.)

f channel friction factor

f_o excitation frequency

g acceleration constant

H magnetic field intensity

h liquid head of hydraulic system

h_f friction head

I_c magnetic circuit excitation current

i_1, i_2, i_3 unit vectors

J current density

$K = K_1 K_3 K_4$ flowmeter calibration factor

K_1 wall conductivity factor

$K_2 = V_m / 2au_o B_o$ motionally induced e.m.f. factor

K_3 velocity profile factor

K_4 end effect factor

K_c combined profile and end effect factor

K_p dielectric polarisation factor

k_c contact resistance factor

k_f leakage flux constant

k_p electromagnetic pump resistance factor

$k_w = \dfrac{w\sigma_w}{b\sigma}$ wall conductivity factor in one-dimensional flow

L_c characteristic length of system

L_f exciting coil inductance

l_g air gap length

l_m magnetic circuit length along flow axis

$M = BL_c \sqrt{\sigma/\rho\nu}$ Hartmann number

Units and List of Symbols (contd.)

$M' = M\left[1 + (2n + 1)^2\pi^2/a^2M^2\right]$ second Hartmann quantity
    $(n = 0,1,2,...)$

$P = \dfrac{1}{\rho v}\left[p + \dfrac{B \cdot B}{2\mu}\right]$ pressure variable

P_d dielectric polarisation

$P_o = -\nabla P$ pressure gradient variable

p hydrodynamic pressure

P_d pump delivery pressure

Q volume flow rate

Q_e electric charge

$R = L_c u/v$ Reynolds number

R_b barrier resistance

R_c Reynolds number at flow transition

R_{ci} flowmeter internal resistance

R_{cw} flowmeter wall resistance

R_{ex} external circuit resistance of e.m. pump

R_f exciting coil resistance

R_{in} amplifier input resistance

$R_M = R\beta$ magnetic Reynolds number

R_o series resistance component of flowmeter impedance

R_s spreading resistance

r radius

r_2 external radius circular channel

r_3 inter-electrode radius

r_a valve slope resistance

Units and List of Symbols (contd)

r_e electrode radius

r_i internal radius, circular channel

$S = B^2/\mu\rho u^2$ energy ratio

T temperature; <u>or</u> turns

t time

$U_D = \omega t/\sigma$ dielectric relaxation facotr

$U_s = \omega\mu\sigma L_c^2$ skin effect factor

U_ω velocity of propagation for m.h.d. waves

u velocity

u_d "field velocity" in skin effect factor

u_o average velocity

$\left.\begin{array}{l} u_v = u + b_e \\[2mm] u_\omega = u - b_e \end{array}\right\}$ velocity variables

V potential difference

V_i amplifier input voltage

V_m motionally induced e.m.f.

V_o resultant flowmeter output voltage

V_P motionally induced dielectric polarisation voltage

V_s flow-dependent component of V_o

V_t transformer e.m.f.

W_M magnetic energy

w channel wall width

w_m magnetic circuit width

X_o series reactance component of flowmeter impedance

$Z = R_o + jX_o$ flowmeter output impedance

α_c integration constant

Units and List of Symbols (contd.)

α_v $\dfrac{\text{mean back emf}}{\text{applied voltage}}$ of electromagnetic pump

$\beta = \mu\sigma v$ Batchelor's number

$\varepsilon = \varepsilon_o\varepsilon_r$ permittivity

ε_o permittivity of free space

ε_r relative permittivity of material medium

η dynamic viscosity coefficient

θ angle

$\lambda = 1/\mu\sigma$ magnetic diffusivity

μ permeability

μ_o permeability of free space

μ_r relative permeability of material medium

ν kinematic viscosity

ν' apparent (m.h.d.) viscosity

ρ fluid density

ρ_e volume electric charge density

ρ_s surface electric charge density

σ electrical conductivity

σ_ω electrical conductivity of channel wall

τ volume

τ_d time constant of skin effect equation

τ_u time constant for decay of fluid motion

τ_ε dielectric relaxation time

ϕ magnetic flux

ϕ_i total magnetic flux linking flow amplifier input circuit

ω angular frequency

$\nabla = \underline{i}_1 \dfrac{\partial}{\partial x} + \underline{i}_2 \dfrac{\partial}{\partial y} + \underline{i}_3 \dfrac{\partial}{\partial z}$

∇^2 Laplace operator

Chapter 1

AN INTRODUCTORY REVIEW

1.1. Measurement of Fluid Flow

Measurement of the flow of liquids and gases is commonly required as a feature of systems and installations in every branch of engineering. A number of electrical methods have been devised for this purpose and one of these — the electromagnetic flowmeter — is the subject of this thesis. As the general principles of flow measurement and what may be termed conventional measuring methods have been fully treated in the extensive literature on the subject (e.g. Refs 1, 2 and 3), only a brief outline of them will be given here to provide a background for the main topic.

A convenient grouping of flowmeter types is based on the form of channel, pipe or conduit in which flow measurement is to be made. Closed channel flowmeters are required for all fluids and are normally installed in channels of a simple cross-sectional form, while open channel flowmeters are restricted to liquids which can be exposed to atmosphere and usually involve the metering of water or aqueous solution.

Within each of the two main groups, basic sub-divisions can be made. Closed channel types include:

(1) Mechanical flowmeters in which a piston, vane or propeller moves continuously at a speed proportional to the flow rate;

(2) Differential pressure flowmeters which require a pressure-generating device (e.g. Venturi tube, orifice plate or nozzle) to be inserted into the channel and an arrangement for measuring the pressure differential. The volume rate of flow is determined from this using Bernouilli's relation of hydrodynamics

and an experimental coefficient of discharge (Ref. 2 pp. 70-77);

(3) <u>Variable aperture flowmeters</u>, usually of the cone-and-float type, in which variation of the channel cross-section at the metering point is a measure of the rate of flow.

Open channel flow measurements can be made using:

(4) Weirs and notches which form a dam across the channel and enable the flow rate to be determined from the depth of flow over the dam crest;

(5) Venturi flumes which introduce a pressure differential by a contraction of the channel cross-section in a manner similar to that of the Venturi tube for closed channels.

The selection of a flowmeter for a particular application requires consideration of a number of factors and it is to be expected that, in many cases, alternative arrangements will be possible. Where the channel has a uniform cross-section, either full-flow or shunt (by-pass) installations may be made, the latter having economic advantages for large channels. The shunt arrangement usually comprises a pressure-generating device in the main channel with a mechanical meter in the by-pass. The flow information required may be either the indication and recording of the volume rate of flow or an integration of the flow rate, or both. Differential pressure and variable aperture types are convenient in the former case while mechanical meters, coupled directly to a simple counter, are useful for obtaining an integrated reading. The minimum flow rate and the range of flow rate to be measured determine the sensitivity and type of flow scale required. As the variable aperture meter can readily be provided with a linear flow scale, or even a scale which is expanded at the lower rates of flow, it is suited to a situation where a wide

variation in flow rate is expected. The physical and chemical properties of the fluid being metered (e.g. corrosive action of liquid sodium) are of prime importance in determining the choice of flowmeter. This topic is too extensive to be dealt with here but is fully covered both in flowmeter literature (e.g. Refs 2 and 3) and in the catalogues of flowmeter manufacturers.

In certain cases involving open channels, river flow gauging being the most common, the methods described above cannot be applied on account of the dimensions and irregular nature of the channel. The volume rate of flow in these circumstances is obtained as the product of the channel cross-sectional area and the mean velocity of flow, these quantities being determined from experimental data on the channel profile and the velocity distribution across it. For measuring the latter a velocity probe is required and this may take the form of a simple timed float arrangement, a small propeller-type current meter or an L-shaped Pitot tube (Ref. 2, pp 276-8).

The determination of velocity distribution profiles is also required in the study of flow through channels and around obstacles. In this case, an important requirement is that the velocity probe should not give rise to any significant rearrangement of the flow pattern and this restricts the size of the probe.

Finding the speed at which a body is propelled through a fluid can be included in the general category of flow measurement problems as it involves the motion of a velocity probe relative to the fluid.

A complete flowmeter system comprises a flow-sensing device with an output 'signal' depending in some manner on the flow being measured, a transmission system which may include signal amplification and a recording instrument to present the flow information in a manner suited to a particular situation. If the flow signal leaving the transmission system is in coded

form, a detector has to be included in the recording instrument which may display its output as the deflection of a pointer on a scale, as a reading on a counter or as a graph made by a pen recorder. Alternatively or additionally, the information may be passes into an overall feedback control system of which the flowmeter forms part.

The calibration of a flowmeter system is undertaken by an actual test such as the measurement of the amount of liquid collected in an accurately calibrated vessel in a given time. It may not be necessary to use the fluid to be metered for calibration purposes (see Ref. 2, p. 102). Analytical prediction of flowmeter calibration is hampered by the difficulties involved in applying the theory of hydrodynamics to the type of three-dimensional situations which flowmeters present.

1.2. Application of Electrical Methods to Flow Measurement

The application of electrical methods to flow measurement may be made in any or all of the main component parts of a flowmeter system. Thus it is necessary to distinguish between (1) electrical recording instruments, (2) electrical data transmission and (3) flow sensing devices having as an output an electrical quantity (voltage, current, resistance, etc.) depending on the flow rate.

A requirement of a flowmeter system with electrical (and electronic) components is that some form of transducer be included to convert flow information to an electrical quantity. In a all-electrical system, the flow-sensing device will act as the transducer; otherwise a suitable arrangement must be included. Variable resistance, inductance and capacitance pick-ups can be employed with a differential pressure-generating device (Ref. 2, Chapter 8) while, with mechanical types, a small magnet built into the rotor converts the assembly into an

electric generator with an output frequency depending on the flow velocity (Ref. 4).

Details of electrical data transmission and recording systems and of electrical telemetering systems have received considerable attention (e.g. Refs 2, 5 and 6). Advantages which may be claimed for them include (i) high speed of response, (ii) power amplification to increase sensitivity and reduce load (head loss) on the flow system, (iii) minimum number of moving parts and (iv) suitability for data transmission to a remote metering point. When the flowmeter data is fed into an overall control system, rather than displayed visually for a human operator, electrical methods may have additional attraction. However, they require a power supply and may be dangerous where explosive or inflammable fluids are involved.

Electrical flow sensing devices depend on either (1) an electrical property of the moving fluid, (2) a fluid property (e.g. thermal or acoustic) which, in turn produces an electrical output depending on the fluid velocity, or (3) electromagnetic induction effects in moving fluids. Examples of the first two types will be given to conclude this Section.

The salt velocity method (Refs 7 and 8) belongs to the first group mentioned in the preceding paragraph and is used in water flow determination. A quantity of concentrated salt solution is introduced into the flow channel at a convenient point. The time taken for the relatively high-conductivity region produced by salt injection to reach measuring electrodes connected to a bridge-type detector, together with the distance between the injection point and the measuring point, enable the flow to be determined. The method requires good mixing of the brine and this is difficult to achieve at low velocities.

In the second group is the <u>hot wire or thermal meter</u>
which consists of a wire element stretched across the flow
channel and heated by passing an electric current through
it. Motion of the fluid tends to cool the element, thereby
changing its electrical resistance and, with a constant
voltage supply, the current it carries. Measurement either
of resistance or current change may be employed to determine
the rate of fluid flow past the element. This scheme is
commonly used for air and gas flow measurements and details
of it are available in the literature (Refs 9 and 10).

The <u>electrocaloric flowmeter</u> (Ref. 11) requires the
fitting of an electrically supplied heater element in the
flow channel, together with a resistance thermometer in a
downstream location. Under conditions of constant
differential temperature, the heat flow is proportional to
the fluid flow rate and thus can be used as a measure of the
volume rate of flow.

<u>Ultrasonic flowmeters</u> (Refs 12 and 13) operate on the
principle of phase comparison of ultrasonic waves before and
after transmission over a fixed distance in a fluid.
Variation of the velocity of the liquid produces phase changes
in the transmitted wave relative to the zero-flow condition.
Detection by a phase-sensitive arrangement (usually an
electronic type) gives an output which is a direct measure of
the flow rate.

The conditions where electrical methods can be employed
to advantage cannot be defined clearly and certainly depend
at least as much on economic as on technical considerations.
It is probably correct to state that the great majority of
cases can be dealt with satisfactorily using a simple
differential pressure or mechanical flowmeter installation.
There remain, however, a significant number of situations
(e.g. where high sensitivity and/or low head loss is a

requirement) in which an all-electrical system is attractive and it is to one of these that attention is now directed.

1.3. Electromagnetic flowmeters

Electromagnetic flowmeters are a class of electrical flow sensing devices which depend on (a) the interaction between magnetic and fluid velocity fields when these are present simultaneously in a defined region, (b) the properties of the fluid and of the solid material(s) forming the region boundaries and (c) boundary or junction effects due to the contact of dissimilar materials, one of which may be in motion. The first-mentioned is the principle by which a flow-dependent signal is produced, the second determines the general nature of the signal while the third may be regarded as a source of secondary effects. In this and the following Section, only the main principles will be outlined and detailed consideration both of these and of practical matters will be taken up in subsequent Chapters.

The first study of the behaviour of a fluid in a region containing a magnetic field was made by Faraday (see Refs 14 and 15) in the course of his experiments in terrestial electromagnetic induction made during December 1831 and January 1832. It has been suggested in several reports on electromagnetic flowmeters that Faraday devised the first meter of this type to measure tidal flow in the river Thames. However, examination of his diary (Ref. 14) shows that the purpose of the experiments conducted from Waterloo Bridge, London was to test his idea that moving part of a conducting loop through the earth's magnetic field would produce a deflection on a galvanometer connected in series with it. He chose to use the Thames as he considered that it would serve as a moving conductor of much greater length than any solid conductor system that he could construct in his

laboratory. His experiments were inconclusive, apparently
due to electrolytic effects, but they were of prime importance
because they originated in the thought that his electro-
magnetic induction law applied to fluid conductors as well as
to solid ones.

As a direct consequence of Faraday's observation it may
be stated that the kinetic energy of a moving, conducting
fluid can be converted to electromagnetic energy and vice-
versa. For reasons to be given in Sections 1.5 and 1.6,
interest in this form of energy conversion has developed
rapidly over the past twenty years. It has become known as
magnetohydrodynamics[1] - the motion of fluids in magnetic
fields - and has brought to electrical engineering a range of
magnetohydrodynamic machines in which the rotating element of
conventional motors and generators is replaced by the flow of
fluid in a channel.

Since the output of a magnetohydrodynamic generator may
be expected to depend on the rate of fluid flow through its
channel, any machine of this type can be used as an electro-
magnetic flow-sensing device or flowmeter. By treating the
electromagnetic flowmeter from this point of view, rather
than simply as a development of Faraday's homopolar disc
generator (although this is a valid approach which may be
useful for some purposes), it is identified with a general
class of electrical machines and with an important area of
study in both theoretical and practical physics.

The action of all electromagnetic flowmeters depends on
the general principles of motional electromagnetic induction.
For discussion purposes, it is convenient to classify flow-
meters by the effect which provides a flow-dependent signal.

---

1. This name was first suggested by Alfven in 1943 (Ref. 25).
   Cowling has proposed the alternative term 'hydromagnetics'.

The three main types result from motional induction of (1) a potential gradient within the fluid, (2) a magnetic field in and around the fluid and (3) dielectric polarisation of the fluid. Only the first-mentioned type has received significant attention in the literature and this report is primarily concerned with versions of it.

The commonly employed form of the electromagnetic flow-meter (to be referred to hereafter as the contact type) is shown in Fig. 1.1(a) to comprise a flow channel, usually of circular cross-section (although the rectangular section has advantages which will be explored later) situated in a transverse magnetic field extending over a short axial length. The flow-induced potential difference is 'collected' by means of a pair of contacts (or electrodes) mounted in the channel wall in contact with the fluid along a line perpendicular both to the direction of fluid flow and to the magnetic field lines.

Viewed from a reference system stationary with respect to the exciting field,[1] the motion of an electrically conducting body at a velocity[2] $\underline{u}$ through a time-invariant magnetic field of flux density $\underline{B}$ produces an electromagnetic force $\underline{F}$ on a unit charge, stationary relative to the fluid, given by

$$\underline{F} = \underline{u} \times \underline{B} \qquad (1\text{-}1)$$

For a homogeneous, isotropic, inviscid fluid, the velocity $\underline{u}_0$ is axially directed and uniform over the cross-section of the flow channel. In a uniform magnetic field $\underline{B}_0$ of infinite axial extent (i.e. two-dimensional model

---

1. The treatment of electromagnetic induction followed here uses Maxwell's equations and is in accordance with first order relativity theory.
2. Each symbol is defined when first introduced and a List of Symbols precedes this Chapter. Unless otherwise stated, rationalised M.K.S. units are used.

representation) for this type of flow, the potential difference appearing across the electrodes is numerically equal to the motionally induced e.m.f. V_m given by the line integral of F between the electrodes B and D as

$$V_m = \int_B^D (\underline{u} \times \underline{B}) \cdot d\underline{l} = 2r_1 u_o B_o \qquad (1\text{-}2)$$

for electrodes mounted diametrically opposite each other in a circular channel of internal radius r_1 and formed from material of infinite resistivity. Equation 1-2 shows that in this idealised case the electrode voltage is directly proportional to the flow velocity. Its polarity can be found by applying Fleming's right-hand rule.

The sensitivity of a flowmeter will be defined as the output signal obtained per unit volume per unit time. In this case, the sensitivity is given by

$$S_i = 2r_1 u_o B_o / \pi r_1^2 u_o = 2B_o / \pi r_1 \qquad (1\text{-}3)$$

and is seen to depend directly on the magnetic flux density and inversely on the channel radius.

In the case of a rectangular channel of internal dimensions 2a and 2b (2a being the longer side) with electrodes mounted in the shorter sides, and for the same conditions, V_m and S_i are

$$V_m = 2au_o B_o \quad (1\text{-}4); \qquad S_i = B_o / 2b \qquad (1\text{-}5)$$

To establish that the electrode voltage is directly proportional to the flow velocity (and hence to the volume rate of flow in any given channel) from simple ideas of electromagnetic induction has required the assumption of a model which departs in several important aspects from any practical situation. However, when such considerations as velocity distribution in the channel, non-uniformity and finite axial length of the magnetic field, fluid turbulence, finite resistivity of the channel walls and fluid conductivity

are taken into account, equations 1-1 to 1-5 are still found
to be a useful guide to the performance of this type of
flowmeter. These matters are taken up again in Chapter 3.

In a discussion of the <u>induced magnetic field flowmeter</u>,
some of the factors listed in the preceding paragraph must
be considered. As the transverse magnetic field extends
over a short axial length of the flow channel and falls to
zero just outside this length, the motional electromagnetic
force has a non-uniform space distribution where the fluid
enters and leaves the main magnetic field. In addition,
the $\underline{F}$ field varies in space due to the velocity distribution
over a cross-section of the fluid as required from well-
known hydrodynamic considerations. The variations in $\underline{F}$
lead to the establishment of circulating currents of density
$\underline{J}$ which in turn produce an induced magnetic field of flux
density $\underline{b}$. The resultant magnetic field $\underline{B}$ is the vector
sum of the main field and the induced field. These effects
correspond to armature reaction in rotating machines.

The dependence of the induced field on the fluid
velocity enables it to be used in the induced field flow-
meter as a measure of the volume rate of flow. The effect
is most marked in high-conductivity fluids (e.g. liquid
mercury and sodium) for which this type would appear to be
suitable. A possible version of it is given in Fig. 1.1(b)
and the operation of this is discussed in Section 1.4.

The <u>dielectric polarisation flowmeter</u> is based on the
following principle which receives further attention in
Chapter 4. In the dielectric of a condenser, the total
displacement is made up of the Maxwellian displacement
current effect and the elastic displacement of the molecular
constituents. If a flow channel of (say) rectangular
cross-section is made from insulating material, fitted with
electrodes and placed in a magnetic field as shown in

flow channel

magnetic field direction

field excitation windings

magnetic circuit

electrical output

electrodes on inner surface of channel wall

direction of fluid motion
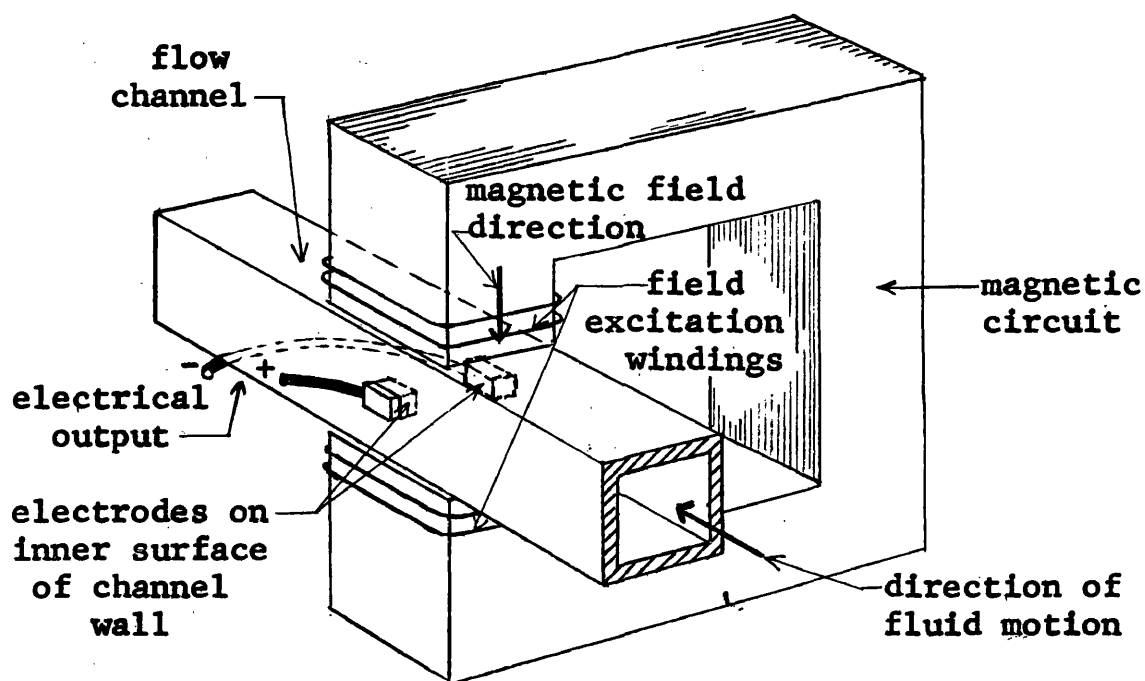
(a) Contact type with rectangular channel section

detector coil B

flow channel of non-conducting material

electrical output

electrical output

detector coil A

electrodes on outer surface of channel wall
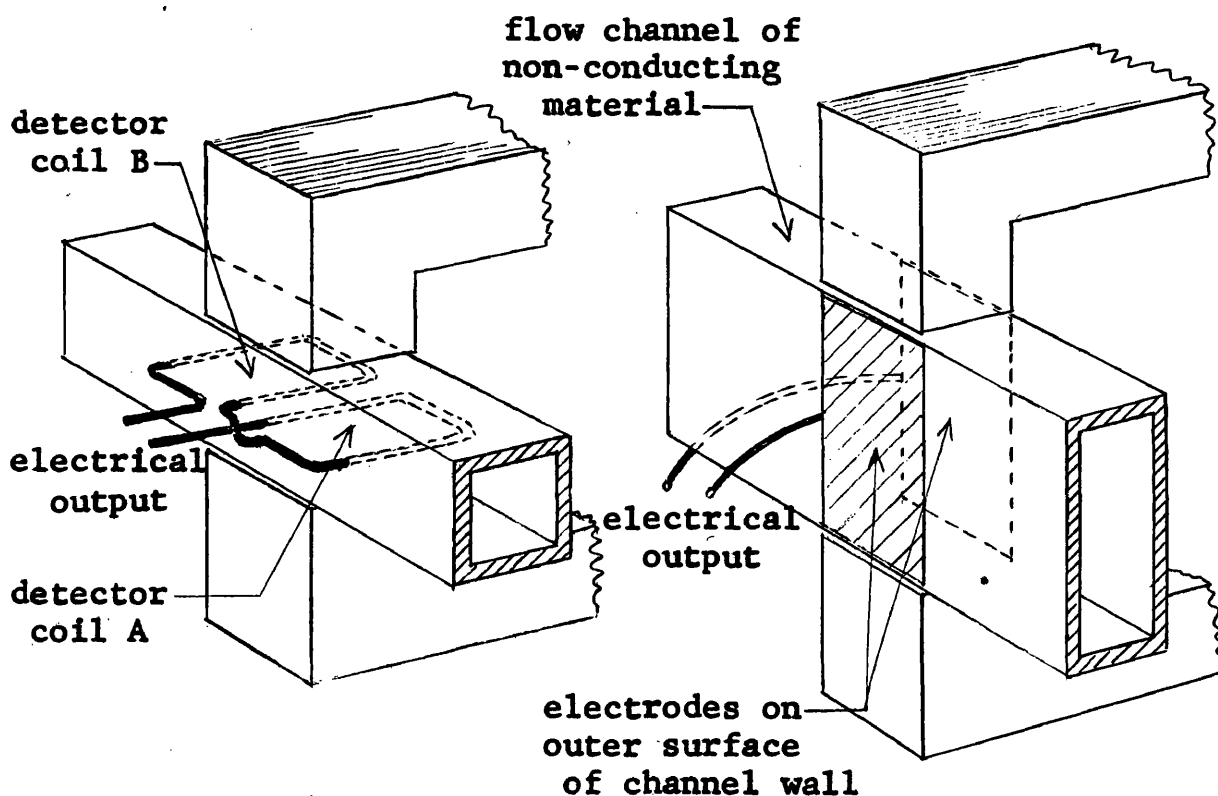
(b) Induced field type

(c) Dielectric polarisation type

Fig. 1.1.   Basic Electromagnetic Flowmeter Arrangements

Fig. 1.1(c), the molecular constituents of a moving fluid
dielectric experience the same force as in the case of an
electrically conducting fluid. Provided the fluid
dielectric is non-magnetic with a relative permittivity
greater than unity, polarisation occurs due to this force
and a flow-dependent potential difference is produced
between the electrodes[1].

Although a flow channel made from insulating material
is clearly required for the dielectric type of flowmeter, a
flow signal output may be obtained in the other two cases
with channels formed from electrically conducting material
provided this is non-ferrous in character. Indeed, chemical,
metallurgical or other considerations may require a metallic
channel to be used as in the case of stainless steel conduits
for liquid metals. The conducting channel 'loads' the
output of the flowmeter and this places restrictions on the
ratio of channel to fluid conductivities if excessive loss of
sensitivity is to be avoided.

1.4. Electromagnetic Flowmeters - Excitation Fields

The magnetic field required for all electromagnetic flow-
meters can be provided either by a permanent magnet or by a
separately excited magnetic circuit although other schemes
have recently been suggested for the metering of high-
conductivity liquids[2]. With separate excitation, the supply
can be selected to give (1) time-invariant (d.c.), (2)
sinusoidally time-varying (a.c.) or (3) pulsed periodic
magnetic field conditions[3].

---

1. For the case of a magnetic dielectric see Ref. 132.
2. Kolin (Ref. 120) has proposed that an axial current flow
   could provide a suitable magnetic field and thus enable
   the external magnetic circuit to be omitted.
3. The pulsed periodic scheme was first suggested by the
   writer in 1951 in a private communication to Prof. Bruce.

The contact type of d.c. electromagnetic flowmeter has found considerable favour in the measurement of the flow of liquid metals (see Section 1.7). A permanent magnet field system is generally employed. To avoid electrode polarisation difficulties when dealing with the flow of electrolytes, a periodically time-varying field is preferred.[1] Realisation of the full inherent sensitivity of electromagnetic flowmeters requires amplification of the flow signal and amplifier design is rather simpler if a.c. signals are involved.

The introduction of time variation into the magnetic field results in the presence of electromagnetically induced e.m.f.'s even when there is no fluid motion. The stationary fluid acts as a loaded secondary winding in a transformer where the field exciting winding forms the primary. For a specified excitation and flowmeter system, eddy currents are set up in the fluid with a magnitude depending on the fluid conductivity (and internal inductance). The situation corresponds to that obtaining in a single-phase induction motor with the rotor at rest. Further, as illustrated by Fig. 1.2, the leads connecting the electrodes to the amplifier (and/or detector system), together with the liquid between the electrodes and the amplifier input impedance, form a single-turn secondary winding in which an e.m.f. is induced under time-varying field conditions.

It is convenient to designate this the transformer e.m.f., V_t, and to distinguish it from the motional e.m.f., V_m, which, as already discussed, results from the space displacement of the fluid relative to the magnetic field. The reference system in which both V_t and V_m are specified is again taken as stationary (in space) with respect to the exciting field.

For the case of a conducting body, all or part of which

---

1. As in electrolytic tank field plotting methods.

is moving through a time-varying magnetic field, equation 1-1
is modified to

$$\underline{F} = \underline{E} + \underline{u} \times \underline{B} \qquad (1-6)$$

where $\underline{E}$ is the intensity of the electric field induced by the
time variation of the magnetic field.

Using Maxwell's equation $\nabla \times \underline{E} = -\partial\underline{B}/\partial t$ and introducing
the magnetic vector potential $\underline{A}$ where $\nabla \times \underline{A} = \underline{B}$, 1-6 becomes

$$\underline{F} = -\partial\underline{A}/\partial t + \underline{u} \times \underline{B} \qquad (1-7)$$

Allowing time variation of the magnetic field in the
simple two-dimensional model already used in Section 1.3 for
the d.c. flowmeter, the amplifier input signal V_i of the
system shown in Fig. 1.2. for an amplifier of infinite input
impedance is given by the line integral of $\underline{F}$ between the
amplifier input terminals around the path ABDE as

$$V_i = -\int_A^E \frac{\partial\underline{A}}{\partial t} \cdot d\underline{l} + \int_A^E (\underline{u} \times \underline{B}) \cdot d\underline{l} \qquad (1-8)$$

The first integral of 1-8 yields the transformer e.m.f.
and the second the motional e.m.f.   Since motional effects
can occur along the section BD only of the path, 1-8 can
be rewritten as

$$V_i = -\int_A^E \frac{\partial\underline{A}}{\partial t} \cdot d\underline{l} + \int_B^D (\underline{u} \times \underline{B}) \cdot d\underline{l} \qquad (1-9)$$

Under the assumed conditions, the path of integration
between B and D is immaterial and it is convenient to follow
the straight line through C joining these points.   Provided
the path ABCDE forms a clearly defined loop (e.g. if the
open-circuited ends are close together), V_i can be obtained
as

$$V_i(t) = 2au_oB_o(t) - \frac{d}{dt}[\phi_i(t)] \qquad (1-10)$$

where ϕ_i is the magnetic flux linking the input circuit,

$V_i(t)$ etc. indicate functions of time and

$$V_m(t) = 2au_oB_o(t) \quad (1\text{-}11); \quad V_t(t) = -\frac{d}{dt}[\phi_i(t)] \quad (1\text{-}12)$$

The simple treatment given above fails to take account of several important aspects of the time-varying field situation. Discussion of these will also be found in Chapter 3.

The arrangement of Fig. 1.2 with sinusoidal time variation of the exciting magnetic field will be referred to as the contact type a.c. electromagnetic flowmeter. Denoting the angular frequency of the exciting field by ω_o, B_o and ϕ_i in this case are given by

$$B_o(t) = B_o \sin \omega_o t ; \quad \phi_i(t) = \phi_i \sin \omega_o t$$

and equation 1-10 becomes

$$V_i(t) = 2au_oB_o \sin \omega_o t - \omega_o \phi_i \cos \omega_o t \quad (1\text{-}13)$$

in which

$$V_m(t) = 2au_oB_o \sin \omega_o t ; \quad V_t(t) = -\omega_o \phi_i \cos \omega_o t$$

The transformer e.m.f. is independent of the flow velocity and is displaced $\pi/2$ in phase from the linearly flow-dependent signal V_m. It is desirable to have zero detector output in the absence of fluid motion and this requires some arrangement such as a phase sensitive detector to discriminate against V_t or the 'balancing' of V_t prior to the detector input with a signal derived from the magnet excitation supply.

An alternative approach to the rejection of the transformer e.m.f. is made in the contact type pulsed flow-meter. In this case, time variation of the magnetic field takes the form of a flat-topped pulse waveform of the type shown in Fig. 1.3(a). Noting that the waveforms of $B_o(t)$ and $\phi_i(t)$ differ only by an amplitude scale factor under

Fig. 1.2. Flowmeter Input Circuit

V_{gd} = detector gating pulses
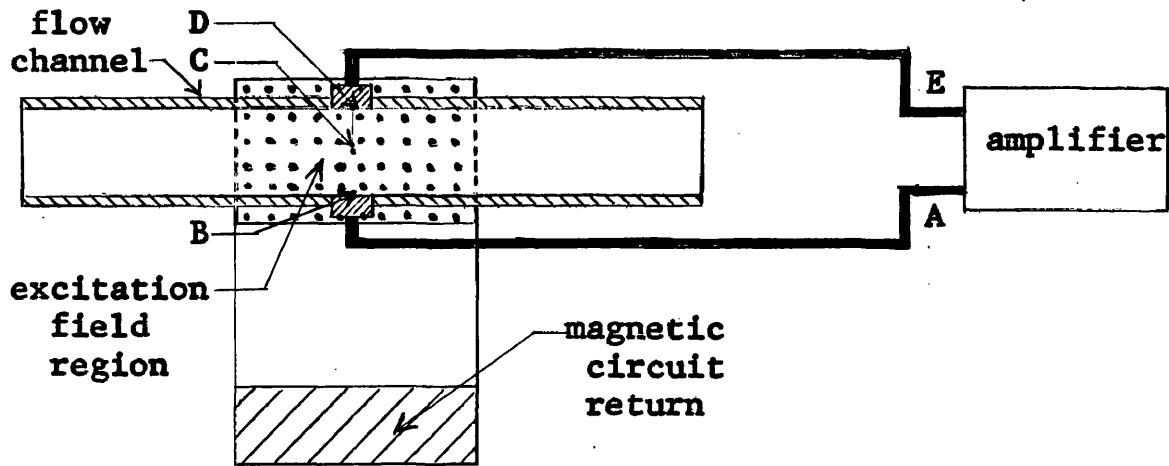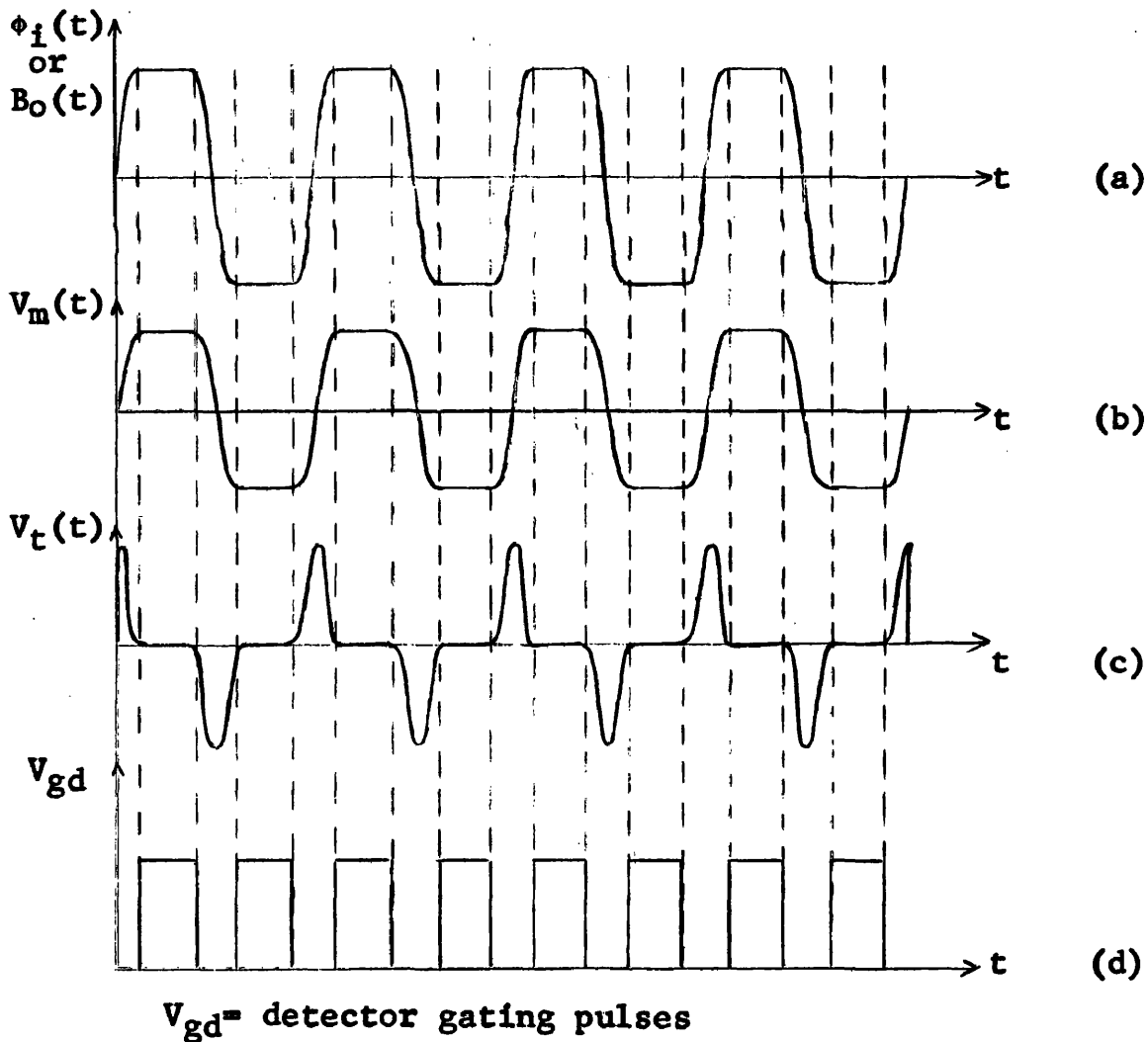
Fig. 1.3. Waveforms for Pulsed Excitation

the assumed conditions, the waveforms of $V_m(t)$ and $V_t(t)$ are seen from equations 1-11 and 1-12 to be proportional to those of $B_o(t)$ and its time derivative respectively as is illustrated by Figs 1.3(b) and 1.3(c). If the detector is arranged to respond to $V_i(t)$ during the time intervals of Fig. 1.3(d) and to be quiescent at other times, its output will depend only on the motional e.m.f. With an amplifier and detector system having a linear input-output relation, equation 1-10 shows that the detector output is directly proportional to the volume rate of flow.

A time varying field can also be applied to the induced field and dielectric polarisation flowmeters. The possible arrangement of the former shown in Fig. 1.1(c) is operated with sinusoidal time variation of the magnetic field. Under stationary conditions, the search coils A and B are positioned so that equal transformer e.m.f.'s are induced in them and are connected in series opposition to give zero output. When fluid flow occurs, the end effects mentioned earlier distort the magnetic field pattern to give unequal signals in the two search coils and hence produce a flow-dependent signal.

1.5. Magnetohydrodynamics

The analysis of electromagnetic flowmeters in subsequent Chapters will make extensive use of magnetohydrodynamic theory, particularly in its application to the flow of fluids in a channel. As this subject has been almost entirely overlooked in other flowmeter discussions, a brief summary of its nature and historical development is given in this Section.

Faraday discussed the purpose of his Waterloo Bridge experiments in his Bakerian Lecture Series of 1832 (Ref. 15) and his pertinent observations are worth quoting directly.

In Article 140 (of his Lectures) he mentions that "it was not difficult to perceive that the earth would produce the same [electromagnetic induction] effect as a magnet and to an extent that would, perhaps, render it available in the construction of new machines." Then, in Article 188: "Although the electricity obtained by magneto-electric induction in a few feet of wire is of but small intensity and has not yet been observed except in metals, and carbon in particular state, still it has the power to pass through brine; and as increased length in the substance acted upon produces increase of intensity, I hope to obtain effects from extensive moving masses of water, though quiescent water gave none." Finally, in Article 192 he speculates that the "Aurora Borealis and Australis may not be a discharge of electricity thus [by electromagnetic induction] urged towards the poles of the earth from whence it is endeavouring to return by natural and appointed means above the earth to the equatorial regions." Although Faraday indicated the possibilities of a study of electromagnetic induction in conducting fluids and guessed at the application of this to terrestrial problems, no significant work seems to have been undertaken for about 100 years.

At the beginning of this century, there was much controversy concerning the Lorentz transformation and the relativity theories of Poincare, Minowski and Einstein, and numerous experiments were devised to test these theories. Those of Blondot (1901, Ref. 16), H.A. Wilson (1905, Ref. 17) and L. Slepian (1914, Ref. 18) are of importance here for they dealt with electromagnetic induction effects in both solid and fluid dielectrics in motion through a steady magnetic field and gave confirmation of the predictions of relativity theory. A review of the Wilson experiment has

been given by Howe (Ref. 19).[1]

The effect of a magnetic field on the electrical resistance of liquid conductors (usually mercury) had been the subject of a number of investigations before the related work of Williams (Ref. 20) and Jones (Ref. 21) in 1925. Williams, recognising the existence of electromagnetic induction effects in liquid conductors, proceeded to devise the first electromagnetic flowmeter (using a d.c. field) in 1930 (Ref. 67). This promising work does not seem to have been continued and it was left to Hartmann and Lazarus, as a result of investigations into the flow of mercury through a closed channel in the presence of a transverse magnetic field, to lay in 1937 the foundations of both theoretical and experimental magnetohydrodynamics (Refs 22 and 23).

In 1943, Alfven (Refs 24 and 25) pointed out that, if a conducting liquid is placed in a constant magnetic field, every motion of the liquid gives rise to an e.m.f. which produces electric currents and that, owing to the magnetic field, these currents give rise to mechanical forces which change the state of motion of the liquid. He suggested that this situation would allow a form of wave motion and derived a wave equation for these magnetohydrodynamic waves on the assumption of infinite electrical conductivity in the liquid. He then applied these ideas to the problem of the origin of sunspots (Refs 26 and 27) and Walen used them as a basis for his 'smoke ring' theory of sunspots (Ref. 28). The existence of magnetohydrodynamic waves was first demonstrated experimentally by Lundquist in 1949 (Ref. 29).

The mechanism responsible for the generation of a magnetic field in rotating bodies such as the sun, earth and the stars has long engaged the attention of geophysicists

---

1. For comments on these experiments, see Whittaker, Ref.132.

(e.g. see Larmor, 1919, Ref. 30). In 1946 Elsasser (Ref. 31) accounted for the earth's magnetic field in terms of the magnetohydrodynamic effects produced by relative motion within its incompressible liquid core. Bullard in 1949 (Ref. 32) used the same approach but followed a different discussion of the problem of electromagnetic induction in a rotating sphere (1949, Ref. 33). In the same year, Truesall speculated on the effect of the compressibility of the earth on its magnetic field (Ref. 34); Elsasser (Ref. 35) gave a useful symmetrical form for the basic equations; and Lundquist, in 1951, investigated the stability of magneto-hydrostatic fields in a further search for a field-generating mechanism (Ref. 36). The self-excited magnetohydro-dynamic dynamo approach has found considerable favour although it does not as yet offer a completely satisfactory solution.[1]

Of more direct and immediate concern in electromagnetic flowmeter theory is the well-known phenomenon of hydrodynamic turbulence. The influence of a magnetic field on liquid turbulence was studied experimentally by Hartmann and Lazarus in the course of their work already cited. The first theoretical treatment was given by Batchelor in 1950 (Ref. 37) when he derived a criterion for the growth of electromagnetic energy in turbulent motion. Lehnert (1952, Ref. 38) gave an impressive demonstration of the damping of turbulence in mercury in the presence of a magnetic field. Murgatroyd (1953, Refs 39 and 40) repeated in modified form the work of Hartmann and Lazarus on the flow of mercury in a closed channel and obtained results generally in agreement. Shercliff (1953, Ref. 41) extended the theory of magneto-hydrodynamic flow in rectangular section channels. More

---

1. See Ref. 47 for a statement of the present position.

recently, the hydrodynamic stability of electrically conducting fluids in magnetic fields has received attention by Stuart (1954, Ref. 42), Lock (1955, Ref. 43), and Taylor (1957, Refs 44 and 45) in the course of work generally related to the problem of controlled thermonuclear fusion.

General studies of magnetohydrodynamics have been undertaken by Lundquist (1957, Ref. 46) and Cowling (1957, Ref. 47), the latter putting emphasis on geophysical and astronomical applications.

1.6. Magnetohydrodynamic Machines

The general problem of energy conversion between moving fluids and magnetic fields has received some attention (e.g. Remeneiras, 1949, Ref. 48) but the main emphasis has been on the engineering design of electromagnetic pumps to handle liquid metals in atomic reactor power plants.

Following Northup's work on the behaviour of mercury in a magnetic field during the period 1906-10 (Ref. 49), several proposals for electromagnetic pumps were made and Hartmann makes passing reference to a successful mercury pump he constructed around 1920. Work on this device which was developed from a mercury magnetometer led to his important magnetohydrodynamic investigations with Lazarus.

Electromagnetic pumps are classified into conduction and induction types, corresponding respectively to the contact and induced field electromagnetic flowmeters. The Hartmann or d.c. conduction arrangement was the first to be developed and successful applications have been described by Barnes, Smith and Whitham (1949, Ref. 51); Collins (1952, Ref. 52); Barnes (1953, Ref. 53); and Watt, O'Conner and Holland (1957, Ref. 54); while Woodrow (1949, Ref. 50) used the approach of Hartmann in his analytical study of this type of pump.

As the d.c. conduction pump requires a low-voltage, high-

current supply, the a.c. conduction type has been developed
to make normal voltage supplies to be used via a suitable
transformer which usually has a magnetic circuit integral with
that of the pump. The analytical treatment for this case has
been given by Murgatroyd (1954, Ref. 55).

The induction pump employs a polyphase supply to obtain a
travelling magnetic field and may take either a spiral or
linear form. Tests on the latter type have been reported by
Barnard and Collins (1951, Ref. 56) and Nixon and Crofts (1954,
Ref. 57), and a design study has been prepared by Watt (1955,
Ref. 58).

Reviews of the electromagnetic pump field given by Watt
(1953, Ref. 59 and 1956, Ref. 60), Blake (1956, Ref. 61 and
1957, Ref. 62) and in Ref. 63, deal in detail with the various
aspects of these machines while a typical nuclear power plant
application is described by Barnes, Koch, Monson, and Smith
(1956, Ref. 64).

1.7. Electromagnetic Flowmeters -- Historical Development

Reference to electromagnetic flow measuring methods are
widely scattered through the literature of a number of
subjects and this probably accounts for the considerable
amount of repetition to be found in flowmeter studies. The
list of 59 references now to be reviewed is believed to be by
far the most extensive to be prepared.

The first record of an application of electromagnetic
induction in fluids to a flow measurement problem is contained
in a United States patent dealing with "An Electromagnetic
Ship's Log", filed by Smith and J. Slepian in 1915 (Ref. 65).
The patent states that it is concerned with a "method of
measuring the speed of a ship relative to the water comprising
a magnetic field moving with the ship through the water and
measuring the electromotive force induced in the water by the

movement of the field." The description of the device includes
details of a field magnet assembly and non-polarisable zinc
sulphate electrodes. The simple theory of electromagnetic
induction is clearly set out and the use of an alternating
magnetic field is suggested to eliminate electrolytic polar-
isation effects.

In 1920, Young, Gerrard and Jevons (Ref. 66) reported on
investigations of tidal and wave motions outside Dartmouth
Harbour using the earth's magnetic field and an arrangement
similar to that employed by Faraday (to whose work reference
is made) but with electrodes specially chosen to be non-polar-
isable. Results obtained agreed with observations made by
other means and included an application to the measurement of
the speed of a ship.

That electromagnetic induction could be utilised to
measure the flow of liquids in closed channels was first
demonstrated by Williams in 1930 (Ref. 67) using a d.c. mag-
netic field, a non-conducting channel, an aqueous solution of
copper sulphate and a galvanometer as a detector. Although
he recognised the existence of circulating electric currents
due to the non-uniform velocity distribution, his analytical
work does not take account of magnetohydrodynamic effects.

The use of the electromagnetic flowmeter for blood flow
measurement was first suggested by Fabre (Ref. 68) and it has
since found considerable application for this purpose. His
scheme involved the use of a d.c. magnetic field, non-polar-
isable electrodes and a thermionic valve amplifier and
detector to increase sensitivity.

Arising out of a newspaper report (Ref. 69) of an
invention which was claimed to produce electrical power directly
from tap water, a lengthy discussion of the flow of fluids
past magnetic poles by Northfield, Howe and Taylor appeared

in the correspondence columns of the Electrician during 1936
(Ref. 70). Howe suggested that the effect on the fluid might
be similar to that in a moving copper strip, discussed the
possibility of a Hall effect appearing and, apparently un-
aware of the work of Williams, recommended the subject for
experimental investigation.

To Kolin must go much of the credit for the development
of the electromagnetic flowmeter as a practical measuring
device. The first of his many reports (Ref. 71) appeared in
1936 and dealt with a simple d.c. arrangement. In the
following year he filed a U.S. patent (Ref. 72) relating to
the flowmeter in rather general terms and dealing specifi-
cally with alternating magnetic field excitation. Jointly
with Katz, he described (1937, Ref. 73) the use of an a.c.
flowmeter system for blood flow measurement.

Independently of Fabre, Kolin and Katz, Zetterer in 1937
developed a d.c. flowmeter for blood flow measurement (Refs
74 and 75). This was followed during the period 1937-41 by
a number of papers (Refs 76-80) by Kolin and his associates
dealing with further blood flow applications and improvements
to the flowmeter system.

A good beginning to the systematic study of electro-
magnetic flowmeters was made by Eindhorn in 1940 (Ref. 82)
using an a.c. flowmeter and a non-conducting channel. In the
following year, Thurlmann repeated in modified form and with
a rather lengthy derivation the analysis of Williams and
extended it to the case of a conducting channel using an
approximate method (Ref. 83). Thurlmann refers to Hartmann's
work but neither Eindhorn nor he give any consideration to
possible magnetohydrodynamic effects.

Kolin next turned his attention to the use of electro-
magnetic induction in the determination of velocity profiles
in channels and around obstacles (1944, Refs 84 and 85). In

1945 he described (Ref. 86) a high-sensitivity a.c. flowmeter which has provided a starting point for nearly all subsequent flowmeter studies, including the one described in this thesis. Guelke and Schoute-Vanneck applied Eindhorn's work to the measurement of sea water velocities (1947, Ref. 87) and in 1948 Lehde and Lang were granted a U.S. patent (Ref. 88) for an electromagnetic ship's log operating on the induced magnetic field principle. Their patent includes the description of a proposed induced field flowmeter on which Fig. 1.1(b) is based.

The use of the electromagnetic flowmeter for blood flow measurement received further attention from Jochim (1948, Ref. 89) and Clark and Randall (1949, Ref. 90). Industrial applications of Kolin's high-sensitivity flowmeter were discussed by Raynsford (1948, Refs 91 and 92) and by Mittleman and Cushing in an as yet unpublished paper (Ref. 93). Oscillatory and transient flow studies using electromagnetic flowmeters were made respectively by Morris and Chadwick (1951, Ref. 94)[1] and Arnold (1951, Ref. 95) and an application to the field of rocket research is mentioned by Jaffe, Coss and Daykin (1951, Ref. 96).

The measurement of liquid metal flow in atomic reactor power plants using e.m. flowmeters offers advantages generally similar to those of electromagnetic pumps. Details of an a.c. flowmeter design for this application has been given by James (1951, Ref. 98 and 1952, Ref. 100) and a d.c. type constructed in 1947 using a stainless steel channel is described briefly by Barnes, Whitham and Smith (1952, Ref. 103). Some systematic testing of both d.c. and a.c. liquid metal flowmeters using mercury has been reported by Elrod and Fouse (1950, Ref. 97 and 1952, Ref. 102) who also

---

1. This and all subsequent references became available during or after the period in which this study was undertaken.

extended Thurlmann's analytical work on the effect of
conducting channel walls. A similar analysis by Astley
(1952, Ref. 101) included consideration of a relatively
high-resistance stagnation layer to represent the 'non-
wetting' condition which may occur between a liquid metal
and a metallic channel or electrode. The calibration of a
liquid sodium d.c. flowmeter has been described by Gray
(1951, Ref. 99) who used the Elrod and Fouse formula.

Hogg, Mittleman and Cushing (1952, Ref. 104) discussed
the circuit problems encountered in the design of their a.c.
flowmeter described in Ref. 93. Kolin (1952, Ref. 105 and
1953, Ref. 109) has dealt with some further improvements to
blood flow measurement apparatus and with Reiche continued
his work on velocity distribution profiles (1953, Ref. 114).
Grossman and Charwat have also applied electromagnetic
induction methods to local velocity determination (1952,
Ref. 106). A further simple d.c. liquid metal flowmeter
has been described by Carroll (1953, Ref. 108). Reports of
a preliminary study of the d.c. liquid metal flowmeter by
Murgatroyd (1952, Ref. 107) and Shercliff (1953, Ref. 110
and 1954, Ref. 115) deal respectively with a proposed test
model and the theory of this type of flowmeter. These
studies were continued by Shercliff (1955, Ref. 119) who
used a d.c. magnetic field excitation and mercury as the test
liquid to investigate the dependence of flowmeter output
voltage on the velocity profile in circular channels.

Further applications of Kolin's 1945 arrangement have
been described by Boeke (1953, Refs 111 and 112), Savastano
and Carravetta (1954, Ref. 113) and Remeneiras and Hermant
(1954, Ref. 116). Some interest has been shown recently in
the use of a rectangular channel section and brief analytical
discussions of this have been presented by Thurlmann (1955,
Ref. 117) and Holdaway (1957, Ref. 123). Elimination of the

external magnet was proposed by Kolin (1956, Ref. 120) and
discussed by Shercliff (1957, Ref. 122). A useful review of
the d.c. liquid metal flowmeter has been given in Ref. 118
while Denison and Spencer (1956, Ref. 121) describe the first
application of the writer's pulsed field excitation scheme
in the course of their work on blood flow measurement.

Chapter 2

THEORETICAL MAGNETOHYDRODYNAMICS

2.1. Hydrodynamics

Classical hydrodynamics is concerned with the behaviour
of fluids in motion in the absence of any electric or magnetic
effects and may be regarded as a special case of the more
general magnetohydrodynamic (m.h.d.) situation. Theoretical
studies of both inviscid and viscous fluids are to be found
in the standard treatments of hydrodynamics such as those by
Lamb (Ref. 124) and Milne-Thomson (Ref. 125). Hydrodynamic
turbulence, the unstable condition which can arise in fluid
flow, is an important aspect of this subject but is as yet
imperfectly understood. A detailed review of the theories of
turbulence has recently been prepared by Lin (Ref. 126).

The dynamical equations for a fluid are the conservation
relations for mass and momentum and these form the basis for
any theoretical study of fluid motion. Restricting attention
to cases where isothermal conditions obtain in a Stokesian
fluid, the so-called Navier-Stokes relation[1] for the conserva-
tion of momentum expressed with respect to a fixed reference
frame is

$$\rho[\frac{\partial \underline{u}}{\partial t} + (\underline{u}\cdot\nabla)\underline{u}] = -\nabla p + \eta[\nabla^2 \underline{u} + \frac{1}{3}\nabla(\nabla\cdot\underline{u}]\qquad(2\text{-}1)$$

where ρ is the fluid density, p the hydrodynamic pressure and
and η the coefficient of dynamic viscosity.

The conservation of mass may be stated formally as

$$\frac{\partial \rho}{\partial t} + \nabla\cdot(\rho\underline{u}) = 0\qquad(2\text{-}2)$$

A further relation is required to enable 2-1 and 2-2 to
be solved for the variables p, ρ and $\underline{u}$ and this is provided

---

1. For a derivation of this relation, see Lamb, Ref. 124, p.2.

by the equation of state which indicates the functional
dependence of fluid pressure on density in the form

$$p = f(\rho) \tag{2-3}$$

The practical situations with which this thesis deals
involve the flow of almost incompressible liquids and for
these 2-2 may be reduced to

$$\nabla \cdot \underline{u} = 0 \tag{2-4}$$

and 2-3 is no longer required. The form of 2-1 for incom-
pressible liquids is

$$\frac{\partial \underline{u}}{\partial t} + (\underline{u} \cdot \nabla)\underline{u} = -\frac{\nabla p}{\rho} + \nu \nabla^2 \underline{u} \tag{2-5}$$

where $\nu = \eta/\rho$ is the kinematic viscosity.

2.2   Electromagnetic Theory

The electromagnetic relations at a point in a material
medium at rest with respect to a reference system are given
by Maxwell's equations and the continuity relations as

$$\nabla \times \underline{H}' = \underline{J}' + \frac{\partial \underline{D}'}{\partial t} \tag{2-6} \qquad\qquad \nabla \times \underline{E}' = -\frac{\partial \underline{B}'}{\partial t} \tag{2-7}$$

$$\nabla \cdot \underline{D}' = \rho_e' \tag{2-8} \qquad\qquad \nabla \cdot \underline{B}' = 0 \tag{2-9}$$

in which $\underline{H}$ denotes the magnetic field intensity, $\underline{J}$ the
current density, $\underline{D}$ the electric displacement, ρ_e the volume
charge density and the primes indicate that the field
quantities are referred to the rest reference system.

In an isotropic, linear medium, the constitutive
relations are

$$\underline{B}' = \mu_o \mu_r \underline{H}' \tag{2-10} \qquad\qquad \underline{D}' = \varepsilon_o \varepsilon_r \underline{E}' \tag{2-11}$$

where μ_o and μ_r are respectively the permeability of free
space and the relative permeability of the material medium,
and ε_o and ε_r are respectively the permittivity of free
space and the relative permittivity of the material medium.
The permeability $\mu = \mu_o \mu_r$ and the permittivity $\varepsilon = \varepsilon_o \varepsilon_r$.

It is shown in standard treatments of relativity (e.g. Stratton, Ref. 127, p. 79) that Maxwell's equations are invariant to a transformation from one reference system to another moving with a linear, uniform relative velocity. The electromagnetic equations of a material medium moving with velocity $\underline{u}$ relative to a fixed reference frame are

$$\nabla \times \underline{H} = \underline{J} + \frac{\partial \underline{D}}{\partial t} \qquad (2\text{-}12) \qquad \nabla \times \underline{E} = -\frac{\partial \underline{B}}{\partial t} \qquad (2\text{-}13)$$

$$\nabla \cdot \underline{D} = \rho_e \qquad (2\text{-}14) \qquad \nabla \cdot \underline{B} = 0 \qquad (2\text{-}15)$$

where
$$\underline{J} = \nabla(\underline{E} + \underline{u} \times \underline{B}) + \underline{u}\rho_e \qquad (2\text{-}16)$$

and ∇ is the electrical conductivity. The usual transformation relations can be employed to obtain these unprimed field quantities in terms of the primed quantities of equations 2-6 to 2-9 and c, the velocity of light in vacuo. As the ratios of $\underline{B}$ to $\underline{H}$ and $\underline{D}$ to $\underline{E}$ are not preserved in both systems, it is necessary to recognise that the constitutive relations as stated in 2-10 and 2-11 do not apply to the fixed frame.[1]

In the theory of rotating machines, electromagnetic induction effects arising from the motion of conductor systems relative to an exciting magnetic field are usually determined without difficulty from Faraday's Law using the flux cutting rule. However, the application of this method to systems with both moving and stationary parts connected through sliding contacts, leads to perplexing, and at times contradictory, results.[2] In addition to being an example of this type, the electromagnetic flowmeter involves a moving system within which there is relative motion due to the liquid velocity distribution over the cross-section of the flow channel. To avoid these difficulties, the approach used here is to apply the basic electromagnetic equations in accordance with

---

1. The general relations are given by Cullwick, Ref. 128, Ch.6.
2. As illustrated by Refs 129 and 130.

established relativity theory and to first order accuracy.

2.3. Formulation of Magnetohydrodynamic Equations

The basic relations of magnetohydrodynamics can be
formulated either by combining the hydrodynamic and electro-
magnetic equations given in the previous two sections (the
'continuum' approach) or by manipulation of the Boltzmann
equation which arises in the theory of ionised gases. This
equation is fully discussed by Chapman and Cowling (Ref. 133)
and the lengthy derivation of the m.h.d. equations from it
has been given by Spitzer (Ref. 134). The continuum approach
is certainly valid for liquids and is appropriate to the
present discussion.   It can be expected to apply to gases
provided the radius of curvature of electron and ion paths
is large compared with their mean free path.

The momentum equation is obtained by modifying the
Navier-Stokes equation to take account of the electromagnetic
body forces and is

$$\frac{\partial \underline{u}}{\partial t} + (\underline{u}\cdot\nabla)\underline{u} = \frac{1}{\rho}(\rho_e \underline{E} + \underline{J} \times \underline{B}) - \frac{1}{\rho}\nabla p + \gamma\nabla^2\underline{u} \qquad (2\text{-}17)$$

to the right-hand side of which may be added such terms as
are required to account for any external body forces.
Subject to the usual restrictions of homogeneity, incompres-
sibility and linearity, this modified Navier-Stokes equation,
together with equation 2-4 and the electromagnetic relations
2-12 to 2-16, provide a set of relations from which the
various vector and scalar variables may be determined.

This set involves a non-linear partial differential
equation which prevents a complete solution from being
obtained in all but a few special cases.   It will be shown
in Chapter 3 that the flow of liquid in a channel is a
situation in which linear relations may obtain and for which
complete solutions can be derived under certain simple

boundary conditions. The remainder of this Chapter is devoted to some general aspects of the m.h.d. relations which will be useful in later analysis and discussion.

2.4. Magnetic Field Relation

An important auxiliary relation for the magnetic flux density can be obtained as follows. By taking the curl of both sides of 2-16, there results

$$\nabla \times \underline{J} = \sigma[\nabla \times \underline{E} + \nabla \times (\underline{u} \times \underline{B})] + \rho_e(\nabla \times \underline{u})$$

Rearranging 2-12 and again taking the curl of both sides gives

$$\nabla \times \underline{J} = \nabla \times (\nabla \times \underline{H}) - \nabla \frac{\partial \underline{D}}{\partial t}$$

These can be combined into the single equation

$$\nabla \times (\nabla \times \underline{H}) - \nabla \times \frac{\partial \underline{D}}{\partial t} = \sigma[\nabla \times \underline{E} + \nabla \times (\underline{u} \times \underline{B})] + \rho_e(\nabla \times \underline{u}) \qquad (2\text{-}18)$$

Writing $\underline{B} = \mu\underline{H}$ and $\underline{D} = \epsilon\underline{E}$ and applying 2-13, equation 2-18, using the vector relation for $\nabla \times (\nabla \times \underline{B})$ and 2-15, becomes

$$\frac{\partial \underline{B}}{\partial t} - \nabla \times (\underline{u} \times \underline{B}) = \frac{1}{\sigma\mu}[\nabla^2\underline{B} - \mu\epsilon \frac{\partial^2 \underline{B}}{\partial t^2} + \mu\rho_e(\nabla \times \underline{u})] \qquad (2\text{-}19)$$

It is useful to note that, for $\underline{u} = 0$, 2-19 reduces to an electromagnetic wave equation

$$\frac{\partial \underline{B}}{\partial t} = \frac{1}{\sigma\mu}[\nabla^2\underline{B} - \mu\epsilon \frac{\partial^2 \underline{B}}{\partial t^2}]$$

The assumption of negligible electromagnetic radiation requires that $\left|\partial\underline{B}/\partial t\right| \gg (\epsilon/\sigma)\left|\partial^2\underline{B}/\partial t^2\right|$

and gives $\quad \dfrac{\partial \underline{B}}{\partial t} - \nabla \times (\underline{u} \times \underline{B}) = \dfrac{1}{\sigma\mu}[\nabla^2\underline{B} + \mu\rho_e(\nabla \times \underline{u})]$

In this case, for $\underline{u} = 0$, the equation reduces to a diffusion or skin effect equation

$$\frac{\partial \underline{B}}{\partial t} = \frac{1}{\sigma\mu} \nabla^2\underline{B} \qquad (2.20)$$

Neglecting $\mu\rho_e(\nabla \times \underline{u})$ in comparison with $\nabla^2\underline{B}$ leads finally to

the <u>Bullard Relation</u>

$$\frac{\partial B}{\partial t} - \nabla \times (\underline{u} \times \underline{B}) = \lambda \nabla^2 \underline{B} \qquad (2\text{-}21)$$

where $\lambda = 1/\mu\sigma$ may be called the magnetic diffusivity from 2-20.

This derivation shows that the Bullard relation differs in form from two of the most important partial differential equations and that its solution is likely to prove difficult.[1]

The two approximations made in the derivation can be stated in the form that Maxwellian displacement currents are negligible and that convection current effects are neglected in the equation for charge continuity. Equation 2-16 then becomes a statement of Ohm's Law as

$$\underline{J} = \sigma(\underline{E} + \underline{u} \times \underline{B}) \qquad (2\text{-}22)$$

This does not mean that the effects of charge accumulation are to be neglected and equation 2-14 may not be written $\nabla \cdot \underline{D} = 0$ as is sometimes done.

Equation 2-20 applies when the liquid is at rest, and, following usual skin effect reasoning, the time constant τ_d for the decay of $\underline{B}$ is given approximately by

$$1/\tau_d = \lambda/L_c^2$$

where L_c is a length of the order of the dimensions of the region in which the field exists. Also, the velocity at which this field moves through the stationary liquid conductor is

$$u_d = \lambda/L_c$$

For a liquid of infinite electrical conductivity, 2-21 reduces to

$$\frac{\partial B}{\partial t} - \nabla \times (\underline{u} \times \underline{B}) = 0 \qquad (2\text{-}23)$$

---

1. See Elsasser (Ref. 31) and Bullard (Ref. 33) for solutions dealing with a conducting sphere rotating in a magnetic field.

This equation has a form identical to that of the vorticity relation for an inviscid liquid obtained in hydrodynamics where the lines of vorticity are taken to move with the liquid.[1] By analogy, equation 2-23 can be interpreted in the same manner and the magnetic field lines thought of as being frozen into the liquid. As a consequence of this, any two points lying on a magnetic line of force will remain on the same line as it is swept along by the flow. This does not mean that any physical entity other than the material liquid is in motion relative to the reference system and represents only a means of accounting for the forces being considered. A simple physical explanation is that, in a perfect conductor, there can be no induced electromagnetic force due to $\underline{B}$. Thus no relative motion is possible between the liquid and the magnetic field.

In general, the lines of magnetic force tend to be carried about with the moving liquid but at the same time to leak or slip through it to some extent. In hydrodynamics, Reynolds number R is defined as

$$R = L_c u / \gamma \qquad (2\text{-}24)$$

and, by analogy, a magnetic Reynolds number R_m can be defined as

$$R_M = L_c u / \lambda = R \gamma / \lambda \qquad (2\text{-}25)$$

Strong interaction between electromagnetic and hydrodynamic phenomena may be expected when the transport of magnetic lines of force dominates the leak, and this will occur when $u \gg u_d$ or $R_M \gg 1$.

From 2-25

$$R_M / R = \mu \nabla \gamma = \beta \qquad (2\text{-}26)$$

where $\beta = \mu \nabla \gamma$ is Batchelor's number.

2.5. Stress and Energy

The electromagnetic body forces per unit volume as included

---

1. See Ref. 125, Chapter 13.

in equation 2-17 become, on application of 2-12 and 2-14,

$$\rho_e \underline{E} + \underline{J} \times \underline{B} = (\nabla \cdot \underline{D})\underline{E} + (\nabla \times \underline{H} - \frac{\partial \underline{D}}{\partial t}) \times \underline{B}$$

$$= (\nabla \cdot \varepsilon\underline{E})\underline{E} + (\nabla \times \underline{H}) \times \mu\underline{H} + \frac{\partial}{\partial t}(\varepsilon\underline{E} \times \mu\underline{H})$$

$$+ (\nabla \times \underline{E}) \times \varepsilon\underline{E}$$

Using the vector identities[1]

$$(\nabla \times \underline{E}) \times \underline{E} = (\nabla \cdot \underline{E})\underline{E} - \nabla|E|^2/2 - \underline{E}(\nabla \cdot \underline{E})$$

$$(\nabla \times \underline{H}) \times \underline{H} = (\nabla \cdot \underline{H})\underline{H} - \nabla|H|^2/2 - \underline{H}(\nabla \cdot \underline{H})$$

and equation 2-15 gives

$$\rho_e \underline{E} + \underline{J} \times \underline{B} = \mu\varepsilon \frac{\partial}{\partial t}(\underline{E} \times \underline{H}) + \varepsilon[(\nabla \cdot \underline{E})\underline{E} - \nabla|E|^2/2]$$

$$+ \mu[(\nabla \cdot \underline{H})\underline{H} - \nabla|H|^2/2] \quad (2\text{-}27)$$

where $(\nabla \cdot \underline{E})\,\underline{E}$ and $(\nabla \cdot \underline{H})\,\underline{H}$ denote the divergence of dyads. The first term on the right-hand side of 2-27 is the rate of change of linear momentum per unit volume, while the remaining terms are a statement of the electromagnetic stress tensor and define a system of stresses which can be regarded as being produced by the lines of electric and magnetic force. Following the established procedure for interpreting this tensor[2], it can be concluded that the electric and magnetic lines of force exert longitudinal tensions $\frac{\varepsilon}{2}|E|^2$ and $\frac{\mu}{2}|H|^2$ per unit area and lateral pressures of the same magnitude respectively. Thus, in general, the curvature of the lines of electric and/ or magnetic force is high in regions where the electromagnetic forces on the liquid are large.

On the assumption that electric force effects are negligible, equation 2-27 reduces to

$$\underline{J} \times \underline{B} = \mu[(\nabla \cdot \underline{H})\underline{H} - \nabla|H|^2/2] \quad (2\text{-}28)$$

1. Stratton, Ref. 127, p.98.
2. Ibid, pp. 97-103.

and only tensions and pressures of magnetic origin are
involved. In this case, the rate of increase of magnetic
energy W_M is found using equation 2-21 and integrating over
the entire volume occupied by the field as

$$\frac{dW_M}{dt} = \int \mu \underline{H} \frac{\partial \underline{H}}{\partial t} d\tau = \int \mu [\underline{H} \cdot \nabla \times (\underline{u} \times \underline{H}) + \lambda \underline{H} \cdot \nabla^2 \underline{H}] d\tau \qquad (2\text{-}29)$$

The first term on the right-hand side of 2-29 can be written
as

$$W_{M1} = \int \mu [\nabla \cdot (\underline{u} \times \underline{H}) \times \underline{H} + (\underline{u} \times \underline{H}) \cdot \nabla \times \underline{H}] d\tau$$

by means of the vector relation for $\underline{H} \cdot \nabla \times (\underline{u} \times \underline{H})$.
By Green's theorem for a finite volume, the first integral
vanishes and, with

$$(\underline{u} \times \underline{H}) \cdot (\nabla \times \underline{H}) = - \underline{u} \cdot (\nabla \times \underline{H}) \times \underline{H} \quad \text{and} \quad \nabla \times \underline{H} = \underline{J}$$

W_{M1} becomes

$$W_{M1} = - \int \underline{u} \cdot (\underline{J} \times \underline{B}) d\tau$$

and gives the work done by the moving liquid against the
magnetic force $\underline{J} \times \underline{B}$.

The second term of 2-29 is

$$W_{M2} = \int [\mu \lambda \underline{H} \cdot \nabla^2 \underline{H}] d\tau = \int [\mu \lambda \underline{H} \cdot (\nabla \times \underline{J})] d\tau$$

$$= - \int \mu \lambda [\nabla \cdot (\underline{J} \times \underline{H}) + \nabla \times (\underline{H} \cdot \underline{J})] d\tau$$

Again, the divergence term vanishes on integration leaving

$$W_{M2} = - \int \frac{|\underline{J}|^2}{\sigma} d\tau$$

as the rate of conversion of magnetic energy into Joule heat.

2.6. Force Effects

The electromagnetic body force $\underline{J} \times \underline{B}$ is perpendicular to
the magnetic field and so cannot influence motion along the
lines of magnetic force. Its effect in the transverse
direction depends on whether the lines of force slip freely

through the liquid (the electromagnetic flowmeter case) or are frozen into it (as is supposed in the discussion of astronomical problems).

Considering first the former case in which electrical conductivity can be expected to be of importance, the momentum equation neglecting electric body forces and using 2-22 is

$$\rho \frac{du}{dt} = - \nabla p + \rho \nu \nabla^2 \underline{u} + \sigma(\underline{E} + \underline{u} \times \underline{B}) \times \underline{B}$$

When the only significant body force is $\sigma(\underline{u} \times \underline{B}) \times \underline{B}$, the approximate equation for the transverse velocity u_{tr} is

$$\frac{du_{tr}}{dt} = - \frac{\sigma B^2}{\rho} u_{tr} \qquad (2-30)$$

which indicates a time constant for the decay of motion

$$\tau_u = \rho/\sigma B_o$$

Equation 2-30 reveals the existence of an induction drag which tends to impede motion across the lines of magnetic force and which may be attributed to a magnetic viscosity, the effects of which have been demonstrated by Lehnert (Ref. 38).

By dimensional agrument, the ratio

$$M^2 = \frac{B^2 \sigma}{\rho \nu/L_c^2} = \frac{\text{magnetic viscous force per unit volume}}{\text{ordinary viscous force per unit volume}}$$

where $M = BL_c \sqrt{(\sigma/\rho \nu)}$ is the Hartmann number first obtained by Hartmann in his work on channel flow.

When the lines of force are almost frozen into the fluid, electrical conductivity is unimportant and discussion of the electromagnetic body forces involves only the stress tensor in equation 2-28. The tension on the lines of force suggests an analogy with the behaviour of a stretched string. If a line of force is displaced from equilibrium, a restoring force is set up and tends to produce oscillations about equilibrium. As the force $\underline{J} \times \underline{B}$ is always normal to $\underline{B}$, it gives a measure

of rigidity to the lines of force. The stretched string analogy may be used as a guide in the manipulation of the momentum and magnetic field relations to obtain the wave equation for magnetohydrodynamic waves. Walen (Ref. 28) has shown that the velocity of propagation of these waves in a medium of infinite conductivity and with a uniform exciting magnetic field B_o is

$$U_W = B_o/\sqrt{\mu\rho}$$

In a liquid, hydrostatic pressure can usually be neglected. The ratio of the magnetic tension stresses to the stresses set up by the inertia forces is given by

$$S = \frac{B^2}{\mu\rho u^2} = \frac{\text{magnetic energy per unit volume}}{\text{material kinetic energy per unit volume}} \quad (2\text{-}32)$$

In this case, S is a measure of the importance of the magnetic field relative to the velocity field in determining the nature of the magnetohydrodynamic effects.

It is useful to note from equations 2-24, 2-25, 2-31, and 2-32 that

$$M^2 = SRR_M \quad (2\text{-}33)$$

Chapter 3

MAGNETOHYDRODYNAMIC CHANNEL FLOW

3.1. Formulation of Equations

The description of the electromagnetic flowmeter given in
Chapter 1 indicates that a detailed analysis of it requires the
solution of magnetohydrodynamic channel flow problems involving
both laminar and turbulent flow conditions. While it is to be
expected that laminar flow will prove to be the more tractable
condition, some indication of turbulent behaviour can be
obtained on the assumption that the relations apply to time
means for turbulent flow. The approach adopted here is first
to examine the one-dimensional case in some detail to obtain
the general character of electromagnetic flowmeter channel
flow. This is followed by extensions to those two-dimensional
cases where the nature of the boundary conditions permits of a
solution. As practical flowmeters frequently involve the use
of electrically conducting channels, the effect of wall con-
ductivity is considered throughout the discussions.

The liquid is subject to the usual assumptions of homo-
geneous, isotropic and linear character. The relations
required in the solution of channel flow problems are
collected from Chapter 2 and repeated here for reference. They
are:

Bullard relation, $\dfrac{\partial B}{\partial t} - \nabla \times (\underline{u} \times \underline{B}) = \lambda \nabla^2 \underline{B}$ (3-1)

modified Navier-Stokes equation,

$$\frac{\partial \underline{u}}{\partial t} + (\underline{u} \cdot \nabla)\underline{u} = \frac{1}{\rho}(\underline{J} \times \underline{B}) - \frac{\nabla p}{\rho} + \gamma \nabla^2 \underline{u} \qquad (3\text{-}2)$$

Ohm's law, $\qquad\qquad \underline{J} = \sigma(\underline{E} + \underline{u} \times \underline{B})$ (3-3)

Maxwell's equations, $\nabla \times \underline{H} = \underline{J}$ (3-4), $\nabla \times \underline{E} = -\dfrac{\partial B}{\partial t}$ (3-5)

and $\nabla \cdot \underline{B} = 0$ (3-6), $\nabla \cdot \underline{u} = 0$ (3-7), $\underline{B} = \mu \underline{H}$ (3-8)

In some cases, solution is facilitated by a change of variable and Elsasser (Ref. 35) has given a scheme leading to a symmetrical form of equations 3-1 and 3-2 which has been used in the analytical treatment of magnetohydrodynamics.[1] A modification of the Elsasser procedure to place M in evidence in the basic relations leads to a more convenient form for channel flow problems.

Using 3-4 and the vector relations for $\nabla \times (\underline{u} \times \underline{B})$ and $(\nabla \times \underline{B}) \times \underline{B}$, 3-1 and 3-2 may be rewritten as

$$\lambda \nabla^2 \underline{B} + (\underline{B} \cdot \nabla)\underline{u} = \frac{\partial \underline{B}}{\partial t} + (\underline{u} \cdot \nabla)\underline{B} \qquad (3\text{-}9)$$

and $$\nu \nabla^2 \underline{u} + \frac{1}{\mu \rho}(\underline{B} \cdot \nabla \underline{B}) - \nabla[\frac{p}{\rho} + \frac{\underline{B} \cdot \underline{B}}{2\mu\rho}] = \frac{\partial \underline{u}}{\partial t} + (\underline{u} \cdot \nabla)\underline{u} \qquad (3\text{-}10)$$

Writing $b_e = \frac{\underline{B}}{\mu \sqrt{\nu \rho \gamma}}$ and substituting only in $\nabla^2 \underline{B}$ and $\nabla \underline{B}$ terms on the left-hand side of 3-9 and 3-10 yields

$$\nabla^2 \underline{b}_e + [\frac{M}{L_c} \cdot \nabla]\underline{u} = \sqrt{\frac{\nu}{\rho\gamma}}[\frac{\partial \underline{B}}{\partial t} + (\underline{u} \cdot \nabla)\underline{B}] \qquad (3\text{-}11)$$

$$\nabla^2 \underline{u} + [\frac{M}{L_c} \cdot \nabla]\underline{b}_e - \nabla[\frac{p}{\rho} + \frac{\underline{B} \cdot \underline{B}}{2\mu\rho}] = \frac{1}{\gamma}[\frac{\partial \underline{u}}{\partial t} + (\underline{u} \cdot \nabla)\underline{u}] \qquad (3\text{-}12)$$

where $\underline{M} = \underline{B}L_c\sqrt{\frac{\nu}{\rho\gamma}}$ is, in general, a function of $\underline{B}$ and $\underline{b}_e$.

The substitutions

$$\underline{u}_v = \underline{u} + \underline{b}_e, \quad \underline{u}_w = \underline{u} - \underline{b}_e, \quad \text{and } \nabla P = \nabla[\frac{p}{\rho} + \frac{\underline{B} \cdot \underline{B}}{2\mu\rho}]$$

can be made to the right-hand sides of 3-11 and 3-12. Then, adding 3-11 to 3-12 gives

$$\nabla^2 \underline{u}_v + [\frac{M}{L_c} \cdot \nabla]\underline{u}_v - \nabla P = \frac{1}{\gamma}[\frac{\partial \underline{u}}{\partial t} + (\underline{u} \cdot \nabla)\underline{u}] - \sqrt{\frac{\nu}{\rho\gamma}}[\frac{\partial \underline{B}}{\partial t} + (\underline{u} \cdot \nabla)\underline{B}]$$
$$(3\text{-}13)$$

and subtracting 3-11 from 3-12 yields

$$\nabla^2 \underline{u}_w + [\frac{M}{L_c} \cdot \nabla]\underline{u}_w - \nabla P = \frac{1}{\gamma}[\frac{\partial \underline{u}}{\partial t} + (\underline{u} \cdot \nabla)\underline{u}] - \sqrt{\frac{\nu}{\rho\gamma}}[\frac{\partial \underline{B}}{\partial t} + (\underline{u} \cdot \nabla)\underline{B}]$$
$$(3\text{-}14)$$

---

1. By Lundquist, Ref. 46.

The retention of both $\underline{B}$ and $\underline{b}_e$ in these equations will be justified in subsequent analytical work where they will be associated with the applied and induced fields, respectively.

3.2. One-dimensional Case - Extended Hartmann Theory

The choice of coordinate system for this case is shown in Fig. 3.1 where liquid flow is entirely in the positive z direction but a function only of x; the exciting magnetic field is uniform, of infinite axial extent and directed along the positive x axis, and the guiding surfaces are electrically conducting flat plates[1] of infinite area parallel to each other and to the yoz plane and distance 2b apart. The one-dimensional situation is a reasonable approximation to the important practical case of a high aspect ratio rectangular channel. Consideration is limited at this stage to time-invariant conditions.

The problem specification is that:

$$\frac{\partial \underline{B}}{\partial t} = 0, \quad \frac{\partial \underline{u}}{\partial t} = 0, \quad \underline{u} = \underline{i}_3 u_z(x), \quad \underline{B} = \underline{i}_1 B_0 + \underline{i}_3 b_z, \quad \underline{J} = \underline{i}_z J_y.$$

Thus $(\underline{u} \cdot \nabla)\underline{u} = (u_x \frac{\partial}{\partial x} + u_y \frac{\partial}{\partial y} + u_z \frac{\partial}{\partial z})\underline{u} = 0,$ $(\underline{u} \cdot \nabla)\underline{B} = 0,$ and

$$\frac{\nabla \underline{B} \cdot \underline{B}}{2\mu\rho} = \frac{\nabla}{2\mu\rho}(\underline{i}_1 B_0 + \underline{i}_3 b_z)^2 = \frac{\underline{i}_1}{2\mu\rho} \frac{\partial (b_z)^2}{\partial x}.$$

where $\underline{i}_1$, $\underline{i}_2$ and $\underline{i}_3$ are unit vectors. The result for $\nabla(\underline{B} \cdot \underline{B})$ shows that a transverse pressure gradient is set up.

The component equations for b_z and u_z are now obtained from 3-9 and 3-10 as

$$\frac{\partial^2 b_z}{\partial x^2} + \frac{B_0}{\lambda} \frac{\partial u_z}{\partial x} = 0 \tag{3-15}$$

$$\frac{\partial^2 u_z}{\partial x^2} + \frac{B_0}{\mu\rho\nu} \frac{\partial b_z}{\partial x} = \frac{1}{\nu\rho} \frac{\partial p}{\partial z} \tag{3-16}$$

The solution of these must meet the requirement that there

---

1. Hartmann dealt only with non-conducting plates.

is no net current flow in the y direction and the velocity boundary condition that $u_z(x) = 0$ at $x = \pm b$.

From 3-15, $\dfrac{\partial b_z}{\partial x} = - \dfrac{B_o}{\lambda} u_z + \dfrac{\partial b_z}{\partial x}\bigg|_{x=\pm b}$

which, on substitution in 3-16, yields the equation for u_z as

$$\frac{\partial^2 u_z}{\partial x^2} - [\frac{\sigma B_o^2}{\rho \nu}] u_z = \frac{1}{\nu \rho}\frac{\partial p}{\partial z} - \frac{B_o}{\mu \rho \nu}\frac{\partial b_z}{\partial x}\bigg|_{x=\pm b}$$

Using the definition of $M = B_o b\sqrt{\dfrac{\sigma}{\rho \nu}}$ and noting that differentiation with respect to z gives

$$\frac{\partial^2 p}{\partial z^2} = 0 \quad \text{or} \quad \frac{\partial p}{\partial z} = - p_o, \quad \text{a constant,}$$

this equation over a length L in the z-direction is

$$\frac{\partial^2 u_z}{\partial x^2} - [\frac{M}{b}]^2 u_z = - \frac{p_o}{\nu \rho L} - \frac{B_o}{\mu \rho \nu}\cdot\frac{\partial b_z}{\partial x}\bigg|_{x=\pm b}$$

The total current per unit width in the y-direction is obtained by integrating Ohm's Law as $2b\sigma(B_o u_o + E_y)$ and this, when equated to the total wall current $-2w\sigma_w E_y$ yields

$$E_y = - \frac{u_o B_o}{1 + w\sigma_w/b\sigma} = \frac{1}{\mu \sigma}\frac{\partial b_z}{\partial x}\bigg|_{x=\pm b}$$

where w and σ_w are respectively the wall thickness and wall conductivity.

A general solution for $u_z(x)$ is

$$u_z(x) = C_1 e^{Mx/b} + C_2 e^{-Mx/b} + [\frac{b}{M}]^2 [\frac{p_o}{\nu \rho L} + \frac{M^2 u_o}{b^2(1 + k_w)}]$$

where $k_w = w\sigma_w/b\sigma$ is the wall conductivity factor and C_1 and C_2 are integration constants to be determined using the boundary condition. Straightforward manipulation leads to

$$u_z(x) = u_o \left[\frac{\cosh M - \cosh (Mx/b)}{\cosh M - (\sinh M)/M}\right] \qquad (3\text{-}17)$$
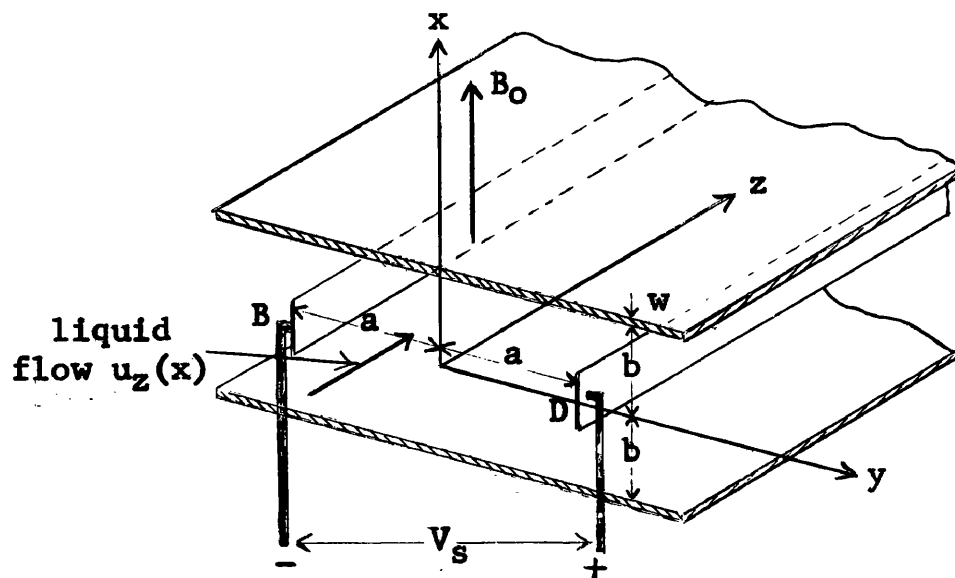
Fig. 3.1.   Coordinate System for One-Dimensional Channel Flow Analysis
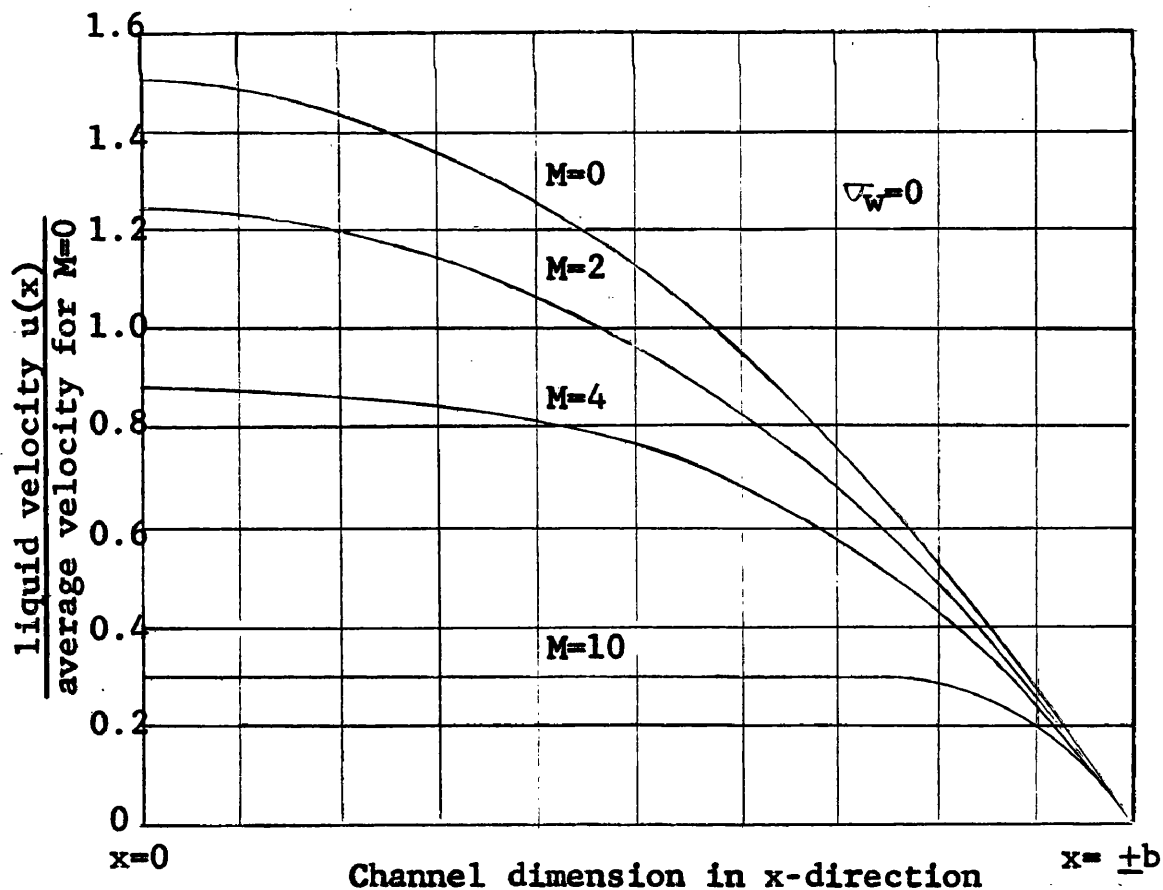
Fig. 3.2.   Hartmann Velocity Profiles for One-Dimensional Flow

where
$$u_o = \frac{P_o b^2}{\nu \rho L M^2}\left[\frac{1 - (\tanh M)/M}{k_w/(1 + k_w) + (\tanh M)/M}\right] \qquad (3\text{-}18)$$

Equations 3-17 and 3-18 reduce to the results obtained by Hartmann when $k_w = 0$ to give

$$u_z(x)\Big|_{\sigma_w=0} = \frac{P_o M}{\sigma B_o^2 L}\left[\frac{\cosh M - \cosh (Mx)/b}{\sinh M}\right] \qquad (3\text{-}19)$$

$$u_o\Big|_{\sigma_w=0} = \frac{P_o b^2}{\rho L}\frac{1}{\nu M^2}\left[\frac{1 - (\tanh M)/M}{(\tanh M)/M}\right] \qquad (3\text{-}20)$$

Equations 3-17 to 3-20 give the effect of the applied magnetic field on the laminar flow pattern as a flattening of the velocity profile and a reduction in the average velocity (for a fixed pressure gradient) to an extent depending on the value of M as shown in Fig. 3.2. Putting $M = 0$ in 3-20 gives the field-free average velocity as

$$u_o\Big|_{\substack{\sigma_w=0\\B_o=0}} = \frac{P_o b^2}{\rho L}\frac{1}{3\nu}$$

and the additional losses produced by the application of a magnetic field can, by comparison with 3-20, be ascribed to an apparent viscosity ν' where

$$\nu' = \frac{M^2}{3}\left[\frac{(\tanh M)/M}{1 - (\tanh M)/M}\right] \qquad (3\text{-}21)$$

Examination of equation 3-21 shows that, at low M values $(M < 5)$, ν' varies parabolically while for high M the relation is linear.

The current density $J_y(x)$ is given by Ohm's Law as

$$J_y(x) = \sigma(- \partial V/\partial y + u_z B_o)$$

and substitution for $\partial V/\partial y$ and u_z yields

$$J_y(x) = -\frac{\sigma u_o B_o}{1 + k_w} + \sigma u_o\left[\frac{\cosh M - \cosh (Mx/b)}{\cosh M - (\sinh M)/M}\right] \qquad (3\text{-}22)$$

The induced current profiles, particularly for the case $\sigma_w = 0$, are evidently characterised by high densities in the

boundary layer near the wall where the viscous and electro-magnetic forces predominate, while over most of the cross-section the velocity and current are nearly uniform, indicating equilibrium between the pressure and electromagnetic forces. Some discussion and analysis of the boundary layer have been given by Lernhert (Ref. 38), Murgatroyd (Ref. 40) and Shercliff (Ref. 110).

3.3. One-dimensional Case - Flow Signal

The results of the preceding Section apply only to laminar flow conditions but the flow-induced potential difference V can be obtained from 3-3 by integrating with respect to y and without using 3-2.

Referring to Fig. 3.1, if electrodes are inserted into the channel at B and D, distance 2a apart, the flow signal V_s is

$$V_s = \int_B^D -E_y \, dy = \frac{2au_oB_o}{1 + w\sigma_w/b\sigma} = 2au_oB_oK_1 \qquad (3-23)$$

where $K_1 = 1/(1 + w\sigma_w/b\sigma)$ is the wall correction factor which expresses the departure of V_s from the value $2au_oB_o$ due to finite wall conductivity. This result is independent of the velocity profile, flow conditions and M (for laminar flow) and shows that the flow signal can be considered to be generated by a source of internal resistance and terminal shunt resistance proportional to $1/\sigma b$ and $1/w\sigma_w$ respectively and internal e.m.f. $2au_oB_o$. The internal resistance and wall resistance are respectively $R_i = a/\sigma b$ and $R_w = a/w\sigma_w$ per unit length in the z-direction.

The motionally induced e.m.f. is obtained from the integration of $\underline{u} \times \underline{B}$ between B and D as

$$V_m = B_o \int_B^D u_z(x) \, dy = 2aB_ou_z(x) = 2au_oB_oK_2 \qquad (3-24)$$

where K_2 in this case is an x-dependent quantity and in general gives the ratio $V_m/2au_oB_o$. It shows that, unlike the integral of $\partial V/\partial y$, V_m is not constant over the cross-section.

Analysis of the one-dimensional case shows that magneto-hydrodynamic channel flow considerations are not required in the determination of the flow signal but are necessary to a proper discussion of the velocity distribution, pressure drop and induced current and field distributions. Failure to appreciate this[1] leads to results which apply only to M values sufficiently low for electromagnetic viscosity effects to be negligible relative to the normal viscous forces.

3.4. Two-dimensional Case - Formulation of Equations

Using the rectangular coordinate system of Fig. 3.1 and again considering time-invariant conditions, the problem is specified in the following statements.

$$\frac{\partial \underline{B}}{\partial t} = 0, \quad \frac{\partial \underline{u}}{\partial t} = 0, \quad \underline{u} = \underline{i}_3 u_z(x,y), \quad \underline{J} = \underline{i}_1 J_x + \underline{i}_2 J_y,$$

$$\underline{B} = \underline{i}_1 B_o + \underline{i}_3 b_z(x,y).$$

These lead to $\quad (\underline{u}\cdot\nabla)\underline{u} = 0, \qquad (\underline{u}\cdot\nabla)\underline{B} = 0$

$$(\underline{B}\cdot\nabla)\underline{u} = (B_o\frac{\partial}{\partial x} + b_z\frac{\partial}{\partial z})\underline{i}_3 u_z = \underline{i}_3 B_o \frac{\partial u_z}{\partial x}$$

$$(\underline{B}\cdot\nabla)\underline{B} = (B_o\frac{\partial}{\partial x} + b_z\frac{\partial}{\partial z})[\underline{i}_1 B_o + \underline{i}_3 b_z] = \underline{i}_3 B_o \frac{\partial b_z}{\partial x}$$

$$\nabla \frac{\underline{B}\cdot\underline{B}}{2\mu\rho} = \frac{(\underline{i}_1 B_o + \underline{i}_3 b_z)^2}{2\mu\rho} = \frac{\underline{i}_1(\partial/\partial x)b_z^2 + \underline{i}_2(\partial/\partial y)b_z^2}{2\mu\rho}$$

The component equations obtained for 3-9 and 3-10 in this case are

$$\nabla^2 b_z + \frac{B_o}{\lambda}\frac{\partial u_z}{\partial x} = 0 \tag{3-25}$$

$$\nabla^2 u_z + \frac{1}{\mu\rho\nu}\frac{\partial b_z}{\partial x} = \frac{\nabla p}{\rho} = -\frac{p_o}{\rho\nu L} \tag{3-26}$$

There are small transverse pressure gradients in both x and y directions and, by the same reasoning as in the one-dimensional case, the longitudinal pressure gradient can be written as $-\nabla p = p_o/L$.

---

1. As in Refs 67, 83, 86, 97, 101 and 102.

The component form of 3-3, using 3-4 is

$$J_x = -\sigma \frac{\partial V}{\partial x} = \frac{1}{\mu} \frac{\partial b_z}{\partial y} \tag{3-27}$$

$$J_y = \sigma(B_o u_z - \frac{\partial V}{\partial y}) = -\frac{1}{\mu} \frac{\partial b_z}{\partial x} \tag{3-28}$$

and it is useful to note from these equations that the current flow lines in the xoy plane give, the contours of b_z and that b_z and V are orthogonal only if $u_z = 0$.

By eliminating b_z between 3-27 and 3-28, a relation connecting V and u_z is obtained as

$$\nabla^2 V - B_o \frac{\partial u_z}{\partial y} = 0 \tag{3-29}$$

which has the same form as 3-25 (except for a minus sign) and enables V to be found directly when the velocity profile is known. Comparing 3-25 and 3-29, it is important to note that a solution for b_z with a known velocity profile will contain dependence on the liquid conductivity while it is possible for V to be independent of this quantity.

Writing $P_o = -\nabla P$ gives the component form of 3-13 and 3-14 as

$$\nabla^2 u_v + \frac{M}{b} \frac{\partial u_v}{\partial x} + P_o = 0 \tag{3-30}$$

$$\nabla^2 u_w - \frac{M}{b} \frac{\partial u_w}{\partial x} - P_o = 0 \tag{3-31}$$

3.5. Two-dimensional Case - Boundary Conditions

The boundary conditions at the wall surfaces are obtained from the requirements that the normal component of current and the tangential component of magnetic field intensity must be continuous across the liquid-wall boundary and vanish at the outer wall boundary, and that the tangential component of the liquid velocity must be zero at the liquid-wall boundary.

Using the subscripts n and s to denote normal and tan-

gential directions respectively and the subscript w to refer
to the wall, the boundary conditions can be stated as follows:

At the liquid-wall boundary assuming ideal contact,

$$V = V_w, \quad J_n = J_{wn}, \quad \text{or} \quad \frac{\partial V}{\partial n} = \frac{\sigma_w}{\sigma} \frac{\partial V_w}{\partial n}$$

$$u_s = 0, \quad \text{and} \quad b_t = b_{ws} \quad \text{provided} \quad \mu = \mu_w.$$

At the outer wall boundary,

$$J_{wn} = 0, \quad \text{or} \quad \frac{\partial V}{\partial n} = 0 \quad \text{and} \quad b_{ws} = 0.$$

3.6. Two-dimensional Case - Note on Solutions

A general laminar flow solution for the velocity, poten-
tial and current distributions in a channel of either rectan-
gular or circular cross-section has not so far been obtained
due to the difficulties encountered in attempting to solve
the equations of Section 3.4 with the boundary conditions of
Section 3.5. It is usually necessary to infer the behaviour
in these cases from the extended Hartmann theory of Section
3.2, although an exact solution has been obtained for a non-
conducting, rectangular section channel and is given in
Section 3.9. When the velocity profile is known or may be
assumed, 3-29 can be solved for V in the cases of a circular
channel and of a rectangular channel with highly conducting
ends. The circular section channel with a radially symmetric
profile has received considerable attention and it should be
noted that treatment given in the next section combines, ex-
tends (and corrects) the work of Williams (Ref. 67),
Thurlmann (Ref. 83), Kolin (Ref. 86), Elrod and Fouse (Refs
97 and 102) and Astley (Ref. 101). It will be demonstrated
in later chapters that the use of a rectangular section
channel offers several advantages over the circular section
which has hitherto been employed. This type of channel is
considered in Sections 3.8 and 3.9 where the results
obtained are readily shown to agree with those given with

only brief derivation by Shercliff (Refs 41 and 110).

3.7. Circular Channel Section - Symmetrical Velocity Profile

(a) Solution of Equations

It is convenient to use the cylindrical polar coordinates of Fig. 3.3 for this solution. The velocity is then a function of r only and can be written as $u_2 = u_2(r)$. If r_i and r_2 are the inner and outer radii of the channel, respectively, the equations to be solved are obtained by putting $\partial/\partial y = (\partial/\partial r)\sin\theta$ and $\partial/\partial x = (\partial/\partial r)\cos\theta$ in 3-25 and 3-29 as

$$\left. \begin{array}{l} \nabla^2 V - B_o \sin\theta \dfrac{\partial u_z}{\partial r} = 0 \\[2mm] \nabla^2 b_z + \dfrac{B_o}{\lambda}\cos\theta \dfrac{\partial u_z}{\partial r} = 0 \end{array} \right] \qquad r < r_i$$

and $\nabla^2 V_w = 0$ or $\nabla^2 b_z = 0$, $\qquad r_i < r < r_o$

For two-dimensional conditions, $(\partial^2 V/\partial z^2) = 0$ and $(\partial^2 b_z/\partial z^2) = 0$ and the equations for the liquid region are

$$\frac{1}{r^2}\frac{\partial^2 V}{\partial\theta^2} + \frac{1}{r}\frac{\partial}{\partial r}[r\frac{\partial V}{\partial r}] - B_o\frac{\partial u_z}{\partial r}\sin\theta = 0 \qquad (3\text{-}32)$$

$$\frac{1}{r^2}\frac{\partial^2 b_z}{\partial\theta^2} + \frac{1}{r}\frac{\partial}{\partial r}[r\frac{\partial b_z}{\partial r}] + \frac{B_o}{\lambda}\frac{\partial u_z}{\partial r}\cos\theta = 0 \qquad (3\text{-}33)$$

Assuming solutions of the form $V = V(r)\sin\theta$, $b_z = b_z(r)\cos\theta$ and considering first equation 3-32, substitution of the assumed solution yields, on division by $\sin\theta$

$$-\frac{V(r)}{r^2} + \frac{1}{r}\frac{\partial}{\partial r}[V(r)] + \frac{\partial^2}{\partial r^2}[V(r)] - B_o\frac{\partial u_z}{\partial r} = 0 \qquad (3\text{-}34)$$

Now, $\qquad \dfrac{\partial}{\partial r}[V(r)/r] = \dfrac{1}{r}\dfrac{\partial}{\partial r}[V(r)] - \dfrac{V(r)}{r^2}$

so that 3-34 may be integrated without resort to Green's function solution methods.[1] This substitution yields on integration and use of $u_z = 0$ for $r = r_i$

---

1. As are employed in Ref. 83. The direct integration scheme was suggested by H.W. Lamb and first used by Kolin (Ref. 86).

$$\frac{\partial}{\partial r} V(r) + \frac{V(r)}{r} = B_o u_z + \frac{\partial}{\partial r} V(r)\Big|_{r=r_i} + \frac{V(r_i)}{r_i}$$

Multiplication by r, followed by integration using the derivative of rV(r) with respect to r, gives

$$rV(r) = B_o \int u_z r \, dr + [\frac{\partial}{\partial r} V(r)\Big|_{r=r_i} + \frac{V(r_i)}{r_i}]\frac{r^2}{2} + C_3$$

Now $C_3 = 0$ since $V(r) = 0$ for $r = 0$ and the final result is

$$V(r) = \frac{B_o}{r}\int u_z r \, dr + [\frac{\partial}{\partial r} V(r)\Big|_{r=r_i} + \frac{V(r_i)}{r_i}]\frac{r}{2} \qquad (3\text{-}35)$$

By entirely similar reasoning,

$$b_z(r) = -\frac{B_o}{\lambda r}\int u_z r \, dr + [\frac{\partial}{\partial r} b_z(r)\Big|_{r=r_i} + \frac{b_z(r_i)}{r_i}]\frac{r}{2} \qquad (3\text{-}36)$$

In the channel wall, the Laplace equation to be solved for V_w is

$$\frac{1}{r^2}\frac{\partial^2 V_w}{\partial \theta^2} + \frac{1}{r}\frac{\partial}{\partial r}[r \frac{\partial V_w}{\partial r}] = 0$$

Assuming again a solution of the form $V_w = V_w(r)\sin \theta$, a similar procedure leads to

$$V_w(r) = [\frac{\partial}{\partial r} V_w(r)\Big|_{r=r_i} + \frac{V_w(r_i)}{r_i}]\frac{r}{2} + \frac{C_4}{r}$$

where C_4 is an integration constant to be determined using the boundary condition $\frac{\partial}{\partial r}[V_w(r_2)] = 0$.

Thus $V_w(r) = \frac{1}{2} V_w(r_i)[\frac{r}{r_i} + \frac{r_2^2}{rr_i}] + \frac{r}{2}[1 + \frac{r_2^2}{r^2}]\frac{\partial}{\partial r} V_w(r)\Big|_{r=r_i}]$

$$(3\text{-}37)$$

At the liquid-wall boundary, $V_w(r_i) = V(r_i)$ and $\sigma_w\frac{\partial}{\partial r}V_w(r_i) = \sigma\frac{\partial}{\partial r} V(r_i)$. Thus

$$[1 + \frac{r_2^2}{r_i^2}] r_i \frac{\sigma}{\sigma_w}\frac{\partial}{\partial r}[V(r)\Big|_{r=r_i}] = V(r_i)[1 + \frac{r_2^2}{r_i^2}]$$

or $\qquad \frac{\partial}{\partial r} V(r)\Big|_{r=r_i} = \frac{V(r_i)[1 - r_2^2/r_i^2]\sigma_w}{r_i[1 + r_2^2/r_i^2]\sigma} \qquad (3\text{-}38)$

(b) Flow Signal - Electrodes Mounted in Channel Wall

Integration of 3-35 gives the flow signal appearing between electrodes B and D in Fig. 3.3 as

$$V_s = 2V(r_i) = \frac{2B_0}{r_i}\int_0^{r_i} u_z r \, dr + r_i \frac{\partial}{\partial r} V(r)\Big|_{r=r_i} + V(r_i).$$

Now $\frac{2B_0}{r_i}\int_0^{r_i} u_z r \, dr = u_o r_i$ since $u_o = \frac{1}{\pi r_i^2}\int_0^{r_i} 2\pi r u_z(r) \, dr$

Substitution of this result and the expression for $\frac{\partial}{\partial r} V(r)\Big|_{r=r_i}$ obtained from 3-38 yields

$$V_s = \frac{2B_0 u_o r_i}{1 + \frac{\sigma_w}{\sigma}[\frac{r_2^2 - r_i^2}{r_2^2 + r_i^2}]} = 2B_0 u_o r_i K_1 \qquad (3\text{-}39)$$

where K_1 again denotes the wall conductivity factor.

This important result shows the flow signal to be independent of the velocity profile (and hence flow conditions) provided this depends only on r. Further, when the channel is made from insulating material, V_s has the same value as given by the simple theory leading to equation 1-2. The form of 3-39 can again be recognised as giving the terminal voltage of a generator of internal e.m.f. $2B_0 u_o r_i$ and with $k_w = R_i/R_w$.

Rewriting 3-39 leads directly to

$$V_s = 2B_0 u_o r_i \frac{[1 + (r_i/r_2)^2]}{1 + (r_i/r_2)^2 + (\sigma_w/\sigma)[1 - (r_i/r_2)^2]}$$

which differs from the Elrod and Fouse formula in that they give the numerator term as $2r_i/r_2$. This leads to the conclusion that V_s depends on the ratio r_i/r_2 when the walls are non-conducting, a result which is not in accord with physical reasoning applied to a practical flowmeter. The solution of Laplace's equation for the channel walls applies to both conducting and non-conducting conditions but, in the latter case, gives the electrostatic field. Derivation of the Elrod and Fouse formula involves integration from B' to D'

in Fig. 3.3 and so includes the electrostatic potential difference from B' to B and D to D' in the non-conducting case. The procedure followed here to obtain 3-39 is evidently appropriate in relation to the practical electrode arrangement used in circular channel flowmeters.

For a thin channel wall, 3-39 reduces to

$$V_s = \frac{2B_0 u_0 r_i}{1 + \overline{\nabla_w} w / \overline{\nabla} r_i} \tag{3-40}$$

which is identical in form to equation 3-24 and is the result obtained by Thurlmann.

An estimate of the effect of 'contact resistance' may be made by assuming that the contact voltage drop is linearly related to the radial current density.[1] Matching solutions at the liquid-wall boundary then requires that

$$V(r_i) + k_c \frac{\partial V(r)}{\partial r}\bigg|_{r=r_i} = V_w(r_i)$$

where k_c is a conductance factor for the thin contact region. This modifies 3-38 and leads to

$$V_s = \frac{2B_0 u_0 r_i}{1 + (1 + k_c)[\overline{\nabla_w}(r_2^2 - r_i^2)] / [\overline{\nabla}(r_2^2 + r_i^2)]} \tag{3-41}$$

(c) <u>Potential, Current and Magnetic Field Distribution</u>

The distribution of potential, induced magnetic field and induced current density over the entire channel cross-section can be obtained in any particular case using equations 3-35 and 3-37 together with 3-27 and 3-28 in cylindrical polar form. Complete solutions for the Poiseuille distribution laminar flow case with a non-conducting channel were first obtained by Williams and have been repeated in greater detail by Thurlmann whose distribution diagram is reproduced in

---

1. The contact resistance may be non-linear and a function of time as discussed in Section 4.3.
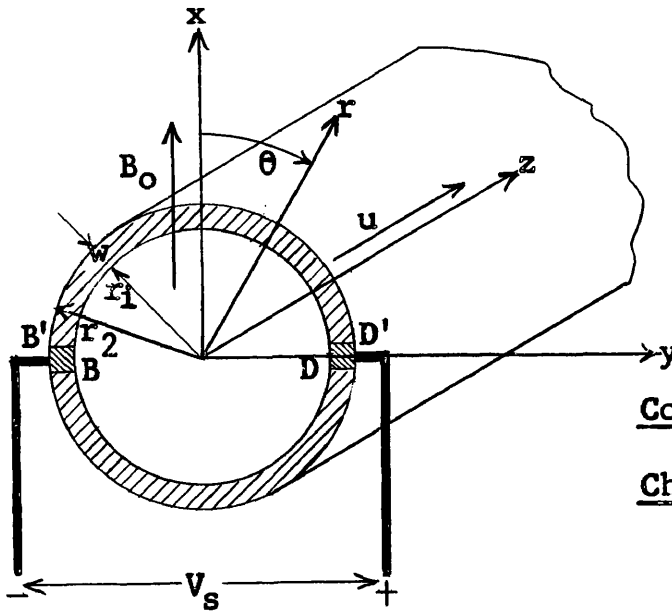
Fig. 3.3.
Coordinate System
for Circular
Channel Analysis

Drawn for:

B_O = 0.6Wb/m^2
r_i = 0.5cm
u_O = 10cm/sec
$R \approx 500$
σ = 10 $\mho$/m (8% NaCl soln)

solid lines:
    current flow
dashed lines:
    equipotentials
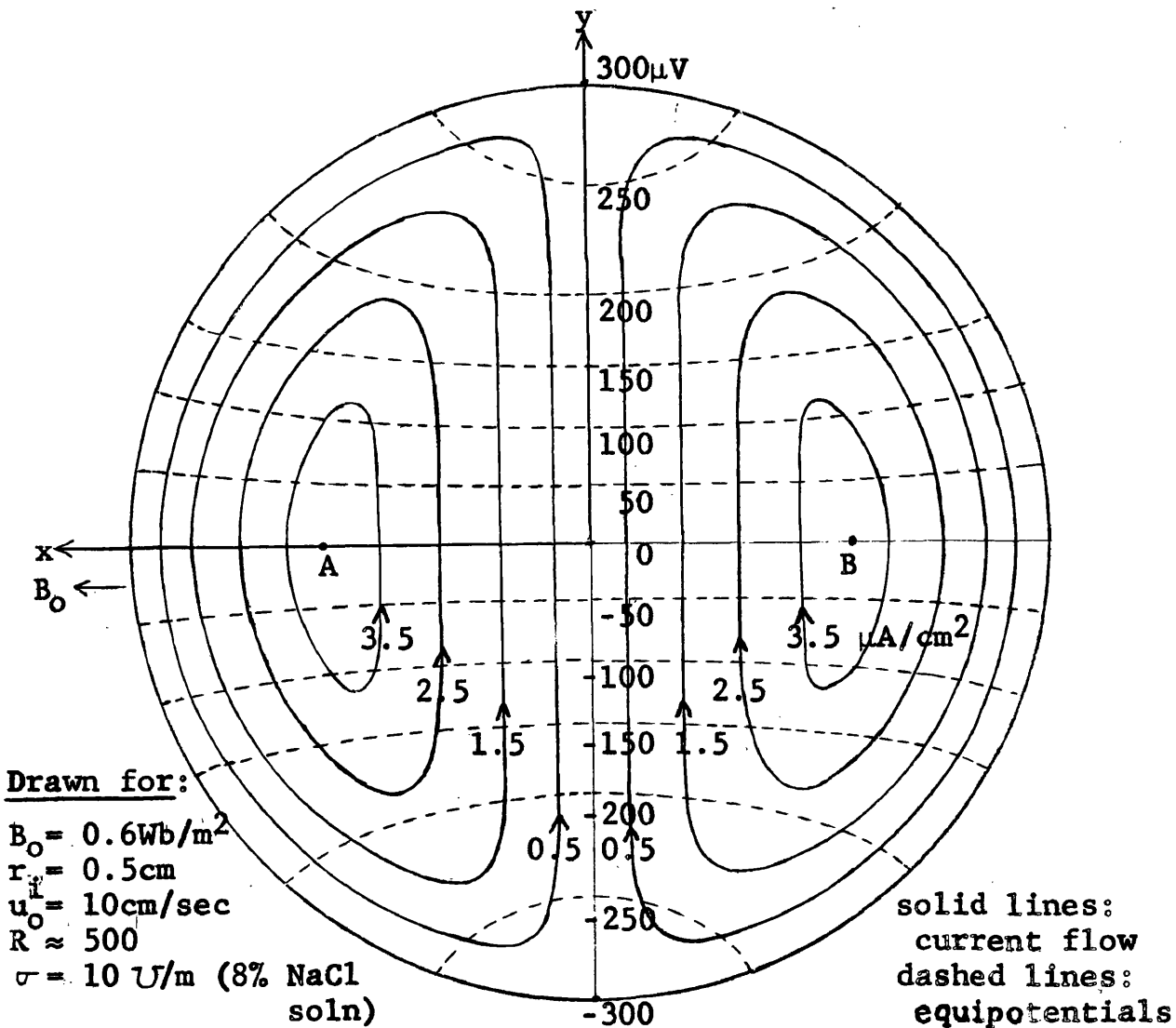
Fig. 3.4. Potential and Current Distributions for low-M
Laminar Flow in a Circular Channel

Fig. 3.4.

It is readily possible to envisage electromagnetic flow-meter applications in which low-conductivity liquids flow in highly conducting channels. While equation 3-39 indicates that V_s tends to zero when $\sigma_w \gg \sigma$, it is useful to investigate alternative electrode arrangements by which a flow signal may still be obtained. A reasonable approximation for this case is to regard the channel wall as forming a perfectly conducting, zero potential boundary at which the boundary condition is that of zero tangential current density. As the boundary condition is stated in terms of b_z, it is appropriate to consider equation 3-33 and its solution 3-36 rather than 3-32. Now the boundary condition applicable to 3-32 for an insulated wall is that

$$\left. \frac{\partial V(r)}{\partial r} \right|_{r=r_i} = 0, \quad \text{compared with} \quad \left. \frac{\partial b_z(r)}{\partial r} \right|_{r=r_i} = 0$$

for 3-33. This comparison, together with the form of 3-32 and 3-33, allows the perfectly conducting and insulated wall cases to be regarded as dual problems provided the dual relationships

$$V(r) \text{ to } b_z(r); \text{ and } B_0 \sin \theta \text{ to } - \frac{B_0}{\lambda} \cos \theta$$

are recognised.

Application of these to Fig. 3.4 shows that a flow-dependent potential difference exists within the liquid and that a flow signal may be obtained from electrodes mounted at the points A and B in Fig. 3.4. To avoid modification of the distribution patterns, it is necessary that the electrodes and their circuit connections produce negligible disturbance of the liquid flow and that the connections be electrically insulated.

(d) Flow Signal - Highly Conducting Channel

On the assumption of infinite wall conductivity, a solutions of Laplace's equation is not required in the wall region and V_s can be obtained directly from 3-35.

For $r = r_i$, $V(r) = 0$, giving

$$\frac{\partial}{\partial r} V(r) \bigg|_{r=r_i} = - B_0 u_0$$

from which

$$V(r) = \frac{B_0}{r} \int u_z r \, dr - B_0 u_0 r/2$$

and

$$V_s = 2V(r) = \frac{2B_0}{r} \int_0^r u_z r \, dr - B_0 u_0 r \qquad (3\text{-}42)$$

If u_{or} denotes the average velocity over a cross-section of radius r,

$$V_s = B_0 r (u_{or} - u_0) \qquad (3\text{-}43)$$

In this case, the flow signal depends on the velocity profile and would be zero if the velocity reaches a constant value over the entire cross-section due, say, to high-M conditions.

For low-conductivity liquids where normal viscous forces predominate, the velocity distribution has the Poiseuille form

$$u_z(r) = 2u_0(1 - r^2/r_i^2)$$

Substitution of this in 3-42 gives

$$V_s = B_0 u_0 (r - \frac{r^3}{r_i^2})$$

which has a maximum value of $\quad 2B_0 u_0 r_i/3\sqrt{3} \qquad (3\text{-}44)$

when

$$r = r_i/\sqrt{3} \qquad (3\text{-}45)$$

Equations 3-44 and 3-45 indicate that the electrodes must be inserted a distance $r_i(1 - 1/\sqrt{3})$ to obtain the maximum flow signal which is about 19% of the corresponding insulated wall value and is linearly related to the average velocity. It is to be expected that this arrangement will continue to provide an increasing signal with turbulent flow conditions but that the linear relation will no longer be obtained.

3.8. Rectangular Channel Section - High-Conductivity End Walls

For the rectangular channel section of Fig. 3.5, the end walls (parallel to the exciting magnetic field) are of sufficiently high conductivity to be regarded as perfect conductors forming regions of constant potential at the surface of which

$$J_x \bigg|_{y \,=\, b} = \frac{\partial b_z}{\partial y} \bigg|_{y \,=\, b} = 0$$

The flow signal in this case is developed between the high-conductivity end walls and is given from 3-28 as

$$V_s = \int_{-a}^{a} (B_o u_z - \frac{J_y}{\sigma}) dy$$

and is a constant for any path.

Integration over the entire cross-sectional area yields

$$\int_{-b}^{b} V_s dx = \int_{-b}^{b}\int_{-a}^{a} B_o u_z \, dy dx - \int_{-b}^{b}\int_{-a}^{a} \frac{J_y}{\sigma} \, dy dx$$

or

$$V_s = 2au_o B_o - \frac{1}{2b} \int_{-b}^{b}\int_{-a}^{a} \frac{J_y}{\sigma} \, dy dx \qquad (3\text{-}46)$$

since

$$4abu_o = \int_{-b}^{b}\int_{-a}^{a} u_z \, dy dx$$

Now, the net current flow in the y direction must be zero so that for any value of y,

$$\int_{-b}^{b} J_y dx = - \int_{-(w+b)}^{-b} J_{yw1} dx - \int_{b}^{w+b} J_{yw2} dx$$

Also, in the side walls,

$$\frac{1}{\sigma_w}\int_{-a}^{a} J_{yw1} dy = -V_s = \frac{1}{\sigma_w}\int_{-a}^{a} J_{yw2} dy$$

Combining these results leads directly to

$$- \frac{1}{\sigma_w}\int_{-(w+b)}^{-b}\int_{-a}^{a} J_{yw1} \, dy dx - \frac{1}{\sigma_w}\int_{b}^{w+b}\int_{-a}^{a} J_{yw2} \, dy dx$$

$$= \int_{-(w+b)}^{-b} V_s dx + \int_{b}^{w+b} V_s dx = \frac{1}{\sigma_w}\int_{-a}^{a}\int_{-b}^{b} J_y \, dx dy$$

giving that

$$2V_s w = \frac{\sigma}{\sigma_w} \int_{-b}^{b} \int_{-a}^{a} \frac{J_y}{\sigma} \, dx \, dy \quad \text{or} \quad \frac{1}{2b} \int_{-b}^{b} \int_{-a}^{a} \frac{J_y}{\sigma} \, dx \, dy = V_s \frac{w\sigma_w}{b\sigma}$$

where J_{yw1} and J_{yw2} are the current densities in the side walls at $x = -b$ and $x = +b$, respectively. Substitution of this result in 3-46 yields

$$V_s = \frac{2au_oB_o}{1 + w\sigma_w/b\sigma} = 2au_oB_oK_1 \qquad (3-47)$$

This is the same expression as was obtained in the one-dimensional analysis given earlier. It shows that V_s is independent of the velocity distribution for this rectangular arrangement and is given by the simple formula 1-5 where the side walls are non-conducting. The derivation given here is a rigorous treatment of the effect of side wall conductivity and extends Holdaway's result (Ref. 123) which deals with non-conducting side walls.

3.9. Rectangular Channel Section - Laminar Flow Solution for Non-conducting Walls

An alternative to the electrode configuration just considered is the placing of small electrodes at the mid-point of the end walls as shown in Fig. 3.6. For the particular case of non-conducting walls both the induced magnetic field and the liquid velocity are zero at the inner wall surface and the substitutions used in equations 3-13 and 3-14 lead to the simple boundary conditions in 3-30 and 3-31 that $u_v = u_w = 0$ at the channel walls.

Inspection of 3-30 and 3-31 shows that, for the coordinate system of Fig. 3.6, $u_v(x,y) = u_w(-x,y)$ so that it is sufficient to solve for (say) u_v. The equation to be solved is 3-30 which has the component form

$$\frac{\partial^2 u_v}{\partial x^2} + \frac{\partial^2 u_v}{\partial y^2} + [\frac{M}{b}] \frac{\partial u_v}{\partial x} + P = 0 \qquad (3-48)$$
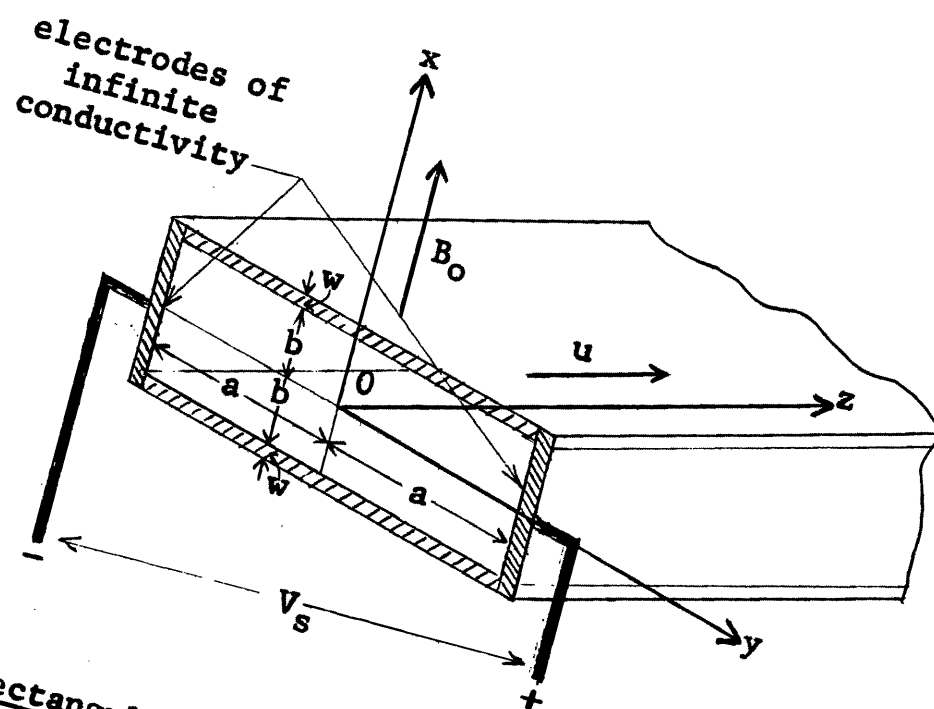
Fig. 3.5.   Rectangular Channel - Highly Conducting End Walls
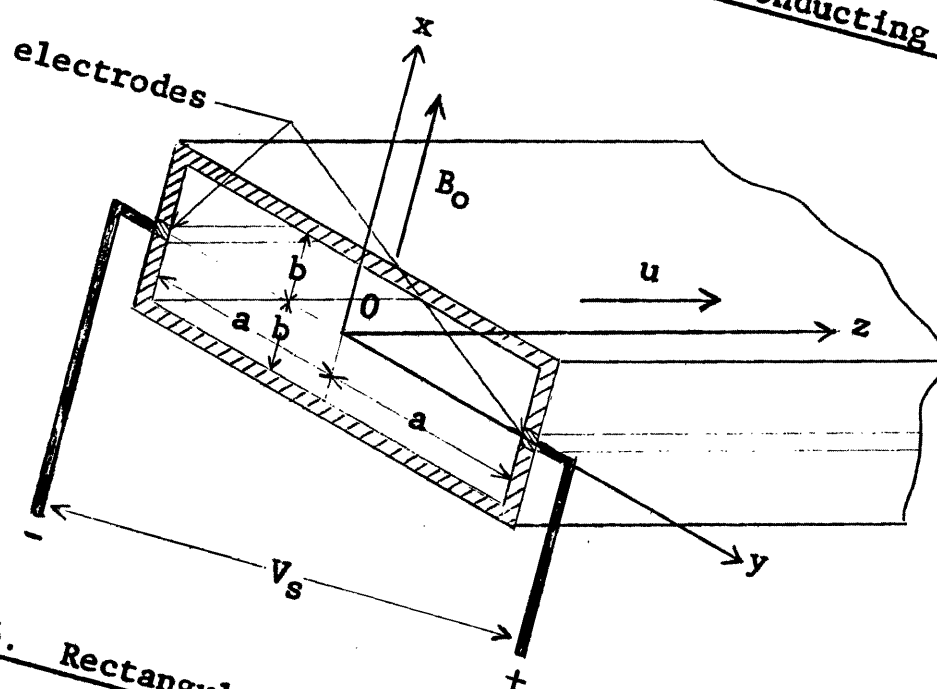
Fig. 3.6.   Rectangular Channel - Insulated Walls

Following established Fourier methods for boundary value problems involving second order, linear, inhomogeneous partial differential equations, 3-48 is rendered homogeneous by the substitution $u_v(x,y) = [1 + X_v(x)]Y_v(y)$ giving

$$\frac{\partial^2 X_v}{\partial x^2} + [1 + X_v]\frac{\partial^2 Y_v}{\partial y^2} + \frac{M}{b} Y_v\frac{\partial X_v}{\partial x} + P = 0$$

which is homogeneous provided $\quad \frac{\partial^2 Y_v}{\partial y^2} + P = 0 \qquad\qquad$ (3-49)

Then, $\qquad \dfrac{\dfrac{\partial^2 X_v}{\partial x^2} + \dfrac{M}{b}\dfrac{\partial X_v}{\partial x}}{X_v} = -\dfrac{\dfrac{\partial^2 Y_v}{\partial y^2}}{Y_v} = \alpha_c$, a constant.

$\qquad\qquad\qquad\qquad\qquad\qquad\qquad\qquad\qquad\qquad$ (3-50)

From 3-50, Y_v must satisfy both 3-49 and $\dfrac{\partial^2 Y_v}{\partial y^2} - \alpha_c Y_v = 0$

for which a general solution is $Y_v = C_1 e^{P_1 y} + C_2 e^{P_2 y}$ where P_1 and P_2 are obtained as roots of the auxiliary equation $p^2 - \alpha_c = 0$ and C_1 and C_2 are constants to be determined from the boundary conditions $u_v(x,a) = u_v(x,-a) = 0$ or $Y_v = 0$ for $y = \pm a$. Hence,

$$Y_v = a_n \cos\left[\frac{(2n + 1)\pi}{2a}\right], \quad (n = 0,1,2 - - -)$$

and $\qquad\qquad \alpha = \dfrac{(2n + 1)^2 \pi^2}{4a^2}$

This can only satisfy 3-49 if the Fourier coefficients a_n are chosen such that $\partial^2 Y_v/\partial y^2$ is the Fourier representation of the constant $-P$ between the limits $y = \pm a$.

Now, $\qquad \dfrac{\partial^2 Y_v}{\partial y^2} = -\dfrac{(2n + 1)^2 \pi^2}{4a^2} a_n \cos\left[\dfrac{(2n + 1)\pi}{2a}\right]y$

while $\qquad P = \dfrac{4P}{\pi} \sum_{n=0}^{\infty} \dfrac{(-1)^n}{(2n + 1)} \cos\left[\dfrac{(2n + 1)\pi}{2a}\right]y$

which are equal in magnitude when $a_n = \dfrac{16Pa^2}{\pi^3}\dfrac{(-1)^n}{(2n + 1)^3}$

and a solution of Y_v which satisfies all the conditions is

$$Y_v = \frac{16Pa^2}{\pi^3} \sum_{n=0}^{\infty} \frac{(-1)^n}{(2n + 1)^3} \cos\left[\frac{(2n + 1)\pi}{2a}\right]y$$

X_v is determined from $\dfrac{\partial^2 X_v}{\partial x^2} + \dfrac{M}{b}\dfrac{\partial X_v}{\partial x} - \alpha_c X_v = 0$

which has a general solution $X_v = C_3 e^{p_3 x} + C_4 e^{p_4 x}$ where p_3 and p_4 are determined as the roots of

$$p^2 + \frac{M}{b} p - \frac{(2n + 1)^2 \pi}{4a^2} = 0.$$

The boundary conditions require that $X_v = 1$ for $x = \pm b$. Then the integration constants C_3 and C_4 are determined as

$$C_3 = \frac{\sinh p_4 b}{\sinh(p_3 - p_4)b} \; ; \qquad C_4 = - \frac{\sinh p_3 b}{\sinh(p_3 - p_4)b}$$

Putting $p_3 + p_4 = - M/b$ and $p_3 - p_4 = M'/b$ where

$$\frac{M'}{b} = [\frac{M^2}{b^2} + \frac{(2n + 1)^2 \pi^2 b^2}{a^2}]^{\frac{1}{2}}$$

makes the solution for u_v

$$u_v(x,y) = \frac{16Pa^2}{\pi^3} \sum_{n=o}^{\infty} \frac{(-1)^n}{(2n+1)^3} F_1(x) \, F_2(x) \, \cos[\frac{(2n+1)\pi}{2a}]y$$

where

$$F_1(x) = [1 - \frac{\sinh\frac{M'+M}{2} \exp\frac{(M'-M)x}{2b} + \sinh\frac{M'-M}{2} \exp\frac{(M'+M)x}{2b}}{\sinh M'}]$$

and

$$F_2(x) = [1 + \frac{(\sinh p_4 b)e^{p_3 x} - (\sinh p_3 b)e^{p_4 x}}{\sinh(p_3 - p_4)b}]$$

Using $u_z = \frac{1}{2}(u_v + u_w)$,

$$u_z(x,y) = \frac{16Pa^2}{\pi^3} \sum_{n=o}^{\infty} F_3(x) \frac{(-1)^n}{(2n+1)^3} \cos[\frac{(2n+1)\pi)}{2a}]y \qquad (3\text{-}51)$$

where

$$F_3(x) = 1 + \frac{\sinh\frac{M'+M}{2} \cosh\frac{(M'-M)x}{2b} - \sinh\frac{M'-M}{2} \cosh\frac{(M'+M)x}{2b}}{\sinh M'}$$

The one-dimensional Hartmann solution is readily obtained using the foregoing method rather than that of Section 3.2. Only X_v requires to be found from the equation

$$\frac{\partial^2 X_v}{\partial x^2} + \frac{M}{b} \frac{\partial X_v}{\partial x} = 0$$

which has an auxiliary equation with a non-zero root $p = - \frac{M}{b}$.

The equation for X_w similarly yields a non-zero root at $p = \frac{M}{b}$. Comparison of these roots with those obtained in the derivation of 3-51 shows directly that this equation applies to the one-dimensional case when $Y_v = Y_w = C_5$, a constant, $p_3 = M/b$ and $p_4 = - M/b$ and gives

$$u_z(x) = C_6[1 - \frac{\cosh(Mx/b)}{\cosh M}]$$

which corresponds to 3-20.

Although equation 3-51 has an inconvenient form for detailed investigation, it is of particular importance in that it shows (1) the velocity profile in the direction of the applied magnetic field depends on that field and has a form similar to that found in one-dimensional Hartmann theory and (2) the velocity profile transverse to the field is not greatly affected by the field and tends to a parabolic form for high-M conditions.

It is to be expected that a similar result applies in the non-conducting circular case and that the flow signal usually depends on M to an extent which can at least be assessed using 3-51. In a practical flowmeter with an exciting field of limited axial length, establishment of full profile distortion requires an 'entry length' l_e which has been estimated by Shercliff (Ref. 110) at

$$l_e = \frac{3\rho u_o}{B_o^2 \sigma} = \frac{3Rb}{M^2} \tag{3-52}$$

using an adaptation of a flat plate boundary layer solution method in which the non-linear space situation is solved approximately through consideration of the analogous linear time variation problem.

The flow signal is, as usual, obtained by integration of 3-28 between B and D of Fig. 3.6. Now 3-28 gives

$$\frac{\partial V}{\partial y} = B_o u_z - \frac{1}{\sigma \mu B_o} \frac{\partial b_z}{\partial x}$$

where $\qquad b_z = \mu(\sqrt{\rho\sigma})^{\frac{1}{2}}(u_v - u_w)/2$

and yields $\qquad V_{AB} = V_s = \int_o^a B_o[(u_v + u_w) - \frac{b}{M}\frac{\partial}{\partial x}(u_v - u_w)]dy$

which, on integration leads to

$$V_s = \frac{64B_o a^3 P}{\pi^4}\sum_{n=o}^{\infty}\frac{1}{(2n+1)^4}[1 - \frac{1}{2}\frac{\cosh M/2}{\cosh M'/2}(1 - \frac{M'}{M}\frac{\tanh M/2}{\tanh M'/2})]$$

(3-53)

The average velocity is obtained by integrating over the cross-section as

$$u_o = \frac{32Pa^2}{\pi^4}\sum_{n=o}^{\infty}\frac{1}{(2n+1)^4}[1 - \frac{4M'}{M'^2 - M^2}(\frac{\tanh\frac{M'+M}{2}\tanh\frac{M'-M}{2}}{\tanh\frac{M'+M}{2} + \tanh\frac{M'-M}{2}})]$$

(3-54)

Multiplying 3-53 by u_o and dividing by 3-54 gives a result of the form

$$V_s = 2B_o au_o K_3$$

(3-55)

where K_3 is the average velocity profile factor and gives the ratio of V_s obtained from 3-53 to that given by equation 1-4. K_3 depends on M and on the a/b ratio and approximate calculations of these dependences are shown in Figs 3.7 and 3.8. It may be noted that at high-M Values (>100), K_3 is independent of the a/b ratio and that, under low-M conditions where only normal viscous forces are considered, V_s is no longer given by the simple formula 1-4 as in the circular section channel.

Comparison of these results with the high-conductivity end case indicates that there the effect of the end conductors is to modify the cross-section potential distribution in such a fashion as to make the integral of $\partial V/\partial y$ between the channel ends an average value for any particular flow rate.

3.10. Turbulent Flow Conditions

The discussion of turbulent flow conditions is hampered by the continued existence of obscure points in its theoretical study and must be based on the experimental work of
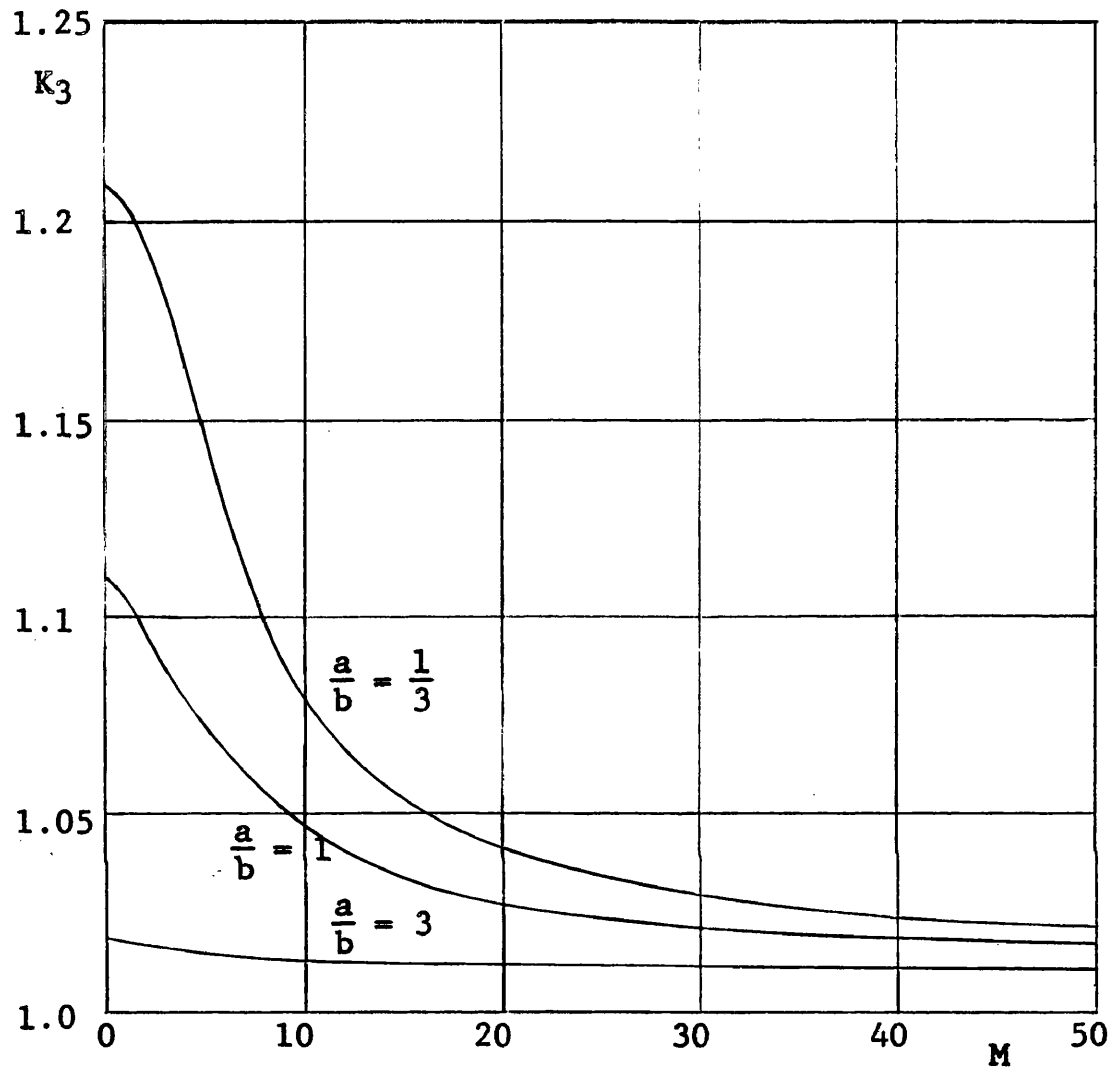
Fig. 3.7. Velocity Profile Factor K_3 Versus Hartmann Number M
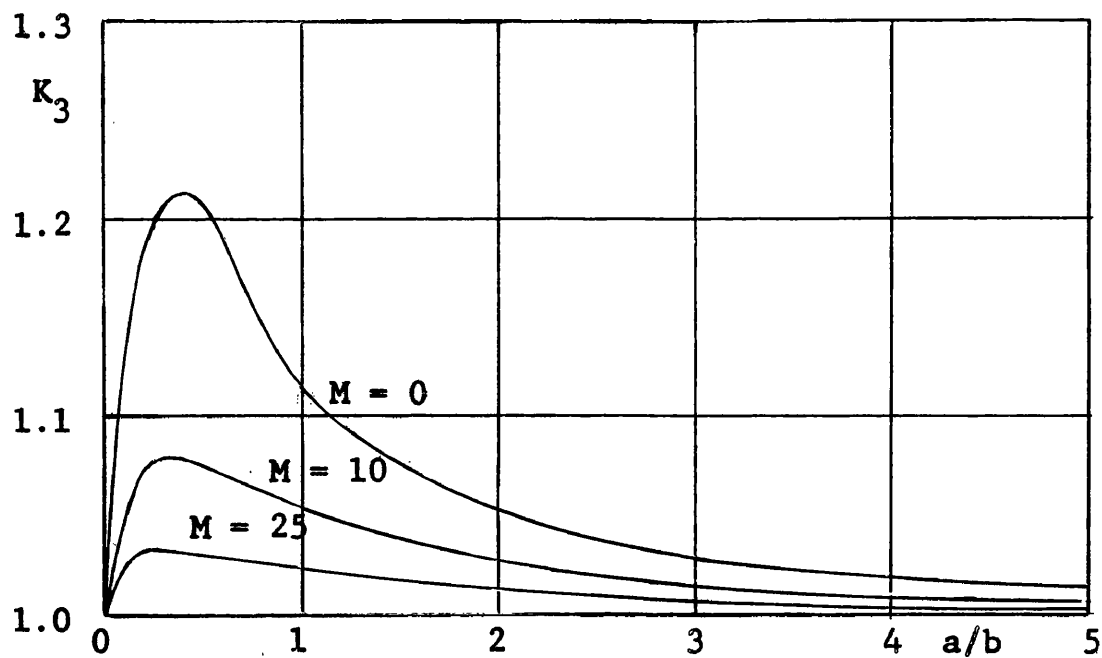
Fig. 3.8. Velocity Profile Factor K_3 Versus Aspect Ratio $\frac{a}{b}$

Hartmann and Lazarus (Ref 23) and Murgatroyd (Ref. 40). It should be recalled, however, that the flow signal may be determined in circumstances where it is independent of the velocity profile provided the assumptions stated in Section 3.1 can be applied.

In the one-dimensional theory of Section 3.2, the apparent increase of viscosity with magnetic field is expressed by equation 3-21 from which it may be inferred that the effect of a transverse magnetic field is to delay the onset of turbulent conditions in laminar flow as the average velocity is increased and even to suppress them altogether. The experimental evidence generally supports this contention as well as giving good agreement with laminar theory for high aspect ratio rectangular channels. The results obtained by Hartmann and Lazarus showed the pressure head required for magnetic flux densities in the range 0 to 1.2 Wb/m^2 to maintain various volume flow rates of mercury. For a small cross-sectional area they found that turbulence was completely suppressed while in other larger area cases a considerable magnetic field was required to achieve this. In some instances, the pressure head required to maintain a constant volume flow rate was actually reduced while turbulence was being suppressed. They also showed that the onset of turbulence was delayed in the presence of a transverse magnetic field.

When M is large, equation 3-20 becomes, approximately,

$$u_o = \frac{p_o b^2}{\rho L M \nu} = \frac{p_o b}{L \rho M u_o} R$$

or

$$\frac{M}{R} = \frac{p_o b}{\rho L u_o^2} \qquad (3-56)$$

Murgatroyd, also using mercury, found that this condition was roughly supported by his experiments provided $R/M < 225$ and concluded that turbulence should not occur when this inequality is met. However, this conclusion may be questioned as M/R in 3-56 depends on the liquid viscosity (see also Section 4.6).

3.11. Axial Direction Non-uniformity of Applied Magnetic Field

The assumption of a non-uniform space distribution for the exciting magnetic field is required to account for the important end effects which occur where the liquid enters and leaves this field. As the three-dimensional nature of this boundary value problem precludes any general solution, it is necessary to seek a suitable approximate treatment. For the contact type of electromagnetic flowmeter, the points requiring consideration are (1) the effect on the flow signal and (2) the additional pressure drop and these are investigated here with the assumptions that (a) the velocity is everywhere constant and axially directed over the channel cross-section, (b) the channel is of rectangular section with non-conducting walls, (c) the exciting field is entirely in the direction transverse to that of the liquid, and (d) the component of the induced field in the direction of the exciting field has negligible effect. The problem is thus reduced to a two-dimensional situation involving no variation in the x-direction of the coordinate system of Fig. 3.9.

The distance 2c is a measure of the axial length over which the exciting field is within 3db (say) of its maximum flux density. The equations to be solved are

$$J_y = \sigma(u_o B - \frac{\partial V}{\partial y}) \quad (3\text{-}57); \qquad J_z = -\sigma\frac{\partial V}{\partial z} \quad (3\text{-}58)$$

where, on the assumption of symmetry, $B(z)$ and $V(z)$ are even functions of z with $B(z)$ having values B_o at z = 0 and zero at z = $\pm\infty$ and $\partial V/\partial z$ = 0 for z = 0, and $V(y)$ is an odd function of y with (say) V = 0 for y = 0. With the basic requirement $\nabla \cdot J$ = 0, 3-57 and 3-58 yield the Laplace equation

$$\frac{\partial^2 V}{\partial y^2} + \frac{\partial^2 V}{\partial z^2} = 0 \quad (3\text{-}59)$$

The relevant boundary conditions are that, at y = $\pm$ a, J_y = 0 and $\partial V/\partial y$ = $u_o B$ while, as z $\rightarrow \pm\infty$, V $\rightarrow$ 0.

These conditions suggest that a Fourier Integral solution should be obtained to accommodate the entire z-axis over which a non-periodic solution is required.[1] The problem is similar to that of finding the potential between plates of infinite extent parallel to the xoz plane and distance 2a apart when the potential on one plate is zero and on the other is some specified function of z.

A variable separable solution of 3-59 is $V(y,z) = YZ$ which, on substitution yields

$$(1/Y)\ \partial^2 Y/\partial y^2 = -(1/Z)\ \partial^2 Z/\partial z^2 = \alpha$$

where α is now a continuously variable parameter. By the usual procedure,[2] a particular solution of 3-59 which is bounded for all y and z is found as $\sinh \alpha y \cos[\alpha(z + c)]$, where α and c are to be regarded as arbitrary constants. The function

$$\frac{u_0}{\pi \alpha \cosh \alpha a}\ B(z')\sinh \alpha y \cos[\alpha(z - z')]$$

is also a solution, the continuously variable parameters α and z' being independent of both y and z. The integral of this with respect to these parameters is the required solution for $V(y,z)$ and is

$$V(y,z) = \frac{u_0}{\pi} \int_0^\infty \frac{\sinh \alpha y}{\alpha \cosh \alpha a}\ d\alpha \int_{-\infty}^\infty B(z')\cos[\alpha(z' - z)]dz'$$

which reduces to

$$V(y,z) = u_0 B_0 [\frac{2}{\pi} \int_0^\infty \frac{\sinh \alpha y}{\alpha \cosh \alpha a} \cos \alpha z \int_0^\infty f(z')\cos \alpha z'dz'd\alpha] \quad (3\text{-}60)$$

as $B(z) = B_0 f(z)$ is a real, even function. On differentiation with respect to y, 3-60 gives the Fourier Integral for $u_0 B(z)$ when $y = \pm a$ as required by the boundary conditions. Writing

$$V_s = 2V(b,0) = 2au_0 B_0 K_4 \quad (3\text{-}61)$$

---

1. Eindhorn (Ref. 82) assumes a double Fourier series solution which does not satisfy 3-59 and is not immediately applicable to the z-axis conditions.
2. Fourier methods throughout follow Ref. 135.

K_4 can be recognised as an end effect constant giving the departure of V_s from the value $2au_oB_o$ and to be determined in any particular case by the integrations indicated in 3-60 for $y = a$, $z = 0$. It is to be noted that K_4 is a function of the magnetic field distribution over the yoz plane but is independent of the conductivity.

A useful approximation to aid the calculation of K_4 in any particular case is a piecewise-linear representation of $B(z)$. From equation 3-57,

$$V(y,z) = B(z)u_oy - \frac{1}{\sigma} \int_o^y J_y(y,z)dy = B(z)u_oy - V_j(y,z)$$

Double differentiation with respect to both y and z shows that $V_j(y,z)$ may be determined by a separation of variables solution of Laplace's equation when $B(z)$ is either a constant (including zero) or a linear function of z. The boundary condition $\partial V/\partial y = u_oB(z)$ for $y = \pm a$ is replaced by $\partial V_j/\partial y = 0$ for $y = \pm a$.

Provided $B(z)$ is approximated by sections of constant amplitude or constant slope as indicated in Fig. 3.10, a Fourier series solution for any one of these sections and meeting the boundary conditions is

$$V(y,z) = B(z)u_oy - \sum_{n=o}^{\infty} b_n\cosh[\frac{2n+1}{2a}\pi z]\sin[\frac{2n+1}{2a}\pi y]$$

where b_n is the Fourier coefficient to be obtained by matching solutions at the section boundaries across which both V and $\partial V/\partial z$ must be continuous. For any but the simplest approximations, the procedure is lengthy as it involves the solution of $2N_B$ simultaneous equations where N_B is the number of section boundaries. It is illustrated here for the case where

$$B(z) = B_o, \quad -c < z < c ; \qquad B(z) = 0, \quad z > c$$

By writing $\quad y = \sum_{n=o}^{\infty} \frac{8(-1)^n a}{\pi^2(2n+1)^2} \sin[\frac{2n+1}{2a}]\pi y$
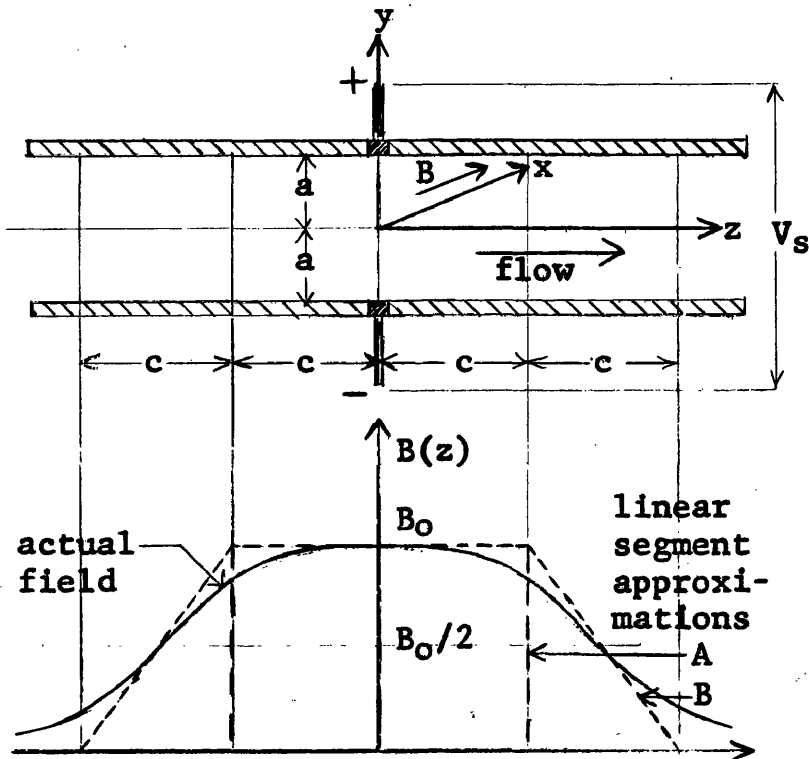
Fig. 3.9. Coordinate System for End Effect Analysis

Fig. 3.10. Magnetic Field Distribution and its Approximation by Linear Segments
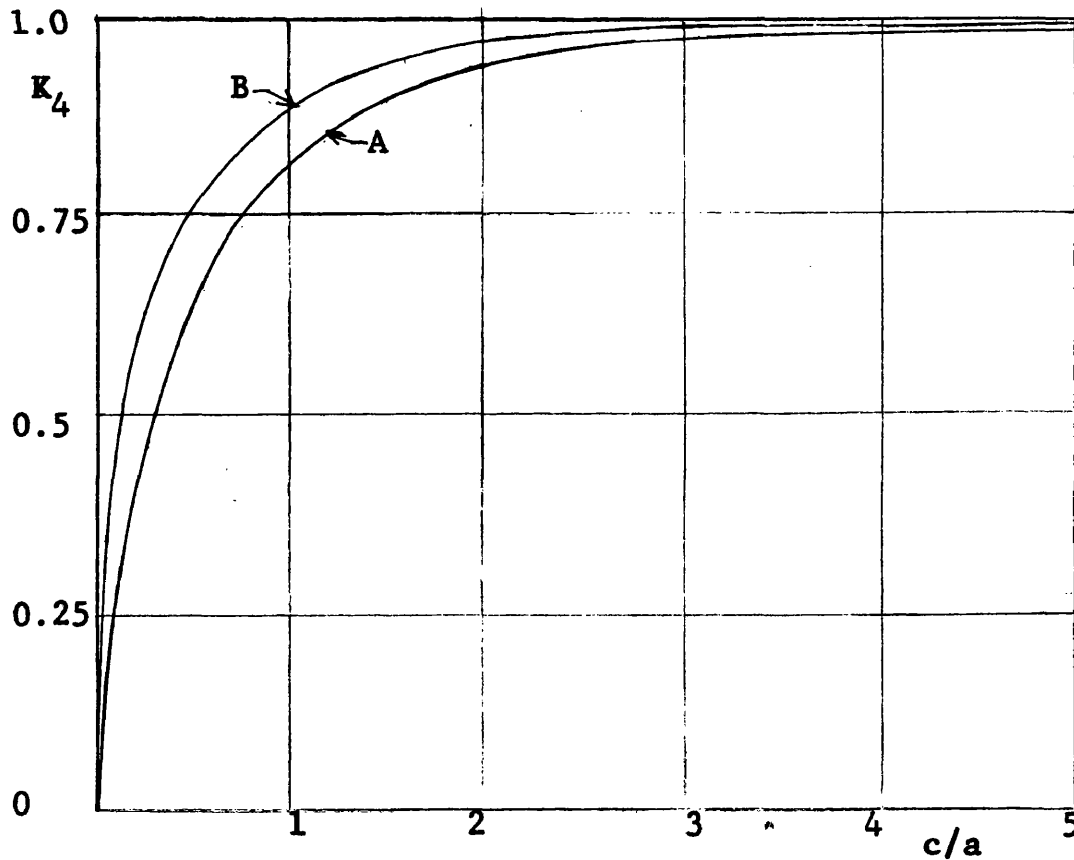
Fig. 3.11. End Effect Constant K_4 Versus c/a Ratio

then
$$B_o u_o \frac{8(-1)^n a}{\pi^2 (2n+1)^2} + b_{n1} \cosh[\frac{2n+1}{2a}]\pi c = b_{n2} \exp[\frac{2n+1}{2a}]\pi c$$

and
$$b_{n1} \sinh[\frac{2n+1}{2a}]\pi c = - b_{n2} \exp[\frac{2n+1}{2a}]\pi c$$

where b_{n1} and b_{n2} indicate the regions $z < c$ and $z > c$ respectively. Solution for b_{n1} and b_{n2} now yields

$$V(y,z)\Big|_{|z|<c} = B_o u_o y - \frac{8u_o B_o a}{\pi^2} \sum_{n=0}^{\infty} \frac{(-1)^n}{(2n+1)^2}[\sin(\frac{2n+1}{2a})\pi y] \cdot$$
$$\exp-(\frac{2n+1}{2a})\pi c[\cosh(\frac{2n+1}{2a})\pi z] \quad (3\text{-}62)$$

$$V(y,z)\Big|_{|z|>c} = \frac{8u_o B_o a}{\pi^2} \sum_{n=0}^{\infty} \frac{(-1)^n}{(2n+1)^2}[\sin(\frac{2n+1}{2a})\pi y][\sinh(\frac{2n+1}{2a})\pi c] \cdot$$
$$\exp-(\frac{2n+1}{2a})\pi |z| \quad (3\text{-}63)$$

The flow signal is

$$V_s = 2V(a,0) = 2u_o B_o a[1 - \frac{8}{\pi^2} \sum_{n=0}^{\infty} \frac{1}{(2n+1)^2} \exp-(\frac{2n+1}{2a})\pi c]$$
$$(3\text{-}64)$$

where
$$K_4 = [1 - \frac{8}{\pi^2} \sum_{n=0}^{\infty} \frac{1}{(2n+1)^2} \exp-(\frac{2n+1}{2a})\pi c]$$

The end effect constant as a function of the ratio of c/a is plotted in Fig. 3.11 both for the case considered and the improved approximation

$$B(z) = B_o, \quad |z| < c; \quad B(z) = B_o(2 - \frac{|z|}{c}), \quad c < z < 2c;$$
$$B(z) = 0, \quad |z| > 2c.$$

In the latter case, K_4 is within 1% of $2u_o B_o a$ for $c/a > 2$.

A rough estimate of the extra pressure drop introduced by the circulating end currents may be made following the method commonly employed in electromagnetic pump analysis.[1] The pressure gradient due to the transverse current J_y is given by

$$\frac{\partial p}{\partial z} = -B_o J_y = \sigma B_o (\partial V/\partial y - u_o B_o)$$

When field distortion effects are neglected and $B(z)$ is

---

1. See Woodrow, Ref. 50.

is assumed to have the form used in the derivation of 3-62 and 3-63, $\partial p / \partial z$ is given by

$$\frac{\partial p}{\partial z} = \sigma B_o^2 u_o \sum_{n=o}^{\infty} \frac{4(-1)^n}{(2n+1)\pi} \exp-(\frac{2n+1}{2a})\pi c \, [\cosh(\frac{2n+1}{2a})\pi z] \cdot$$
$$[\cos(\frac{2n+1}{2a})\pi y]$$

from which the pressure drop P_1 is found by averaging with respect to y and integrating from $z = -c$ to $z = c$ as

$$P_1 = \frac{16B_o^2 u_o \sigma a}{\pi^3} \sum_{n=o}^{\infty} \frac{1}{(2n+1)^3} [1 - \exp-(\frac{2n+1}{2a})\pi c] \qquad (3-65)$$

When the channel walls are electrically conducting, it is to be expected that the extra circulating current will increase the pressure drop.

3.12. Time Variation of Applied Magnetic Field

Practical applications of the electromagnetic flowmeter may involve the use of a time-varying magnetic field in situations where a time-invariant velocity may be assumed. For such cases, it is useful to determine the conditions under which the time-invariant analysis of the preceding sections can be applied, at least to a good approximation, for peak or r.m.s. quantities.

For a uniform, time-varying applied magnetic field the two-dimensional components, using the rectangular coordinate system of Fig. 3.1, are

$$\frac{\partial \underline{u}}{\partial t} = 0, \quad \underline{u} = \underline{i}_3 u_z(x,y), \quad \underline{B}(t) = \underline{i}_1 [B_o(t) + b_x(x,y,t)]$$
$$+ \underline{i}_2 b_y(x,y,t) + \underline{i}_3 b_z(x,y,t)$$

which give again $(\underline{u} \cdot \nabla)\underline{u} = 0, \quad (\underline{u} \cdot \nabla)\underline{B} = 0$
while

$$(\underline{B} \cdot \nabla)\underline{u} = [(B_o + b_x)\frac{\partial}{\partial x} + b_y \frac{\partial}{\partial y} + b_z \frac{\partial}{\partial z}]\underline{i}_3 u_z(x,y)$$
$$= \underline{i}_3 [(B_o + b_x)\frac{\partial u_z}{\partial x} + b_y \frac{\partial u_z}{\partial y}]$$

$$(\underline{B} \cdot \nabla)\underline{B} - \nabla \frac{\underline{B} \cdot \underline{B}}{2} = (\nabla \times \underline{B})\underline{B}$$

$$= [\underline{i}_1 \frac{\partial b_z}{\partial y} - \underline{i}_2 \frac{\partial b_z}{\partial x} + \underline{i}_3 (\frac{\partial b_y}{\partial x} - \frac{\partial b_x}{\partial y})] \times$$

$$[\underline{i}_3(B_o + b_x) + \underline{i}_2 b_y + \underline{i}_3 b_z]$$

$$= \underline{i}_1 [b_z \frac{\partial b_z}{\partial x} + b_y (\frac{\partial b_y}{\partial x} - \frac{\partial b_x}{\partial y})] + \underline{i}_2 [(B_o + b_x)(\frac{\partial b_y}{\partial x} - \frac{\partial b_x}{\partial y}) -$$

$$b_z \frac{\partial b_z}{\partial y}] + \underline{i}_3 [(B_o + b_x)\frac{\partial b_z}{\partial x} + b_y \frac{\partial b_z}{\partial y}]$$

The component equations of the Bullard relation 3-9 can now be written as

$$\frac{\partial}{\partial t}(B_o + b_x) = \frac{1}{\mu\sigma} \nabla^2 (B_o + b_x) \qquad \text{(a)}$$

$$\frac{\partial b_y}{\partial t} = \frac{1}{\mu\sigma} \nabla^2 b_y \qquad \text{(b)} \qquad \text{(3-66)}$$

$$\frac{\partial b_z}{\partial t} = \frac{1}{\mu\sigma} \nabla^2 b_z + B_o \frac{\partial u_z}{\partial x} + b_x \frac{\partial u_z}{\partial x} + b_y \frac{\partial u_z}{\partial y} \qquad \text{(c)}$$

and for the modified Navier-Stokes equation 3-10 as

$$- \frac{1}{\mu\rho}[b_y (\frac{\partial b_y}{\partial x} - \frac{\partial b_x}{\partial y}) + \frac{1}{2}\frac{\partial}{\partial x}(b_z)^2] = 0 \qquad \text{(a)}$$

$$\frac{1}{\mu\rho}[(B_o + b_x)(\frac{\partial b_y}{\partial x} - \frac{\partial b_x}{\partial y}) - \frac{1}{2}\frac{\partial}{\partial y}(b_z)^2] = 0 \qquad \text{(b)} \qquad \text{(3-67)}$$

$$\frac{1}{\mu\rho}[(B_o + b_x)\frac{\partial b_z}{\partial x} + b_y \frac{\partial b_z}{\partial y}] + \nu\nabla^2 u_z = - \frac{P_o}{\rho L} \qquad \text{(c)}$$

Considering first 3-66, it is to be noted that equations (a) and (b) are independent of b_z and u_z and are the component form of the skin effect equation for a conductor in a stationary transverse magnetic field. This leads to the important conclusion that the resultant field due to the skin effect may be obtained independently of the flow conditions by the usual procedure[1] and the motional fields may then be found using the third equation of 3-66 when the velocity distribution is known. Evidently, the motional behaviour is due to the applied field

---

1. E.g. Smythe, Ref. 131, Chap. 11.

alone when the skin effect is negligible or U_s, the skin effect parameter, satisfies the relation

$$U_s = \omega\mu\sigma L_c^2 \ll 1 \qquad (3\text{-}68)$$

It may be noted that $U_s/R_M = \omega L_c/u_o$ and hence ωL_c may be regarded as the electrical propagation velocity.

As the velocity profile can be determined directly from the normal hydrodynamic form of the Navier-Stokes equation when $M \ll 1$, equation 3-68 gives the condition under which time-invariant analysis may be expected to apply to the case of low-M flowmeters with time-varying field excitation.

The effect of axial direction non-uniformity of the applied field in the d.c. case has been shown to be the introduction of additional circulating electric currents and an increase of the overall pressure drop across the flowmeter. However, when the field quantities vary with time and the value of M and the device dimensions are sufficiently high to produce significant energy conversion effects, examination of the appropriate components of $\underline{J} \times \underline{B}$ shows that certain combinations of spacial field distributions, time phasing of the field quantities, liquid velocity and liquid conductivity can produce a pressure rise in a manner analogous to torque production in an induction motor. As this condition was not obtained in the experimental system described later, analysis of it is not attempted here.

The topic is of obvious importance in the induced field type of flowmeter and would require attention in any treatment of that device. It also indicates that it should be possible to develop single-phase induction pumps in addition to the polyphase types now available. Such a pump, like its induction motor counterpart, would not be self-starting without auxiliary equipment.

Chapter 4

FLOWMETER ANALYSIS AND TESTING

4.1. Introduction

The magnetohydrodynamic channel flow theory of Chapter 3 has dealt with situations which are idealised in several ways with respect to practical flowmeter arrangements. Attention is now directed to analysis and discussion of further physical effects which arise in flowmeters, to the derivation of a circuit model representation of the device and to a brief review of the factors requiring attention in any system design. The concluding section outlines a testing programme which is appropriate both for device evaluation and for an experimental study of earlier theoretical predictions.

4.2. Dielectric Polarisation

The assumption of negligible displacement current in magnetohydrodynamic theory is entirely justified as signifi-cant effects are only obtained in liquids which are reason-ably good electrical conductors. When sinusoidal time variation of field quantities is involved, the condition for insignificant displacement current may be stated as

$$U_D = \frac{\omega \varepsilon}{\sigma} \ll 1 \qquad (4\text{-}1)$$

In Section 1.3, the principle of the dielectric flowmeter was described as an application of electromagnetic induction in a moving dielectric where, for a useful flow signal to be obtained, it is to be expected that the liquid must possess a dielectric relaxation time $\tau_\varepsilon = \varepsilon/\sigma$ comparable to the characteristic time of the measuring system. Although detailed examination of dielectric polarisation and its application to the dielectric flowmeter will not be attempted here, some consideration is necessary for the application of

the a.c. contact flowmeter to liquids of low conductivity. Under conditions where the inequality 4-1 does not apply, motional dielectric effects may occur.

Fig. 4.1 shows the coordinate system to be used for an approximate analysis of the flow of a non-magnetic dielectric through a non-conducting rectangular channel which is situated in a uniform, time-invariant, transverse magnetic field of infinite axial extent. The outer surfaces of the thin channel walls are covered with a metallic contact, the whole arrangement forming a parallel plate capacitor. To permit a simple, one-dimensional analysis to be made it is assumed that (1) the channel is of effectively infinite extent in the direction of the magnetic field, or a>>b, (2) the dielectric liquid is inviscid so that $\underline{u}$ may be taken as axially directed and constant everywhere on the cross-section, and (3) the thickness of the channel walls is negligible in comparison with the distance b.

The usual definition[1] of dielectric polarisation $\underline{P}_d$ is

$$\underline{P}_d = \underline{D} - \varepsilon_o \underline{E}$$

and for a homogeneous, isotropic and linear medium as may be assumed for this case, $\underline{D} = \varepsilon_o \varepsilon_r \underline{E}$ so that

$$\underline{P}_d = \varepsilon_o \varepsilon_r (1 - \frac{1}{\varepsilon_r})\underline{E} \qquad (4\text{-}2)$$

In general, $\underline{D} = \underline{D}_o + \underline{D}_p = \varepsilon_o \underline{E}_o + \varepsilon_o \underline{E}_p + \underline{P}_d$

where the subscripts o and p refer to the external and polarising components respectively. Now, for a parallel plate capacitor, $\underline{D}$ must be continuous through the boundary so that $\underline{D}_p = 0$ and

$$\underline{E}_p = - \frac{\underline{P}_d}{\varepsilon_o} = - (1 - \frac{1}{\varepsilon_r})\underline{E}_o \qquad (4\text{-}3)$$

---

1. Stratton, Ref. 127, p. 11.

When the dielectric is in motion, the polarising force $\underline{F}_p$ in the fixed reference frame is produced by the combined effects of the surface charge density ρ_s on the plates and motional induction through the magnetic field B_o as

$$\underline{F}_p = \underline{E}'_o = \underline{E}_q + \underline{u}_o \times \underline{B}_o$$

to first order accuracy. The component of electric field produced by molecular displacement is

$$\underline{E}_p = (1 - \frac{1}{\varepsilon_r})(\underline{E}_q + \underline{u}_o \times \underline{B}_o).$$

Thus the total (electrostatic) electric field intensity between the plates is

$$\underline{E} = \underline{E}_q + \underline{E}_p = \frac{\underline{E}_q}{\varepsilon_r} - (\underline{u}_o \times \underline{B}_o)(1 - \frac{1}{\varepsilon_r})$$

From Fig. 4.1,

$$\underline{u}_o = \underline{i}_3 u_o, \quad \underline{B}_o = \underline{i}_1 B_o, \quad \underline{E}_q = -\underline{i}_2 E_q$$

Now $E_q = Q_e/2a\varepsilon_o$ where $Q_e = 2a\rho_s$ is the total charge on the metal plates per unit axial length and hence

$$E = \frac{Q_e}{2a\varepsilon_o\varepsilon_r} - u_o B_o(1 - \frac{1}{\varepsilon_r})$$

The potential rise from the lower to the upper plate is given by[1]

$$\int_{-b}^{b} -E \, dy = -\frac{Q_e b}{a\varepsilon_o\varepsilon_r} + 2bu_o B_o(1 - \frac{1}{\varepsilon_r})$$

or

$$V_s = 2bu_o B_o(1 - \frac{1}{\varepsilon_r}) - \frac{Q_e}{C} \qquad (4-4)$$

where $C = a\varepsilon_o\varepsilon_r/b$ is the capacitance per unit length when the liquid is at rest.

Equation 4-4 shows that the effect of liquid motion from the lumped circuit viewpoint is to add a voltage generator of e.m.f. $V_p = 2bu_o B_o(1 - 1/\varepsilon_r)$ in series with the normal

---

1. This corresponds to the result obtained by Wilson (Ref. 17) and Howe (Ref. 19) for a rotating, dielectric cylinder.

capacitance C. Although V_p is given by an integral similar to that used to obtain the motionally induced e.m.f. in equation 1-2, it is to be distinguished from the latter quantity which represents the integration of the electromagnetic force acting on free unit charges at rest relative to the moving medium and is independent of the physical constants of the medium. V_p is linearly related to the flow velocity but depends on ε_r, being zero for $\varepsilon_r = 0$ as demonstrated by Blondot (Ref. 16) and Slepian (Ref. 18). For liquids of high relative permittivity, the dependence on ε_r is small and, for distilled water where $\varepsilon_r = 81$, V_p is about 98.7% of $2bu_oB_o$.

If the channel in Fig. 4.1. is rotated so that the short dimension lies along the x-axis, the boundary requirement is for $\underline{E}_o$ to be continuous. In this case, the electric field inside the dielectric will be negligibly different from that outside and, in consequence, polarisation effects will be insignificant. In general, it can be supposed that V_p depends on the channel dimensions and the velocity profile and thus

$$V_p = 2L_c u_o B_o (1 - \frac{1}{\varepsilon_r})K_p \qquad (4-5)$$

where K_p is a factor to be determined and L_c here denotes the appropriate internal channel dimension. In a study of the dielectric flowmeter, more detailed analysis would be needed.

4.3. Contact Effects

Throughout the two-dimensional analysis of Chapter 3, all junctions between the liquid and the channel walls or electrodes were assumed to be ideal (except in the derivation of 3-41 where a linear contact resistance was allowed) and the electrodes or contact by which the flow signal is collected were implied to be of infinite axial extent. In any practical device, both the interface or junction phenomena and the
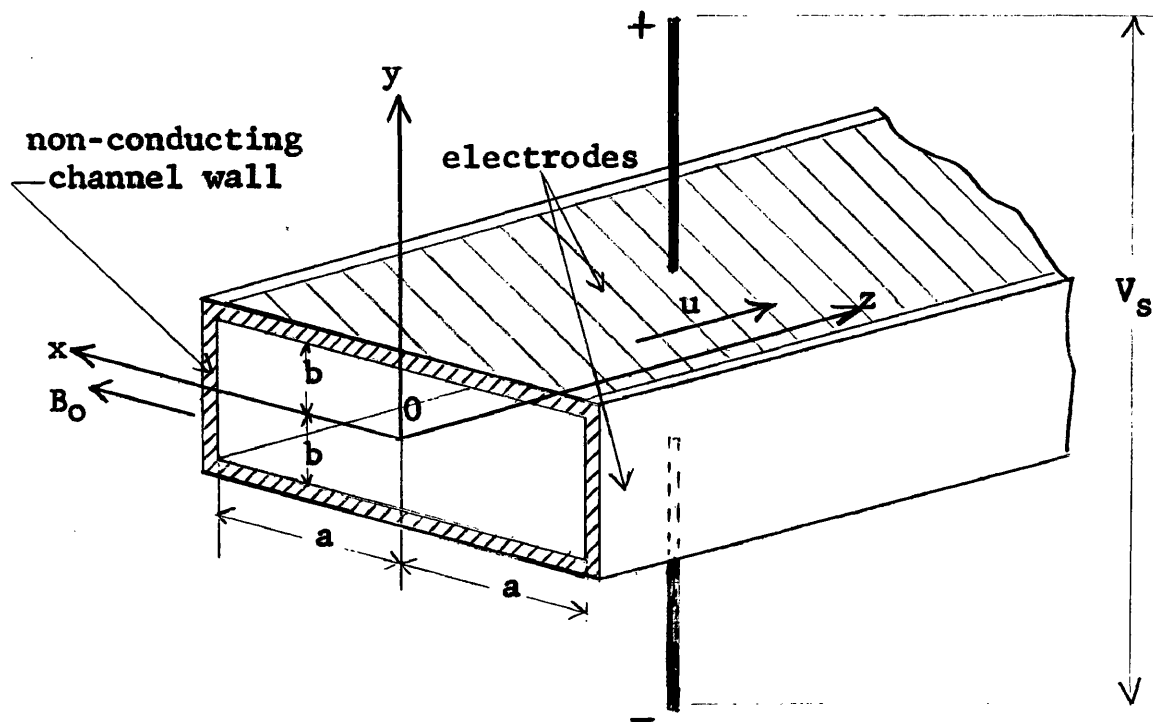
**Fig. 4.1.   Coordinate System for Dielectric
Polarisation Analysis**
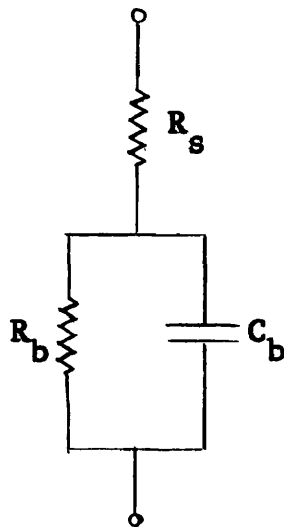
Fig. 4.2.   Circuit Model for a Point Contact

contact area may be expected to modify the ideal behaviour to some extent.

At any junction between dissimilar conducting materials there is set up a potential difference of the magnitude required to maintain thermodynamic equilibrium. The region over which this 'barrier' potential is developed is confined to thin layers on either side of the junction as the constituent phases, as a whole, are required to be electrically neutral. On one side of the 'barrier layer' there is an excess of positive charge and on the other side an excess of negative charge as required by the potential difference while the layer itself is a region of charge depletion and may be regarded as a parallel plate capacitance. The junctions of interest here involve a solid-liquid interface across which electrical conduction usually occurs with a non-linear, potential difference/current characteristic.[1] The complex phenomena responsible for setting up the contact potential involved are as yet not fully understood, but are known to be time-dependent. They have received much attention in the literature of the subject and are reviewed in detail by Butler (Ref. 137). In addition, where liquid motion occurs due to the application of external forces, static equilibrium is destroyed and electrokinetic effects must be considered.

The remarks of the foregoing paragraph apply when intimate contact occurs between the two phases forming the junction. In certain cases, notably with liquid metals, the liquid fails to make such a contact due to the non-wetting phenomenon which produces a relatively high-resistance junction unsuitable for the collection of the flow signal.

---

1. Rectification of an alternating supply by means of this non-linear characteristic is known as Faradaic rectification. See Ref. 140.

Three contact conditions can be recognised in electromagnetic flowmeters as:

(1) electrode contact only - non-conducting walls;

(2) good electrode contact but poor wall contact - conducting walls with non-wetting of the walls by the liquid;

(3) good contact at both electrodes and walls - conducting walls with good wetting by the liquid.

In all these cases, the contact dimensions are likely to be small relative to the channel cross-section and the axial length of the applied magnetic field. It is, therefore, appropriate to regard the electrodes, particularly in cases (1) and (2), as small area or point contacts and to associate with them a spreading resistance to account for the increase of inter-electrode resistance over that predicted by two-dimensional analysis, due to the convergence of current flow lines.

Following usual practice[1], a circuit model representation of a point contact may be made as shown in Figure 4.2 where R_b is the barrier resistance, C_b the depletion layer capacitance and R_s the series spreading resistance. R_b and C_b may be non-linear but R_s, at least in most cases, is a linear parameter.[2] When time-varying signals are involved, it is appropriate to use incremental parameters in this circuit model. Under these conditions, it is important to note that the interface phenomena may give rise to a slow time variation of the barrier potential which constitutes a 'bias' on the non-linear characteristic and produces a 'drift' in the incremental value of R_b (and possibly also of C_b). This effect also occurs in electrolytic tank work and has been noted by Makar, Boothroyd and Cherry, (Ref. 140).

---

1. Ref. 138, p. 23.
2. Ref. 139.

4.4. Flowmeter Circuit Model

The outer ends of the conductors connecting the flowmeter contacts to the input of the amplifying and detecting system provide a 'terminal-pair' at which the total flowmeter output V_o is developed and with respect to which a circuit representation of the flowmeter may be devised.

In Chapter 3, the flow signal at the electrode contacts was found to differ from the value $2L_c u_o B_o$ by an amount depending on (1) channel wall currents, (2) velocity profile distortion arising from magnetohydrodynamic effects and (3) circulating electric currents due to non-uniformity of the applied magnetic field in the axial direction. On the assumption that conditions determined using one and two-dimensional analysis apply to the actual three-dimensional situation, equations 3-23, 3-39, 3-47, 3-55 and 3-61 may be taken as the basis for writing

$$V_s = 2L_c u_o B_o K \qquad (4-6)$$

where $K = K_1 K_3 K_4$ is the flowmeter calibration factor.

The first three equations cited in the previous paragraph indicate the dependence of V_s on the ratio R_i/R_w for particular boundary configurations but may be applied to all linear circuit conditions by the use of Thevenin's theorem. The corresponding circuit model is shown in Fig. 4.3. where K_c is now dependent only on the velocity profile and field end effects, R_{cw} is the actual resistance of the walls between the electrodes with the channel emptied of liquid and R_{ci} is the effective flowmeter internal resistance, incorporating the effect of both R_b and R_s when these are introduced by the electrode arrangement. If R_t is the total resistance between the electrodes with the channel filled, R_{ci} is obtained as

$$R_{ci} = \frac{R_t}{R_{cw}/R_t - 1} \qquad (4-7)$$
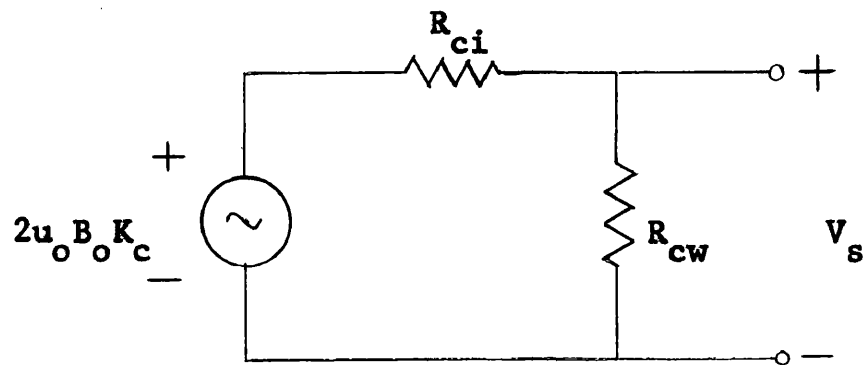
Fig. 4.3.   Basic Flowmeter Circuit Model
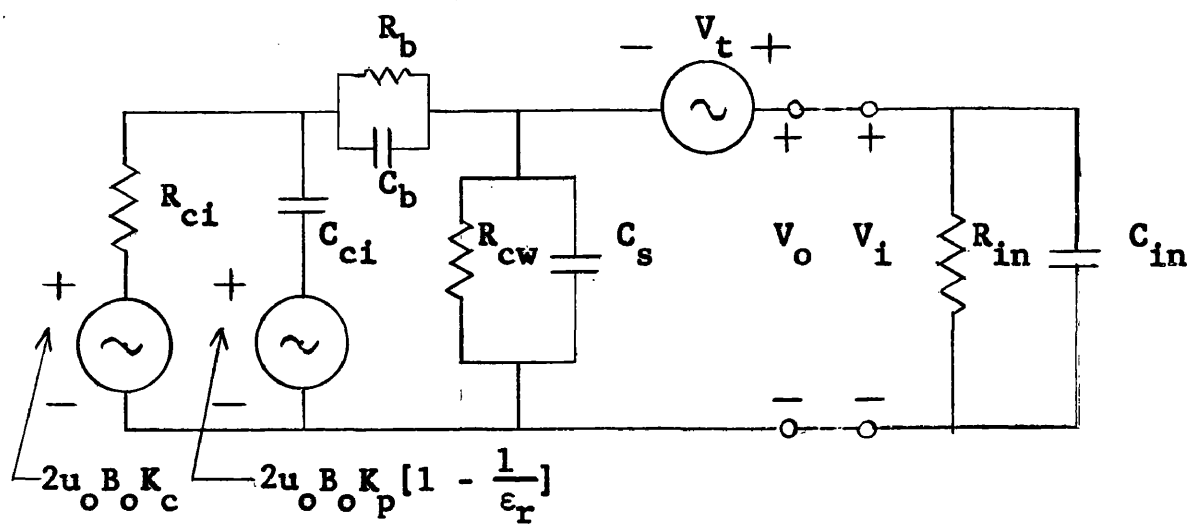
Fig. 4.4.   Complete Circuit Model

In the presence of a contact potential barrier, $R_{ci} = R_b + R_{ci}'$ where R_{ci}' denotes the true internal resistance.

To complete the circuit model and render it suitable for time-varying conditions, the transformer e.m.f., dielectric polarisation and the internal, barrier and external shunt capacitances must be included. As the non-linear barrier effects may be expected to be of small importance in an otherwise linear system, interaction between V_m, V_t and V_p may be neglected and generators representing the latter two may be superimposed on the circuit already given. Recalling from equation 1-8 that V_t is obtained by integrating $- \partial \underline{A}/\partial t$ around the input circuit and is in series with V_m, a source representing it may be included in one of the connecting leads. Dielectric polarisation is added in accordance with 4-5 as a voltage source in series with the internal capacitance C_{ci}, the combination being placed in parallel with the generator representing motional induction effects on the free charges. Addition of the barrier capacitance and external shunt capacitance C_s in parallel with R_b and R_{cw} respectively, completes the circuit model which is shown in Fig. 4.4. with the amplifier input resistance R_{in} and input capacitance C_{in} included.

4.5. System Design Considerations

(a) Selection of Test Liquids

In principle, the contact flowmeter can be applied to liquids with an exceedingly wide range of electrical conductivities. The physical properties[1] of some of these are listed in Table 4.1 while Table 4.2 gives typical values of the various magnetohydrodynamic and other numbers which have been introduced in earlier discussions. These Tables indicate that significant magnetohydrodynamic effects are to be found only in liquid metals while dielectric effects occur in

---

1. Values were obtained from Refs 63 and 151-153.

(a) <u>Liquid Metals</u>

	Melting Point °C	Density gm/cm³	°C	Dyn.Viscosity kg/m sec x10⁻³	°C	Resistivity Ω-m x10⁻⁸	°C
Gallium	29.92	6.093	32.4	1.894	52.9	25.9	29.7
Mercury	-38.87	13.55	20	1.55	20	94.07	0
Potassium	63.7	0.819 0.783	100 250	0.515 0.331	69.6 167.4	13.16 18.7	64 150
Rubidium	39.0	1.442 1.423	99 140	0.673 0.413	38 140	23.15 27.47	50 100
Sodium	97.8	0.928 0.891	100 250	0.686 0.504	104 168	9.65 13.18	100 200
Na-K Alloy A 56%-44% by wt.	19.0	0.886 0.850	100 250	0.546 0.316	104 250	33.0 38.0	50 150
Na-K Alloy B 22%-78% by wt.	-11.0	0.847 0.811	100 250	0.468 0.279	104 250	37.5 44.0	50 150

(b) <u>Electrolytes</u>

	Conductivity $\mho$/m	°C
Sulphuric Acid (max. conductivity)	76.4	20
Hydrochloric Acid*	76.2	18
Potassium Chloride (normal)	10.2	20
Copper Sulphate*	4.6	15
Sodium Chloride (saturated)	2.26	20
Potassium Chloride (1/10 normal)	1.16	20
Acetic Acid*	0.161	18
Potassium Chloride (1/100 normal)	0.128	20

(c) <u>Water</u>

	Conductivity $\mho$/m; x10⁻⁴, 20 °C
Manchester Tap Water	73.2
Distilled Water	1
Purest Water	0.04

* 20 gm salt in 100 gm solution

<u>Table 4.1. Physical Constants of Liquids</u>

	Temp °C	M $B_o = 1$ Wb/m^2 $L_c^o = 1$ cm	R $u_o = 1$ m/sec $L_c^o = 1$ cm $\times 10^4$	R_M $u_o = 1$ m/sec $L_c^o = 1$ cm $\times 10^{-2}$	U_S $f = 50$ c/s $L_c = 1$ cm
Gallium	50	470	3.21	4.85	0.152
Mercury	20	265	8.82	1.32	0.042
Potassium	70	1200	1.61	9.75	0.305
Rubidium	50	831	2.14	5.44	0.171
Sodium	100	1230	1.35	13.1	0.411
Na-K Alloy A	20	745	1.62	3.81	0.120
Na-K Alloy B	20	755	1.82	3.36	0.105
H_2SO_4 (max σ)	20	2.5	1.12	96×10^{-6}	314×10^{-6}
$CuSO_4$	20	0.7	≈ 1.0	5.8×10^{-6}	18.2×10^{-6}
KCl (1/100N)	20	0.1	≈ 1.0	0.2×10^{-6}	0.5×10^{-6}
Distilled Water	Temp °C 20		U_D, $f = 10$ kc/s 0.45		

Table 4.2. Typical Magnetohydrodynamic, Flow and Skin Effect Numbers

(a) Shell type   (b) Core type
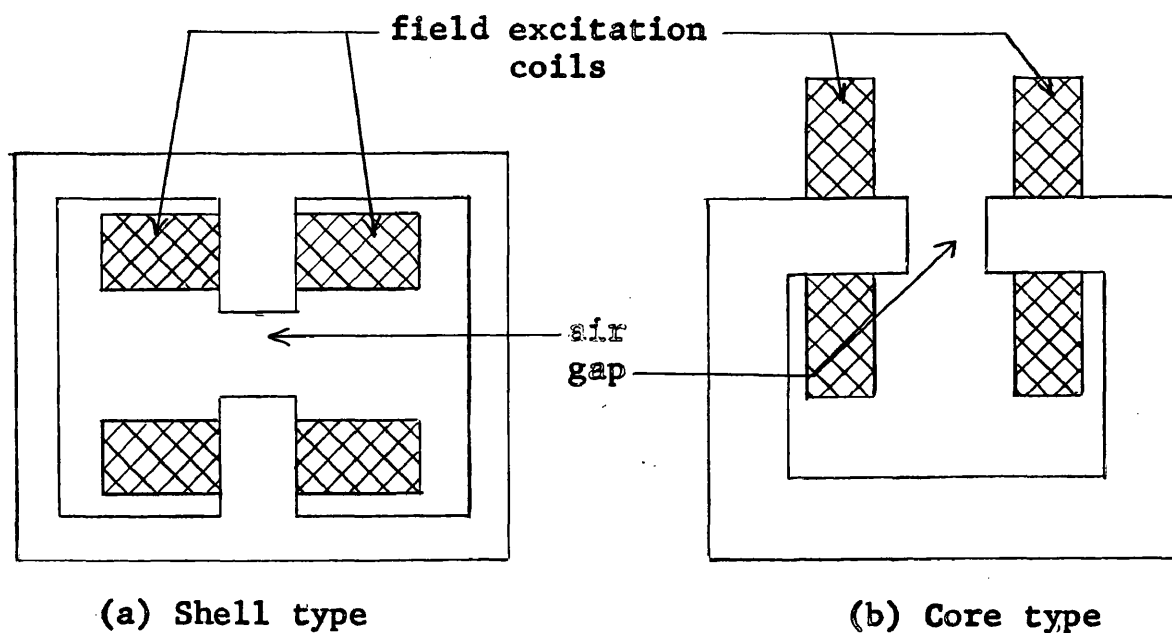
Fig. 4.5. Alternative Magnetic Circuit Configurations

liquids such as distilled water where electrical conduction is due to impurities. Electrolytes form an intermediate range for which the modified Navier-Stokes relation is not required and it is sufficient to consider the circulating electric currents and wall conductivity effects for a velocity profile determined from normal hydrodynamic theory. It may be remarked that, at the outset of any electromagnetic flowmeter design, a determination of the numbers M and U_D is required to enable the correct type classification to be made.

From Table 4.2, sodium has the best characteristics for the attainment of high-M conditions but is difficult to handle[1] and is solid at normal ambient temperatures. While gallium might be considered as it has a reasonably low melting point and is chemically much less active than sodium, it is costly and mercury is probably the most suitable liquid for this aspect of experimental work under normal laboratory conditions. Low-M conditions are conveniently provided by electrolytic solutions such as potassium chloride and offer a very wide range of conductivity. The extensive information available in the literature on contact effects between electrodes and these solutions is a further factor in favour of their use. For low-conductivity tests where dielectric effects are required, distilled water or conductivity water may be used.

(b) Magnetic Circuit for Exciting Field

The magnetic circuit design centres on the problem of producing a substantial flux density (>0.1 Wb/m^2) in the air gap required to accommodate the flow channel and is particularly difficult when high-M conditions are required. The two possible magnetic circuit configurations, corresponding to shell-type and core-type transformer structures, are shown in Fig. 4.5. While the former provides a more nearly symmetrical

1. The techniques of sodium plumbing are discussed in Ref. 144.

configuration, use of the latter enables channel sections to be interchanged more readily. To minimise leakage troubles, it is important to locate the coils carrying the exciting current on the limb which includes the air gap as indicated for both cases in Fig. 4.4.

(c) Amplifier and Detector

While equation 4-6 shows that sufficient output is available at large volume flow rates to operate directly a detecting instrument, amplification of the flow signal is normally required. The main amplifier requirement is that the bandwidth should be selected to minimise noise but allow transmission of the full frequency spectrum of the flow signal. In the latter connection, it should be noted that time variation of both B_o and u_o in 4-6 causes V_s to take the form of a double-sideband, suppressed carrier signal. Hence the amplifier bandwidth should be sufficient to handle the highest significant frequency associated with the maximum time rate of change of velocity.

(d) Amplifier Input Circuit

The design and layout of the amplifier input circuit and the electrical output of the flowmeter involve some novel instrumentation problems which may be listed as (1) elimination of capacitance-coupled voltages under time-varying conditions, particularly with liquids of low conductivity, (2) either complete rejection of the transformer e.m.f. or at least a reduction in its level to a value where amplifier overloading cannot occur, (3) establishment of a stable output under no-flow conditions, (4) selection of electrode materials which are immune from chemical action yet provide an intimate contact with the liquid, and (5) minimisation of loading of the flowmeter by the amplifier input impedance and associated cable connections.

4.6. Formulation of a Test Programme

It is apparent that an experimental investigation of the various factors already discussed cannot properly be undertaken using only one liquid and a particular design of flowmeter. Since all published experimental studies conform to this pattern they are of limited value and there is a need for a more general approach.

Apart from the basic dependence on L_c, B_o and u_o, the flow signal output of an electromagnetic flowmeter has been predicted to depend on the principal dimensions of the device, liquid and channel wall conductivities, the kinematic viscosity and density of the liquid, and the channel flow conditions. Claims[1] that the calibration is independent of these are not justified, except in special circumstances with non-conducting walls, and it should be noted that the temperature dependence of these properties and dimensions may further modify device performance.

Referring to equation 4-6, the functional dependence of the factor K for time-invariant conditions at a specified temperature may be expressed formally as

$$K = F_1 (L_c, c, w, \sigma, \sigma_w, \rho, V, u_o) \qquad (4\text{-}8)$$

where the right-hand side is an arbitrary function of eight quantities with L_c again denoting the channel internal dimension(s). The first seven quantities have appeared in the course of the channel flow analysis conducted in Chapter 3 and the eighth is included to recognise that the establishment of profile distortion and the effect of turbulent flow conditions are necessarily related to the hydraulic Reynolds number. It is desirable to rearrange 4-8 to express the functional relation in terms of dimensionless parameters and

1. As are made in Ref. 86.

equations 3-23, 3-39, 3-47, 3-55 and 3-61 indicate that a suitable choice for laminar flow conditions in a circular channel flowmeter with a fully established velocity profile is

$$K = F_2[\frac{c}{r_i}, \frac{R_{ci}}{R_{cw}}, M]$$
(4-9)

and for the corresponding rectangular case

$$K = F_3[\frac{b}{a}, \frac{c}{a}, \frac{R_{ci}}{R_{cw}}, M]$$
(4-10)

The selection of an alternative or additional parameter to M is less straightforward in the case of turbulent magneto-hydrodynamic flow on account both of theoretical difficulties and a lack of experimental data of the type available for normal hydrodynamic turbulence. The particular flow characteristic of interest here is the velocity profile which is known to depend on R in hydrodynamic turbulence and assumed to be independent of liquid viscosity over most of the channel cross-section. It is suggested that the ratio $M/\sqrt{R}$ is appropriate as it does not involve γ but the matter cannot be resolved satisfactorily without further examination of the general channel flow problem.

Shercliff's entry length relation (equation 3-52) indicates that $M/\sqrt{R}$ is of importance when the dimensions of the flowmeter and the magnetic forces are such that a steady profile cannot be established. This is additional evidence that the form of 4-9 and 4-10 for other than two-dimensional laminar flow should be respectively

$$K = F_4[\frac{c}{r_i}, \frac{R_{ci}}{R_{cw}}, M/\sqrt{R}]$$
(4-11)

$$K = F_5[\frac{b}{a}, \frac{c}{a}, \frac{R_{ci}}{R_{cw}}, M/\sqrt{R}]$$
(4-12)

In all cases, the ratio σ_w/σ may be used in place of the measured quantities in the ratio R_{ci}/R_{cw}.

While this discussion indicates some of the parameters which require attention in any experimental investigation, it does not cover all the quantities on which the flowmeter output may be expected to depend. These include ε_r, ω, the temperature T, electrode area and position, and the location of any sources of profile distortion which are of purely hydrodynamic origin (e.g. channel bends).

The data obtained in a test programme is thus required to:

(1) Establish the dependence of flowmeter calibration in accordance with the foregoing selection of parameters and quantities;

(2) compare the overall calibration of particular flow-meter systems with that predicted by channel flow analysis;

(3) allow a comparison to be made of the alternative methods of magnetic field excitation;

(4) enable the most satisfactory input circuit arrangements to be determined.

Chapter 5

A FLOWMETER SYSTEM FOR EXPERIMENTAL STUDIES

5.1. System Requirements and Specification

The basic requirement in the design and construction of a
system suitable for the systematic study of electromagnetic
flowmeters is that it should be capable of being operated
over a wide range of flow conditions with differing
excitation, electrodes and input circuit arrangements. This
implies a degree of elaboration and a measure of compromise
in its design such as would not be needed for specific
instrumentation applications.

The essential features of the system required to carry
out the test programme of Chapter 6 are shown in Fig. 5.1 and
the design, construction and performance of its component
units are discussed in this Chapter. These units included:

(1) an hydraulic circuit capable of constant head
    operation on both mercury and aqueous solutions.

(2) magnetic circuits and channel section assemblies;

(3) d.c., a.c. and pulsed supplies for magnetic circuit
    excitation;

(4) amplifier input stages, one of which featured extra-
    high input impedance with capacitance neutralisation;

(5) transformer e.m.f. and noise rejectors;

(6) main high-gain amplifier;

(7) detectors for sinusoidal and pulsed excitation;

(8) flow signal display devices.

Provision was made for a variety of interconnection schemes
and to facilitate testing over a sufficiently wide range of
frequencies with both sinusoidal and pulsed excitation, a system
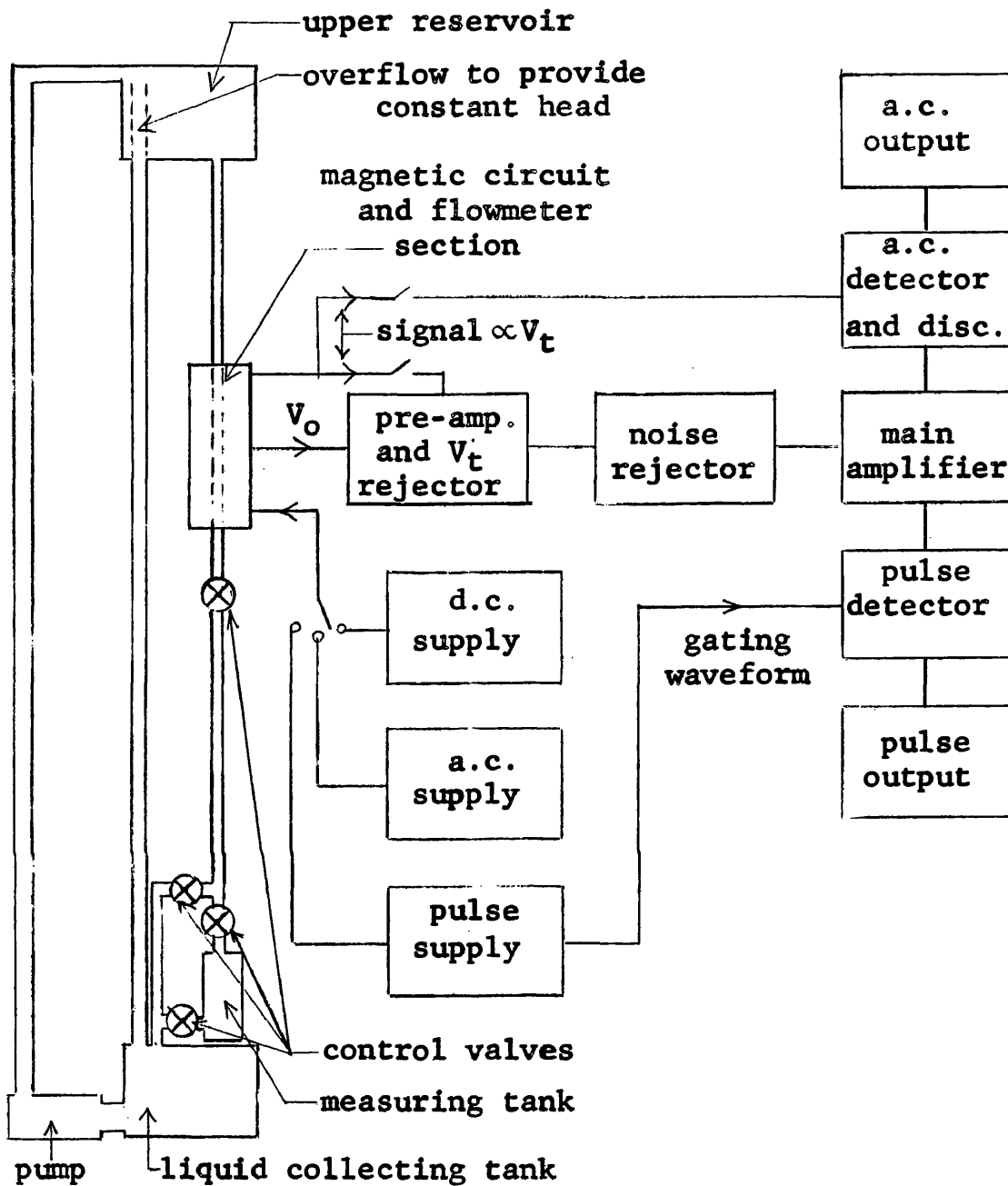
Fig. 5.1. Block Diagram of Experimental System

Liquid	B_o, Wb/m^2	$2r_i$, in	u_c,* in/sec	V_m at $u=u_c$, μV
Mercury	1.0	0.375	0.97	235
Water	1.0	0.375	8.26	2010
	0.2	1.50	2.06	402

* based on $R_c = 2\rho r_i u_c / \eta = 2000$

Table 5.1. Transition Velocity Values of V_m

bandwidth of at least 10 kc/s was adopted with the lower half-power frequency of the capacitance-coupled amplifying stages located at leas than 5 c/s. In the case of d.c. excitation, the amplifiers were operated with a chopper modulator driven directly from the flowmeter output.

5.2. Hydraulic Circuit

The hydraulic circuit was required to be of the recirculatory type to conserve the test liquid and also to be totally enclosed (except for small air vents) to avoid the escape of toxic vapours when mercury was used. While a circuit for the tests to be described may be laid out either horizontally or vertically, the latter arrangement was chosen on the grounds that (a) a constant head tank using an overflow to control the level could readily be incorporated and (b) the head tank would permit trapped air bubbles to escape from the test liquid. The total weight of mercury required in a vertical system raises problems of structural strength and for magnetohydrodynamic experiments where large volume rates of flow are to be examined, a horizontal circuit may be preferred.

The maximum flow rate for mercury was set at 3 gall/min because of limitations imposed by the method of flow rate measurement used. The amount of mercury arriving in a collecting tank over a specified time interval was weighed and from this information the flow rate was determined. Taking 5 sec as the shortest time interval over which a reasonably accurate determination may be made, a flow rate of 3 gall/min involves the collection of about 33 lb of mercury. When this amount was added to the 90-95 lb required to fill the system, it appeared that cost limitation as well as handling difficulty made 3 gall/min the upper limit. The inner radius for circular channels was chosen at 3/16 in to meet the air

gap restrictions imposed by magnetic circuit design discussed
in Section 5.3. It is easily shown that the liquid velocity
in a channel of this size at a volume rate of 3 gall/min is
about 10 ft/sec.

Before finally settling on these values, they were checked
to determine if (a) a range of laminar flow velocities could
be obtained with values of V_m above the noise level of the
amplifier input stages and (b) the head required would be
within the capacity of a small electromagnetic pump.
Rearranging equation 2-24 to express u_c, the velocity of
transition from laminar to turbulent flow in terms of R_c,
the critical Reynolds number gives

$$u_c = \frac{R_c}{2\rho r_i} \tag{5-1}$$

Taking $R_c = 2000$, the value of u_c for mercury at 20° C is
found to be 0.97 in/sec in a 3/8 in diameter channel. Substitu-
tion of this value in equation 1-2 with an applied field of
1 Wb/m^2 yields a value of V_m of 235 μV which is satisfactorily
above the noise level to be expected from amplifiers of the
required bandwidth.

The head required to achieve a liquid velocity of 10 ft/sec
is determined from the well-established empirical formulae of
hydraulics. Weisbach's equation[1] gives h_f, the head required
to overcome friction losses in pipes, as

$$h_f = \frac{fl}{2r_i} \cdot \frac{u^2}{2g} \tag{5-2}$$

where f is the friction factor and 1 is the overall pipe
length. Neglecting entry and exit losses, the total head
required is given by

---

1. See Ref. 142, p. 105.

$$h = \frac{u^2/2g}{1 - fu^2/4gr_i} \qquad (5\text{-}3)$$

The friction factor for mercury at $u = 3$ ft/sec in a 3/8-in diameter smooth pipe is given by standard curves[1] as 0.016 and using this value in 5-3 gives the minimum h required as 7.55 ft. The value of 9 ft was adopted for it is readily attained by a conduction-type electromagnetic pump.[2]

In the case of aqueous solutions, the volume restriction is much less severe but the channel width limitation remains. Nikuradse (Ref. 143) has shown experimentally that Reynolds numbers in excess of 10^5 are necessary if fully developed turbulent flow is to be attained. Taking $R = 10^5$ and using the relation $2ur_i = R\eta/\rho$ yields $r_i = 0.092$ in as the pipe radius required with a 9-ft head. The corresponding flow velocity and volume flow rate are 7.1 ft/sec and 49 gall/min respectively. As the latter value can be obtained with a small centrifugal pump against a 9-ft static head, it was decided to include provision for operation with aqueous solutions in a 1.5-in diameter pipe and to accept the lowering of the magnetic flux density brought about by the increased air gap. The values of u and V_m at $R_c = 2000$ for 3/8-in and 1.5-in diameter pipes are given in Table 5.1. and again meet noise level requirements.

The general layout and principal dimensions of the hydraulic circuit are shown in Fig. 5.2. Aqueous solutions were pumped using a commercially obtained centrifugal pump while mercury was handled by an electromagnetic pump built specially for the purpose. The design of the latter pump followed closely the method given by Woodrow (Ref. 50) and is dealt with in Appendix I. Cooling of mercury after it had passed through the e.m. pump was essential because of the

---

1. Ref. 142, p. 106.
2. See Appendix I.
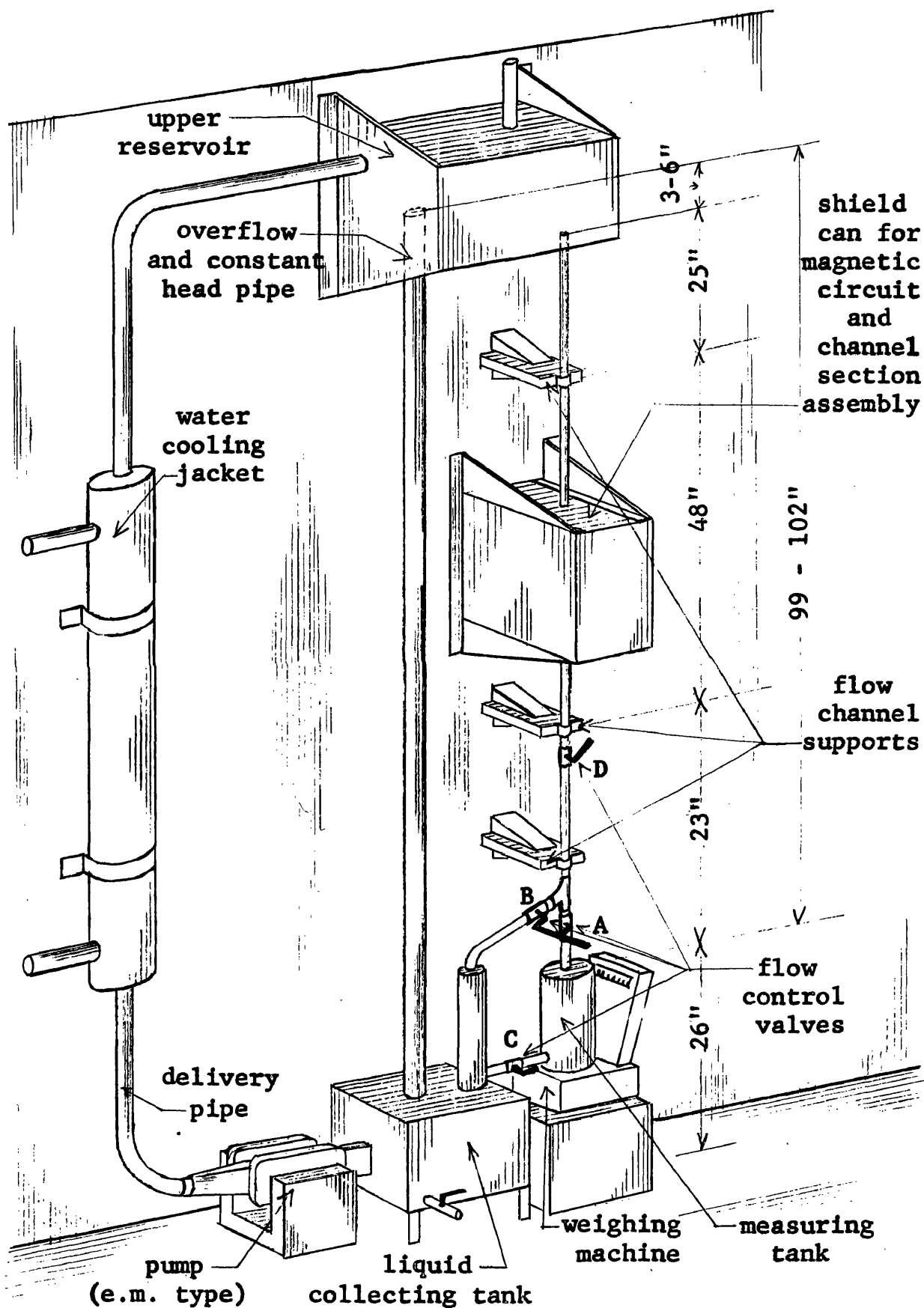
Fig. 5.2. Layout and Principal Dimensions of Flow Circuit

low efficiency of this device and was accomplished by surrounding the head tank delivery pipe with a water jacket. It was found to be necessary to cool aqueous solutions by the same method at high volume flow rates. Materials used in the construction of the system were limited to glass, stainless steel, rubber and plastics to minimise interaction with the test liquids and all surfaces in contact with these liquids were carefully cleaned at frequent intervals using benzene. Care was taken at all joints to ensure leak-proof connections with hose clamps being used at the high-pressure points.

The measured maximum flow rates for mercury and tap water are shown by Table 5.2. to agree satisfactorily with the values required. The procedure in all flow measurements was first to close valve C and then simultaneously to close B and open A (these valves were mechanically coupled) to allow a quantity of liquid to flow into the collecting tank over a suitable time interval after which the valves A and B were restored to their original positions. After the weight of the collected liquid had been noted, it was returned to the system by opening valve C. This arrangement avoided sudden stoppage of the liquid in the test channel and allowed the weight determination to be made under truly static conditions. The flow was controlled by valve D which was placed below the flowmeter to ensure that the test pipe could be filled completely for static tests.

5.3. Magnetic Circuit and Channel Section Assembly

To ensure that strong magnetohydrodynamic effects occur in mercury, a Hartmann number of the order of 100 is required and Table 4.2 shows that this is exceeded in a 3/8-in internal diameter channel with $B_o = 1$ Wb/m^2. Accordingly, magnetic circuit design was aimed at the production of this flux

density (r.m.s. value in the case of sinusoidally time-varying conditions) in a space capable of containing the channel section assembly. An iron return path was used and was laminated from special "Stalloy" stampings (0.013 in) to permit operation with time-varying fields. Air gaps of 5/8 in and 2 in were used but only in the former was the maximum required flux density attained.

In the circumstances of interest here, where the air gap length l_g exceeds 1% of the total magnetic path length, a reasonable estimate of the ampere-turns required may be made from the relation

$$I_c T = k_f \frac{B_o l_g}{\mu} \tag{5-4}$$

where I_c is the exciting current, T the number of coil turns and k_f a constant which allows for leakage flux and depends on geometry and coil location relative to the air gap. Using the core-type arrangement of Fig. 4.5(b), a value of $k_f = 1.5$ was estimated and the product $I_c T$ from 5-4 is then 19000 A-T. To avoid eddy current losses, each of the four coils was wound in layers of 16 s.w.g. insulated copper wire with supplementary inter-layer insulation. Connections to each layer were provided to enable the total excitation voltage to be held within the limits of a 400-V, 50-c/s supply by suitable series-parallel connection of the layers. The coil dimensions were chosen to limit dissipation to about 0.3 W per in^2 of surface area with an operating current density of 1000 A/in^2. While this proved to be satisfactory, it was necessary to use forced air cooling and to limit the period of use to about 10 min at full current.

The magnetic circuit dimensions were selected to provide (a) an approximately uniform field across a 1.5-in diameter channel and (b) c/a ratios of a sufficient magnitude to enable velocity profile distortion by magnetohydrodynamic effects to become fully established. To meet condition (a), the width w_m

Liquid	Test Channel Diameter in	Test Channel* Max. Flow Rate gall/min	Total Flow Rate Incl. Overflow gall/min
Mercury	0.375	2.7	3.1
Water	0.375	2.2	3.5
	1.50	36	40

* Circular cross-section glass tubing

Table 5.2.   Maximum Volume Flow Rates of Hydraulic Circuit

Magnetic Circuit	No. of Coils	T per Coil	Wire Gauge s.w.g.	d.c. value[b] of R_f per coil at 18°C Ω	L_f[b] per coil at f=50c/s H	B_0[c] Wb/m^2 l_g= 5/8"	l_g= 2"
M1, l_m=2in	4	1456[a]	16	7.52	0.316	0.92[e]	0.26[e]
M1, l_m=10in	4	1456[a]	16	12.4	1.37	0.96[e]	0.30[e]
M2	4	9500	28	235	1.52	0.16[f]	-

a. 52 layers of 28 turns each. b. average value measured with coils in position on magnetic circuit and with all turns (per coil) connected in series. c. d.c. excitation with I_c=1 kA/in^2 measured at air gap centre. e four coils in series. f two coils in series.

Table 5.3.   Electrical Characteristics of Magnetic Circuits

Channel Section	Cross-Section	Dimensions (nominal) 2r$_i$ in	2a in	2b in	a/b	w in	Material[b]	Eleectodes Type[d] in Fig 3.6	r_e in
1	Circ.	3/8				1/16	Tufnol	A	3/64
2	Circ.	3/8				1/16	S.S.	A	3/64
3	Circ.	3/8				1/16	Ni on Cu	C	3/64
4	Square		0.33	0.33	1	1/8	Perspex	A/B	e
5	Square		0.33	0.33	1	1/16	S.S.	A/B	e
6	Square		0.33	0.33	1	1/64[a]	Ni on Cu	C	3/64
7	Rect.		0.58	0.19	3	1/8	Perspex	A/B	e
8	Rect.		0.58	0.19	3	1/16	S.S.	A/B	e
9	Rect.		1.05	0.10	10	1/8	Perspex	B	0.10
10	Circ.	1.5				1/8	Tufnol	A	1/16
11	Circ.	1.5				1/16	S.S.	E	1/32

a. reinforced with 3/64 in Perspex. b S.S. = stainless steel, Ni on Cu = nickel plate on copper. c. electrode material selected from: carbon, nickel plated copper, platinum and stainless steel. d. when two electrode types are indicated, these were mounted on opposite ends of the channel section. e. sizes specified in Chapter 6.

Table 5.4.   Channel Section Details
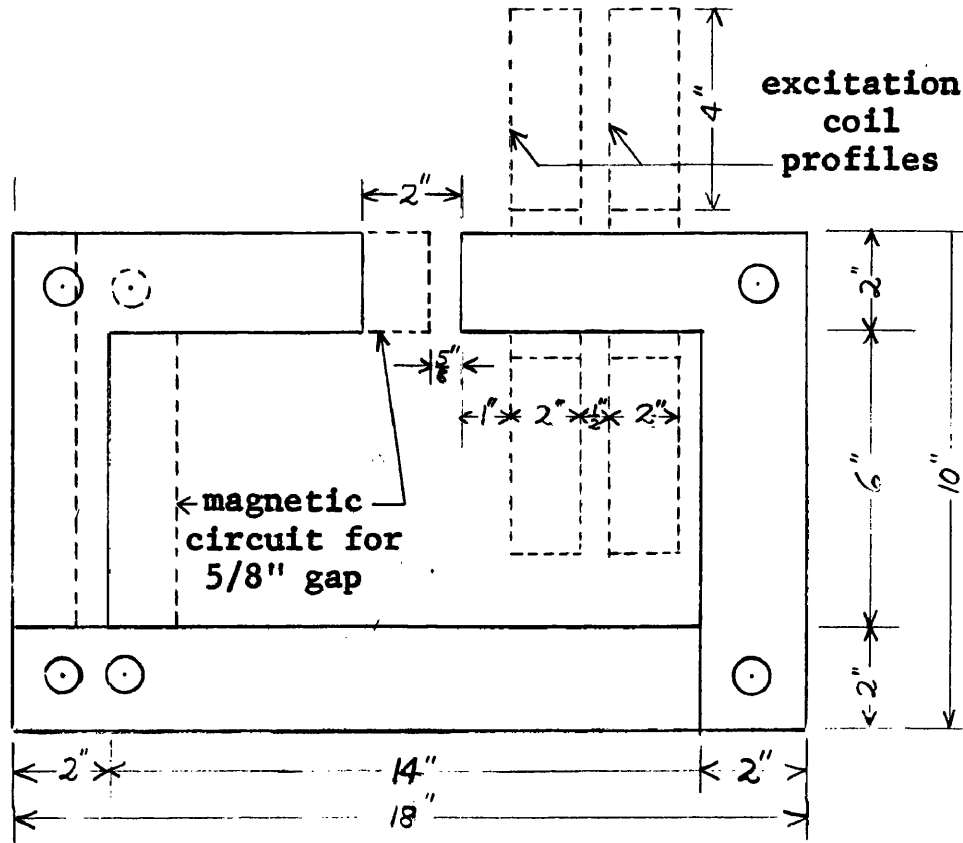
(a) Magnetic circuit M1 assembled for 2 in air gap

(b) Magnetic circuit M2

Fig. 5.3. Details of Magnetic Circuits

of the magnetic circuit and the thickness l_m of the lamination stack were chosen at $2\frac{1}{2}$ in and 10 in respectively to give c/a ~ 27 with a 3/8-in diameter channel. Two sets of coils were made, one for a $2\frac{1}{2}$-in stack and the other for the full 10-in length to enable both short and long flowmeter arrangements to be tested. The laminations were punched to 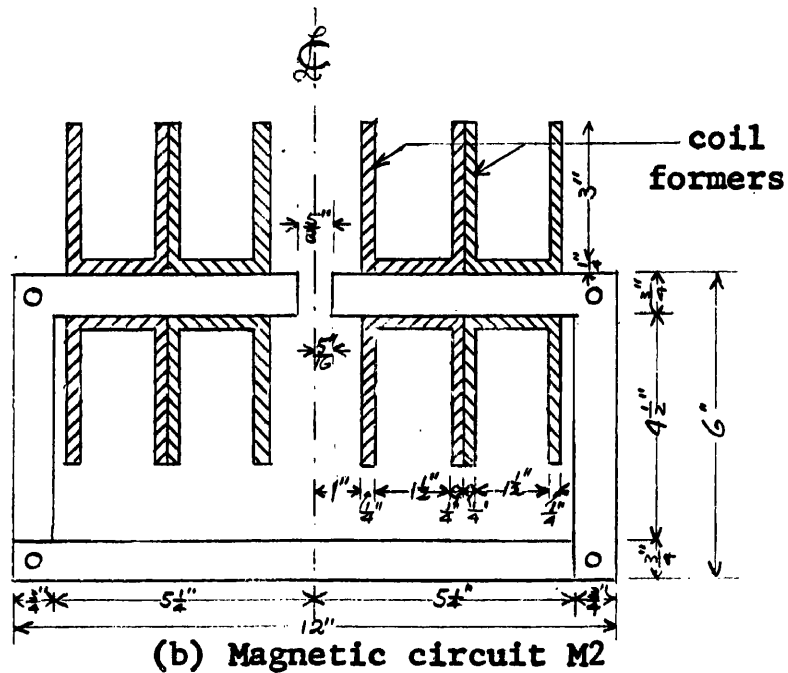enable assembly for either 5/8 in or 2 in air gaps and the structure was braced with suitable supports to ensure mechanical rigidity. The form and dimensional details of this magnetic circuit M1 are given in Fig. 5.3(a) and its important characteristics are summarised in Table 5.3.

A second, smaller magnetic circuit M2 with an air gap of 5/8 in only was designed and constructed in a similar manner for tests with a variable supply frequency and with pulsed magnetic fields where the inductance of the excitation windings and the peak exciting current are determined by the driving power amplifier as discussed below. The dimensions and characteristics of this second circuit appear in Fig. 5.3(b) and Table 5.3 respectively while the coil design is given in Section 5.4.

A total of 11 channel section assemblies were built for the experimental programme and details of their dimensions, wall materials and electrode mountings are given in Table 5.4. In all cases, the section length was 2 ft and the electrodes were normally mounted 18 in from the entry end to ensure the establishment of a truly two-dimensional flow pattern in the flowmeter region. Both electrically insulating and conducting materials were used and in the latter case nickel-plated copper and stainless steel served to produce wetting and non-wetting conditions respectively with mercury. Channels with rectangular cross-sections were assembled from sheet material, the component parts being carefully machined to ensure accuracy and constancy of the internal dimensions.

When section changers were necessary, they were formed from glass or nickel-plated copper and all joints were made with short lengths of rubber hose, clamped to prevent leakage.

It was judged to be important for the successful correlation of theory with experiment that, when separate electrodes were used and mounted in the channel wall, they should be exactly flush with it. To achieve this condition and also to enable a good determination of the inter-electrode distance to be made, the following procedure was adopted. The electrodes were first assembled to project slightly beyond the inner channel wall and, in the case of circular channels, the tube was carefully bored and reamed to finish the electrodes flush with the wall and establish the value of r_i. For rectangular sections, the electrodes were machined flush with their mounting wall before assembly of the channels and the dimensions 2a and 2b were measured with an internal micrometer.

Experimental investigation of the input circuit arrangements using channel section Cl (see Section 6.3) indicated a need for thorough shielding against stray electric fields. This was accomplished by surrounding all channel sections made from insulating material with aluminium foil and connecting this to the shield of the amplifier input cable. The electrode connections to this cable were enclosed in a small shielding can and contact was made with the liquid column at each end of the test section. The complete magnet and channel section assembly was enclosed in a box made from $\frac{1}{4}$-in thick aluminium sheet and this was also connected to the cable shield. To minimise circulating currents due to flux linkage of the shielding system, the channel section was insulated from the external shielding at the points where it passed through the latter. The appearance and layout of a typical complete assembly, including shielding arrangements,

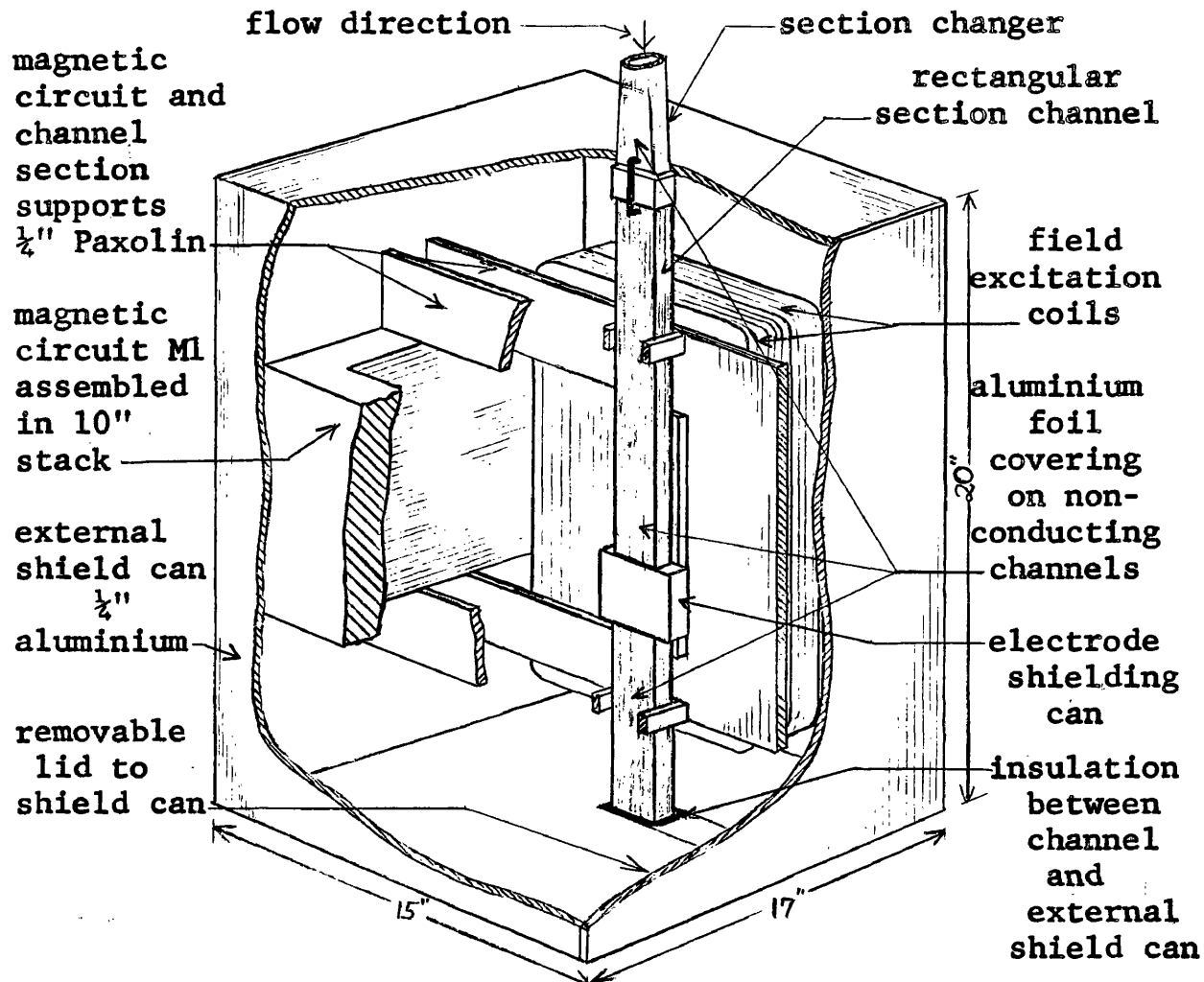**Fig. 5.4. Cut-Away View of Typical Magnetic Circuit and Flow Channel Assembly**

(a) Type A (circular)

(b) Type A (rectangular)

(c) Type B (rectangular)
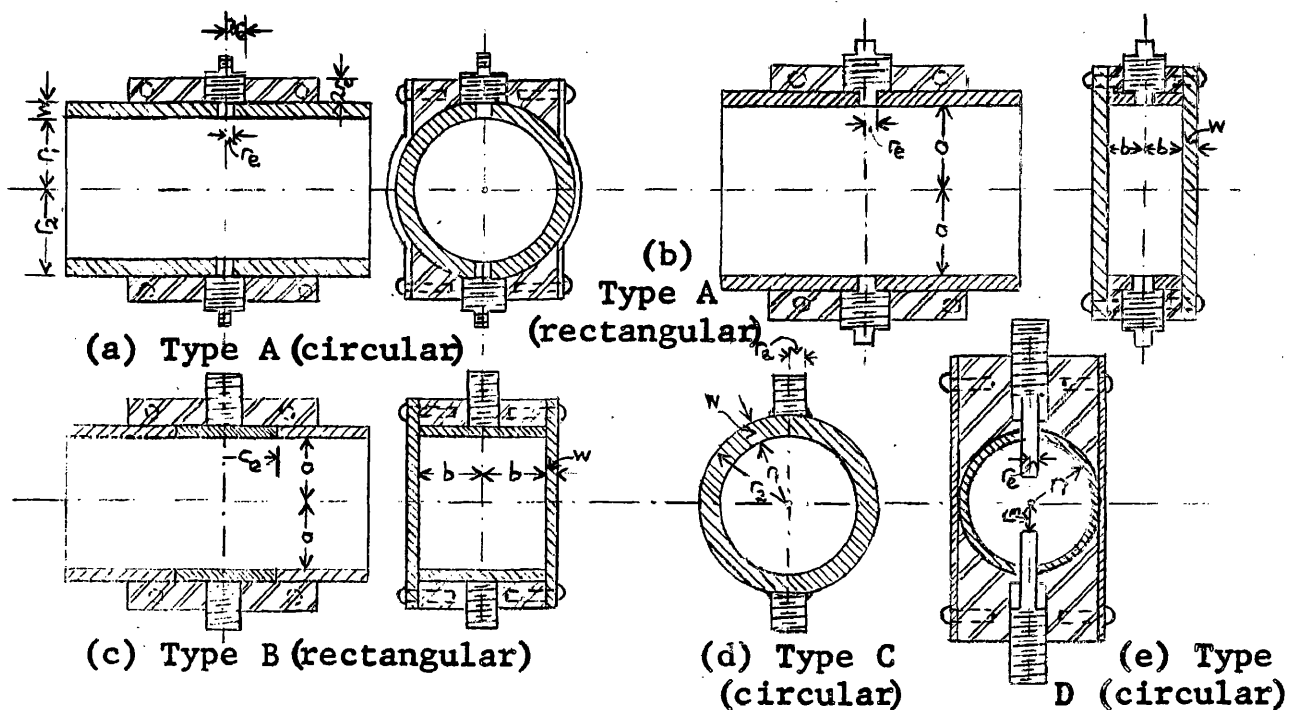
(d) Type C (circular)

(e) Type D (circular)

Fig. 5.5. Cross-Sectional Views of Channel Assemblies through Electrodes

is sketched in in Fig. 5.4 where a rectangular section is
shown in position between the magnet pole faces while details
of the channel and electrode assemblies appear in Fig. 5.5.

5.4. Magnetic Field Excitation Supplies

The excitation current for the magnetic field was taken
from a d.c. generator for time-invariant conditions and from
the local mains supply for 50-c/s a.c. operation. To handle
other frequencies and for pulsed excitation, a power amplifier
was designed and built to work into the matched coils of
magnetic circuit M2. In all cases, the constancy of exciting
current was maintained by manual adjustment to correct for
supply voltage fluctuations and changes in coil resistance due
to heating, "Variac" auto-transformers being used with the
50-c/s a.c. supply.

For d.c. and a.c. mains supply operation, the individual
coils were connected in a series-parallel grouping appropriate
to the exciting current required but only series connection
could be employed with the power amplifier because of the
limitations imposed on the peak exciting current by the KT66
valves used. For sinusoidal operation, the use of a series
capacitor for power factor correction proved helpful in
obtaining the required exciting current, particularly with
the power amplifier.

The presence of harmonics in the 50-c/s a.c. mains proved
troublesome in certain phases of the experimental work as is
discussed in Chapter 6. The method adopted to eliminate these
harmonics was to place a filter of novel design between the
coils and their supply. This filter comprised two "bridged-T"
sections connected in cascade to reject completely the 3rd
and 5th harmonics and to provide substantial attenuation of
all higher-order components. Design details and performance
characteristics are given in Appendix II.

The production of the pulse waveform of Fig. 1.3(a) requires an exciting current rise time of not more than about 10% of the pulse duration if the necessary flat top is to be produced. A straightforward method of obtaining an approximately rectangular current pulse in an inductive load employs a tetrode valve power amplifier with an appropriately shaped pulse signal applied to its input. The relevant circuit model for a preliminary discussion is given in Fig. 5.6 where r_a, R_f and L_f are respectively the valve slope resistance, coil resistance and coil inductance. Recalling that the current in this circuit attains 86.5% of its maximum value after two time constants when the excitation is a voltage step function, a criterion for satisfactory performance can be stated as

$$\frac{2L_f}{r_a + R_f} = \frac{1}{20f_o} \qquad (5-5)$$

where f_o is the repetition frequency of the pulse waveform. The inductance of an iron-cored coil is given by

$$L_f = \mu T^2 A_g / l_g \qquad (5-6)$$

where A_g is the effective air gap area and the reluctance of the iron path has been neglected. The maximum value of T allowed by the rise time restriction is immediately obtained from 5-5 and 5-6 as

$$T_{max} = [\frac{(r_a + R_f)l_g}{40f_o \mu A_g}]^{\frac{1}{2}} \qquad (5-7)$$

Rearrangement of 5-4 and substitution in it of this expression for T_{max} yields that the peak flux density available is

$$B_{o(max)} = \frac{I_c}{k_f}[\frac{(r_a + R_f)\mu}{40f_o A_g l_g}]^{\frac{1}{2}} \qquad (5-8)$$

Using a channel of 3/8-in internal diameter, the minimum dimensions for the magnetic circuit are of the order l_g = 5/8 in, w_m = 3/4 in and l_m = 3/4 in and a reasonable value of A_g

which allows for the fringing field is $A_g = 1$ in^2. Typical operation of a KT66 tetrode valve from a 300-V anode supply can attain a peak current of about 250 mA with an anode load of 1000 Ω and has $r_a \simeq 60$ kΩ. Substitution of these values in 5-7 and 5-8 for $f_o = 50$ c/s and $k_f = 1.5$ gives the corresponding numbers for T_{max} and $B_{o(max)}$ as 24600 turns and 0.325 Wb/m^2 respectively. The value of $B_{o(max)}$ can be further improved by using additional valves in parallel but the increase in I_c is offset by a reduction in $r_a + R_f$ to make the net gain proportional to the square root of the number of parallel valves provided $r_a \gg R_f$.

These calculations indicated that the power amplifier scheme would give useful values of $B_{o(max)}$ in a frequency range up to at least 200 c/s and provided a basis for magnetic circuit design. The amplifier circuit consisted of two pairs of KT66 valves connected in a push-pull arrangement and driven by a pair of cathode followers to enable the grids of the power valves to be driven positive. A phase-splitter amplifier completed the circuit which is given in Fig. 5.7. Circuit time constants were chosen to locate the lower and upper half-power frequencies at 5 c/s and 20 kc/s. The amplifier input was derived from a commercial variable frequency oscillator (Advance type J1) capable of providing both sinusoidal and square wave signals. In the latter case, it was found that the inclusion of a phase advance network in the amplifier input improved the flatness of the top of the flux waveform, the transmission characteristic of this network being adjusted to give the most satisfactory performance at each repetition frequency. The power valves were operated in class B for pulse excitation but, for sinusoidal time variation of the magnetic field, it was necessary to use class AB operation to keep waveform distortion to an acceptable level.

The magnetic circuit was assembled from 0.005 in lamina-
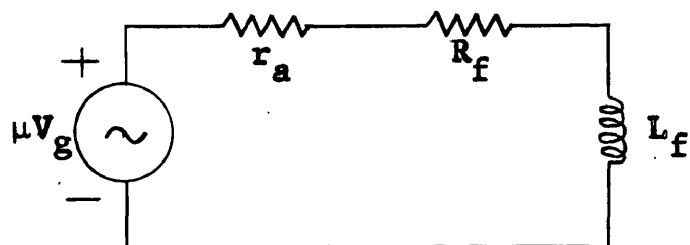
Fig. 5.6. Circuit Model for Power Amplifier Discussion
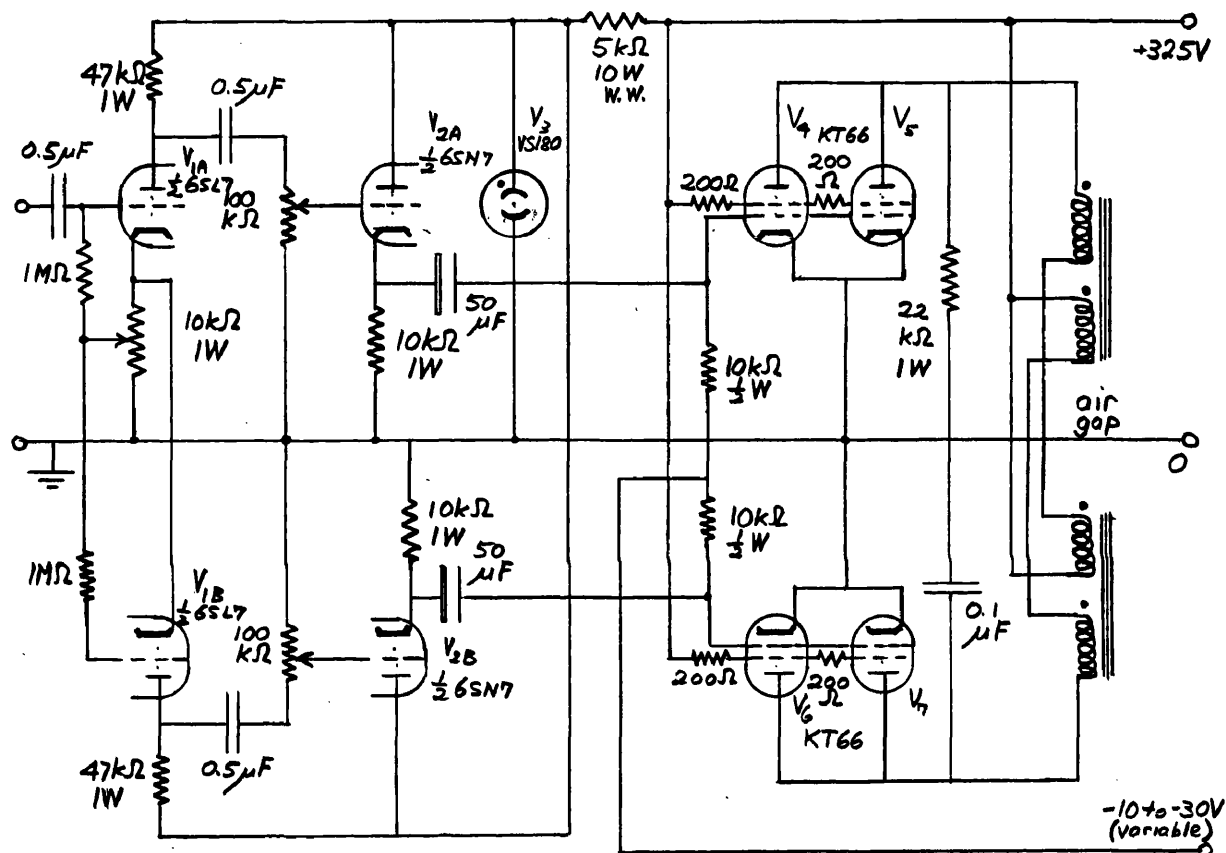
all resistors ¼W, 20% carbon except as noted

Fig. 5.7. Power Amplifier Circuit Diagram

Effective Field Coil Turns (½ of total)	Peak Excitation Current mA	Peak Flux Density Wb/m^2	Maximum f_o for Useful Flat Top to Pulse c/s
19000	470	0.42	140
9500*	470	0.22	520
4250*	470	0.11	1050

* series resistance added to restore anode load to matched value

Table 5.5. Power Amplifier Performance for Pulsed Excitation

tions to minimise iron losses and each of the four coils was wound with 9500 turns of 28 s.w.g. wire, tapped at 4250 and 2125 turns. Paper insulation was used between winding layers and each coil was fully impregnated to eliminate the risk of voltage breakdown. A series RC combination was connected between the valve anodes to make a resonant circuit with approximately critical damping, eliminating both ringing in the pulse top and high reverse voltages on the trailing edge. Additional capacitors were connected in series with the field coils when power factor correction was required with sinusoidal excitation. Data on this magnetic circuit M2 has already been given in Fig. 5.3(b) and Table 5.3.

The performance of the power amplifier was rather better with respect to rise time than was assumed above and it proved to be possible to obtain a useful flat top in the waveform up to f_o = 140 c/s at the maximum attainable value of B_o. Use of the coil tappings raised the limit on f_o at the expense of a reduced $B_{o(max)}$ as detailed in Table 5.5. With sinusoidal excitation, operation at $B_{o(rms)}$ = 0.27 Wb/m^2 was acheived up to f_o = 60 c/s but above this value a reduction in B_o was necessary to avoid excessive coil voltages.

5.5. Amplifier Input Stages and Capacitance Neutralisation

The amplifier input stages for time-varying magnetic field conditions comprised a double-triode pre-amplifier and a special input cathode follower circuit of exceedingly high input impedance for use with high-resistivity liquids (ρ > 10^2 Ω-m). The double triode section had a push-pull circuit for tests with a differential input stage but the input cathode follower, which included an input capacitance neutralisation arrangement, was constructed for use with an unbalanced flow signal only. The input stage for tests with d.c. field excitation consisted of a 50-c/s mechanical

chopper and its associated transformer.

Design of the double-triode stage to conform to the system pass band followed standard procedures (Ref. 146), the complete circuit being shown in Fig. 5.8. Provision was made for the injection of a transformer e.m.f. balancing signal via the grids of the second pair of triodes. All valve sockets incorporated anti-microphonic mountings and the valves were enclosed in shield tubes. The overall mid-band gain was measured using a calibrated attenuator and found to be 26.4 db while the input impedance was represented by approximately 3 MΩ in parallel with 15 $\mu\mu$F.

The high input impedance cathode follower was based on a design by Lettvin et al (Ref. 147) for biological work where source impedances of the order of $10^8 \Omega$ are encountered. The circuit was stabilised with three feedback loops to obtain a gain of 1.00 ($\pm$ 0.1%) and a d.c. input resistance greater than $10^{13} \Omega$ was achieved through grid current cancellation. A fourth feedback loop provided an adjustable negative Miller capacitance to hold the total input capacitance to less than 0.1 $\mu\mu$F over a 20-kc/s bandwidth when the capacitance to be neutralised did not exceed 50 $\mu\mu$F. Details of the design and operation of the circuit are given in Ref. 147 and the circuit diagram appears in Fig. 5.9. It was necessary to allow the residual grid current to flow in the input circuit but it was judged that the low value of this ($<10^{-13}$ A) would have a negligible effect on flowmeter performance.

5.6. Transformer e.m.f. Rejector

When the flowmeter channel section is located so that the electrode axis passes through the centre of the air gap field, the maximum obtainable value of V_t occurs if the conductors of the input circuit are oriented to link a magnetic flux $\phi_i/2$. In principle, the winding of a single-turn coil on the
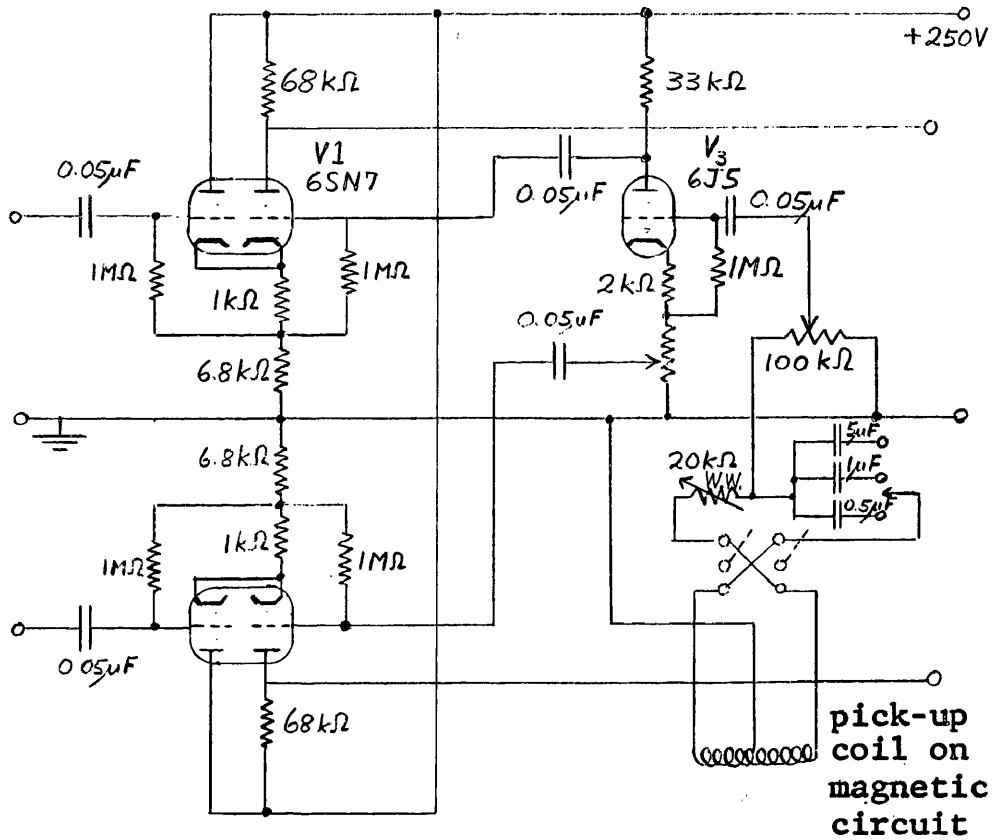
all resistors 1W, 20% carbon except as noted

Fig. 5.8. Double-Triode Pre-Amplifier and Transformer e.m.f. Rejector
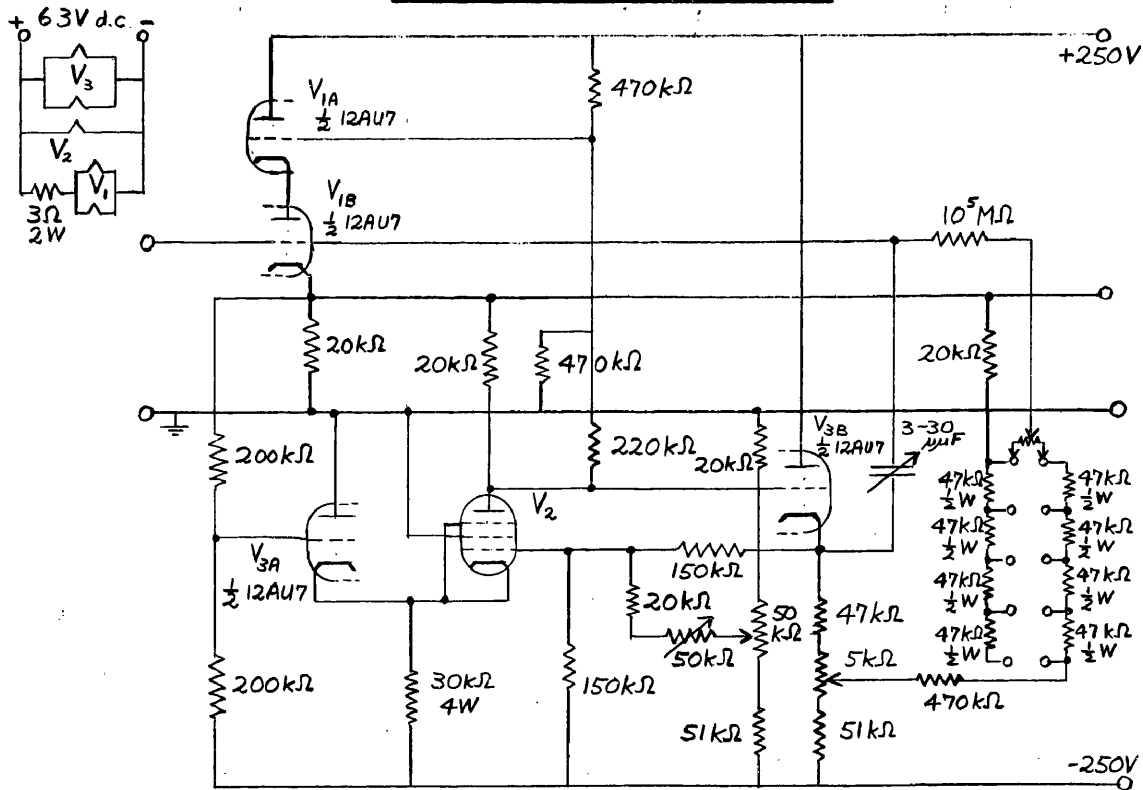
Fig. 5.9. High Input Impedance Cathode Follower

magnetic circuit to link the same flux would provide exact cancellation of V_t but with sinusoidal excitation it is convenient to have some control over the magnitude and phase of the balancing signal to correct for non-uniformities in the magnetic field. In addition to balancing V_t, there is the possibility of cancelling other unwanted signals (e.g. capacitance-coupled) at the excitation frequency.

In the experimental system, the balancing signal was obtained by winding a centre-tapped, 20-turn auxiliary coil on the magnetic circuit and it was passed through a constant-amplitude phase-shift network before being applied to the second pair of grids of the double triode pre-amplifier as shown in Fig. 5.8.

Rejection of the transformer e.m.f. was also achieved by the alternative metod of positioning the input circuit conductors in the manner indicated in Fig. 5.10. The connections between the electrodes and the input screened cable were made with 16 s.w.g. wire and adjustment for optimum rejection was made by finally positioning these connections with the channel section installed in the magnetic field.

5.7. Frequency-selective Amplifier for Noise Reduction

It has already been pointed out in Section 4.5. that the output of an electromagnetic flowmeter has the form of a double-sideband, suppressed carrier signal. Accordingly, a useful reduction in system noise can be obtained by the inclusion of a filter with a pass band sufficient only to handle the sidebands corresponding to the highest time rate of change of velocity. In the range of excitation frequencies employed, the parallel-T feedback amplifier scheme (Refs 148 and 149) can be used to provide the required characteristic and may be stagger-tuned to obtain sufficient bandwidth (Ref 150). However, it cannot be used with pulsed excitation where

electrode   electrode   screened cable
mount   shield can   to amplifier

channel
section

adjustable
conductor

views in direction X
with
can side removed

(a) for unbalanced amplifier operation
    (circular channel)

X

(b) for balanced amplifier operation
    (rectangular channel)
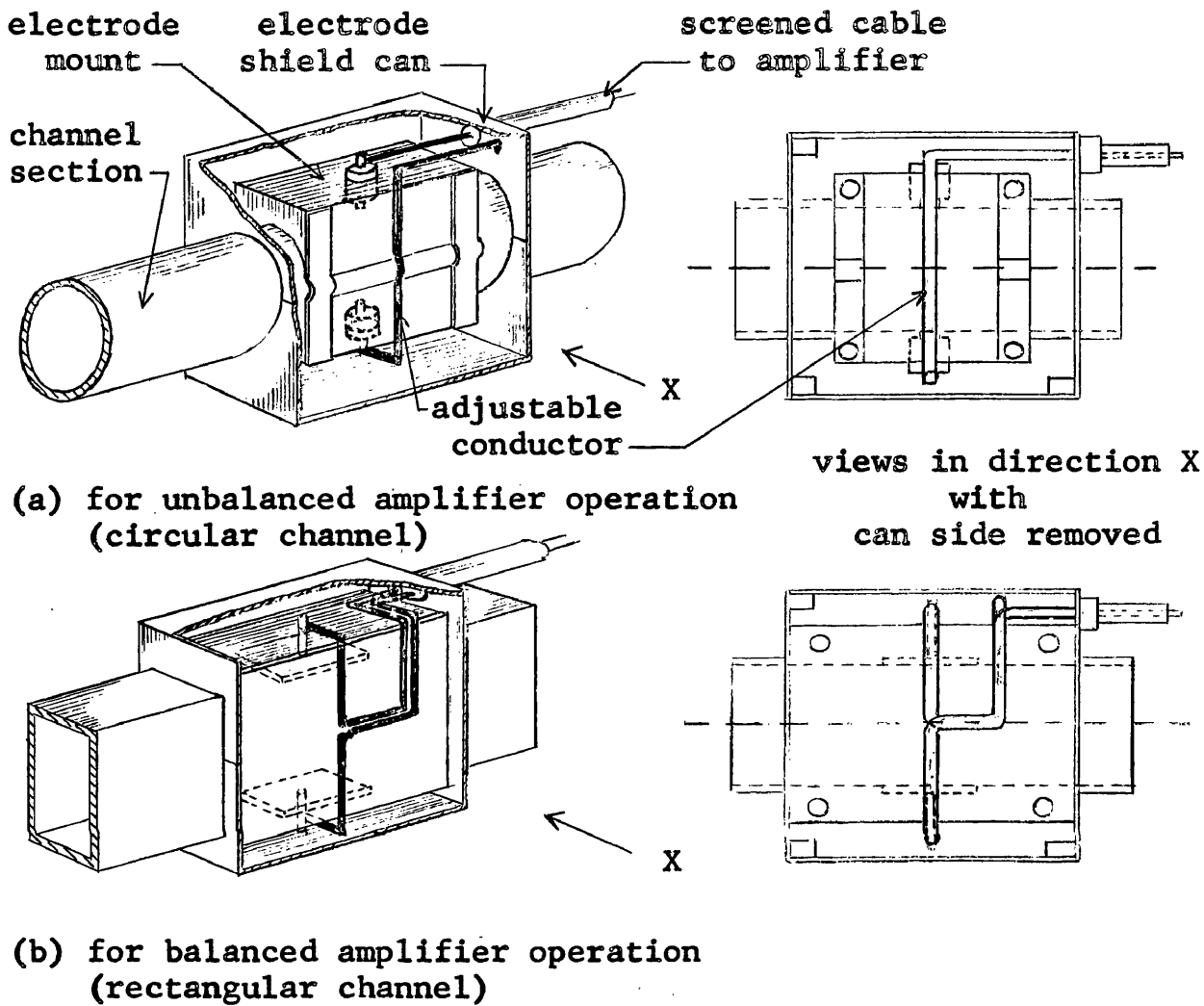
Fig. 5.10.   Transformer e.m.f. Rejection by Input
              Conductor Positioning

all resistors
½W, 20% carbon
except as noted

R = 1M, 1%
C selected for
frequency from

$$C = \frac{1}{2\pi f} \mu F$$

250V

330kΩ

V_1
6SN7

47kΩ
1W

0.2μF

0.2μF

0.2μF

1MΩ

1MΩ

R   R

C
R/2

C
2C

12kΩ
1W

50kΩ

8μF

Fig. 5.11.   Frequency-Selective Amplifier

preservation of the rectangular pulse shape is desired.

For the experimental investigation of Chapter 6, a single-stage, double-triode circuit was found to be adequate. It was designed following Ref. 149 and was constructed with the circuit of Fig. 5.11 to be adjustable over the frequency range from 10 c/s to 1 kc/s. The stage provided a centre-frequency gain of 24 db, a Q-factor of 5.6 and a second harmonic rejection of better than 18 db.

5.8. Main Amplifier

Calculations in Section 5.2. have shown that the value of V_m for the transition velocity in the experimental system may be as low as about 100 μV and hence the main amplifier should be capable of handling signals down to 10 μV for a reasonable laminar flow range. The detector circuits described in the next Sections were designed to operate with an input signal of 10 V and this established the overall amplifier require-ments to be a gain of 100 db with a 5-c/s to 20-kc/s pass band. While a total of about 57 db of gain was available from the double-triode pre-amplifier and the frequency-selective amplifier, provision had to be made for operation with the input cathode follower only and thus a maximum gain of 100 db was required from the main amplifier.

Three similar amplifiers were constructed and used either singly or in cascade as required. Each amplifier comprised the three-stage feedback circuit shown in Fig. 5.12 wit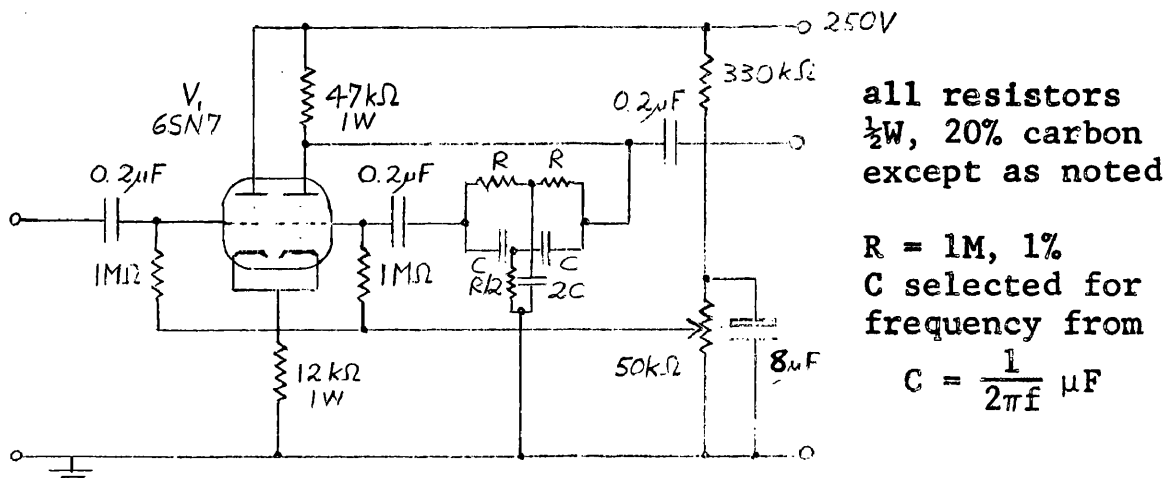h staggered time constants to obtain stable operation at a mid-band gain of 32 db with half-power frequencies at 3.2 c/s and 28.6 kc/s. Low-noise EF37A valves were used in each stage of one of the amplifiers and in the first stages of a second while anti-microphonic valve mountings were used throughout. Both the valve heater and h.t. supplies were obtained from batteries to eliminate hum voltages and the degree of

negative feedback applied (32 db) gave adequate gain stability against drift in these supplies. The r.m.s. value of the noise signal referred to the input with the three amplifiers in cascade (low-noise valves at the input end) was 3.5 μV for an input source resistance of 10 kΩ.

5.9. Detector for Sinusoidal Excitation

A simple phase-sensitive detector was used to provide further discrimination against the transformer e.m.f. and was built to the circuit diagram of Fig. 5.13. An operating signal level of 10 V was chosen and for all experiments the gain of the amplifiers was adjusted to provide this value. The reference signal was derived from a second auxiliary winding on the magnetic circuit and shifted in phase by 90° by means of a constant amplitude phase-shift network. The double-triode cathode follower driver stage was included to allow balanced operation throughout the amplifying system. With a 10-V anode-to-anode signal on the detector diodes, the discrimination against V_t was 35 db when the output was measured using a d.c. valve voltmeter.

5.10. Detector for Pulsed Excitation

The detector in this case used the diode gate circuit shown in detail in Fig. 5.14. The double diode was driven by cathode followers and the gate was held in the closed position by connecting the cathode of the diode V_{2B} to a negative line. The gate control pulse was derived from the power amplifier drive through an integrating and delay network which allowed any part or all of the positive-going signal available at the cathode of V_1 to be examined. The detector output was measured on a peak reading valve voltmeter and the waveform monitored using a cathode-ray oscilloscope (Cossor Model 1035).

all resistors ½W, 20% carbon except as noted
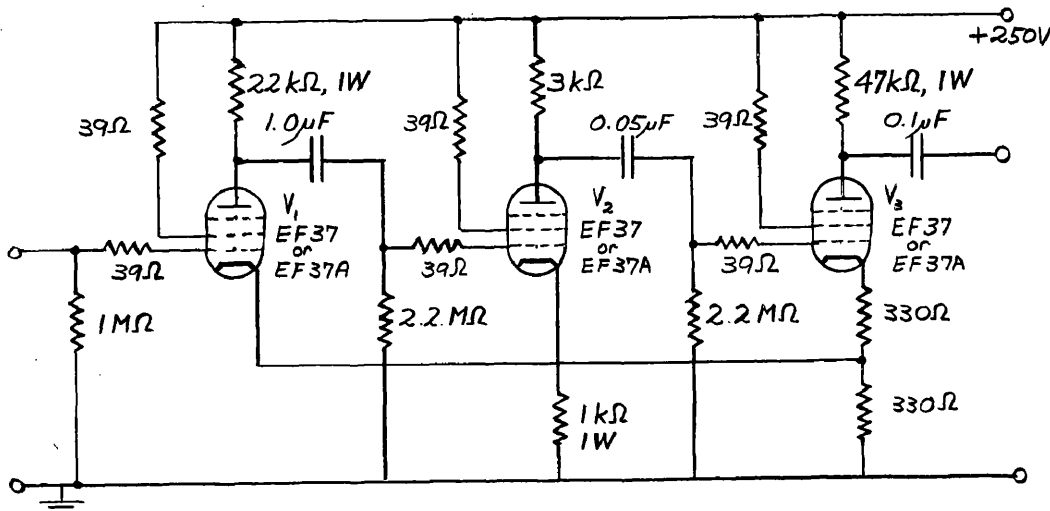
Fig. 5.12.   Main Amplifier Circuit
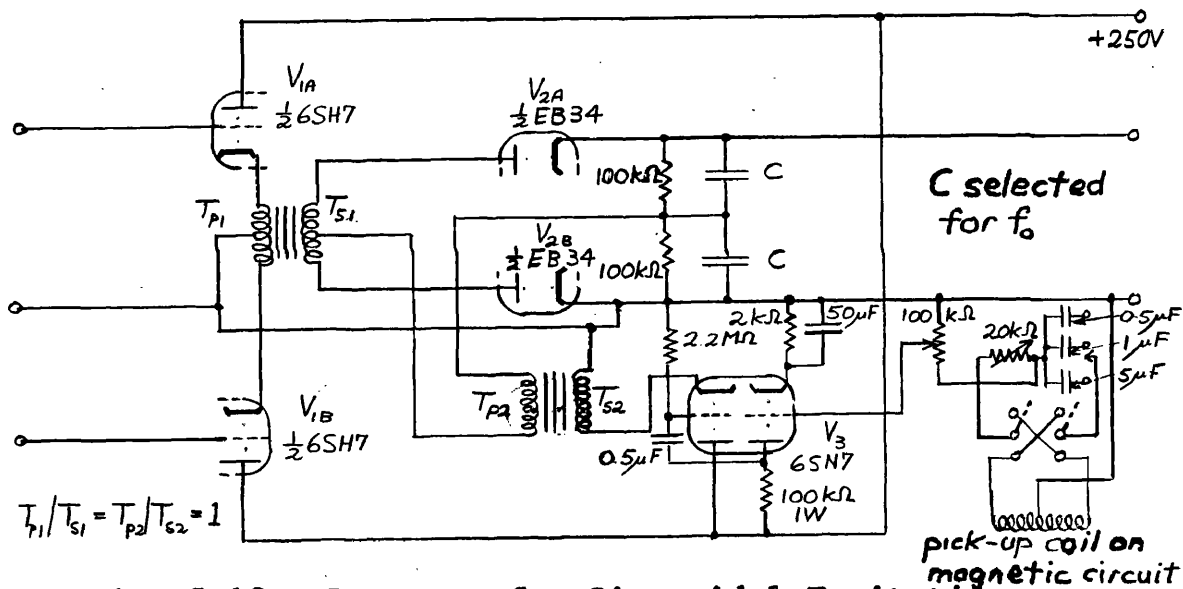
Fig. 5.13.   Detector for Sinusoidal Excitation
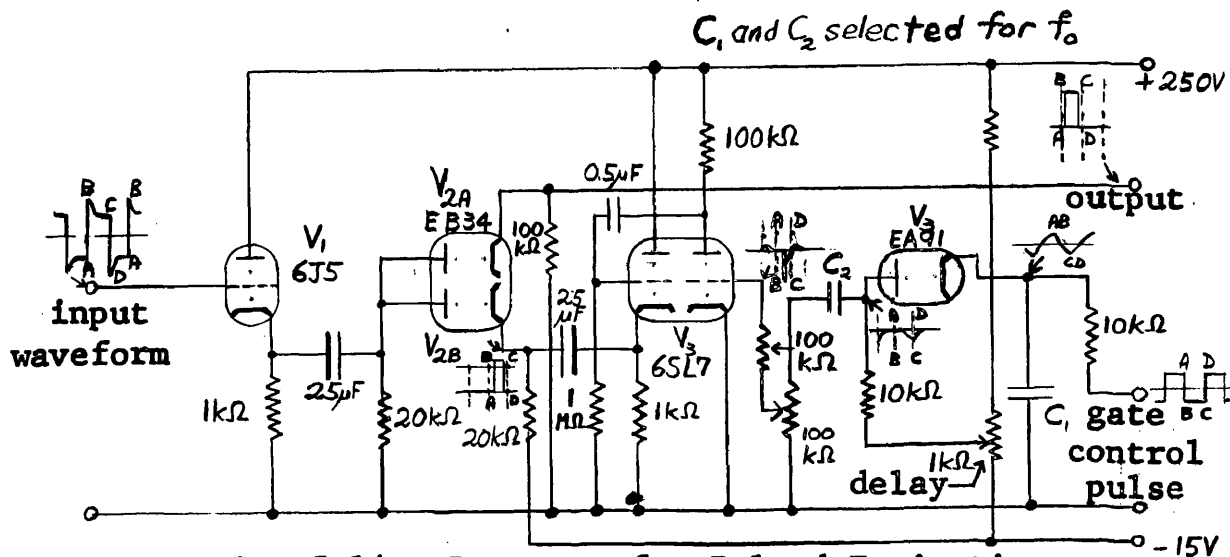
Fig. 5.14.   Detector for Pulsed Excitation

Chapter 6

EXPERIMENTAL INVESTIGATION

6.1. Objectives

The main purpose of the experimental investigation reported here was to secure a sufficiently wide range of data for the detailed evaluation of the design and performance of the contact type of electromagnetic flowmeter. The work was undertaken in three stages in the following order which has been adhered to in preparing the Chapter:

(1) An investigation of input circuit arrangements for rejecting the transformer e.m.f. and stray effects with time-varying magnetic field excitation;

(2) A comparative study of d.c., a.c. and pulsed field excitation over a wide range of liquid conductivity in the absence of significant magnetohydrodynamic effects;

(3) The calibration of several flowmeter arrangements with wall conductivity and velocity profile distortion effects, the latter including those of magnetohydrodynamic origin.

Certain measuring techniques which were used throughout are first considered and the procedure in each test is then given. For later reference, the tests are numbered consecutively and the results derived from them are presented together at the end of the Chapter.

The experimental system in all tests was of the form indicated by Fig. 6.1., units being selected to give the performance appropriate to the particular situation. Reference to it is accordingly limited to special requirements and to features not mentioned in Chapter 5.

6.2. Measurement Techniques

The quantities which it was necessary to measure at all

stages of the experimental programme were: (1) the output
signal from the flowmeter; (2) the magnetic flux density;
(3) the volume flow rate Q of the test liquid; (4) liquid
conductivity; (5) the flowmeter output impedance, Z_o; and
(6) dimensions of the channel section and magnetic circuit
air gap. The procedures with respect to items (3) and (6)
have already been given in Sections 5.2 and 5.3 respectively.

Although great care was taken to ensure the short-term
stability of the amplifier gain, this quantity was not meas-
ured directly. Values of V_o were obtained by the low-level
attenuation method using a calibrated attenuator. To achieve
satisfactory operation of the detectors, the gain of the
amplifiers was adjusted to provide a signal of about 10 V
(peak) at the detector and waveforms were at all times
monitored to guard against waveform distortion. The estimated
accuracy of the method ranged from 3 per cent with V_o of the
order of 10μV to better than 1 per cent for V_o above 100μV.
Where r.m.s. values of non-sinusoidal waveforms were required,
the a.c. detector was replaced by an instrument with a square
law characteristic.

The magnetic flux density for each magnetic circuit was
measured for d.c. excitation using a commercial (Cambridge)
fluxmeter, the relation between the value of B_o at the centre
of the air gap and the excitation current being obtained to
better than 2 per cent accuracy. For time-varying excitation,
a 10-turn coil of 1 cm^2 area was located in the air gap
between one of the magnet pole faces and the channel section.
The output of this coil was applied to a simple resistance-
capacitance integrating circuit to obtain directly the value
of the time varying flux, and hence of B_o, to an estimated
accuracy again of 2 per cent.

The conductivity of liquid mercury was taken from standard
tables (Ref. 153) but the conductivity of electrolytic

solutions was measured using a commercial bridge (Electronic
Switchgear Type MC1) designed specially for this purpose and
operated at a frequency of 1 kc/s. Output impedance measure-
ments for electrolytes were made using a standard impedance
bridge (General Radio Type 714).

The method adopted for measuring the volume flow rate was
least accurate at high values with mercury due to the limited
amount of that liquid which was available. The duration of
a liquid run was measured by a timer actuated by a mercury
switch mechanically coupled to the flow control lever. By
careful adjustment of the setting of this switch, the uncer-
tainty in time measurement was reduced to 1/5 sec to give a
minimum overall accuracy of 5 per cent and of better than 0.5
per cent for liquid runs of 1 min or more.

6.3. Investigation of Input Circuit Arrangements

(a) General Comments

The importance of input circuit conditions in establishing
the overall performance of electromagnetic flowmeters has
already been indicated in Chapter 4, yet previous investiga-
tions have not included the experimental data necessary to a
detailed comparison of the methods available. To enable
subsequent stages of the experimental work to be carried
through satisfactorily, it was deemed appropriate to deal with
this first.

The analysis and discussion of flowmeter parameters in
Chapters 3 and 4 have shown the dependence of Z_o on the
channel dimensions. As the actual flow-induced voltage is not
of concern here and a change in Z_o can be obtained using
liquids of different conductivities, one channel section and
magnetic circuit sufficed for this work. These were respec-
tively circular cross-section channel C1 (Table 5.4) and
magnetic circuit M2.

Apart from electrolytic polarisation effects at the electrodes with d.c. excitation (these have been treated quite fully by Kolin, Refs 71, 72 and 77), sinusoidal excitation is adequate for the study of all circuit problems in this basically linear system. It was used throughout these tests, being derived from either the 50-c/s supply mains or the power amplifier. The phase sensitive feature in the detector circuit was disconnected to ensure equal sensitivity to all components of V_o.

Four liquids; mercury, sodium chloride solution, tap water and distilled water were used to give a conductivity range from $10^6 \mho/m$ to less than $10^{-4} \mho/m$. The excitation frequency was varied over the range 20 c/s to 1 kc/s and magnetic flux densities up to 0.1 Wb/m^2 were employed.

This phase of the work involved five related objectives:

(1) Determination of the relative effectiveness of capacitance-coupled voltage elimination using (a) the transformer e.m.f. balancing arrangement proposed by Kolin (Ref. 86), (b) a balancing signal derived specially for this purpose in the manner of Hogg et al (Ref. 104), and (c) a metallic shield as described in Section 5.3;

(2) Comparison of the Kolin and Eindhorn (Refs 79 and 82, respectively) methods of transformer e.m.f. rejection;

(3) Measurement of the magnitude of unwanted noise and its dependence on system bandwidth, magnetic flux density and excitation frequency;

(4) Comparison of balanced and unbalanced amplifier operation;

(5) Examination of contact effects.

(b) **Test Details**

(1) **Test 1. Elimination of Capacitance-Coupled Voltages**

For this test, channel section C1 was stripped of all

metallic shielding and, using tap water and carbon electrodes[1], V_o was measured before and after cancellation of capacitance-coupled voltages at the excitation frequency. The balancing signal was derived from either the transformer e.m.f. rejector or from a separate source, capacitance coupled directly to the electrode terminals. Measurements were made, with both balanced and unbalanced amplifier operation and the external screening can in position, for $B_o = 0.075$ Wb/m^2 and $f_o = 50$ c/s and 200 c/s. In the case of excitation using the 50-c/s mains supply, the effects of (a) including the bridged-T filter and (b) removing the external screening can were also recorded.

Details of the flowmeter input circuit for unbalanced conditions are given in Fig. 6.1; those for balanced operation differed only in earthing connections. To avoid inclusion of the effect of V_t in the values of V_o obtained, the channel was first filled with mercury and the input conductors adjusted to obtain a minimum in V_o. This procedure eliminated inductively voltages in liquids of any conductivity.

Results of a typical test sequence are tabulated in Table 6.1, together with ratios showing the degree of rejection achieved and its level with respect to V_m calculated from equation 1-2 for $u_o = 10$ cm/sec. For ease of comparison, this information is also displayed in Fig. 6.4.

(2) Test 2. Dependence of V_t, noise and residual harmonic components on method of transformer e.m.f. rejection, liquid conductivity, frequency, flux density and system bandwidth.

The metallic shielding was restored to channel section C1 and, for both balanced and unbalanced operation with power amplifier excitation, readings were taken to establish the above relations over the ranges of f_o, B_o and σ stated earlier.

---

1. Modified "Variac" auto-transformer brushes were found to be satisfactory for this purpose.

The overall system bandwidth was reduced by inserting the selective amplifier when required.

To simulate the situation with Kolin-type rejection in which V_t would normally reach its maximum value, the input conductors were oriented in such a manner as to be linked by approximately one-half of the total magnetic flux. In these circumstances, a drift of zero after balancing was noted both with water and electrolytic solutions, the rate of this decreasing slowly with time. The factors responsible for this drift were examined in a later test and, for the present measurement, it was found that the use of freshly cleaned electrodes reduced the effect to negligible proportions.

Separation of the residual value of V_o into components due to random noise and harmonic components of the excitation frequency was accomplished by turning off the field supply and measuring the former alone. Where random fluctuations predominated, it was observed that these did not depend on B_o and this was assumed to apply in all cases. Amplifier noise was obtained separately and subtracted from overall values to yield the true noise generation in the flow channel.

Fig. 6.5 gives the performance observed under balanced amplifier operating conditions and includes the value of V_t calculated for equation 1-12. Results for unbalanced operation showed agreement generally within the limits of experimental accuracy and are not presented separately.

(3) Test 3.   Small-signal flowmeter output impedance

To obtain information on the nature of the flowmeter output impedance in the case of electrolytic solutions and without introducing either non-linear contact effect or irreversible changes at the electrode surfaces, the small-signal value of Z_o was measured as a function of frequency using a voltage which did not exceed about 50 mV. As this impedance may depend strongly on impurities and be likely to

vary widely in apparently similar situations, measurements were confined to the electrode-liquid combinations used in the experimental programme and, to minimise time dependent effects, freshly cleaned electrodes were used.

R_o and X_o, respectively the series resistance and capacitive reactance components of Z_o, as measured for carbon electrodes in tap water and platinised platinum electrodes in NaCl solution are given in Figs 6.6 and 6.7. On the assumption that the measured series resistance tends to the value of the effective spreading resistance as the frequency is raised, values of barrier resistance and capacitance were calculated in both cases and added to the plots of measured data. It is to be noted that both Figs 6.6 and 6.7 give the results for two barriers in series.

(4) <u>Test 4. Drift of zero balance</u>

The drift of zero balance with the transformer e.m.f. rejector observed in Test 2 was most marked immediately after circulation of the test liquid and required that the electrodes be in contact with the liquid for a period of at least 6-8 hours. Measurements of the values of V_o and Z_o over a period of 3 hours immediately following rapid circulation of the liquid for 30 min were made using the same liquid-electrode combinations as in Test 3. Adjustment of the e.m.f. rejector was made at the beginning of the measurement period to ensure exact cancellation of V_t.

The change ΔV_o in V_o and in the series resistance component of Z_o are given in Fig. 6.8, together with the value of ΔV_o calculated from the measured values of V_o and R_o and using the circuit model of Fig. 6.2. Further tests indicated that (a) the drift was independent of B_o and (b) no drift occurred when the liquid was in motion. The procedure in the latter case was to establish a constant flow rate and then to use the V_t rejector to balance out both V_t and V_m.

(c) <u>Input Circuit Arrangements in the Remaining Tests</u>

Tests 1 and 2 demonstrated the clear superiority of careful shielding and input conductor positioning as the methods for eliminating unwanted voltages in the input circuit. It was found, however, that extremely precise manipulation of the balancing conductor(s) was necessary to achieve complete V_t rejection. A compromise arrangement, which proved to be both convenient and satisfactory, was used when required. With this, an approximate balance (say to 100 μV) was first obtained and further elimination of V_t was provided by the e.m.f. rejector and/or the phase-sensing character of the detector.

6.4. Methods of Magnetic Field Excitation

(a) General Comments

The alternative methods of magnetic field excitation were next examined and the mimimum detectable flow signal was also determined. The use of d.c. excitation was confined to mercury but the other two methods were applied to all of the liquids listed in Section 6.3. In addition, specially pure distilled water ($\sigma \approx 0.5 \times 10^{-4}$ U/m) was used to determine the lowest conductivity for which a flow signal could be obtained and also to demonstrate the existence of the dielectric polarisation effect.

Magnetic circuit M2 was again employed and, as $c/a = 1.2$ in this case, significant end effects were obtained. To avoid any significant magnetohydrodynamic effects in mercury, the flux density was held to the low value of 65 mWb/m^2 (M = 8.2 with channel Cl). Using equation 3-52, this gives a laminar flow entry length of about 3 m at the transition Reynolds number. Circular channel section Cl and square section C4 were used, except for the demonstration of dielectric polarisation, for which rectangular section C7 proved to be most effective.
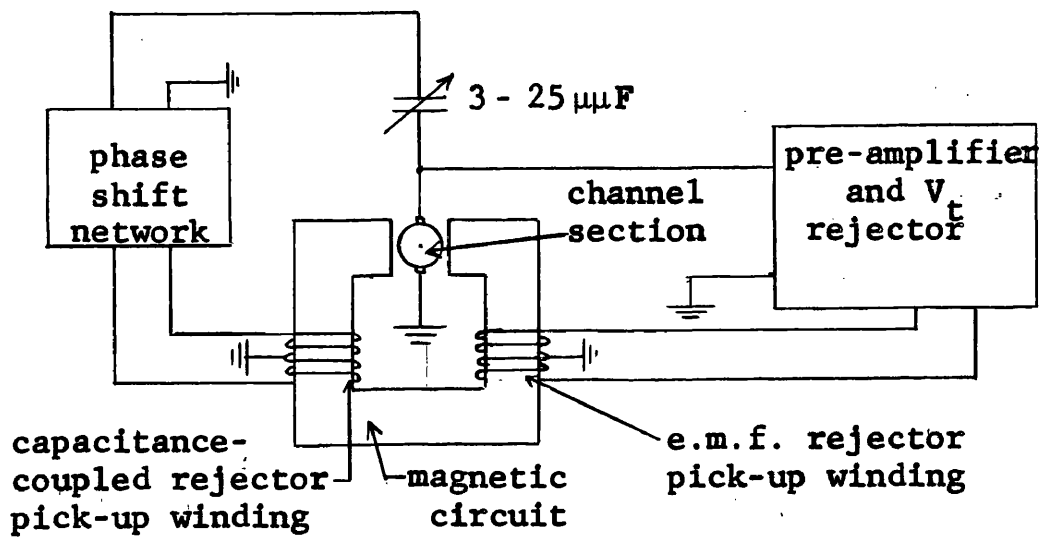
Fig. 6.1. **Input Circuit Arrangements for Capacitance-Coupled**
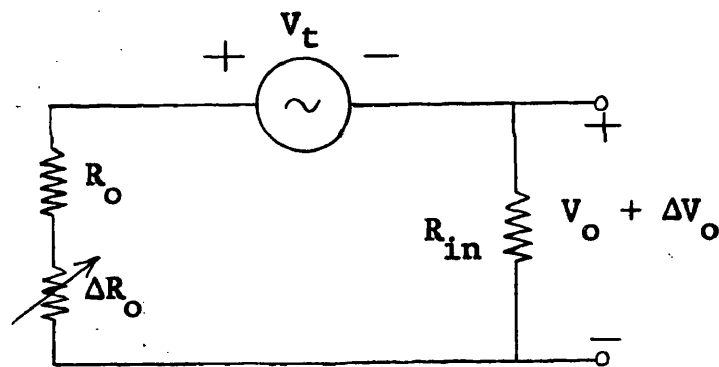
Voltage Elimination Tests

Fig. 6.2. **Circuit Model for Drift Calculations**

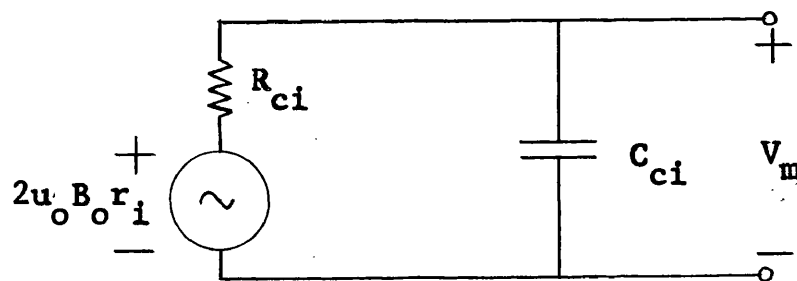**Fig. 6.3.** **Circuit Model for Dielectric Polarisation Calculations**

(b) <u>Test Details</u>

(1) <u>Test 5.   Calibration of a non-conducting circular</u>
<u>channel using mercury</u>

The measured values of V_o for excitation using d.c., a.c.
at 50 c/s and 1000 c/s and pulsed conditions at 50 c/s and 200
c/s are given in Fig 6.9 as functions of u_o, Q and R.   The
relation for V_s obtained from equation 3-39 is also included.
It is to be noted that the transition velocity u_c = 2.5 cm/sec
is below the range of experimental measurement in this case.

(2) <u>Test 6.   Calibration of a non-conducting circular</u>
<u>channel using aqueous solutions</u>

Fig 6.10 shows the corresponding results to Test 5
obtained using 8% NaCl solution, tap water and distilled
water.   The transition velocity of 25 cm/sec was sufficiently
high to allow measurements to be made for both laminar and
turbulent flows.

(3) <u>Test 7.   Dependence of calibration on liquid</u>
<u>conductivity and electrode dimensions</u>

The data obtained in Tests 5 and 6 for 50-c/s a.c.
excitation at u_o = 50 cm/sec are presented in Fig 6.11 versus
conductivity, together with the corresponding data for square
channel section C4 using type B electrodes (see Table 5.4)
0.33 in square.

(4) <u>Test 8.   System noise as a function of conductivity</u>

In Test 2, the random noise component of V_o was determined
as a function of frequency.   In this case, the total system
noise at the detector output, including all random and
excitation frequency harmonic components, was measured as a
function of conductivity for a.c. excitation at 50 c/s for
channels C1 and C4.   The high input impedance cathode follower
and low noise main amplifier were used to minimise noise from
the electronic equipment and the selective amplifier was

included to provide bandwidth limitation.

The apparent r.m.s. noise component of V_o (i.e. the value measured at the detector referred to the amplifier input) is plotted in Fig 6.12 versus conductivity for both channel sections.

(5) Test 9. Demonstration of the dielectric polarisation
    effect

The value of U_D given in Table 4.2 for distilled water indicates that field excitation frequencies of at least 10 kc/s are required to produce a substantial dielectric polarisation effect in this liquid. Magnetic circuit M2 and the power amplifier were found to be capable of sinusoidal operation up to f_o = 15 kc/s at B_o = 20 mWb/m^2 and thus create a time-varying magnetic field of the required frequency. Type B electrodes were installed in both the long and short sides of channel section C7 and their dimensions were chosen such that R_{ci} was of about the same magnitude in each case. Use of the high input impedance cathode follower in the pre-amplifier stage ensured negligible loading of the flowmeter output over the frequency range involved.

The measured values of V_o, expressed in terms of their low-frequency amplitudes, are given in Fig. 6.13 versus frequency for both pairs of electrodes and are compared with the performance predicted using the circuit model of Fig. 6.3 in which the polarisation voltage is omitted. For the pure distilled water used, σ = 0.6 x 10^{-4} U/m, and this gives τ_d = 12 x 10^{-6} $\approx R_{ci}C_{ci}$ secs.

6.5. Flowmeter Calibration

(a) General Comments

Tests described in the preceding Section indicate only the dependence of K on the ratio c/r_i in equations 4-9 to 4-12 and attention is now directed to the measurement of the

effects of the remaining parameters in these equations. Magnetic circuit M1 was used in this work and, when assembled with l_m = 10 in, enabled the (two-dimensional) magnetohydrodynamic effects predicted in Chapter 3 to be established in mercury. The c/a and c/r_i ratios were at least 4:1 in all tests involving l_g = 5/8 in and, from previous experience and the relations given in Fig. 3.11, it was concluded that end effects could safely be neglected.

Magnetic field excitation conditions included both d.c. and 50-c/s a.c. for mercury but were restricted to the latter for low-M tests with 8% NaCl solution.

The presence of a comparatively thick oxide layer on the surface of stainless steel is responsible for the non-wetting condition with mercury and this leads to poor electrical contact. The flow signal obtained using stainless steel channels fluctuated widely and was not suitable for measurement purposes until the oxide layer was removed from the surfaces in contact with mercury. This was done[1] by introducing mercury-lithium amalgam and allowing it to react with a small amount of water. The hydrogen thus produced removed the oxide layer and immediate contact was established with mercury to prevent this layer reforming.

Figs 6.14 to 6.22 give the results of these calibration tests and include the values of V_m predicted by the appropriate relations in Chapters 1 and 3.

(b) <u>Test Details</u>

(1) <u>Test 10. Magnetohydrodynamic velocity profile distortion</u>

The magnetohydrodynamic velocity profile distortion predicted by equations 3-53, 3-54 and 3-55 was first examined using mercury in non-conducting circular channel C1 and square

---

1. This procedure was suggested by Storrow (private communication). It has also been used by Watt (Ref. 54).

channel C4. In the latter case, the type A electrodes had r_e = 3/64 in and the type B electrodes were 0.33 x 0.33 in.

The measured values of V_o with $B_o \approx 0.75$ Wb/m^2 (high-M condition) for $1_m = 2\frac{1}{4}$ in (short flowmeter) and $1_m = 10$ in (long flowmeter) appear in Fig. 6.14 for Reynolds numbers up to 5000 and in Fig. 6.15, using log scales, up to R = 10^5.

(2) **Test 11. Low-M flow in rectangular channels**

Non-conducting rectangular channels C4, C7 and C9 were used to compare the electrode arrangements of Figs 3.5 and 3.6 under low-M conditions with 1_m = 10 in. NaCl solution served as the working liquid and the electrode sizes are specified in Fig. 6.16 which presents the results of these measurements.

(3) **Test 12. Wall conductivity effect**

Stainless steel channels C2, C5 and C8 and nickel-plated copper channels C3 and C6 respectively provided moderate and high wall loading conditions with mercury. Figs 6.17 and 6.18 give the calibration relations obtained for conducting wall conditions in short flowmeters ($1_m = 2\frac{1}{4}$ in) under relatively low-M conditions (M < 8) with B_o = 65 mWb/m^2 and Fig 6.19 shows the high-M behaviour of a stainless steel circular channel.

(4) **Test 13. Velocity profile distortion by channel irregularities**

Test 10 has confirmed the departure of the measured flow-meter calibration from that given by equation 1-2 for non-conducting circular channels in the presence of velocity profile distortion. To demonstrate[1] that this can also occur due to channel irregularities, 3/16 in plugs were inserted approximately half-way into channel sections C1 and C4 at

---

1. Shercliff (Ref. 119) has recently obtained this effect under high-M conditions using a jet directed into the main stream to distort the velocity profile.

distances of $4r_i$ or $4b$ and $10r_i$ or $10b$ upstream from the electrodes in two different orientations as shown in Fig. 6.20. The observed values of V_o fluctuated considerably as is indicated by the scattering of experimental points in Figs 6.20 and 6.21 which deal respectively with mercury and NaCl solution in short flowmeter arrangements.

(5) Test 14.   Calibration of a circular channel flowmeter
   with highly conducting walls

The insertion of electrodes into a circular channel to obtain a flow signal in cases where $w\sigma_w \gg r_i\sigma$, as proposed in Section 3.7, was examined using a short flowmeter, NaCl solution and channel section C11.   The type E electrodes were 1/16 in diameter and had all but their tips covered with shellac. Fig. 6.22 shows the calibration of this arrangement with the inter-electrode distance $2r_3 = 0.89$ in as required by equation 3-45 and also for $2r_3 = 1.11$ in which was found to give the most satisfactory performance in the flow transition region. The measured and calculated calibrations for the non-conducting $1\frac{1}{2}$ in circular channel C10 are also included in Fig. 6.22.

Fig. 6.4. Comparison of Capacitance-Coupled Voltages in Various Tap Water Flowmeter Arrangements

amplitude of V after balance - μV (r.m.s.)

V_m for→

B_o = 75mWb/m²
u_o = 10cm/sec
L_c = 3/8 in
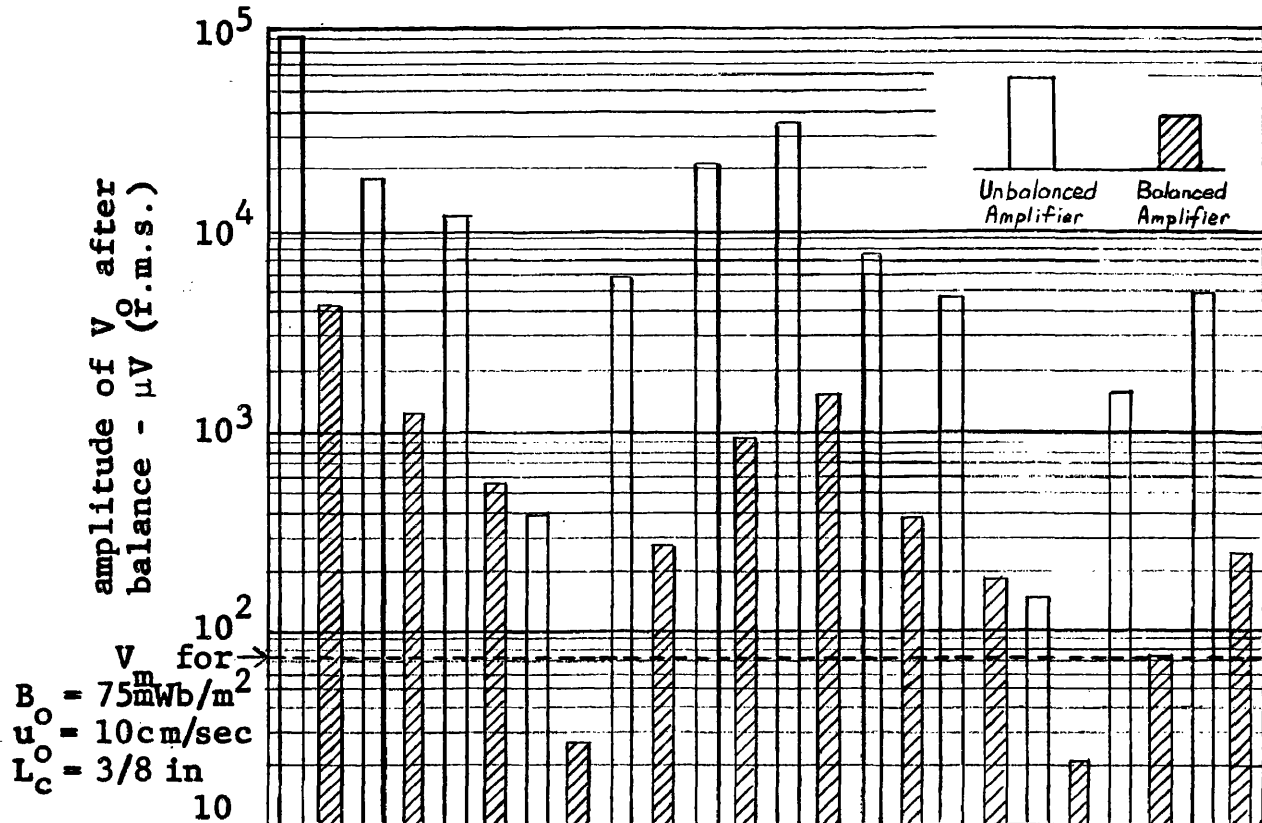
Rejector Type		Transformer e.m.f.						Capacitance-Coupled					
Ext. Shield Can		Off		On				Off		On			
Supply		Mains		Mains		P.A.		Mains		Mains		P.A.	
Frequency c/s		50	50F*	50	50F	50	200	50	50F	50	50F	50	200
Unbalanced Amplifier	V_{o1}/mV	834	834	110	110	95.1	326	834	834	110	110	95.1	326
	V_{o2}/mV	92.3	18.4	12.2	0.39	5.95	20.2	34.1	7.44	4.98	0.14	1.48	4.96
	V_{o1}/V_{o2} db	18.4	33.1	19.1	49.0	24.1	24.3	27.8	41.0	28.0	57.8	36.2	36.4
	V_m/V_{o2} db	-62.6	-48.2	-44.6	-14.8	-38.4	-49.0	-53.6	-40.9	-35.7	-5.9	-26.3	-36.8
Balanced Amplifier	V_{o1B}/mV	37.9	37.9	5.03	5.03	4.32	14.7	37.9	37.9	5.03	5.03	4.32	14.7
	V_{o2}/μV	4230	1200	552	26.8	281	937	1420	396	186	20.3	73	241
	V_{o1}/V_{o2} db	19.0	30.1	19.2	45.5	23.1	23.8	28.5	39.7	28.7	48.0	35.4	35.7
	V_m/V_{o2} db	-35.5	-24.6	-17.9	8.26	-12.0	-22.4	-26.0	-14.9	-8.34	10.9	-0.2	10.9

* indicates inclusion of 50-c/s supply filter (see Appendix II)

Notes: 1. $V_{o1} = V_1$ before connection of rejector (unbal. amp.)

2. V_{o1B} = apparent V_o before connection of rejector (balanced amp.)

3. V_{o2} = apparent V_o after rejector adjustment

4. All values for B_o = 75 mWb/m²; σ = 73.6 x 10⁻⁴ ℧/m

5. V_m computed for u_o = 10 cm/sec, L_c = 3/8 in

Table 6.1. Capacitance-Coupled Voltages in Tap Water
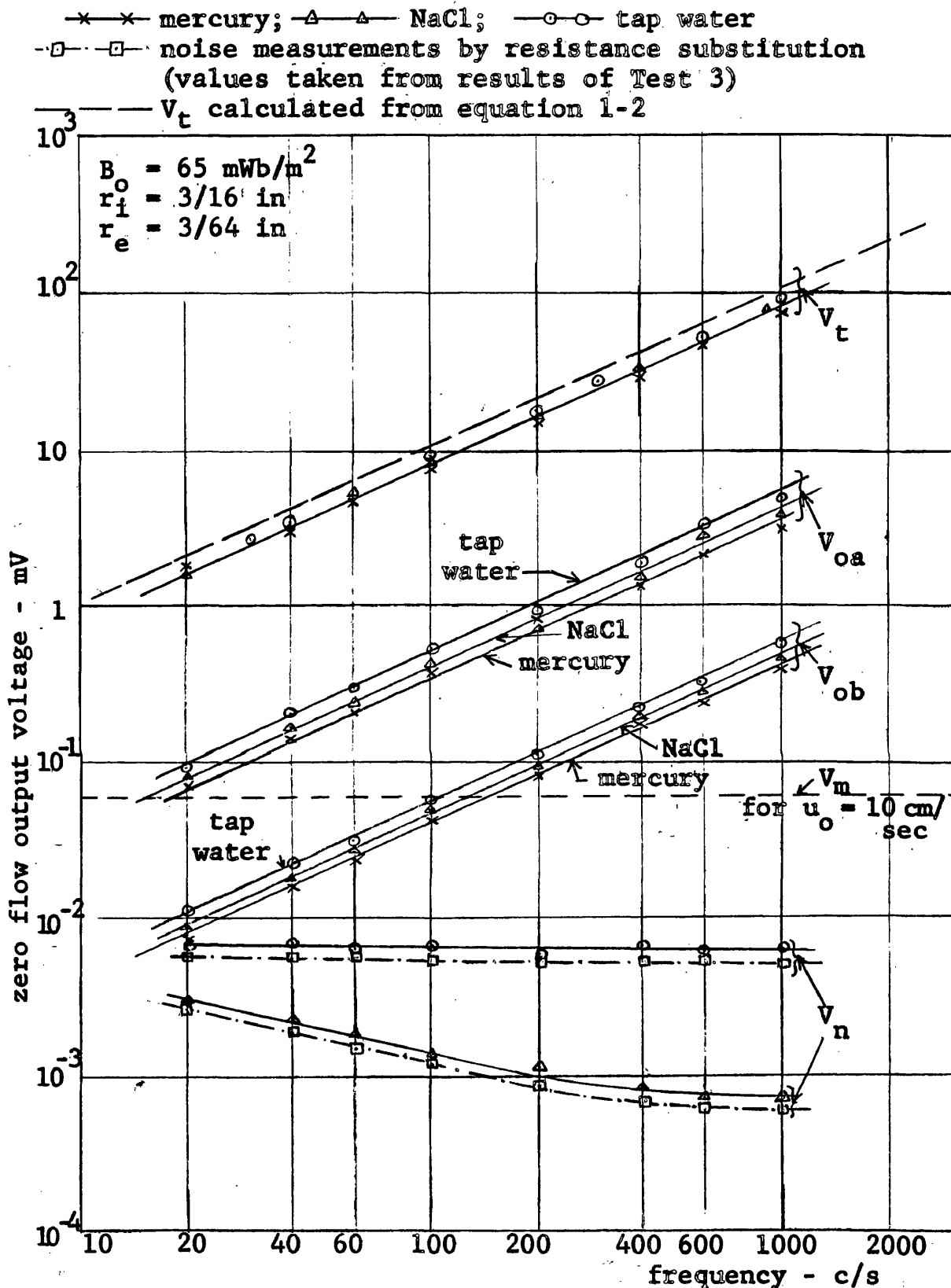
Fig. 6.5. Zero-Flow Output Voltage Versus Frequency for
Several Liquids and Input Circuit Arrangements

Figs 6.6 and 6.7
—×—×— measured series resistance compt. of Z_o
—o—o— measured series reactance compt. of Z_o
—□—□— calculated R_b and C_b - see Sec. 6.3(b)
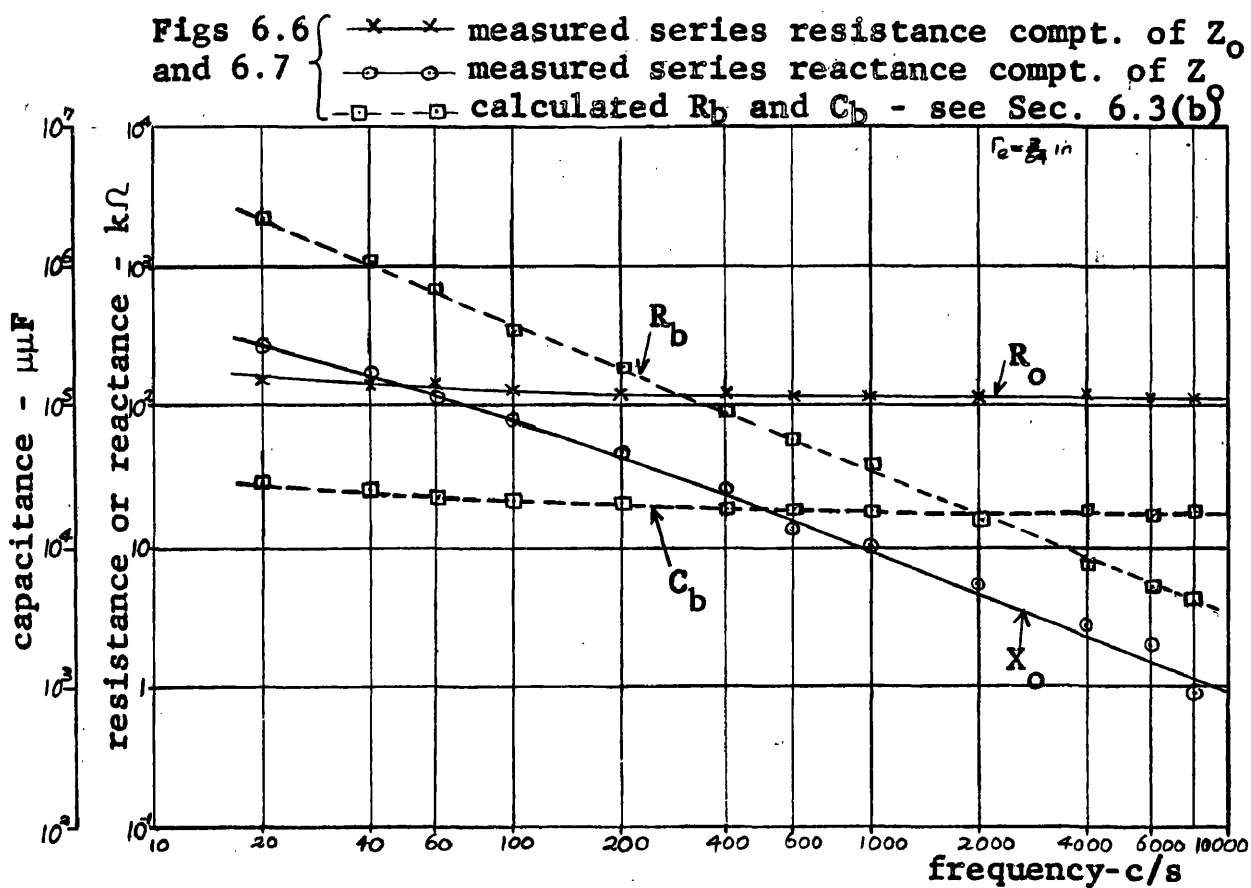
Fig. 6.6. Small-Signal Flowmeter Impedance Versus Frequency for Carbon Electrodes in Tap Water
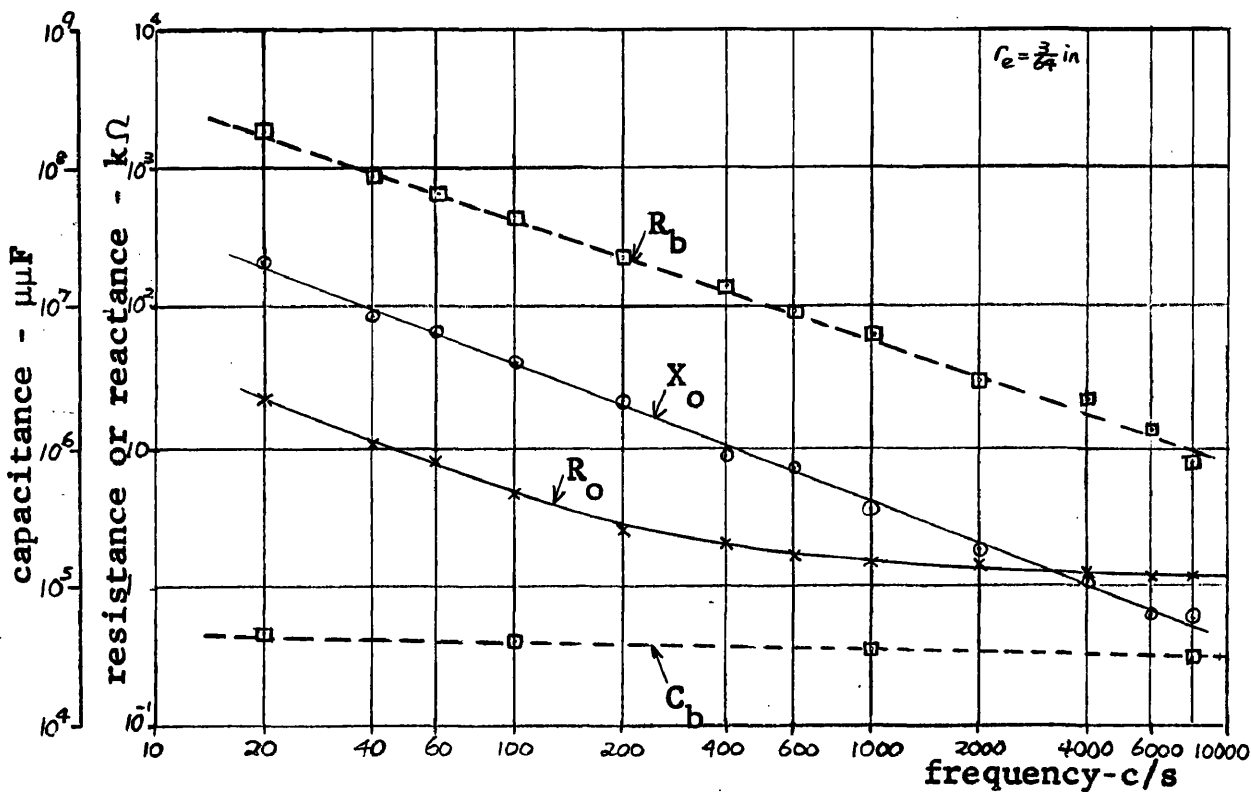
Fig. 6.7. Small-Signal Flowmeter Impedance Versus Frequency for Platinum Electrodes in NaCl

— ✕ — ✕ — measured ΔV_O; — △ — △ — measured ΔR_O

— ☐ — — ☐ — ΔV_O calculated using measured ΔR_O and circuit model of Fig. 6.2
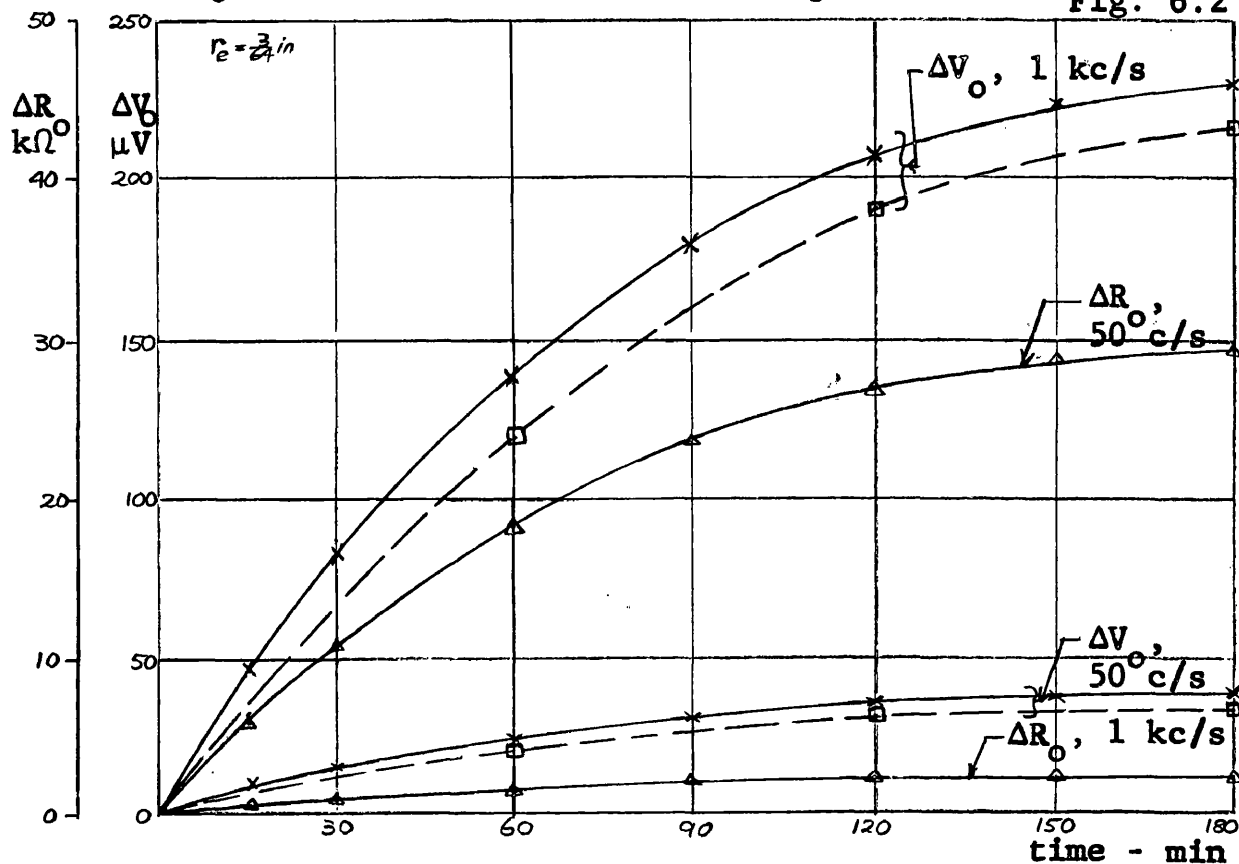
(a) Carbon electrodes in tap water at 50 c/s and 1 kc/s
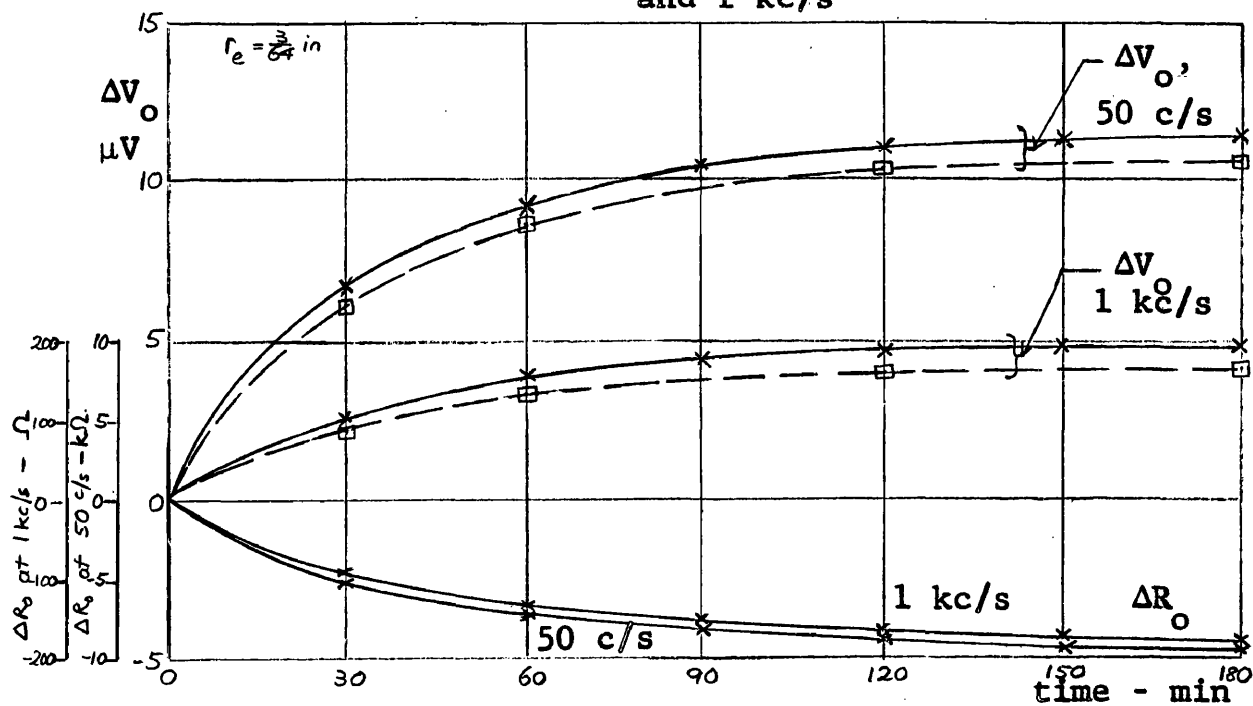
(b) Platinum electrodes in NaCl solution at 50 c/s and 1kc/s

Fig. 6.8. Drift of V_O Versus Time Using Transformer E.M.F. Rejector

V_m calculated from equation 1-2 —— —— ——

V_o measured: d.c.   —△—△—   pulse, 50 c/s —▽—▽—

                 a.c., 50 c/s —×—×—   pulse, 200 c/s —□—□—

                 a.c., 1 kc/s —○—○—
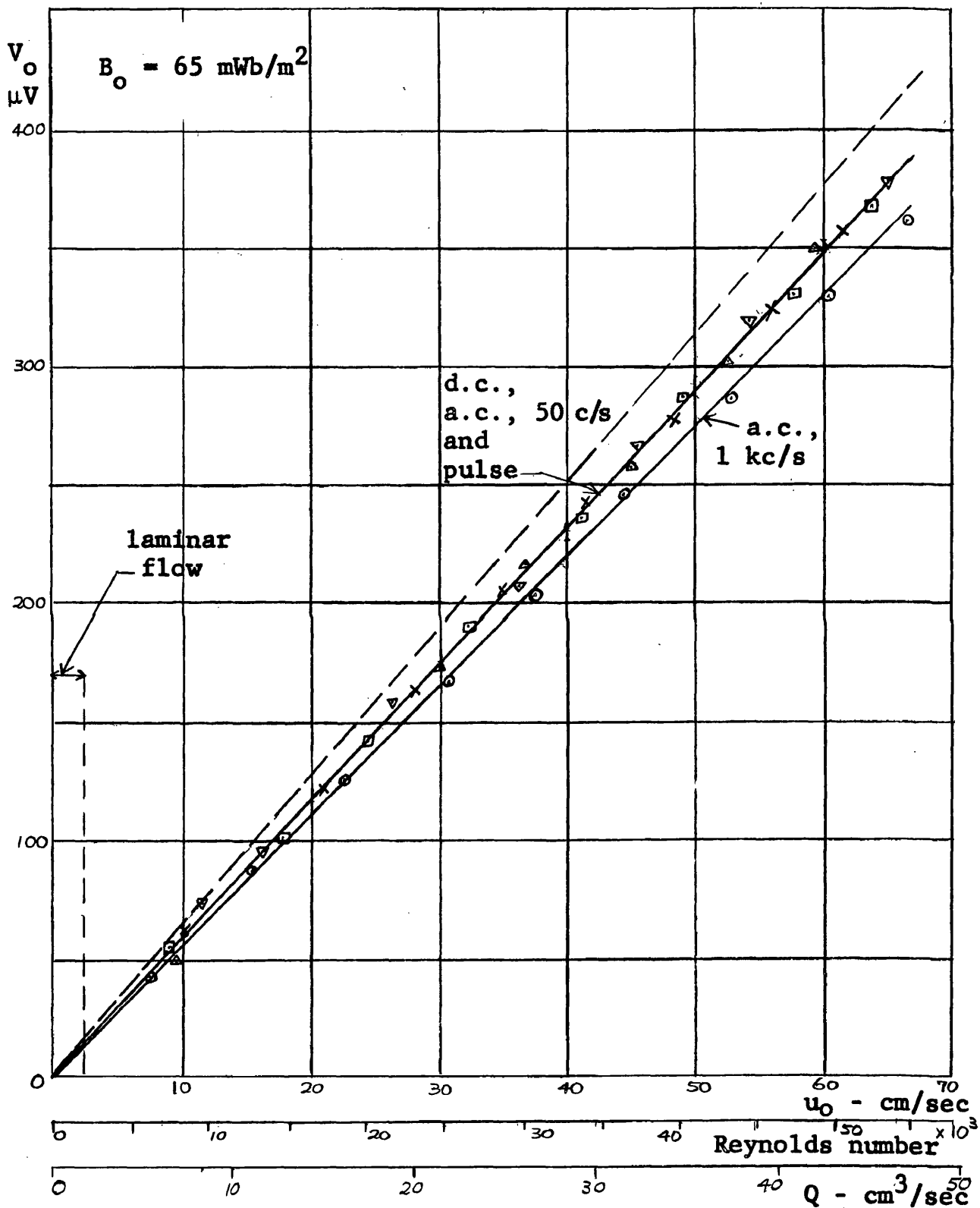
Fig. 6.9. Flowmeter Calibration for Mercury in a Circular
Channel Using Alternative Magnetic Field Excitation Methods
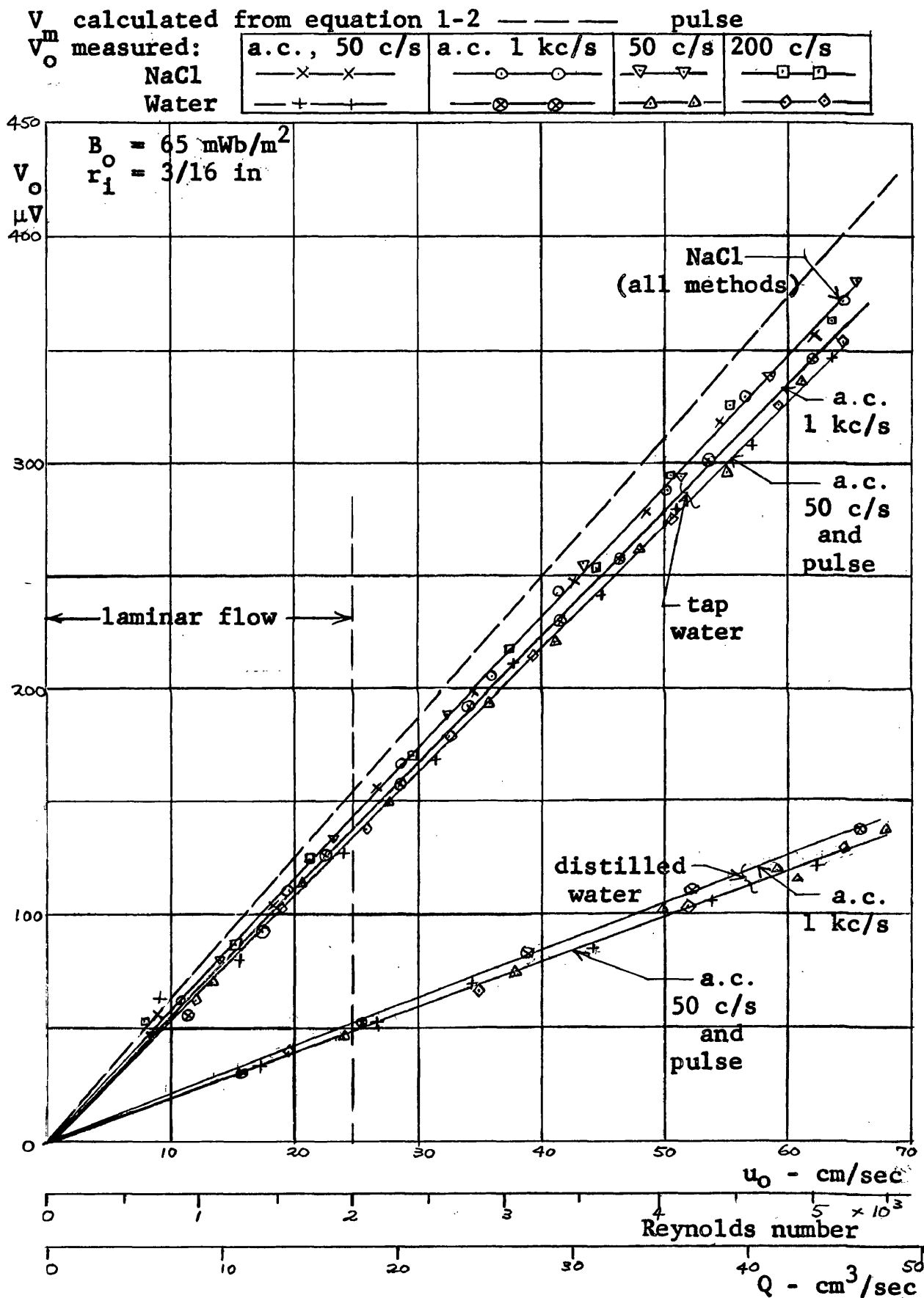
Fig.6.10. Flowmeter Calibration for Aqueous Solutions in a
Circular Channel Using A.C. and Pulse Excitation

Figs 6.11 ⎫ —✗——✗— circular channel, r_i= 3/16 in r_e= 3/64 in
and 6.12 ⎬ —△-△— square channel,type B electrodes 0.332 x
         ⎭   0.332 in

V_o
μV

B_o = 65 mWb/m^2
u_o = 50 cm/sec
f_o = 50 c/s a.c.

circular
channel

square
channel

σ -℧/m
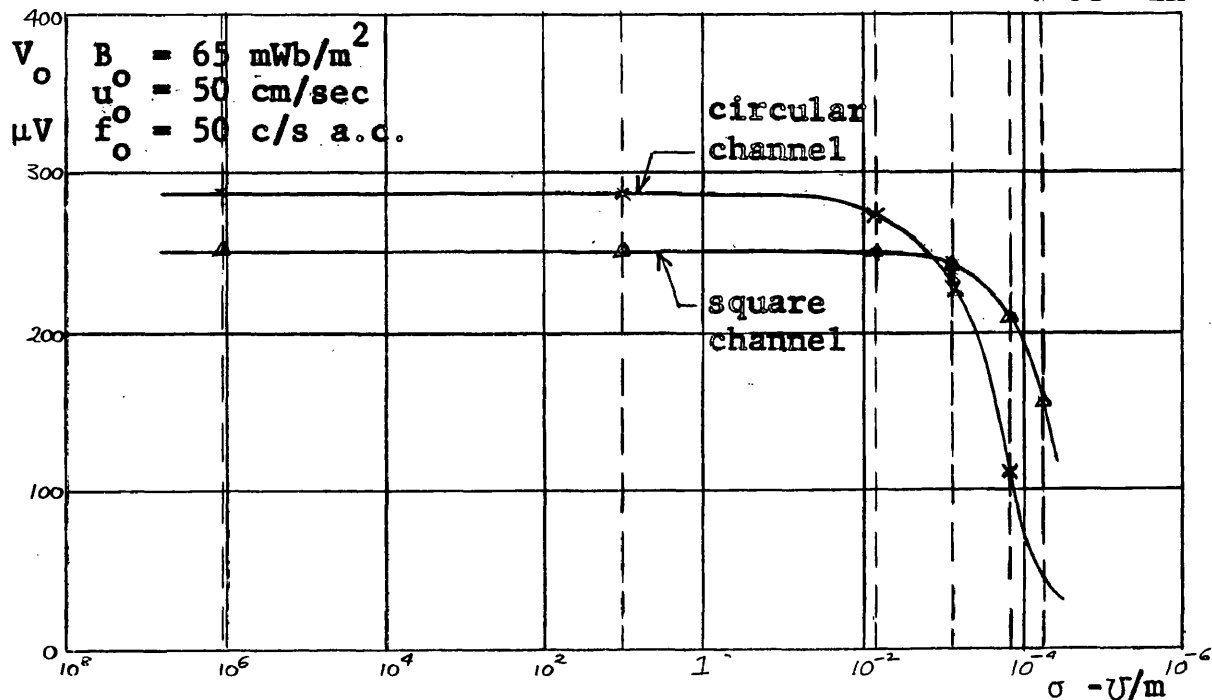
Fig. 6.11. Dependence of Calibration on Liquid Conductivity
and Electrode Dimensions

apparent noise compt. of V_o - μV r.m.s.

B_o = 65 mWb/m^2
u_o = 50 cm/sec
f_o = 50 c/s a.c.

circular→
channel

square
channel

mercury   8% NaCl   tap water σ -℧/m
                                distilled water
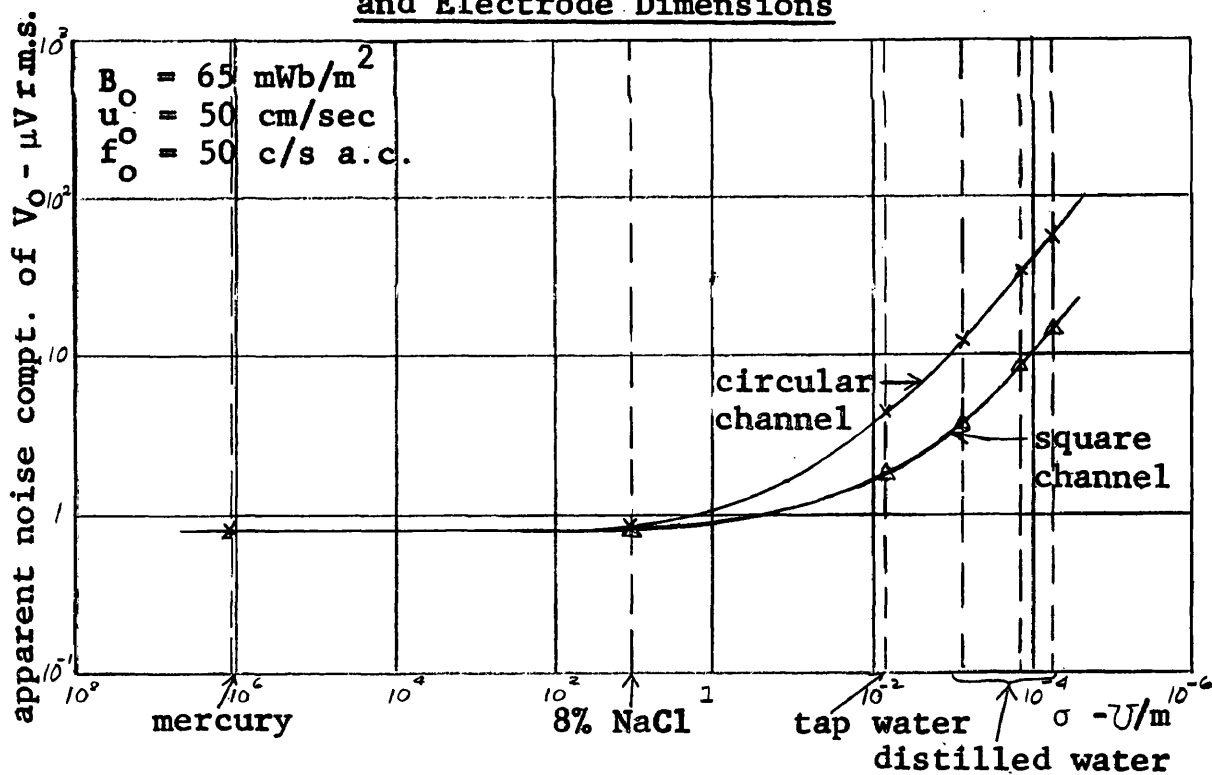
Fig 6.12. Apparent Noise Component of V_o Versus Liquid
Conductivity

(a) Electrode arrangements

—— — — calculated using circuit model of Fig. 6.3

——▫——▫—— measured with electrode arrangement A

——△----△—— measured with electrode arrangement B

(b) Results
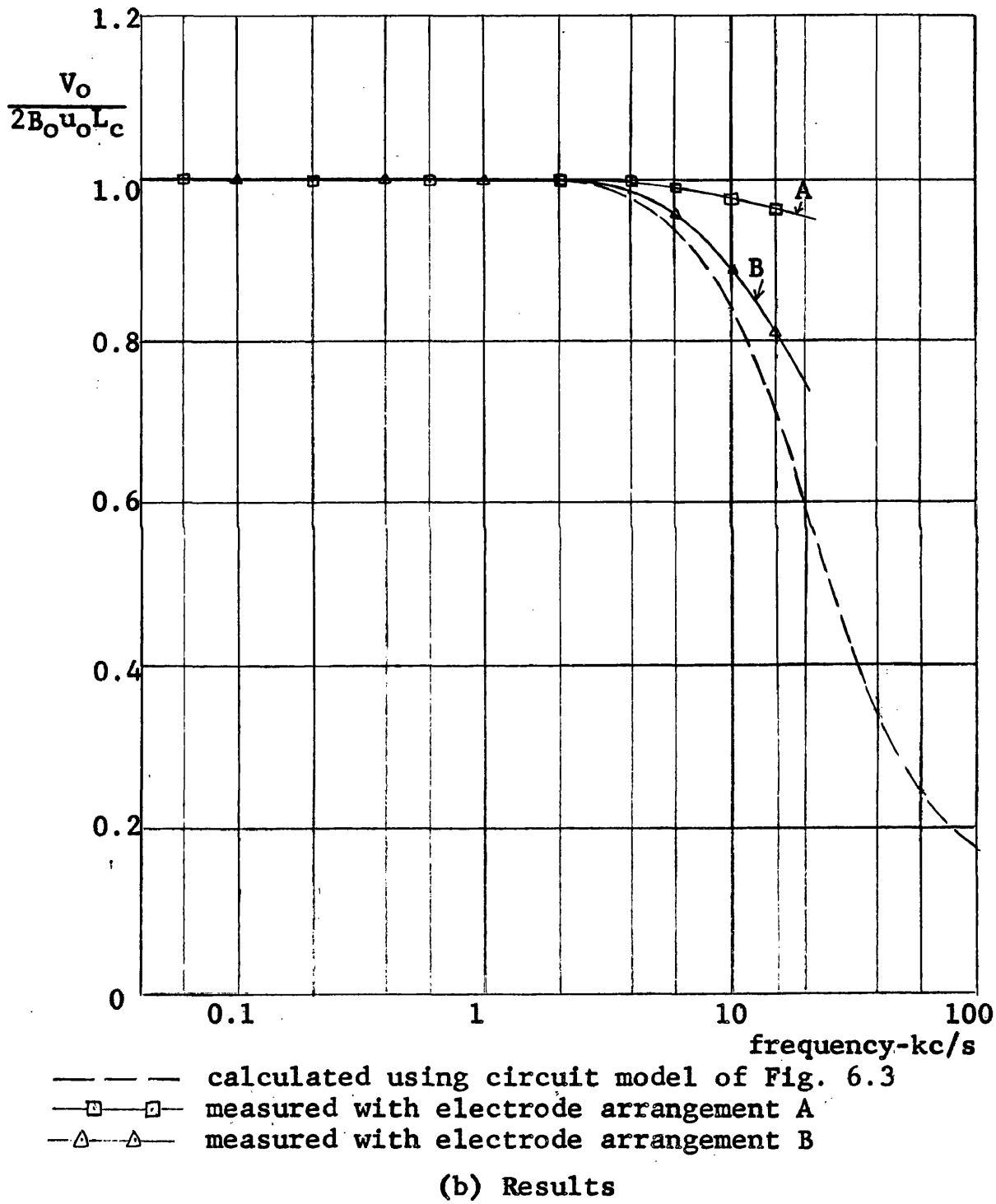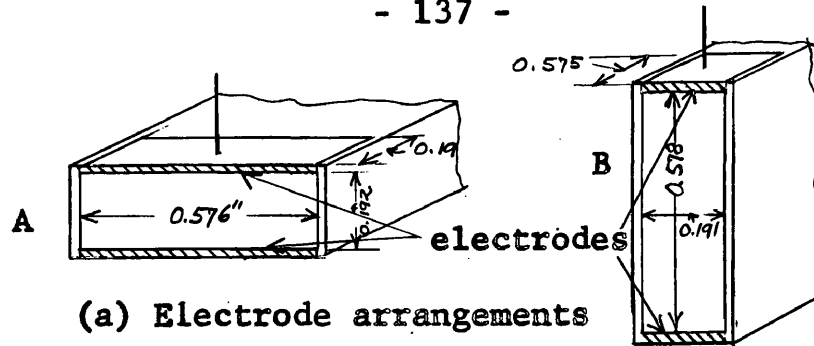
Fig. 6.13. Dielectric Polarisation Effect
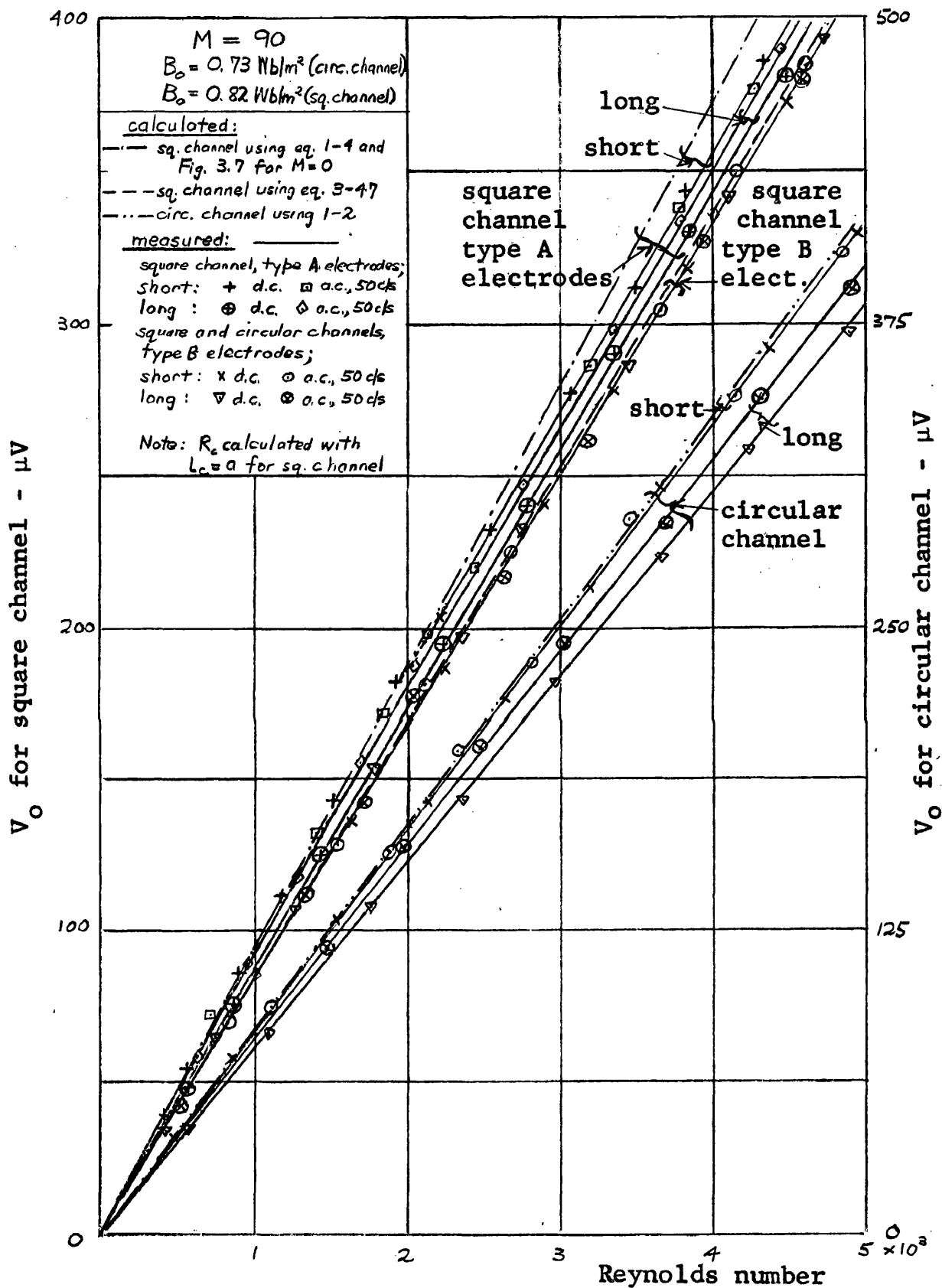
Fig. 6.14. Magnetohydrodynamic Effects in Laminar
and Transition Flow Regions

(a) Circular channel

(b) Square channel
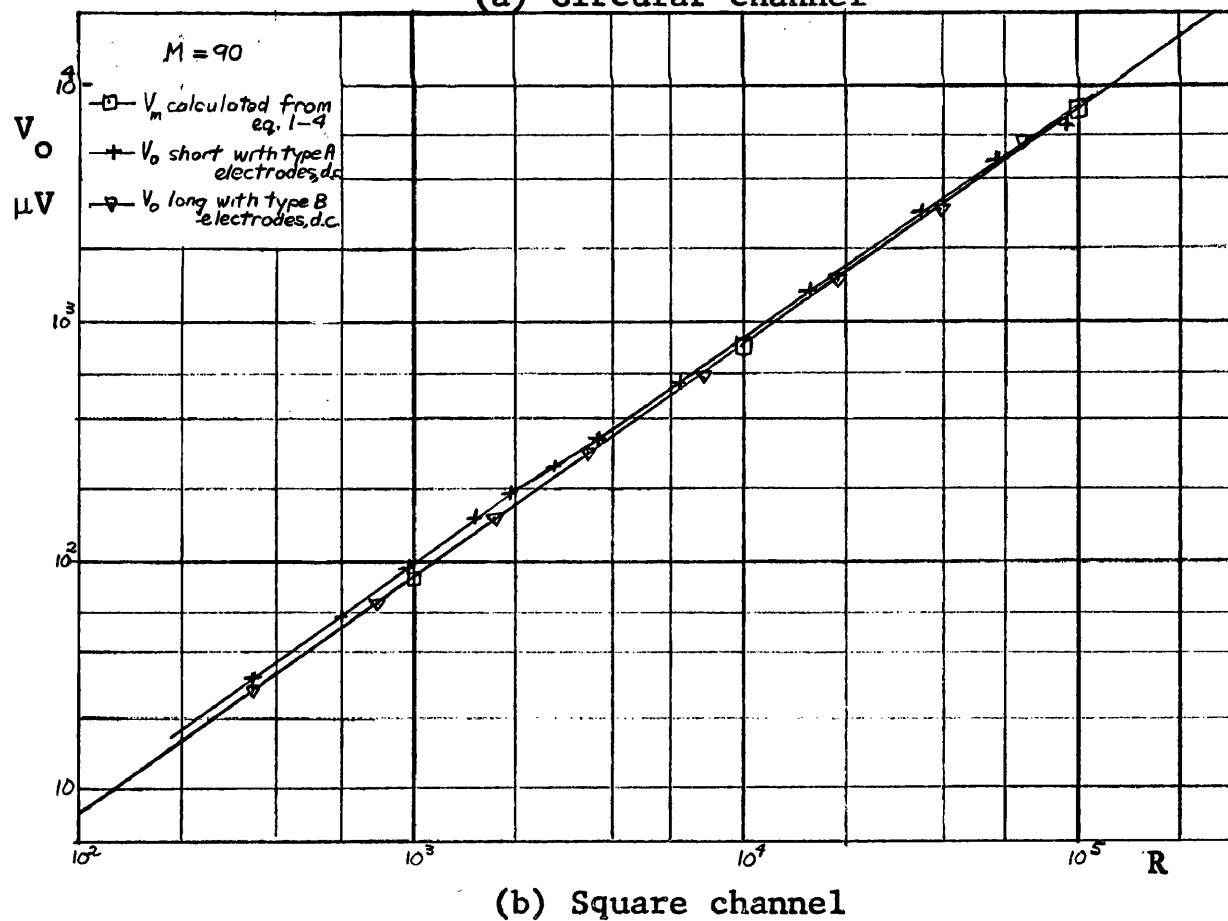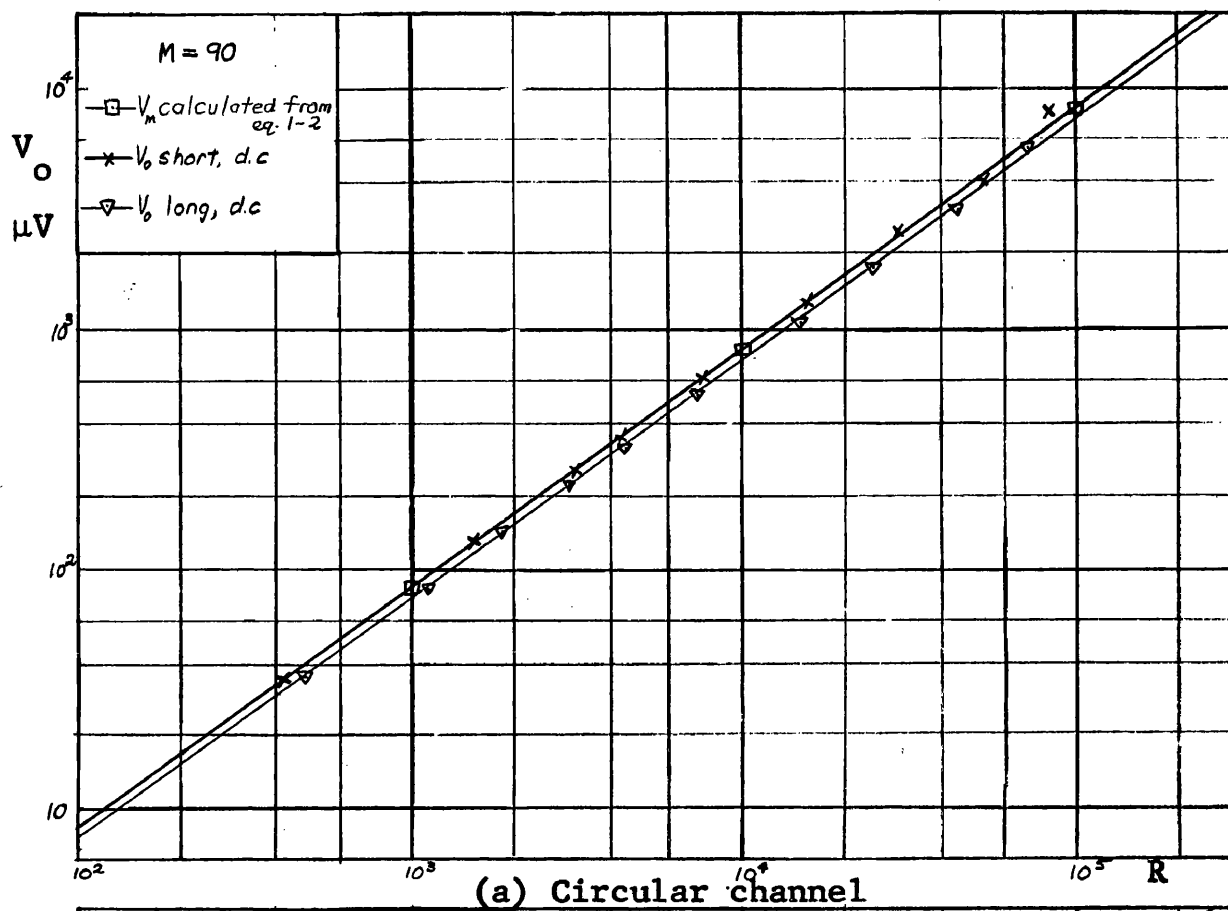
Fig. 6.15. Magnetohydrodynamic Effects in Turbulent Flow
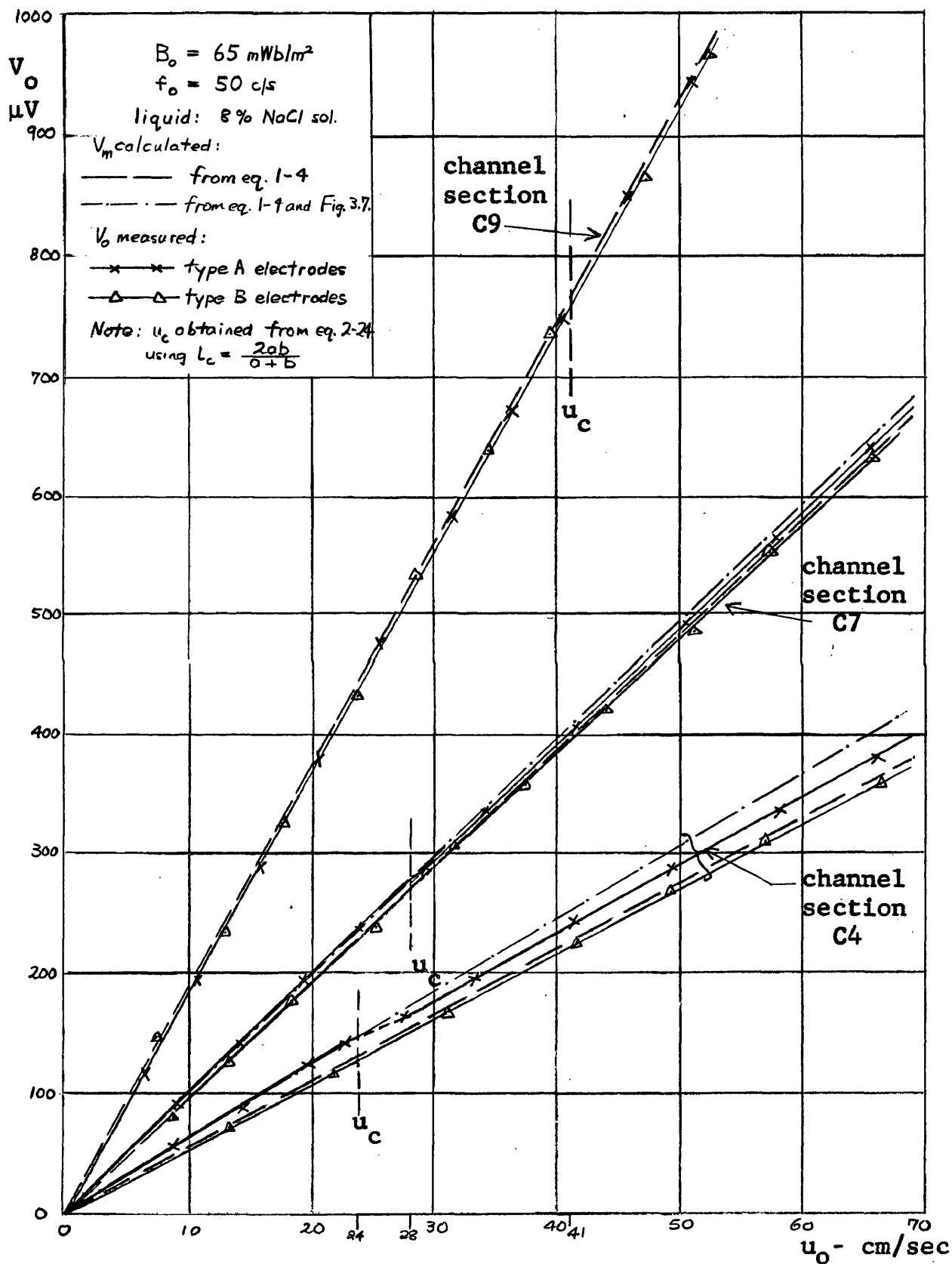
Fig. 6.16. Calibration of Non-Conducting Rectangular
Channel Flowmeters
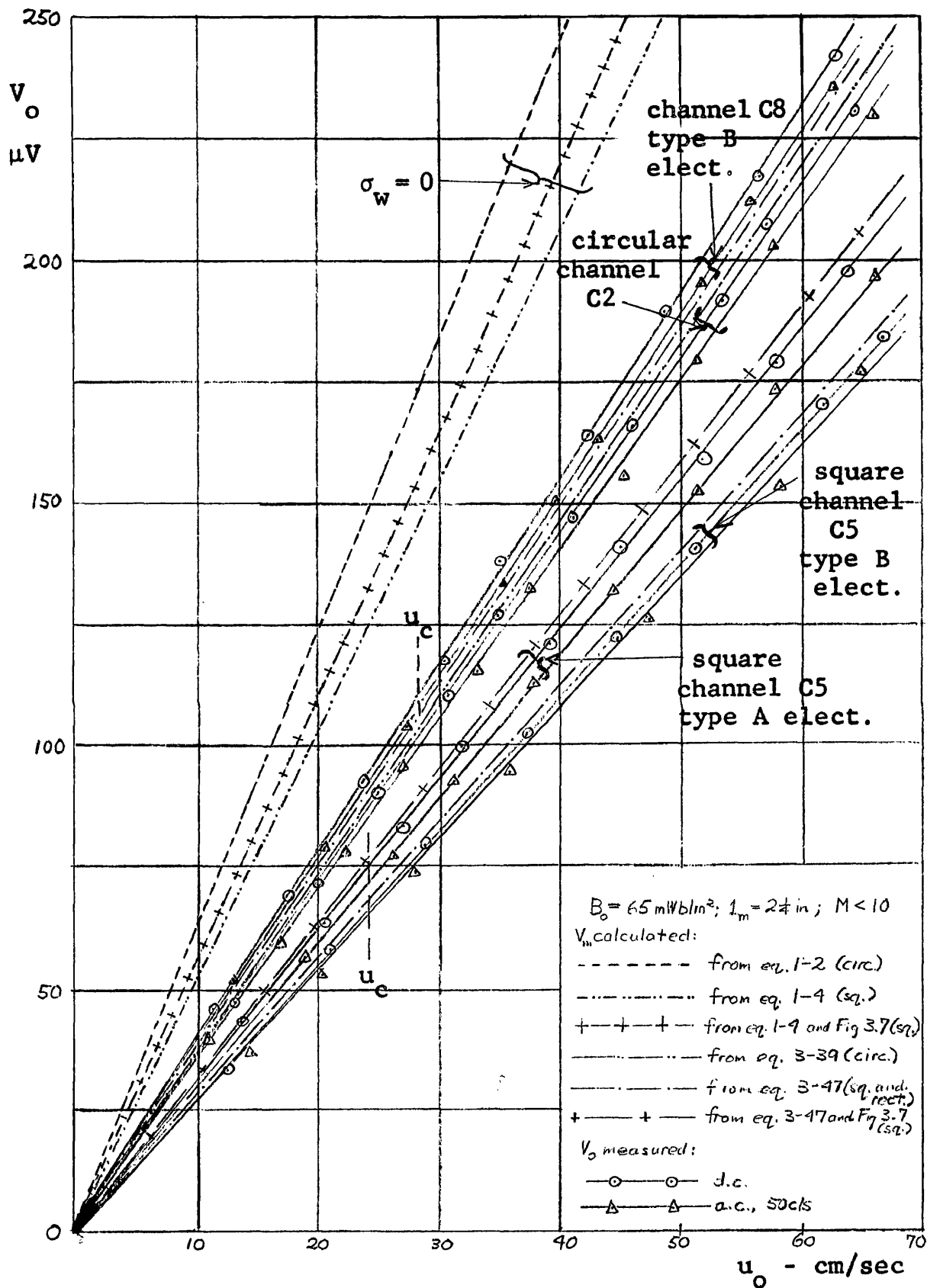
Fig. 6.17. Wall Conductivity Effect for Mercury in
Stainless Steel Channels - Low-M Conditions
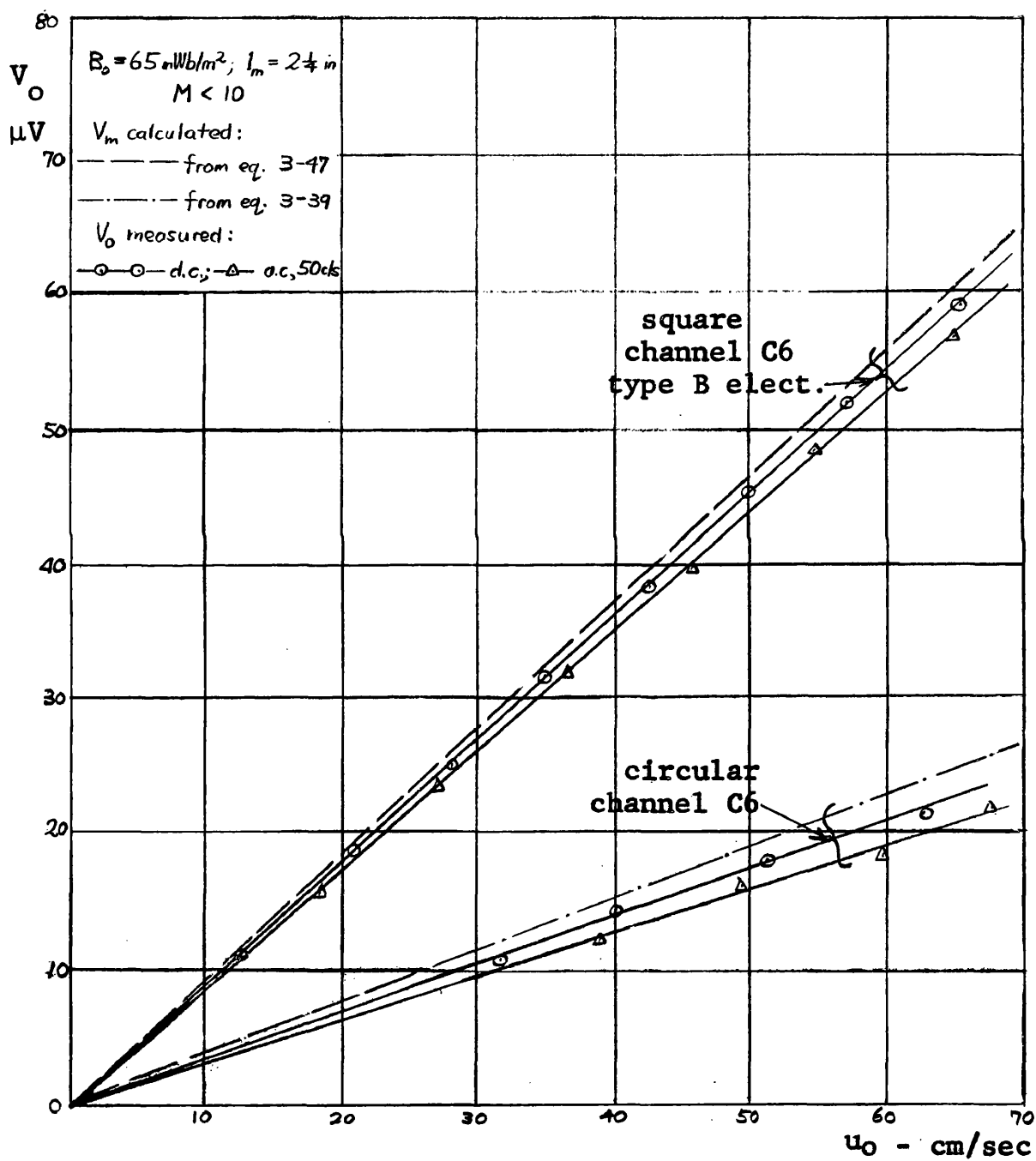
Fig. 6.18. Wall Conductivity Effect for Mercury in Nickel-Plated Copper Channels - Low-M Conditions
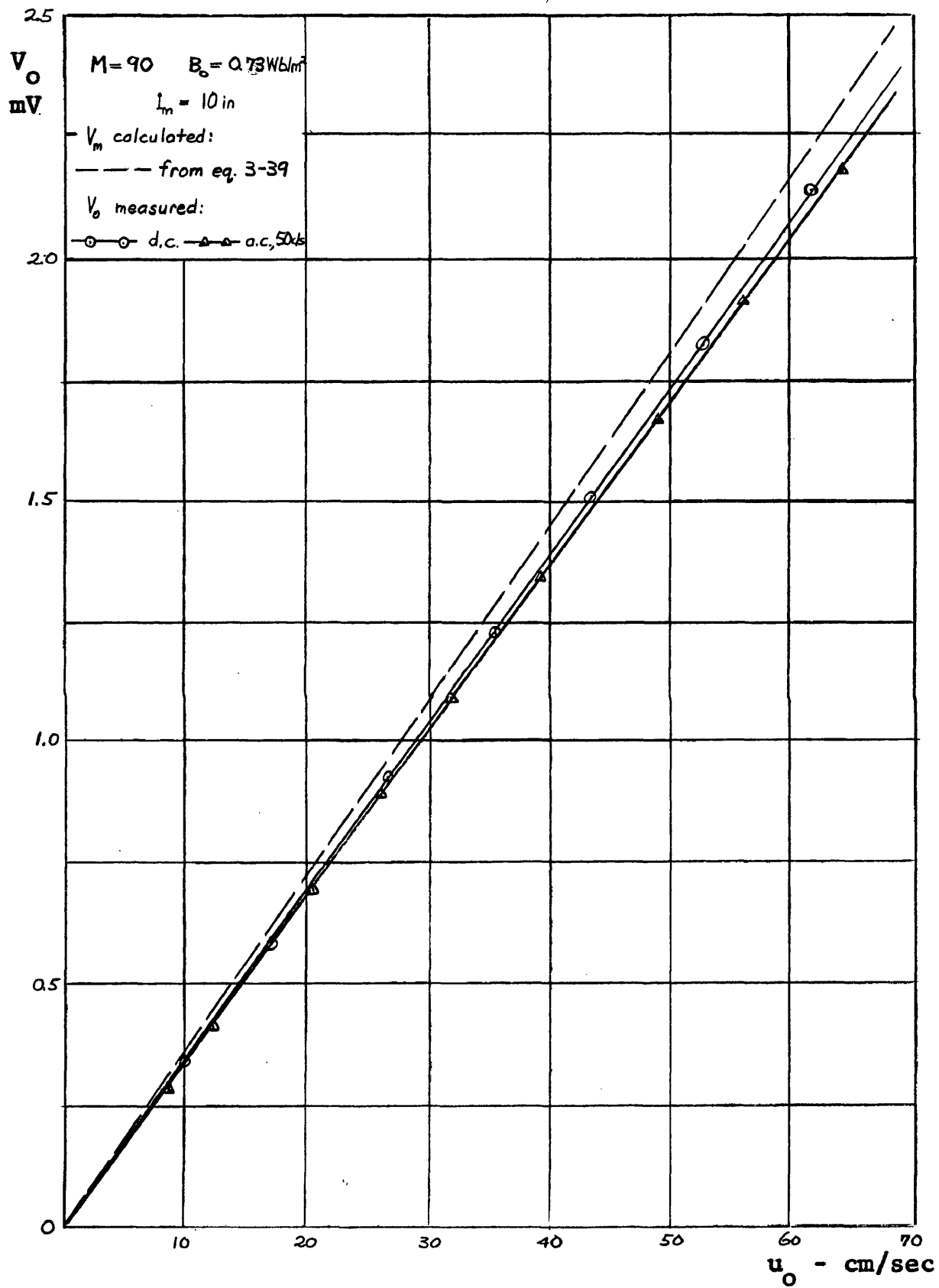
Fig. 6.19. Wall Conductivity Effect for Mercury in a
Circular Stainless Steel Channel - High-M Conditions
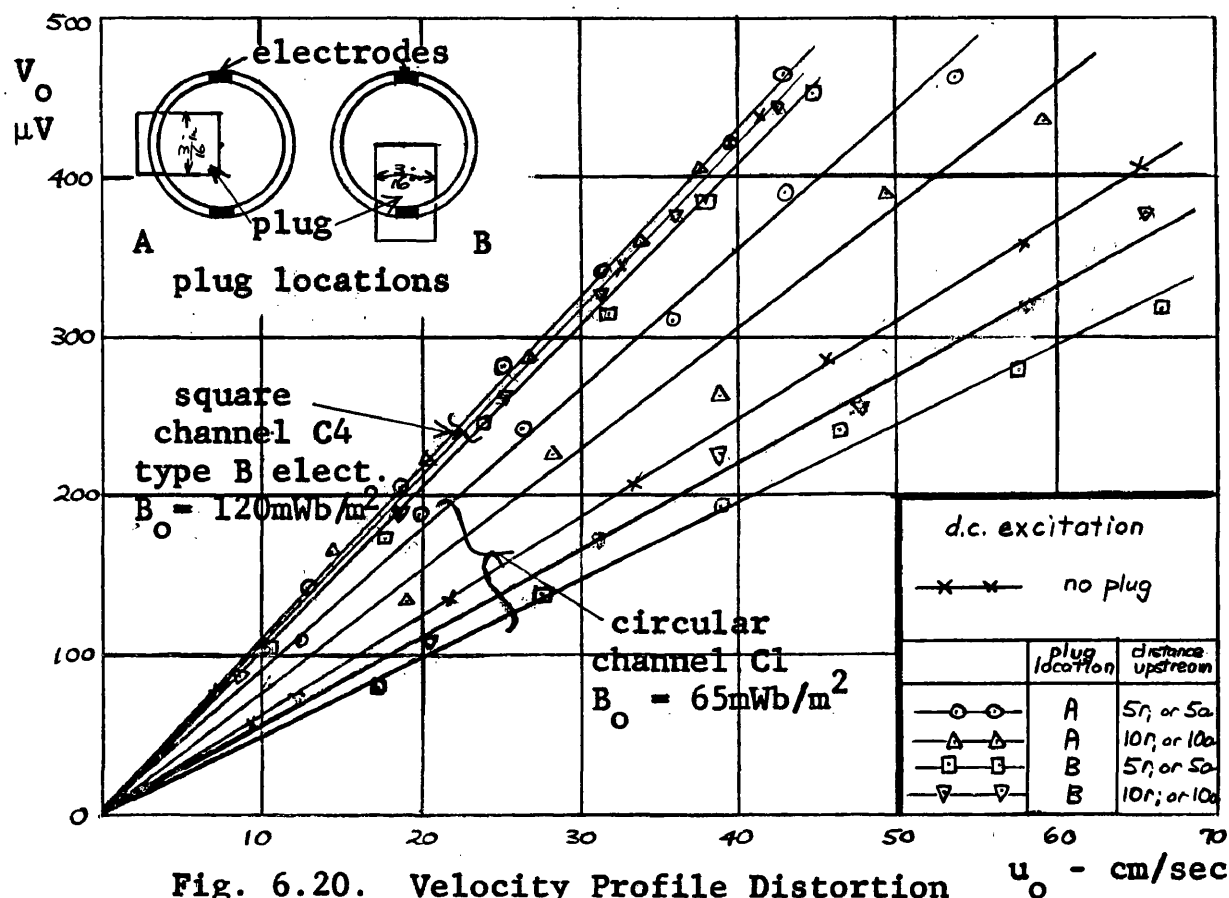
Fig. 6.20. Velocity Profile Distortion
for Mercury in a Short Flowmeter
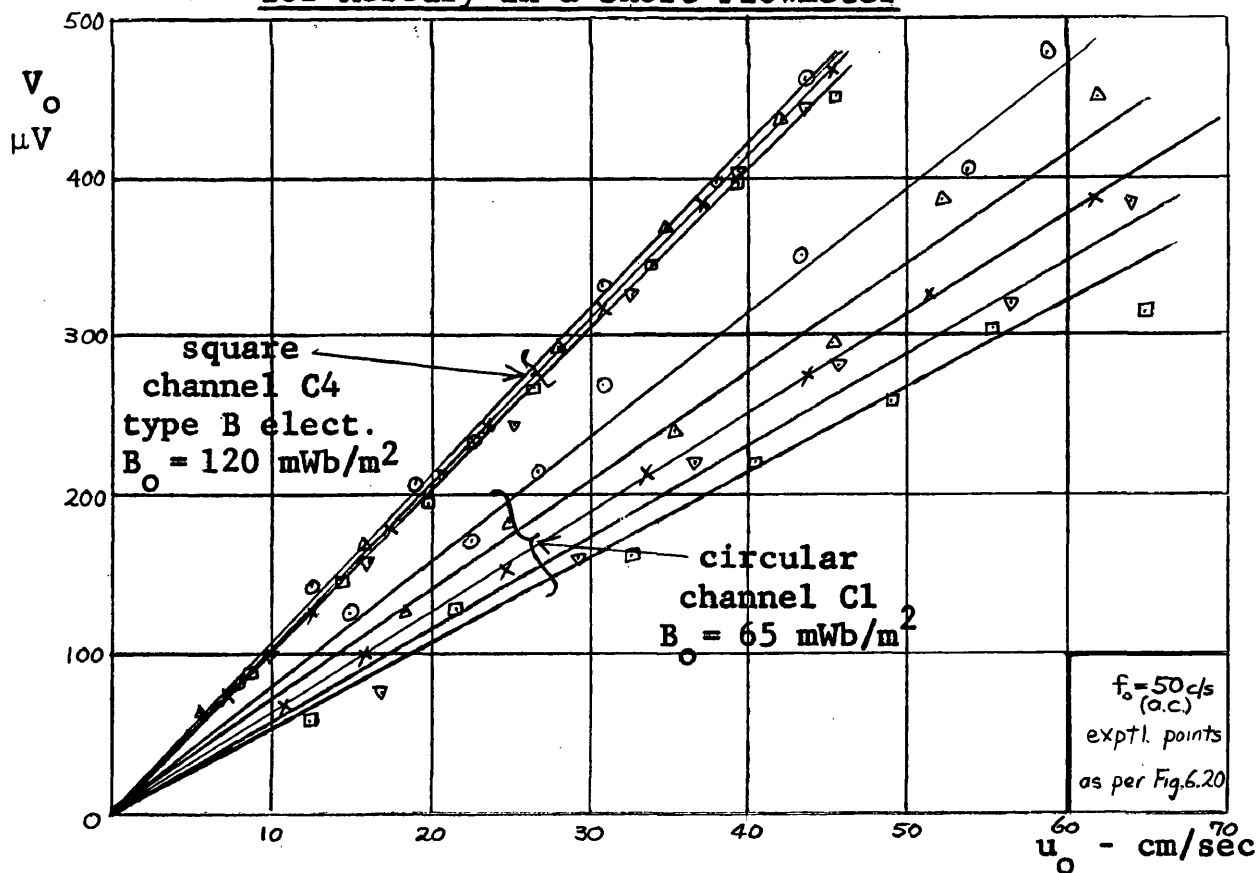
Fig. 6.21. Velocity Profile Distortion for
NaCl Solution in a Short Flowmeter
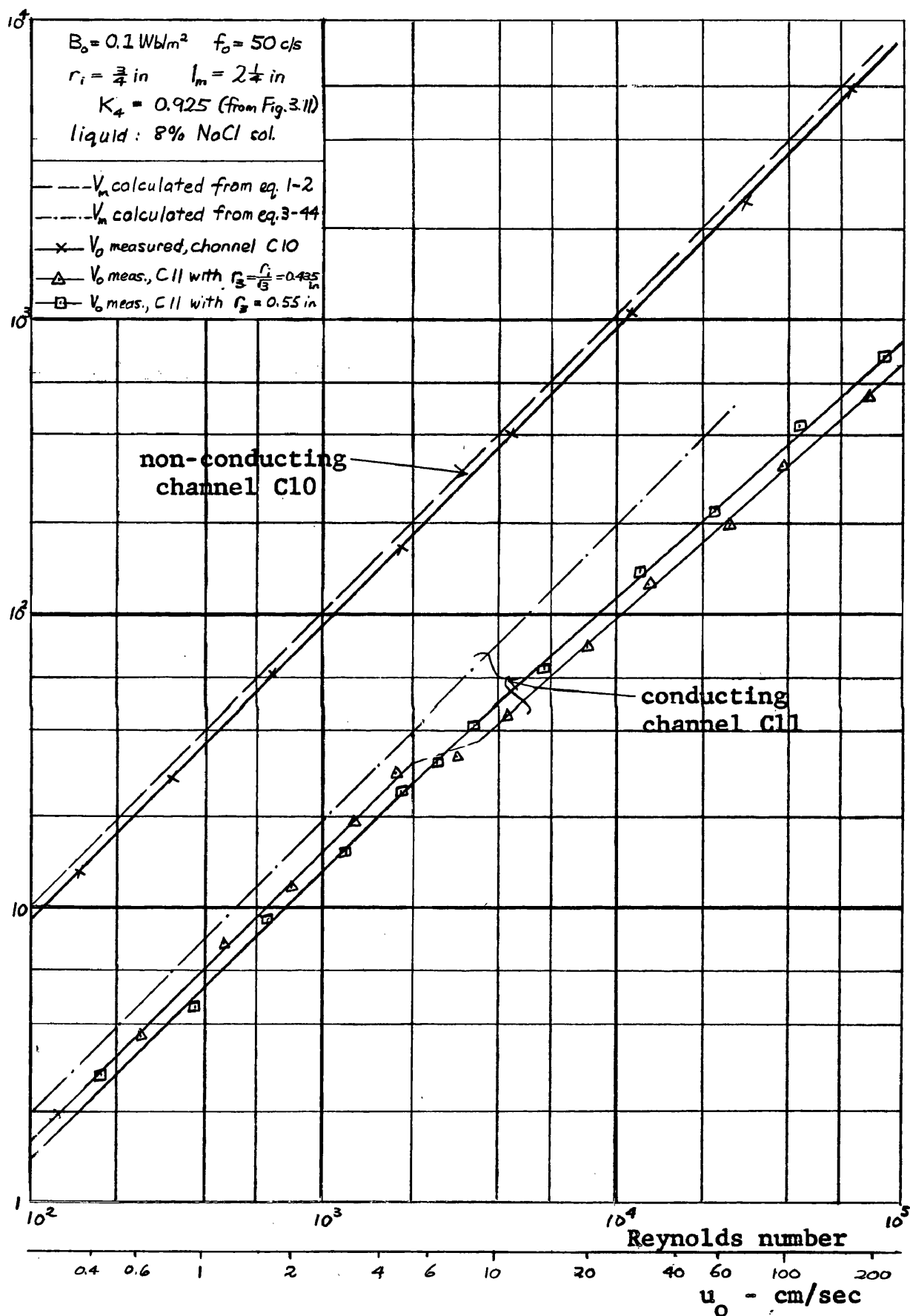
Fig. 6.22. Calibration of a Circular Channel Flowmeter
with Highly Conducting Walls

Chapter 7

EVALUATION OF THE ELECTROMAGNETIC FLOWMETER

7.1. Preliminary Considerations

The measured calibration relations for the electromagnetic
flowmeter arrangements considered in the previous Chapter
demonstrate that a usable flow signal can readily be obtained
over an exceedingly wide range of liquid electrical conduc-
tivity and that, in most cases, it is within 10 per cent of
the predicted value. While it may be both convenient and
satisfactory to carry through a design to this order of
accuracy and to calibrate the completed instrument using
standard techniques, the situations in which improved agree-
ment can be obtained (say to 1 per cent) require definition.
This is of particular importance when a flowmeter is intended
for operation with fluids of differing properties but is
calibrated using only one or with a fluid which is difficult
to handle in a test system.

The basic design requirements for the magnetic circuit
and amplifier input have already been given in Section 4.5
but the relative merits of the various alternatives remain to
be examined. One of the attractive features of the electro-
magnetic flowmeter has been demonstrated to be its suitabil-
ity for the measurement of low flow rates ($Q < 10 \text{ cm}^3$/sec) and
in these applications the choice of field excitation and
input circuit arrangements requires special consideration.

7.2. Input Circuit Arrangements

(a) D.C. Field Excitation

The input circuit arrangements discussed in this Section
are principally those for time variation of the magnetic
field but the case of d.c. excitation and liquid metal flow

is first briefly considered. For this, the only important requirement is good electrical contact between the electrode material and the liquid and this is met provided wetting occurs. Where the electrode and channel wall materials differ, as in Test 12, contact to the latter may also be required[1]. A similar effect with mercury and brass electrodes in a non-conducting plastic pipe has recently been observed and will be reported on separately.

(b) Capacitance-Coupled Voltage Rejection

The difficulties with capacitance-coupled voltages are greatest with low-conductivity fluids and high excitation coil voltages The results given in Table 6.1 and Fig. 6.4 illustrate the typical magnitudes of this effect in a tap water flowmeter without shielding. For comparison purposes, the value of V_m at u_o = 10 cm/sec and B_o = 75 mWb/m^2 (representative of the conditions encountered in blood flow measurement) is also included.

Although considerably higher values of B_o can readily be obtained, this would have to be accomplished without raising the coil supply voltage to improve the V_t/V_m ratio. In addition, the bulk and cost of the field system required may be an objection when increased amplifier gain can readily be provided.

Figure 6.7 shows that the rejection obtained in the experimental system of Test 1 was sufficient to permit a clear indication of V_m at the reference level in only two cases. While an external shield can was of considerable help when the excitation current was provided by the supply mains, the chief source of the coupling electric field was found to

---

1. This difficulty was also experienced by Elrod and Fouse (Refs 97 and 102) but they were apparently unaware that it could be overcome using the technique described in Section 6.5.

be the excitation coil supply voltage. After balance using either method, harmonic components of the excitation frequency predominated, except in the two satisfactory situations, where some random noise was also observed. The bridge circuit formed by the capacitance-coupled rejector was 9-12 db better than the e.m.f. rejector in reducing the amplitude of the residual harmonics but both were inferior to complete shielding, even when balanced amplifiers and the bridged-T supply filter were used.

To be completely effective, the shielding described in Section 5.3. should extend at least 20 channel diameters on either side of the electrodes and sections of electrically conducting channel should be inserted at its ends and be electrically connected to it. As an alternative, the use of a highly conducting channel section and type E electrodes, as in Test 14, gives a comparable performance. Either of these schemes reduces the level of the capacitance-coupled voltages at least to that of the system random noise for low-conductivity liquids, without requiring either balanced amplifiers or supply filters. For the conditions of Test 1, the zero-flow value of V_o was in the range 10-14μV.

When full shielding is not possible, balanced amplifiers and/or a capacitance-coupled rejector should be employed. Better harmonic rejection than that of Test 1 should be possible if care is taken with the phase characteristic of the latter component. In general, use of the V_t rejector is to be avoided on account of the zero drift discussed later, but it is probably satisfactory in situations where the voltages to be eliminated are of the order of the minimum value of V_m.

(c) <u>Transformer e.m.f. Rejection</u>

The chief difficulties with the Kolin-type transformer e.m.f. rejector are that the harmonic components of V_t and the balancing voltage may differ slightly in magnitude and phase

and that the presence of V_t in the input circuit causes drift in the zero setting. Positioning of the input conductor(s) eliminates both of these and, on the basis of experience gained with the flowmeter tests described in the previous Chapter, is recommended as the method to be used in all cases.

Figure 6.5 indicates that the magnitude of the harmonic voltage obtained with the Kolin-type rejector for $B_o = 65$ mWb/m^2 exceeded the value for V_m (for $u_o = 10$ cm/sec) over the entire frequency range above 20 c/s and increased linearly with f_o as is to be expected from equation 1-13 (provided that the harmonic content of the source of field excitation does not depend on f_o). Inclusion of the selective amplifier achieved a reduction in the harmonic voltage of about 20 db and accordingly raised the upper limit on f_o to about 100 c/s for the stated conditions. Further improvement of this method is certainly possible and might include an increased amount of harmonic rejection by the selective amplifier. Work in this direction would not be profitable, however, in view of the magnitude of the zero drift.

Input conductor positioning has been examined and discussed in relation to approximately sinusoidal time variation of the excitation field. For pulsed excitation, its use is essential in almost all cases to avoid amplifier overloading by the impulsive-type transformer e.m.f. produced by the rectangular flux waveform but it is not necessary to obtain exact cancellation.

As already indicated, the positioning of the input conductor requires special care with sinusoidal excitation when the zero-flow value of V_o is to be of the order of 10 μV or less and this becomes increasingly difficult to attain as B_o and/or f_o are raised. Supplementary rejection facilities are useful and, in addition, it is important to ensure that the condutor system is rigidly mounted.

(d) Electrodes

The small-signal characteristics given in Figs 6.6. and 6.7
are representative of the behaviour of contacts between metal
electrodes and electrolytes when polarisation occurs and
current flow is due to the charging and discharging of the
barrier capacitance. The method used to apportion the measured
values of series resistance and reactance between R_b, C_b and
R_{ci} yields the result that C_b varies only slightly with
frequency while R_b has a 1/f dependence. For present purposes,
the important result is that the electrodes used in the experi-
mental work are adequately represented from the circuit view-
point by R_{ci} in series with C_b. Calculation of the spreading
resistance for a flat 3/32-in diameter contact in tap water
and 2 per cent NaCl solution gives 58 kΩ and 640 Ω respectively
and these, when the channel geometry is taken into account,
are in reasonable agreement with the measured values.

Zero drift when V_t is present in the input circuit is
shown by the results of Test 4 (Fig. 6.8) to be due to slow
changes in the series resistance component of Z_o. The magni-
tude of this effect is at least comparable with V_m at low flow
rates and in some cases (e.g. carbon electrodes in tap water
with $f_o = 1$ kc/s) mask it completely. It is presumably caused
by the formation of an insoluble surface layer on the elec-
trodes and this is not sufficiently adherent to resist at
least partial removal by circulation of the test liquid.

In comparison with the magnitude of amplifier input
impedance which can be attained with careful circuit design,
the measured changes in R_o are quite negligible. However,
the design requirement when V_t is rejected by some balancing
arrangement is that any change in R_o should produce a
negligible change in V_t. When V_t is upwards of 10^3 times
the required zero-flow value of V_o, this becomes difficult
to meet and the simpler procedure is to eliminate V_t effects.

7.3. Methods of Magnetic Field Excitation

(a) Discussion of Experimental Results

It has already been fully established, both in this and other flowmeter studies, that d.c. excitation of the magnetic field is suitable for liquid metals but leads to electrode difficulties with electrolytic solutions. The discussion in this Section is concerned with the relative merits of d.c. and time-varying conditions for the former and with sinusoidal and pulsed excitation for the latter. In liquid metals, magneto-hydrodynamic effects may introduce additional factors (as discussed in Section 7.5) and the following remarks apply only to relatively low-M conditions in a short flowmeter.

The magnetic circuit M2 used in obtaining the data presented in Figs 6.9 and 6.10 had $c/a = 1.2$ and, from Fig. 3.10, the applicable value of the end effect constant should lie between about 0.88 and 0.92. This may be compared with the average values of K obtained from the measured data and set out in Table 7.1. For d.c. excitation with mercury, only K_4 should be significant and this is confirmed by the measured value of K which, at 0.93, is in good agreement with curve B of Fig. 3.10. The same value of K (within the limits of experimental accuracy) was found for pulsed excitation with mercury and also for both types of time-varying field conditions with 8 per cent NaCl solution. In other cases, K departed from 0.93 and the causes of this are next considered.

The skin depth of mercury at $f_o = 1$ kc/s is about 1.5 cm and, in accordance with the discussion of Section 3.12, the magnetic field at the centre of a 3/8-in diameter channel should be weakened. The value of $K = 0.86$ obtained for this frequency may be taken to indicate a reduction in V_m due to this and hence the need for a skin effect (or eddy current) factor in a.c. flowmeter calibration.

The calibration relation for pulsed excitation and mercury

is indistinguishable from the d.c. case. The time constant $\tau_d \approx 30$ μsec for mercury and indicates that the magnetic field can diffuse into a 3/8-in diameter channel in a time substantially less than the pulse duration at $f_o = 500$ c/s. On this basis, measurements using this method were effectively made under d.c. conditions over the frequency range used and this is confirmed by the experimental results.

Loading of the flowmeter output by the amplifier input impedance (in the system considered, $R_{in} = 3.2$ MΩ, $C_{in} = 15$ μμF) introduces additional errors with low-conductivity liquids and these are clearly demonstrated for tap water and distilled water in Fig. 6.10. The situation here is complicated by the frequency-dependent character of Z_o already given in Fig. 6.6 and the difference in calibration between 50 and 1000-c/s a.c. excitation may, as shown in Table 7.1, be attributed to this effect. The values of K obtained with distilled water were between 0.32 and 0.34, the spread being again due to the dependence of Z_o on f_o. They indicate that the amplifier input impedance was inadequate for full sensitivity in this case.

Figure 6.11 illustrates the amplifier loading effect and also the improvement which can be gained by increase of electrode area, in this case with type B electrodes in a square channel. A high input impedance cathode follower is required for low-conductivity liquids and the results of Test 10, in addition to showing motional dielectric polarisation, indicate the gain in K obtained with the Lettvin circuit (Fig. 5.9).

(b) Comparison of Methods

When an electromagnetic flowmeter is to be calibrated empirically, Figs 6.9 and 6.10 show that the choice of field excitation is unimportant (within the restrictions mentioned at the beginning of this Chapter), provided the minimum value of V_m to be detected is not obscured by system noise. Figs

6.5 and 6.12 give the results of measuring this noise under different conditions.

Referring first to Fig. 6.12, the approximately constant value obtained for conductivities greater than 1 U/m was composed of supply harmonics while, at lower values of σ, random noise predominated. These harmonics were traced to non-uniformities in the magnetic circuit and were found to increase almost linearly with B_0 and f_0. Random noise from the flowmeter, as shown in Fig. 6.5, was of thermal origin and varied with f_0 and electrode area in accordance with the dependence of R_0 on these quantities. With pulsed field excitation, only the random noise component was observed.

For flow measuring applications involving liquid metals, d.c. excitation is entirely satisfactory unless the anticipated flow signal is of such a low level as to incur difficulties with d.c. amplifiers. In these cases, pulsed excitation gives a stable zero-flow level free from supply harmonics and, in effect, serves as a scheme for "chopping" the flow signal prior to a.c. amplification without the limitations of the mechanical device which would otherwise be used.

With relatively high-conductivity electrolytic solutions, the freedom of the pulse method from supply harmonics gives it a substantial advantage over sinusoidal excitation for which these would provide the chief component of system noise. For low-conductivity liquids, however, the narrower bandwidth required by the sinusoidal method is an advantage in that random noise reduction by bandwidth limitation can be more effective. From the experimental evidence presented here, the two methods are likely to prove about equally satisfactory for liquid conductivities of the order of 1 U/m.

(c) <u>Selection of Excitation Frequency</u>

For measurements of transient flow conditions, the excitation frequency must be sufficiently high to enable it to be

modulated by the highest rate of change of flow without distortion. Analysis of transients in channel flow would involve the solution of equations such as 3-13 and 3-14 for appropriate boundary and initial conditions and is likely to prove difficult in all but a few simple cases. Some experimental work on time-varying flow conditions has been reported by Morris and Chadwick (Ref. 94) and Arnold (Ref. 95) and is also to be found in the metering of blood flow. While transient flows have not been considered in this study, it may be remarked that an instantaneous response will no longer be obtained if the field diffusion time τ_d is a significant fraction of the transient duration. This is likely to prove troublesome in liquid metals.

In other respects, the choice of excitation frequency represents a compromise between the various frequency-dependent effects already determined. An increase in f_o improves, in general, input circuit performance with respect to noise and electrode polarisation but increases the difficulties involved in the provision of an adequate value of B_o and in the higher V_t/V_m ratio. This is confirmed by the results of Test 2 (Fig. 6.5) and it is suggested from these that a value of f_o within the range 200-500 c/s is to be preferred unless rapid changes in flow rate indicate the need for a higher value. This applies to both pulsed and sinusoidal excitation, whichever is appropriate to the flow situation being metered.

The 50-c/s mains supply is certainly convenient for field excitation but also has important disadvantages. With small electrodes and low-conductivity liquids, the series resistance component of Z_o is likely to have a 1/f dependence at this value of f_o and thus to raise noise generation in the flowmeter. In addition, 1/f noise from the associated electronic equipment makes a significant addition to the zero-

flow noise level. Stabilisation of the air gap flux density against supply voltage fluctuations and changes in excitation coil resistance is required in any instrument intended to give good accuracy. This largely negates the initial advantage of the supply mains and constitutes a further factor in favour of a power amplifier in which stabilisation is readily attained.

7.4. Fluid Properties and Flow Conditions

The experimental results obtained in Tests 9-14 show that the calibration of an electromagnetic flowmeter depends, in general, on the fluid properties and flow conditions. The errors introduced are usually of the order of 10 per cent of the performance predicted by simple theory and may depend on the type of flow conditions (laminar or turbulent) established in the flowmeter channel. It is perhaps unfortunate that the calibration in the radially symmetric, circular channel case, as considered by Williams (Ref. 67), Thurlmann (Ref. 83) and Kolin (Ref. 86), is independent of the flow conditions for this has been tacitly assumed to apply in all situations. Discussion of calibration factors and errors is limited here to low-M conditions and magnetohydrodynamic effects are treated in the next Section.

The demonstration of motional dielectric polarisation given by Test 10 (Fig. 6.13) is included to confirm qualitatively the results of Section 4.2 and to show that it is a possible method for metering the flow of liquid dielectrics. As distilled water is not a particularly satisfactory liquid for the conditions of this Test, the effect appears only as a high-frequency modification of the performance predicted without considering it. The substantially greater flow signal obtained with electrodes in the longer channel side (curve A of Fig. 6.13) is, however, in accordance with the results of Section 4.2 and is sufficient to illustrate them.

The values of K obtained for the low-M calibration of
square and rectangular channels with type A electrodes (Fig.
6.16) are given in Table 7.2 where they are shown to give
reasonable agreement with the calculated values of K_3 from
Fig. 3.7 under laminar flow conditions. For turbulent flow,
however, the K values changed through the transition region
and tended to those of type B electrodes for which calibrations
are also included in Fig. 6.16. Comparison of the results for
the two types of electrodes shows the performance of the type
B configuration to be superior in that there is no dependence
on flow conditions. There is also good agreement with the
predicted values at all Reynolds numbers. The effect with
type A electrodes is greatest in low aspect ratio channels and,
for a/b = 10 in Fig. 6.16, the choice of electrodes is
unimportant.

The calibration is also affected by velocity profile
distortion, as shown in Figs 6.20 and 6.21 for both a circular
and a square channel, the latter with type B electrodes.
Positioning the profile-distorting plug along an axis perpen-
dicular to that of the electrodes (location A in Fig. 6.20)
should increase the velocity along the electrode axis but this
should be decreased when the two axes are parallel (location B
in Fig. 6.20). Thus V_m should be respectively larger and
smaller than its radially symmetric profile value and this is
confirmed by the experimental results. These also show that
the square channel calibration in Test 13 was insensitive to
profile distortion as predicted in Section 3.8. The circular
channel section was much less satisfactory in this respect and
the qualitative explanation of the cause as given above has
been confirmed by Shercliff (Ref. 110) in an analytical
treatment.

The highly conducting circular channel with type E elec-
trodes is a further example of a calibration relation which

Liquid	K from Figs 6.9 and 6.10					K_4 from Fig. 3.11 Curve B	$\dfrac{R_o}{Z_o + R_o}$ a.c.	
	d.c.	a.c.		pulse				
		50c/s	1kc/s	50c/s	200c/s		50c/s	1kc/s
Mercury	0.93	0.925	0.86	0.94	0.935	0.92		
8% NaCl	-	0.93	0.94	0.94	0.93	0.92	1.0	1.0
Tap Water	-	0.975	0.90	0.87	0.885	0.92	0.94	0.97
Dist. Water	-	0.315	0.335	0.32	0.33	0.92	0.28	0.30

Table 7.1.   End Effect Factors

Aspect Ratio	Electrode Type	K from Data of Fig. 6.16		K_3 from Fig. 3.7
		Laminar Flow	Turbulent Flow R > 5000	Laminar Flow
1 (C4)	A	1.12	1.04	1.11
	B	0.99	0.99	-
3 (C7)	A	1.02	1.01	1.03
	B	0.995	0.995	-
10 (C9)	A	1.0	1.0	<1.01
	B	0.995	0.995	-

Table 7.2.   Velocity Profile Factors in Square and
Rectangular Channels - Low-M Conditions

Channel Material	Cross-Section	Electrode Type	K from Figs 6.17 and 6.18. f_o=50c/s		K predicted by eqs 3-39, 3-47, Fig. 3.7
			d.c.	a.c.	
Stainless Steel	circular	A	0.58	0.57	0.59
	square	A	0.56	0.54	0.58*
		B	0.49	0.48	0.52
	rect.(C8)	B	0.405	0.39	0.38
Nickel-Plated Cu	circular	A	0.057	0.054	0.0605
	square	B	0.165	0.16	0.17

* laminar flow only

Table 7.3.   Wall Conductivity Factors

Channel Section	Excitation f_o=50c/s	K from Data of Figs 6.14, 6.15				Predicted K_2 (high-M)
		Laminar Flow		Turbulent Flow		
		Short	Long	Short	Long	
circular	d.c.	0.985	0.92	0.985	0.92	1
C1	a.c.	0.98	0.95	0.98	0.97	1
square*	d.c	1.13	1.02	1.06	1.02	<1.01
C4	a.c	1.11	1.05	1.06	1.04	<1.01
square**	d.c.	0.995	0.995	0.995	0.995	1.0
C4	a.c.	1.0	1.0	1.0	1.0	1.0

* type A electrodes.   ** type B electrodes

Table 7.4.   Flowmeter Calibration Factors - High-M Conditions

Note: All data in above Tables are given to nearest 0.5 per
cent and are subject to overall expmtl. error of 2 per
cent

depends on flow conditions. Fig 6.22 shows a marked irregularity in the transition region when the inter-electrode distance for maximum V_m in laminar flow was used but that this was removed by repositioning the electrodes. In turbulent flow, the development of a flow signal depends on the average velocity of the flow between the electrodes exceeding u_o, as required by equation 3-43. The slow decline of this ratio with increasing Reynolds number accounts for the lack of linearity in the V_m versus u_o relation above the transition velocity. The calibration of a non-conducting circular channel with wall-mounted electrodes is also included in Fig. 6.22 and shows no dependence on the character of the flow.

The effect of electrically conducting walls under low-M conditions for wall-mounted electrodes and mercury flow, as shown in Figs 6.17 and 6.18 and summarised in Table 7.3, was generally to increase the calibration errors, particularly when K was small. The accuracy of conductivity and wall dimension measurements was not sufficient to enable the discrepancies to be fully explained and they may be due in part to contact resistance. While this matter requires further investigation, it is to be noted that the calibration with 50-c/s a.c. was consistently lower than the corresponding d.c. case and this is presumably due to the effect of eddy currents in the channel walls.

7.5. Magnetohydrodynamic Effects

Two alternative viewpoints may be adopted with respect to magnetohydrodynamic effects in that they may either be regarded as further sources of calibration errors or used to create laminar flow conditions for which the relation may be predicted. The second alternative is based on the demonstration by Hartmann and Lazarus (Ref. 23) of the suppression of turbulence in channel flow by a transverse magnetic field. From this experiment, it may be concluded that a flowmeter of

sufficient length will be capable of establishing laminar flow and hence being calibrated using the extended Hartmann theory of Section 3.2, provided a high aspect ratio channel is used. The classification of flowmeters into short and long types as used here is intended to reflect the basis on which they are designed.

The calibration relations obtained in the presence of significant magnetohydrodynamic effects ($M = 90$) are given in Figs 6.14 and 6.15 for non-conducting channel walls and in Fig. 6.19 for conducting walls. The K values thus obtained are summarised in Table 7.4. For the short flowmeter arrangement, the behaviour followed closely the low-M case (Fig. 6.9) and it may be concluded that $l_m = 2\frac{1}{2}$ in was insufficient to permit the establishment of profile distortion. Shercliff's entry length relation, equation 3-52 is directly applicable only when $M^2 \ll R$ and for $R = 10^5$, indicates that $l_e \approx 40r_i$ which is in agreement with the experimental evidence.

In the long flowmeter for which $l_e/a = 50$ and $l_e/r_i = 43$, magnetohydrodynamic profile distortion effects were obtained as is evident from the experimental data. A non-conducting square channel with type A electrodes was about 1 per cent above the value calculated from equation 1-4 while, for the corresponding circular channel, $K = 0.92$. For the stainless steel circular channel, however, the calibration was 96 per cent of the low-M value. From this result, it is apparent that the presence of conducting walls reduces the profile distortion effect and this may be due to the existence of a return path for circulating currents external to the liquid. Use of 50-c/s a.c. excitation also produced an interesting result with non-conducting channels in that the values of K obtained exceeded those of the corresponding d.c. situation by 2-3 per cent. This suggests that a time-varying field requires a greater entry length under comparable conditions to establish magneto-hydrodynamic channel flow than does d.c. excitation.

7.6. Design Principles

The calibration of electromagnetic flowmeters has been shown, by channel flow analysis in Chapter 3 and experiment as described in Chapter 6, to depend on channel dimensions, electromagnetic properties, flow conditions and contact effects. In addition, to the extent that these are functions of temperature, the effect of this also requires consideration.

Design and construction of a flowmeter with an accurately predicted calibration evidently becomes increasingly difficult as the desired operating range of fluid conductivity is increased. Table 7.5, prepared on the basis of the results presented and discussed above, summarises the design problems and indicates for each case the relevant parameters in accordance with the discussion in Section 4.6. In it, a classification of flowmeters has been made into types intended for high, medium and low conductivity fluids for it is this quantity which, in the first instance, determines performance. This division corresponds to liquid metals, strong electrolytes and weak electrolytes while the dielectric polarisation flowmeter would be applicable to those fluids usually classed as non-conductors.

The attainment of a specified accuracy and conductivity range requires that the inter-electrode distance, magnetic flux density and amplifier-detector sensitivity be measured and stabilised within close limits. Using feedback methods, it should be possible to achieve a combined error of less than 0.5 per cent in B_o and amplifier gain while the inter-electrode distance may be measured at least to the nearest 0.001 in. In the case of B_o, experimental work has shown that V_m is insensitive to small non-uniformities ($<$ 2.5 per cent) in the air gap field distribution and is accurately determined by the average value. Extreme care in this respect is, therefore, not required.

Conductivity Range $\mho/m$	$10^7 - 10^3$ high	$10^3 - 10^{-1}$ intermediate	$10^{-1} - 10^{-5}$ low
Typical Liquids	Liquid Metals	Strong Electrolytes	Weak Electrolytes and Water
Magnetohydro-dynamic Effects	yes $(M, M/\sqrt{R}, \frac{c}{a}, \frac{c}{r_i})$	not significant	no
Dielectric Polarisation Effects	no	no	yes (U_D)
End Effect	yes $(\frac{c}{a}, \frac{c}{r_i})$	yes $(\frac{c}{a}, \frac{c}{r_i})$	yes $(\frac{c}{a}, \frac{c}{r_i})$
Eddy Current Effects	yes (U_s)	no	no
Wall Conductivity Effects	operation possible at reduced S (R_{ci}/R_{cw})	operation only possible if electrodes are inserted into channel - see Section 3.7(d)	
Amplifier Loading	no	possible (Z_o/Z_{in})	yes (Z_o/Z_{in})
D.C. Field Excitation	yes	not recommended (but possible with special electrodes)	not recommended
Time-Varying Excitation	pulsed preferred	pulsed or sinusoidal	sinusoidal preferred
Predominant Noise Component with A.C. Excitation	supply harmonics	supply harmonics	random noise $(\frac{a}{r_e}, \frac{r_i}{r_e})$
Capacitance-Coupled Voltages	no	may be present unless input is shielded	yes, careful shielding required

Table 7.5. Summary of Design Parameters

When an overall accuracy of 1 per cent is intended, this allows about 0.5 per cent error in K when the inter-electrode distance is of the order of 1 in. Conductivity-dependent effects have thus to be eliminated as far as possible from multi-purpose flowmeters and at least closely controlled in accordance with earlier discussions when operation is required on one fluid only. With non-conducting walls, an error of around 0.25 per cent should be attainable but further work is required on the conducting wall case before this can be assessed. Accordingly, the use of the latter type of wall cannot yet be recommended though it is likely to prove suitable. Direct measurement of R_{ci} and R_{cw} might provide a useful check on the predicted value of K when w, σ_w or k_c cannot be determined with sufficient accuracy.

The use of a square or rectangular channel with highly conducting end walls (type B electrodes) has been demonstrated through Tests 10 and 13 to give the greatest freedom from velocity profile distortion effects. The rectangular channel has the added advantage that it reduces the air gap length and hence the excitation power required. It is at all times desirable to site electromagnetic flowmeters away from channel bends, valves and other sources of profile distortion. This is particularly true when circumstances dictate the use of a circular channel section. While the accuracy of the experimental work was not sufficnently high to establish conclusively that square or rectangular channels give an error-free measure of the average velocity, the results obtained are certainly consistent with this assertion. It seems reasonable to suppose that the error introduced will not exceed 0.25 per cent provided sources of profile distortion are located at least 40a or $40r_1$ from the electrodes in such channel sections.

It may be mentioned here that a random component was observed in V_m when turbulence was present in the flow.

However, its estimated r.m.s. value of less than $0.05V_m$ on a 20-kc/s bandwidth had a negligible effect and was further reduced by the selective amplifier.

The ratio of c/r_i or c/a requires consideration in relation to end effect and magnetohydrodynamic flow stabilisation. The value of K_4 given by curve B of Fig. 3.12 depends on approximations which may conceal small errors and it would appear to be desirable to use a ratio of at least 6:1 to ensure that K_4 is within 0.1 per cent of unity.

Further increase in this ratio is worthwhile only if flow stabilisation under high-M conditions is the objective. While this method has been demonstrated both by the results of Test 10 and in an observed reduction in the random component of V_m,[1] there is no evidence that it is more effective than normal hydrodynamic methods of flow stabilisation. The calibration errors appear to be of the same order as those for the short flowmeter and a square or rectangular channel with type B electrodes is again to be preferred. The long flowmeter has practical disadvantages in that it requires a large magnet, introduces an increased pressure drop as shown by equation 3-65 and, with circular channels, has a profile distortion effect which is not amenable to exact prediction.[2]

7.7. Concluding Remarks

This study has been concerned with the calibration of the contact type of electromagnetic flowmeter, the liquids for which it is suitable and the basis on which it should be designed. Emphasis has been placed on characterising the

---

1. The results given by Elrod and Fouse (Refs 97 and 102) are for a long, circular channel flowmeter and also show a clear indication of the effect but no explanation for it is given.
2. Shercliff (Ref. 110) has considered this situation and has developed an approximate boundary layer solution of limited validity. For $\sigma_w = 0$, this yields $K = 0.925$ and thus agrees with the results of Test 10 to which it is applicable.

effects which cause the calibration to deviate from the relation predicted by simple theory and which determine the lowest measurable flow rate. This has led to the development of pulsed field excitation, the production of a flow signal in aqueous solutions for the case of a high-conductivity channel, the assessment of design problems as summarised in Table 7.5, the conclusion that it is feasible to construct a flowmeter with a calibration predicted to 1 per cent accuracy and the clarification of a number of practical points. Included in the last mentioned are the choice of input circuit arrangements, field excitation and, with time-varying excitation, frequency and waveform.

Empirically calibrated flowmeters are now used to a considerable extent in the metering of blood flow and of corrosive liquids but further work on the device is still required. In particular, the needs are for the design and construction of an accurately predicted instrument, development of a flowmeter able to handle transients with time durations of the order of 1 msec or less, further work on the performance with time-varying fields and a study of temperature dependence. Application of the method to gases and vapours and investigations of the induced field and dielectric polarisation flowmeters are further areas which require attention.

The electromagnetic flowmeter has been analysed here in terms of magnetohydrodynamic channel flow. Many points concerning these flows are still obscure, including the suppression of turbulence by d.c. and time-varying fields, velocity profiles in the presence of turbulence and laminar flow solutions for time-varying conditions, and all of these present considerable theoretical difficulties. Experimental evidence on the character of channel flow is also required to supplement and extend that of Hartmann and Lazarus (Ref. 23)

and Murgatroyd (Refs 39 and 40). One possibility might be the adaption of the electromagnetic velocity probe developed by Kolin and Reiche (Refs 84, 85 and 114) for profile measurements or for the study of turbulence in magnetohydrodynamic channel flows. Work in the latter case could follow the lines of that by Grossman and Charwat (Ref. 106) who, however, confined their attention to aqueous solutions.

The use of electrically conducting channel walls may be regarded as placing a load on the flowmeter and hence converting it into a simple magnetohydrodynamic generator. Recent interest in the possibilities of large-scale power generation using flows of relatively low-temperature, seeded gases provides a device development problem which should enable the channel flow studies presented here to be of further use. For this case, fluid compressibility and anisotropic conductivity effects would require consideration.

Appendix I

ELECTROMAGNETIC PUMP DESIGN

At the time when the design and construction of the hydraulic system was undertaken, considerable attention was being given to the use of electromagnetic pumps for liquid metals and the work of Woodrow (Ref. 50) on the design of the d.c. conduction type had become available. The relatively modest head and flow rate requirements of the hydraulic system and the lack of a suitable mechanical pump, led to the selection of the electromagnetic type for pumping mercury. Mechanical pumps with the required delivery of 3 gall/min through a 9-ft head are now available and are to be preferred for the type of flow system described in Chapter 5. The chief difficulties with the d.c. conduction pump are the low efficiency obtainable with mercury and the need for a special, low-voltage, high-current supply.

As the pump described here incorporated no special features and its design followed closely the procedure set out by Woodrow, only a brief account of it is given. A magnetic circuit was designed using the same procedure as for the M1 unit described in Section 5.3 and provided a separate excitation field with $B_o \approx 1.2$ Wb/m^2 in the air gap. The iron path in this case, however, was fabricated from solid material and the coils were wound with $\frac{1}{2} \times \frac{1}{8}$ in section copper strip. The air gap length was increased to $\frac{3}{4}$ in, w_m to 3 in and 1_m remained unchanged at 10 in.

A rectangular section channel with 2a = 3 in and 2b = $\frac{5}{16}$ in was used in the pump and connected to the $1\frac{1}{8}$ -in diameter delivery pipe through a section changer as shown in Fig. 5.2. For a properly designed pump,

$$P_d = \frac{B_o^2}{2\mu} \qquad (I-1)$$

where p_d is the pump delivery pressure. Using the value of B_o quoted above yields $p_d = 82$ lb/in^2 and this may readily be shown to be sufficient for the required flow conditions in a smooth pipe with $2r_i = 1\frac{1}{8}$ in.

Woodrow defines three dimensionless parameters for pump design and these, for rationalised equations, are

$$R_M = \mu \sigma u_o c \qquad (I\text{-}2)$$

$$k_p = \frac{\text{liquid electrical resistance}}{\text{total circuit resistance}} = 1 + \frac{2R_{ex}bc}{a} \qquad (I\text{-}3)$$

$$\alpha_v = \frac{\text{mean back e.m.f.}}{\text{applied voltage}} = \frac{R_M(1 + \coth R_M) - 1}{R_M(1 + \coth R_M) + k_p - 1} \qquad (I\text{-}4)$$

where R_{ex} is the circuit resistance external to the pump. It may be noted that he did not recognise that I-2 gives the magnetic Reynolds number appropriate to pump analysis and accordingly failed to point out its significance as established in Section 2.4.

For a volume flow rate of 3 gall/min, $u_o \approx 50$ cm/sec and this value, together with the chosen dimensions of the channel section, yields $R_M \approx 0.065$, $k_p \approx 4.5$ and $\alpha_v \approx 0.01$. The required supply current is then 7400 A and the efficiency is about 1.5%.

The low-voltage, high-current supply was provided by 16 heavy-duty 6-V batteries, individually connected to the pump electrodes by about 6 ft of 19/064 cable through two car starter switches, one in each line. The starter switches enabled the batteries to be completely disconnected from the pump for series charging. This supply arrangement was capable of delivering a short circuit current of about 10^4 A with $R_{ex} = 3 \times 10^{-4} \Omega$ for 5-7 min. Lower currents were obtained for longer periods by connecting equal numbers of batteries in parallel through a correspondingly reduced number of cable

pairs, the cable resistance serving to provide the necessary current limitation.

The channel section was fabricated from stainless steel and nickel-plated copper electrodes were used. The pump, when installed in the hydraulic system, was able to deliver at a maximum rate of 3.1 gall/min for a 6-min period with an input current of about 9000 A.

Appendix II

BRIDGED-T SUPPLY FILTER

It is well known[1] that the transfer function of the bridged-T network shown in Fig. II.1(a) possesses a pair of conjugate zeros on the $j\omega$ axis of the complex frequency plane and thus can provide complete rejection of a selected frequency. By cascading networks of this type, a number of rejection frequencies can be obtained and these, in the case of supply harmonic elimination, are adjusted to the important harmonic frequencies. A suitably high rejection Q-factor is employed to avoid attenuation of the fundamental frequency component and a capacitance is added in parallel with the filter output to provide substantial attenuation of the high-order harmonics, for which complete rejection is usually not required.

For the application considered here, where currents of the order of 1 A were involved, the bridged-T structure was chosen in preference to the commonly employed parallel-T to

---

1. See Ref. 145, p. 384

minimise losses and also to give a higher rejection Q-factor.

Both standard and modified networks are shown in Fig. II.1 and typical voltage transfer characteristics appear in Fig. II.2. The effect of the added capacitance C_2 is to attenuate high frequencies in the ratio $C_2/(C_2 + C/2)$ and to modify the transfer function at frequencies below the null value by peaking it as shown in Fig. II.2. Within limits which are readily derived, the load resistance may be chosen to obtain unity voltage transfer ratio at a specified frequency below the null value   A more detailed analysis and discussion of this filter will be presented eleswhere.

Fig. II.3 gives the complete circuit of the version of this filter developed for flowmeter work and its measured voltage transfer function appears in Fig. II.4. Two bridged-T networks were employed to give complete rejection of both the third and fifth harmonics of the 50-c/s supply. The effectiveness of the arrangements is indicated in Table 6.1 where it is shown to provide a reduction of about 30 db in the zero-flow value of V_o with the external shield can in position.

(a) Basic circuit

(b) Circuit modified by
addition of C_2
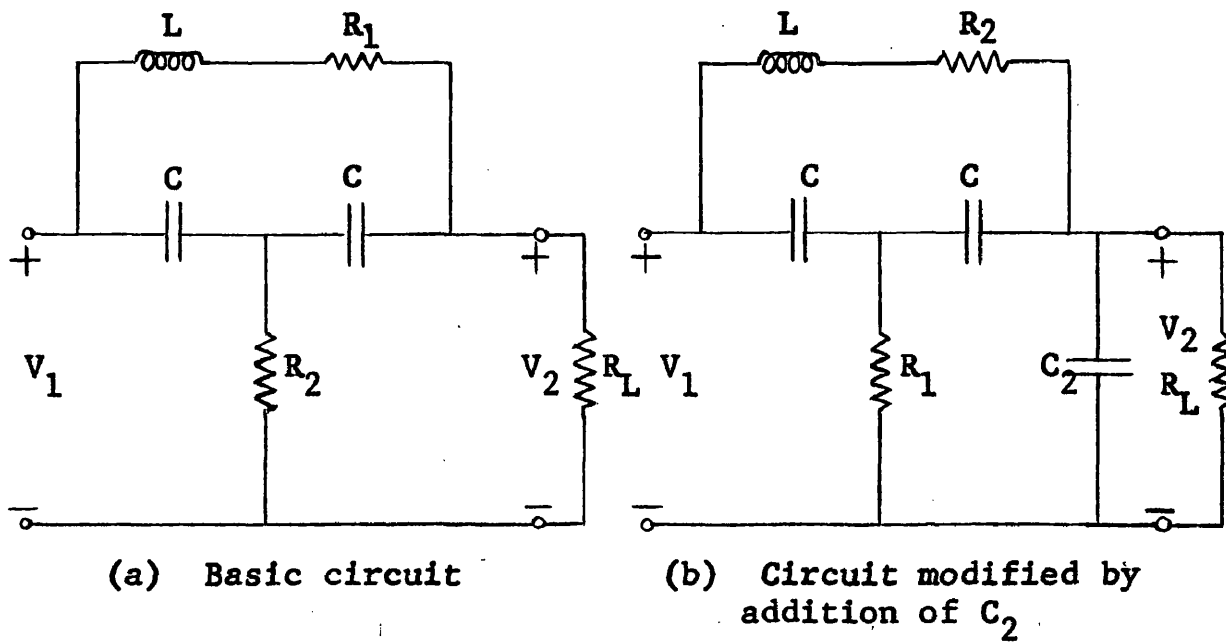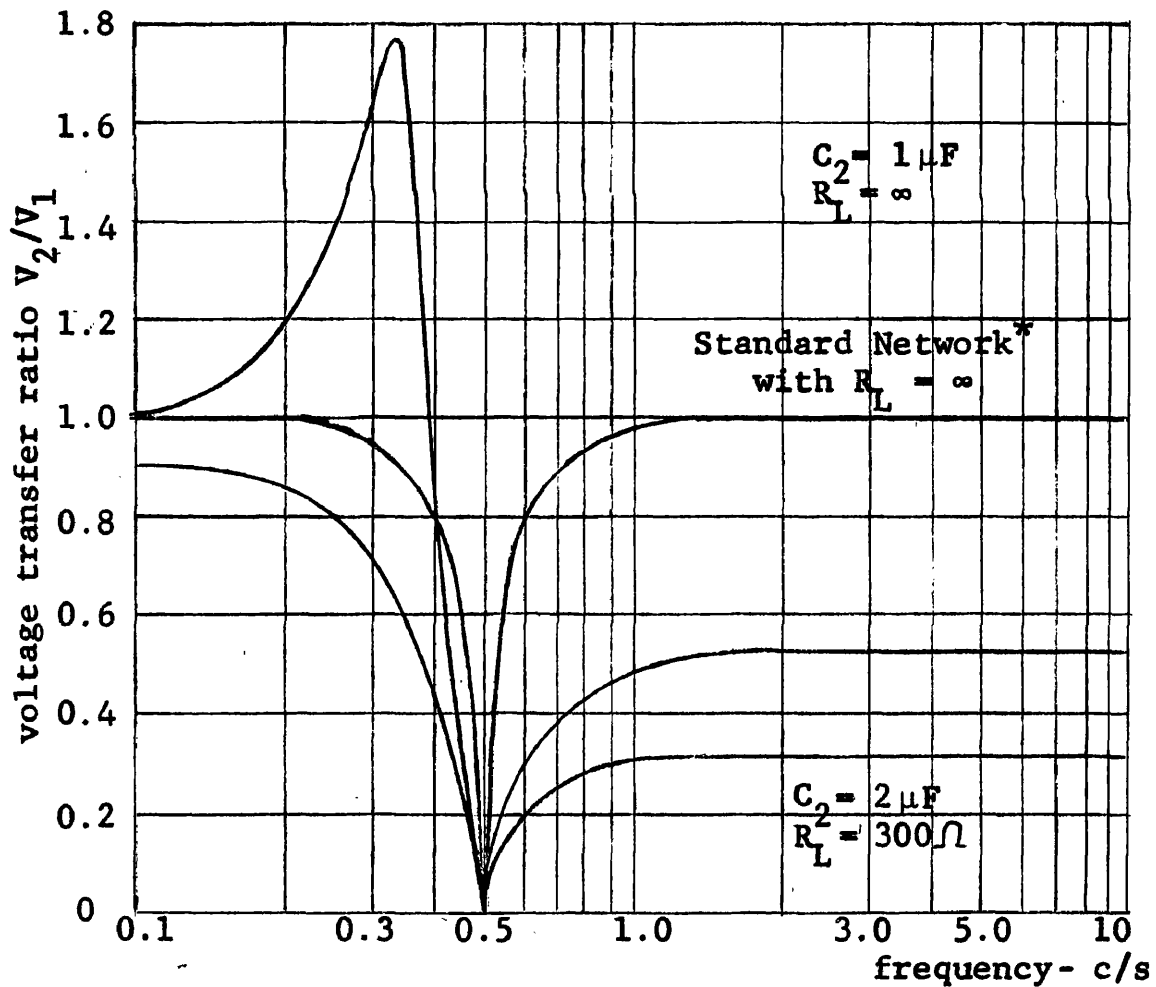
Fig. II.1. Bridged-T Networks

* C = 2 μF, L = 110 mH, R_1 = 37 Ω, R_2 = 770 Ω

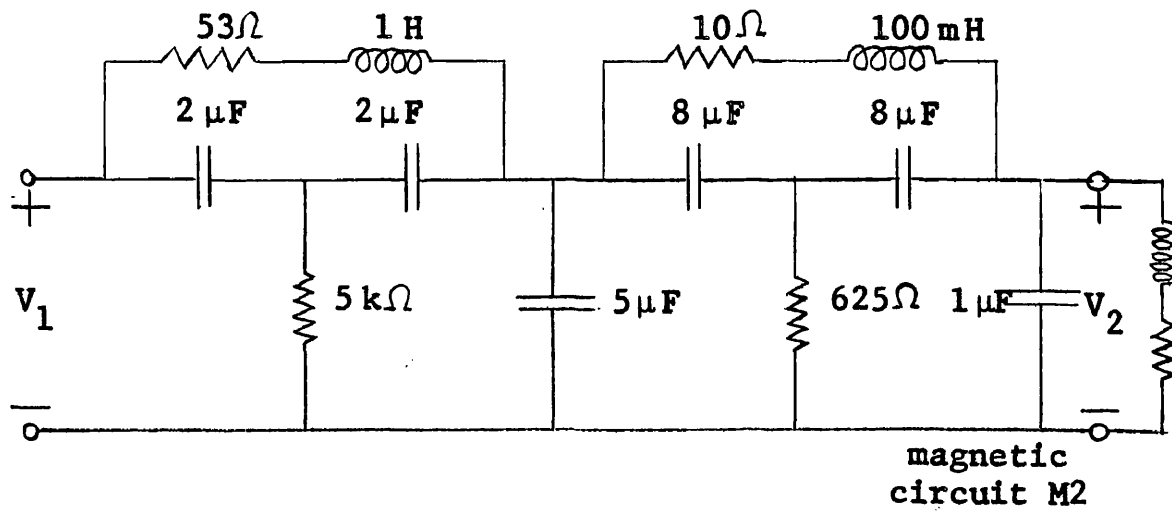Fig. II.2. Typical Voltage Transfer Characteristics for
Bridged-T Networks
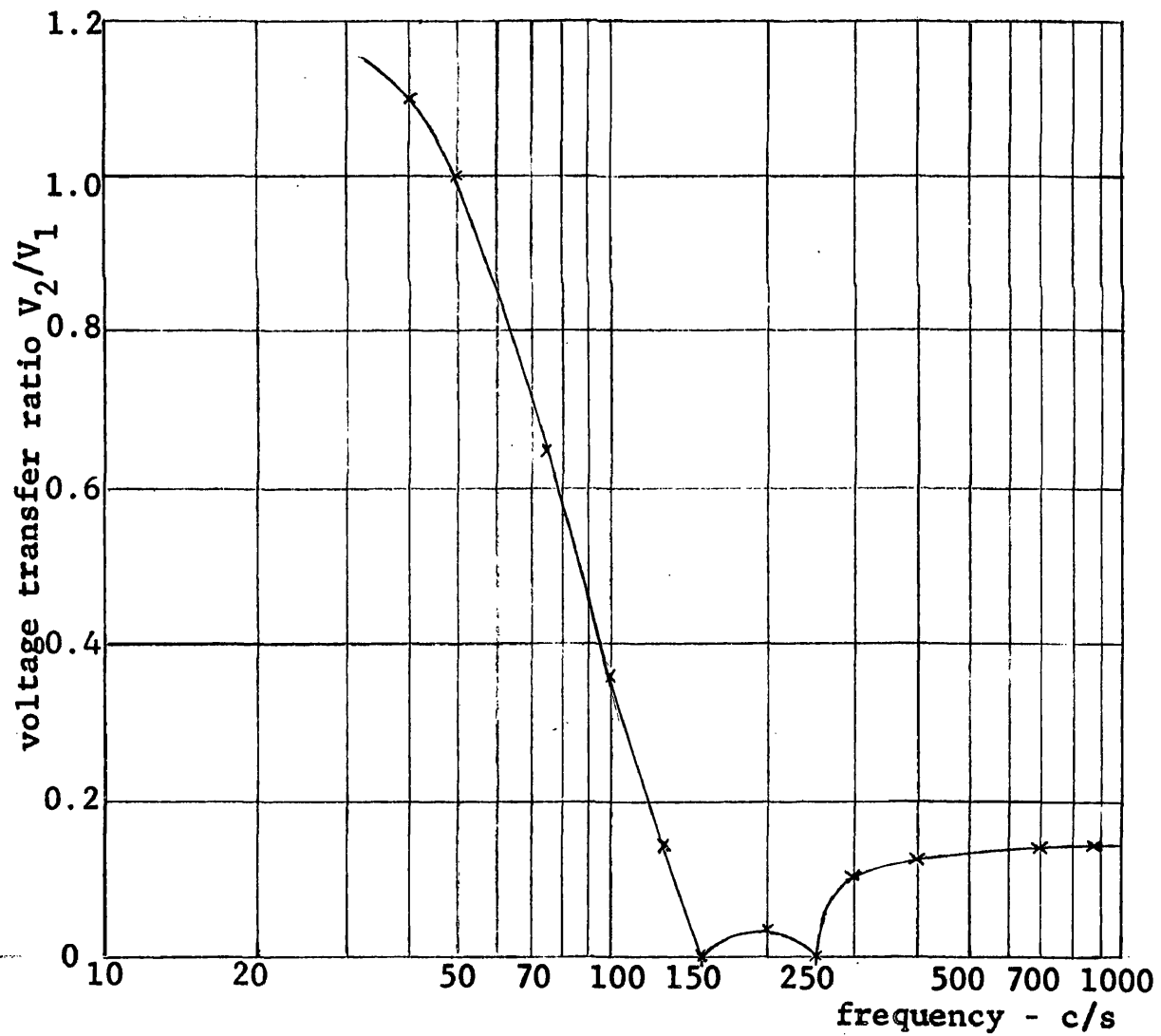
Fig. II.3. Two-Section Bridged-T Supply Filter

Fig. II.4. Supply Filter Characteristic

R E F E R E N C E S

Measurement of Fluid Flow - General

1. "Fluid Meters - Their Theory and Application", A.S.M.E. Research Publication 4th Ed.,(1937).

2. Linford, A. "Flow Measurement and Meters", E. and F. Spon., Ltd., London,(1949).

3. Cole, H.W. "Operating Principles of some Liquid Flowmeters", Prod. Eng., Vol. 22, p. 135, (1951).

Measurement of Fluid Flow - Application of Electrical Methods

4. "Electronic Flowmeter", Rev. Sc. Instrum., Vol. 21, p. 889, (1950).

5. Linford, A. "Electrical Transmission of Flow and Level Records", Beama J., Vol. 47, p. 97; Vol. 48, p. 15; Vol. 49, p. 285, p. 335, and p. 367, (1940-42).

6. Curran, F.J. "Impedance Bridge for Flow Rate Metering", Electronics, Vol. 20, p. 106, (1947).

7. Hooper, L.T. "Salt Velocity Measurements at Low Velocities in Pipes", Trans. A.S.M.E., Vol. 62, p. 651,(1940).

8. Dodkin, O.H. "Field Checks of the Salt Velocity Method", Trans. A.S.M.E., Vol. 62, p. 663, (1940).

9. Weske, J.R. "Measurement of High Air Velocities by the Hot Wire Method", N.A.C.A. Technical Notes No. 880, (Feb. 1943).

10. Sesan, R.A., Hillendahl, W.H., Gallagher, E.J., and London, A.L. "A Thermal Anemometer for Low Velocity Flow", Trans. A.S.M.E., Vol. 64, p. 843, (1943).

11. Lamb, H.J. "An Electric Flow Meter", Electrical Engineering, N.Y., Vol. 66, p. 1216, (1947).

12. "Electronic Flowmeter", Nat. Bur. Stand. Tech. News Bull., Vol. 37, No. 2, p. 30, (Feb. 1953).

13. Kalmus, H.P. "Electronic Flowmeter System", Rev. Sci. Instrum., Vol. 25, p. 201, (1954).

Magnetohydrodynamics

14. Faraday's Diary, Vol. 1, pp. 409-412 (Section dated Jan. 12-13, 1832), G. Bell and Sons, Ltd., London, (1932).

15. Faraday, M. Bakerian Lecture Series, Jan. 12, 1832, Phil. Trans. Royal Soc., Vol. 15, p. 125, (1832)

Magnetohydrodynamics (cont.)

16. Blondot, R., "Sur l'absence de deplacement electrique lors du mouvement d'une masse d'air dans un champ magnetique", Compt. Rend., Vol. 133, p. 778, (1901).

17. Wilson, H.A., "On the Electric Effect of Rotating a Dielectric in a Magnetic Field", Phil. Trans., A, Vol. 204, p. 121,(1905).

18. Slepian, L., "Die Induktin in der Dielietrika die sich im magnetischen Feld bewegen", Ann. d. Phys. (4th Series) Vol. 45, p. 861, (1914).

19. Howe, G.W.O., "A Classic Experiment", Wireless Engineer, Vol. 16, p. 271, (1939).

20. Williams, E.J., "The Effect of a Magnetic Field on the Electrical Resistance of Liquid Metals and Alloys", Phil. Mag. (6th Series) Vol. 50, p. 46, (1925).

21. Jones, T.J., "The Electrical Resistance of Mercury in Magnetic Fields", Phil. Mag. (6th Series) Vol. 50, p. 46, (1925).

22. Hartmann, J., "Hg.-Dynamics", Math-fys. Medd., Vol. 15, No. 6, (1937).

23. Hartmann, J. and Lazarus, F., "Hg.-Dynamics II", Math-fys. Medd., Vol. 15, No. 7, (1937).

24. Alfven, H., "Existence of Electrodynamic-hydrodynamic Waves", Nature, Vol. 150, p. 405, (1942).

25. Alfven, H., "On the Existence of Electromagnetic-hydrodynamic Waves", Arkiv f. mat, astr. o fys. Bd 29B, No. 2, (1943).

26. Alfven, H., "On the Effect of a Vertical Magnetic Field in a Conducting Atmosphere", Arkiv f. mat., astr. o fys. Bd. 29A, No. 11, (1943).

27. Alfven, H., "On Sunspots and the Solar Cycle", Arkiv f. mat., astro. o fys. Bd. 29A, No. 12, (1943)

28. Walen, C., "On the Theory of Sunspots", Arkiv f. mat., astro. o fys. Bd. 30A, No. 15, (1944) and Bd. 31B, No. 3, (1944).

29. Lundquist, S., "Experimental Investigations of Magnetohydrodynamic Waves", Phys. Rev., Vol. 76, p. 1805, (1949).

30. Larmor, J., "How could a Rotating Body such as the Sun become a Magnet?", 1919 Rep. Brit. Ass., p. 159.

31. Elsasser, W.M., "Induction Effects in Terrestial Magnetism", Phys. Rev., Vol. 69, p. 106; Vol. 70, p. 202, (1946); Vol. 72, p. 821, (1947).

Magnetohydrodynamics (cont.)

32. Bullard, E.C., "The Magnetic Field Within the Earth", Proc. Royal Soc. A., Vol. 197, p. 433, (1949).

33. Bullard, E.C., "Electromagnetic Induction in a Rotating Sphere", Proc. Royal Soc. A., Vol. 199, p. 413, (1949).

34. Truesdell, C., "The Effect of the Compressibility of the Earth on its Magnetic Field", Phys. Rev., Vol. 78, p. 183, (1950).

35. Elsasser, W.M., "The Hydromagnetic Equations", Phys. Rev., Vol. 79, p. 183, (1950).

36. Lundquist, S., "On the Stability of Magneto-hydrostatic Fields", Phys. Rev., Vol. 83, p. 307, (1951).

37. Batchelor, G.K., "On the Spontaneous Magnet Field in a Conducting Liquid in Turbulent Motion", Proc. Royal Soc. A., Vol. 201, p. 405, (1950).

38. Lehnert, B., "On the Behaviour of an Electrically Conductive Liquid in a Magnetic Field", Arkiv för fysik, Bd. 5, p. 69, (1952).

39. Murgatroyd, W., "Damping of Turbulence by a Magnetic Field", Nature, Vol. 171, p. 217, (1953).

40. Murgatroyd, W., "Experiments on Magneto-hydrodynamical Channel Flow", Phil. Mag., Vol. 44, p. 1348, (1953).

41. Shercliff, J.A., "Steady Motion of Conducting Fluids in Pipes under Transverse Magnetic Fields", Proc. Camb. Phil. Soc., Vol. 49, Pt. 1, p. 136, (1953).

42. Stuart, J.T., "On the Stability of Viscous Flow Between Parallel Planes in the Presence of a Coplanar Magnetic Field", Proc. Royal Soc. A., Vol. 221, p. 189, (1954).

43. Lock, R.C., "The Stability of the Flow of an Electrically Conducting Fluid Between Planes under a Transverse Magnetic Field", Proc. Royal Soc. A., Vol. 233, p. 105, (1955).

44. Taylor, R.J., "Hydromagnetic Instabilities of an Ideally Conducting Fluid", Proc. Phys. Soc., Vol. 70B, p.31,(1957).

45. Taylor, R.J., "The Influence of an Axial Magnetic Field on the Stability of a Constricted Gas Discharge", Proc. Phys. Soc., Vol. 70B, p. 1049, (1957).

46. Lundquist, S., "Studies in Magneto-hydrodynamics", Arkiv för fysik, Bd. 5, p. 297, (1952).

47. Cowling, T.G., "Magnetohydrodynamics", Interscience Publishers, New York and London, (1957).

Magnetohydrodynamic Machines

48. Remenieras, G., "Sur la possibilite de transformer directement en energie eletrique l'energie d'une veine fluid", La Houille Blanche, No. Special A., (1948).

49. Northup, E.F., "Some Newly Observed Manifestations of Forces in the Interior of an Electric Conductor", Phys. Rev., Vol. 24, Series 2, p. 474, (1907).

50. Woodrow, J., "The D.C. Electromagnetic Pump for Liquid Metals", A.E.R.E. Report No. E/R 452, (1949).

51. Barnes, A.H., Smith, F.A., and Whitham, G.K., "Direct Current Electromagnetic Pumps", U.S. Atomic Energy Commission, Classified Report ANL-4322, (1949). Declassified as AECD-3430, (1952).

52. Collins, G.D., "Operation and Analysis of 100 Psi Electromagnetic Pump", U.S. Atomic Energy Commission, Unclassified Report KAPL-668, (1952).

53. Barnes, A.H., "D.C. Electromagnetic Pumps", Nucleonics, Vol. 11, No. 1, p. 16, (1953).

54. Watt, D.A., O'Conner, R.J., and Holland, E., "Tests on an Experimental D.C. Pump for Liquid Metals", A.E.R.E. Report No. R/R 2274, (1957).

55. Murgatroyd, W., "Theory of the Ideal A.C. Conduction Pump", A.E.R.E. Report No. RD/R 1566, (1954).

56. Barnard, J. and Collins, G.D., "Test of 1200 GPM Linear A.C. Electromagnetic Pump", U.S.A.E.C. Classified Report KAPL-568, (1951). Declassified as AECD-3460, (1952).

57. Nixon, J.D. and Crofts, T.I.M., "Experiment on a 400 GPM, 3-Phase, Flat Linear Electromagnetic Induction Pump at Low Line Pressures", U.K.A.E.A. Report No. R and DB(N)TN 138, (1954).

58. Watt, D.A., "A Study in Design of Travelling Field Electromagnetic Pumps for Liquid Metals", A.E.R.E. Report No. ED/R 1696, (1955).

59. Watt, D.A., "A.C. Liquid Metal Pumps for Laboratory Use", A.E.R.E. Report No. CE/R 1089, (1953).

60. Watt, D.A., "Electromagnetic Pumps for Liquid Metals", Engineering, Vol. 181, p. 264, (1956).

61. Blake, L.R., "A.C. and D.C. Conduction Pumps for Liquid Metals", The Engineer, Vol. 202, pp. 541-544 and pp. 572-576, (1956)

62. Blake, L.R., "Conduction and Induction Pumps for Liquid Metals", Proc. I.E.E., Vol. 104A, p. 49, (1957).

Magnetohydrodynamic Machines (cont.)

63. "The Reactor Handbook: Vol. 2, Engineering", pp. 350-359,
U.S.A.E.C. Publication A.E.C.D.-3646, (May 1955).

64. Barnes, A.H., Koch, L.J., Monson, H.O., and Smith, F.A.,
"The Engineering Design of EBR-II, a Prototype Fast
Neutron Reactor Power Plant" (includes design of elec-
tromagnetic pump), Proc. International Conference on the
Peaceful Uses of Atomic Energy, Geneva, 1955, Vol. III,
p. 330, Paper 501, (1956).

Fluid Flow and Velocity Measurement by Electromagnetic
Induction Methods

65. Smith, C.G. , and Slepian, J., "Electromagnetic Ship's
Log", U.S. Patent Number 1,249,530, Filed Dec. 1915,
Granted Dec. 1917.

66. Young, F.B., Gerrard, H., and Jevons, W., "On Electrical
Disturbances Due to Tides and Waves", Phil. Mag., Vol.
40, 6th Series, p. 149, (1920).

67. Williams, E.J., "The Induction of Electromotive Forces
in a Moving Liquid by a Magnetic Field and its Applica-
tion to an Investigation of the Flow of Liquids", Proc.
Phys. Soc., Vol. 42, p. 466, (1930).

68. Fabre, M.P., "Utilisation des forces electromotrices
d'induction pour l'enregistrement des variations de
vitesse des liquid conducteurs; un nouvel hemodromo-
graphie sans palette de sang", Compt. rend., Vol. 194,
p. 1097, (1932).

69. "Electricity from Tap Water", Sunday Express, Sept. 12,
1935.

70. Northfield, H.J., Howe, G.W.O., and Taylor, J.E., "Fluid
Flow Past Magnet Poles" (Correspondence), The Electrician,
Vol. 116, pp. 14, 40, 68, 151 and 208, (1936).

71. Kolin, A., "Electromagnetic Flowmeter: Principle of
Method and its Application to Blood Flow Measurements",
Proc. Soc. Expmt. Biol. Med., Vol. 35, p. 53, (1936).

72. Kolin, A., "Apparatus for Measuring Fluid Flow", U.S.
Patent Number 2,149,847, Filed July 1937, Granted March
1939.

73. Kolin, A., and Katz, L.N., "Observation de la vitesse
instantanee du sang a l'aide du rheonetre electromag-
netique", Ann. Physiol. Physiochem. Biol., Vol. 13,
p. 1022, (1937).

Fluid Flow and Velocity Measurement...(cont.)

74. Wetterer, E., "Eine neue Methode zur Registrierung der Blutströmungsgeschwindigkeit am uneröffneten Gefäb", ("A New Method for Measuring the Rate of Blood Circulation in an Unopened Vessel"), Zeitschrift für Biologie, Vol. 98, p. 26, (1937).

75. Wetterer, E., "Der Induktionstachograph", ("The Induction Tachygraph"), Zeitschrift für Biologie, Vol. 99, p. 158, (1938).

76. Kolin, A., "An Electromagnetic Recording Flowmeter", (Proc. American Physiological Soc. 49th Annual Meeting), Amer. Jour. Physiol., Vol. 119, p. 355, (1937),(Abstract).

77. Katz, L.N., and Kolin, A., "Flow of Blood in Carotid Artery of the Dog Under Various Circumstances as Determined with Electromagnetic Flowmeter", Amer. Jour. Physiol., Vol. 122, p. 788, (1938).

78. Jochim, K.E., "Some Improvements on the Electromagnetic Flowmeter", (Proc. American Physiological Soc., 51st Annual Meeting), Amer. Jour. Physiol., Vol. 126, p. 547, (1939),(Abstract).

79. Kolin, A., "An A.C. Induction Flowmeter for Measurement of Blood Flow in Intact Blood Vessels", Proc. Soc. Expmt. Biol. Med., Vol. 46, p. 233, (1941).

80. Kolin, A., "A Variable Phase Transformer and its Use as An A.C. Interference Eliminator", Rev. Sci. Instrum., Vol. 12, p. 555, (1941).

81. Kolin, A., Weissberg, J.L., and Gerber, L., "Electromagnetic Measurement of Blood Flow and Sphygmomanometry", Proc. Soc. Expmt. Biol. Med., Vol. 47, p. 324, (1941).

82. Eindhorn, H.D., "Electromagnetic Induction in Water", Trans. Royal Soc. of South Africa, Vol. 28, p. 143,(1940).

83. Thürlmann, B., "Methode zur Elecktrischen Geschwindigkeitsmessung von Flüssigkeit", ("Method of Fluid Flow Measurement"), Helvetica Physica. Acta., Vol. 14, p. 383, (1941).

84. Kolin, A., "Electromagnetic Method for the Determination of Velocity Distribution in Fluid Flow", (American Physical Soc. Annual Meeting, 1942), Phys. Rev.,Vol. 63, p. 218, (1943), (Abstract).

85. Kolin, A., "Electromagnetic Velometry I: A Method for the Determination of Fluid Velocity in Space and Time", Jour. App. Phys., Vol. 15, p. 150, (1944).

Fluid Flow and Velocity Measurement...(cont.)

86. Kolin, A., "An Alternating Induction Flow Meter of High Sensitivity", Rev. Sci. Instrum., Vol. 16, p. 109, (1945).

87. Guelke, R.W., and Schoute-Vanneck, C.A., "The Measurement of Sea Water Velocities by Electromagnetic Induction", Jour. I.E.E., Vol. 94, Pt. II, p. 71, (1947).

88. Lehde, H., and Lang, W.T., "Device for Measuring Rate of Fluid Flow", U.S. Patent Number 2,435,043, Filed Oct. 1944, Granted Jan. 1948. (Assigned to Control Instrument Company, Inc., Brooklyn, N.Y.).

89. Jochim, K.E., "Electromagnetic Flowmeter", Methods in Medical Research (Edited by V.R. Potter), Vol. 1, pp. 108-118, The Year Book Publishing Co., Inc., Chicago, Ill., (1948).

90. Clark, J.W., and Randall, J.E., "Electromagnetic Blood Flowmeter", Rev. Sci. Instrum., Vol. 20, p. 951, (1949).

91. Raynsford, C.L., "Suitability Report on the Magnetic Induction Flow Meter", The Kellex Corp., New York, N.Y., (1948).

92. Raynsford, C.L., "Report on Induction Flowmeter", The Kellex Corp., New York, N.Y., (1949).

93. Mittleman, E., and Cushing, V.J., "An Electronic Flowmeter and its Industrial Applications", Convention of the I.R.E., New York, N.Y., (1950). (Listed in Convention Proceedings but as yet unpublished).

94. Morris, A.J., and Chadwick, J.H., "An Electromagnetic Induction Method of Measuring Oscillatory Fluid Flow", Trans. A.I.E.E., Vol. 70, p. 346 (1951); Electrical Engineering, N.Y., Vol. 70, p. 529, (1951), (Abstract).

95. Arnold, J.S., "Electromagnetic Flowmeter for Transient Flow Studies", Rev. Sci. Instrum., Vol. 22, p.43, (1951).

96. Jaffe, L., Coss, B.A., and Daykin, D.R., "An Electromagnetic Flowmeter for Rocket Research", U.S.N.A.C.A. Research Memorandum RM E50L12, (March 1951).

97. Elrod, H.G., and Fouse, R.R., "An Investigation of Electromagnetic Flowmeters. Technical Report I", U.S. Atomic Energy Commission Unclassified Report No. N.E.P.A.-1451, (1950).

98. James, W.G., "An Induction Flowmeter Design Suitable for Radioactive Liquids", Rev. Sci. Instrum., Vol. 22, p. 989, (1951).

Fluid Flow and Velocity Measurement...(cont.)

99. Gray, W.C., "Magnetic Flowmeter Calibration Results", U.S. Atomic Energy Commission Unclassified Report No. KAPL-613, (1951).

100. James, W.G., "An A.C. Induction Flowmeter", Instruments, Vol. 25, p. 475, (1952).

101. Astley, E.R., "Magnetic Flowmeter Output Potentials", General Electric (General Eng. Lab.), Report No. R52 GL42, (1952).

102. Elrod, H.G., and Fouse, R.R., "An Investigation of Electromagnetic Flowmeters", Trans. A.S.M.E., Vol. 74, p. 589, (1952).

103. Barnes, A., Whitham, G.K., and Smith, F.A., "Electromagnetic Flowmeter", U.S. Atomic Energy Commission Classified Report AMK 4092, (1947). Declassified as A.E.C.D.-3407, (1952).

104. Hogg, W.R., Mittleman, E., Schover, D.S., "Electronic Circuit Problems in Electromagnetic Flow Measurements", Proc. National Electronics Conference, Vol. 8, p. 127, (1952).

105. Kolin, A., "Improved Apparatus and Technique for Electromagnetic Determination of Blood Flow", Rev. Sci. Instrum., Vol. 23, p. 235, (1952).

106. Grossman, L.M., and Charwat, A.F., "The Measurement of Turbulent Velocity Fluctuations by the Method of Electromagnetic Induction", Rev. Sci. Instrum., Vol. 23, p. 741, (1952).

107. Murgatroyd, W., "The Model Testing of Electromagnetic Flowmeters", A.E.R.E. Report No. X/R 1053, (Oct. 1952).

108. Carroll, R.M., "A Simple Electromagnetic Flowmeter For Liquid Metals", U.S. Atomic Energy Commission Unclassified Report No. ORNL-1461, (March 1953).

109. Kolin, A., "A Method for Adjustment of the Zero Setting of an Electromagnetic Flowmeter Without Interruption of Flow", Rev. Sci. Instrum., Vol. 24, p. 178, (1953).

110. Shercliff, J.A., "The Theory of the D.C. Electromagnetic Flowmeter for Liquid Metals", A.E.R.E. Report No. X/R 1052, (1953).

111. Boeke, J., "Vloeistofstroommetig op Basis van Electro-Magnetische Inductie", Electronica, Vol. 6, p.81,(1953).

Fluid Flow and Velocity Measurement...(cont.)

112. Boeke, J., "Een Nieuwe Methode van Vloeistrofstroom-
     meting", Chemisch Weekblad, Vol. 49, p. 133, (1953).

113. Savastano, G., and Carravetta, R., "Apparecchiatura el-
     ettromagnetica per la vistura delle velocita nelle cor-
     renti liquide", Energie Elettrica, Vol. 31, p.81,(1954).

114. Kolin, A., and Reiche, F., "Electromagnetic Velometry II.
     Elimination of the Effects of Induced Currents in Ex-
     plorations of the Velocity Distribution in Axially sym-
     metrical Flow", Jour. App. Phys., Vol. 25, p. 409,(1954).

115. Shercliff, J.A., "Relations Between the Velocity Profile
     and the Sensitivity of Electromagnetic Flowmeters",
     Jour. App. Phys., Vol. 25, p. 817, (1954).

116. Remenieras, G., and Hermant, C., "Mesure electromag-
     netique des vitesses dans les liquids", La Houille
     Blanche, No. Special B/1954, Vol. 9, p. 732, (1954).

117. Thurlmann, B., "Zur Elektromagnetischen Gerschwindig-
     keitsmessung von Flusskeiten", Helvetica Physica Acta,
     Vol. 28, p. 483, (1955).

118. "The Reactor Handbook", Vol. 2, Engineering, pp. 362-
     364, U.S. Atomic Energy Commission Publication AECD-
     3646, (May 1955).

119. Shercliff, J.A., "Experiments on the Dependence of
     Sensitivity on Velocity Profile in Electromagnetic Flow-
     meters", Jour. Sci. Instrum., Vol. 32, p. 441, (1955).

120. Kolin, A., "Principle of Electromagnetic Flowmeter
     Without External Magnet", Jour. App. Phys., Vol. 27,
     p. 965, (1956).

121. Denison, A.B., and Spencer, M.P., "Square-wave Electro-
     magnetic Flowmeter Design", Rev. Sci. Instrum., Vol. 27,
     p. 707, (1956).

122. Shercliff, J.A., "Electromagnetic Flowmeter Without
     External Magnet", Jour. App. Phys., Vo. 28, p. 140,
     (1957).

123. Holdaway, H.W., "A Note on Electromagnetic Flowmeters
     of Rectangular Cross-section", Helvetica Physica Acta,
     Vol. 30, p. 85, (1951).

Hydrodynamics

124. Lamb, H., "Treatise on Hydrodynamics", Cambridge Uni-
     versity Press, 6th Edition, (1945).

Hydrodynamics.(cont.)

125. Milne-Thomson, L.M., "Theoretical Hydrodynamics", The Macmillan Co., London, 3rd Edition, (1956).

126. Lin, C.C., "The Theory of Hydrodynamic Stability", Cambridge University Press, (1955).

Electromagnetic Theory

127. Stratton, J.A., "Electromagnetic Theory", McGraw Hill Book Company, New York, (1941).

128. Cullwick, E. G., "Electromagnetism and Relativity", Longmans, Green and Co., London, (1957).

129. Cramp, W., and Norgrove, E.H., "Some Investigations in the Axial Spin of a Magnet and in the Laws of Electromagnetic Induction", Jour. I.E.E., Vol. 78, p. 481, (1935).

130. Howe, G.W.O., "A Persistent Fallacy", Electrician, Vol. 117, p. 191, (1936).

131. Smythe, W.R., "Static and Dynamic Electricity", McGraw Hill Book Company, New York, 2nd Edition, (1950).

132. Whittaker, E., "The History of the Theories of the Aether and Electricity", Thomas Nelson and Son, London, (1951 and 1953).

Theory of Ionised Gases

133. Chapman, S., and Cowling, T.G., "The Mathematical Theory of Non-Uniform Gases", Cambridge University Press, 2nd Edition, (1952).

134. Spitzer, S., "Physics of Fully Ionized Gases", Interscience Publishers, New York and London, (1956).

Mathematical Methods and Circuit Theory

135. Churchill, R.V., "Fourier Series and Boundary Value Problems", McGraw Hill Book Company, New York, (1941).

136. Guillemin, E.A., "Introductory Circuit Theory", John Wiley & Sons, New York, (1953).

Electrochemistry and Contact Effects

137. Butler, J.A.V. (Editor), "Electrical Phenomena at Interfaces", Methuen and Co., London, (1951).

138. Torrey, H.C. and Whitmer, C.A., "Crystal Rectifiers", M.I.T. Rad. Lab. Series, McGraw Hill Book Company, New York, (1948).

Electrochemistry and Contact Effects (cont.)

139. Jackson, W.D., and Martindale, R.B., "Crystal Admittance Measurements", Quart. Prog. Rept., Res. Lab. of Electronics, M.I.T., p. 107, (June 1957).

140. Barker, G.C., Faircloth, R.L., and Gardner, A.W., "Use of Faradaic Rectification for the Study of Rapid Electrode Processes", Nature, Vol. 181, p. 247, (1958).

141. Maker, R., Boothroyd, A.R., and Cherry, E.C., "An Electrolytic Tank for Exploring Field Distributions", Nature, Vol. 161, p. 845, (1948).

Hydraulics

142. O'Brien, M.P., and Hickox, G.H., "Applied Fluid Mechanics", McGraw-Hill Book Company, New York, (1937).

143. Nikuradse, J., "Gesetzmassigbeiten der Turbulenten Stromung in glatten Rohren", VDI Forschungsheft, p.356, (1932).

144. Cottrell, W.B., and Mann, L.A., "Sodium Plumbing. A Review of the Unclassified Research and Technology Involving Sodium at Oak Ridge National Laboratory", U.S.A.E.C. Report ORNL-1688, (1953).

Electric Circuits

145. Valley, G.E. and Wallman, H., "Vacuum Tube Amplifiers", McGraw-Hill Book Company, New York, (1948).

146. Terman, F.E., "Radio Engineers Handbook", McGraw-Hill Book Company, New York, (1943).

147. Lettvin, J.Y., Howland B., and Gesteland, R.C., "Footnote on a Headstage", IRE Trans. Med. Electronics, PMGE-10, p.26, (1958).

148. Scott, H.H., "A New Type of Selective Circuit and Some Applications", Proc. IRE, Vol. 26, p. 226, (1938).

149. Sowerby, J.McG., "Electronic Circuitry", Wireless World, Vol. 56, p. 223, (1950).

150. Shumard, C.C., "Design of High-Pass, Low-Pass and Band-Pass Filters Using R.C. Networks and Direct Current Amplifiers with Feedback", R.C.A. Review, Vol. 11, p. 534, (1950).

Properties of Liquids

151. Kaye, G.W., and Laby, T.H., "Physical and Chemical Constants", Longman, Green & Co., London, 11th Edition, (1956).

152. "Handbook of Chemistry and Physics", Chemical Rubber Publishing Company, Cleveland, Ohio, 37th Edition, (1955).

153. "Liquid Metals Handbook", U.S. Office of Naval Research, Washington, D.C., 1st Edition, (1950).